
**Enigmatic Intraplate Volcanism:
A geochronological and geochemical approach for the Marie Byrd
Seamounts (Antarctica) and the Christmas Island Seamount
Province
(Indian Ocean)**

DISSERTATION

zur Erlangung des Doktorgrades

der Mathematisch-Naturwissenschaftlichen Fakultät

der Christian-Albrechts-Universität zu Kiel

Vorgelegt von

Andrea Kipf

Kiel, 2014

Erster Gutachter:

Prof. Dr. Kaj Hoernle

Zweiter Gutachter:

Dr. habil. Jörg Geldmacher

Tag der mündlichen Prüfung:

05.05.2014

Zum Druck genehmigt:

.....

.....

Der Dekan

Hiermit erkläre ich, dass ich die vorliegende Doktorarbeit selbständig und ohne Zuhilfenahme unerlaubter Hilfsmittel erstellt habe. Weder diese noch eine ähnliche Arbeit wurde an einer anderen Hochschule im Rahmen eines Prüfungsverfahrens vorgelegt, veröffentlicht oder zur Veröffentlichung vorgelegt. Ferner versichere ich, dass die Arbeit unter Einhaltung der Regeln guter wissenschaftlicher Praxis der Deutschen Forschungsgemeinschaft entstanden ist.

Kiel, den

Andrea Kipf

ABSTRACT:

In the world's oceans, the Hawaii-Emperor Seamounts, the Walvis Ridge and associated Seamount Province as well as the Ninetyeast Ridge and Louisville seamounts are well established examples for age progressive intraplate volcanism related to active upwelling of hot mantle in a stationary plume sensu Wilson (1963). Several seamounts in the Southwest Pacific or in the Northeast Indian Ocean, however, do not comply with the classical mantle plume theory. The South West Pacific, in particular the Amundsen and Bellingshausen Sea off the shelf of Marie Byrd Land (Westantarctica), is an area with several intraplate magmatic events that produced the Marie Byrd Seamounts, Peter I Island and the De Gerlache Seamounts at distinct time intervals, which cannot be explained by a stationary mantle plume. Bathymetric data of the Marie Byrd Seamounts in the Amundsen Sea reveals that the province consists of 8 large volcanic edifices and additional 30 minor volcanic structures (ridges). Further east, the De Gerlache Seamounts and the large active volcanic Island Peter I are situated in the Bellingshausen Sea.

One major goal of this study was to analyze bathymetric and volcanological data to provide an overview about the morphological characteristics of the Marie Byrd Seamounts and Peter I Island. With a detailed $^{40}\text{Ar}/^{39}\text{Ar}$ data set on mineral separates, the ages of the Marie Byrd Seamounts and the submarine base of Peter I Island were constrained in order to understand their temporal and spatial evolution. Further geochemical and petrological investigations aimed to characterize the geochemistry of the mantle sources and causes of melt generation that led to the formation of the Marie Byrd Seamounts, Peter I Island and De Gerlache Seamounts.

The first chapter of this study contains new $^{40}\text{Ar}/^{39}\text{Ar}$ ages of 65-56 Ma of the Marie Byrd Seamounts indicating that these intraplate volcanoes are not directly linked to the activity of a mantle plume as they do not align with spatially age progressive volcanism. The new ages from the eastern submarine flank of Peter I Island indicate that the submarine shield stage is about 1.5 million years older than subaerial volcanism based on earlier ages K-Ar ages of Prestvik and Duncan 1991.

In addition major and trace elements and Sr-Nd-Hf-Pb (double spike) isotope measurements were carried out for all 3 locations. These data reveal for the Marie Byrd Seamounts, the De Gerlache Seamount and Peter I Island that the lavas possess Ocean Island Basalts (OIB) signatures. The isotopic source flavour of the Marie Byrd Seamounts and De Gerlache Seamounts contains a distinct μ ($\mu = ^{238}\text{U}/^{204}\text{Pb}$) HIMU component mixed with a

depleted, possibly Pacific-MORB, component similar to Late Cretaceous–Cenozoic volcanics of the Hikurangi Seamounts off New Zealand (Hoernle et al. 2010), intraplate volcanic fields in New Zealand (e.g. Tappenden 2003), sub-Antarctic islands (Panter et al. 2006) and the West Antarctic rift system (WARS) (e.g. Rocholl et al. 1995). These observations suggest a common mantle source for these volcanic provinces. On the contrary Peter I Island displays a strong enriched mantle (EM) affinity probably caused by shallow mantle recycling of a continental fragment. In the absence of a long-lived hotspot, reactivation of HIMU material, initially accreted to the base of continental lithosphere during the pre-rifting stage of Marie Byrd Land/Zealandia, is proposed to generate magmatism forming the Marie Byrd Seamounts. Continental insulation flow (King and Anderson 1989) is suggested as the likely mechanism to transfer the sub-continental accreted plume material into the shallow oceanic mantle. Crustal extension at the southern boundary of the Bellingshausen Plate (Wobbe et al. 2012) may have triggered adiabatic rise of the HIMU material from the base of Marie Byrd Land to form the Marie Byrd Seamounts. The De Gerlache Seamounts are most likely related to a preserved zone of lithospheric weakness underneath the De Gerlache Gravity Anomaly.

Aspects of the onland geology of Marie Byrd Land (MBL) and Ellsworth Land in West Antarctica are subject of the second chapter to explore the history of the magmatism prior to intraplate magmatism in the Amundsen and Bellingshausen Sea. The West Antarctica coastline provides a very oblique cross section across the Mesozoic-Paleozoic orogenic belts of Gondwana. Pankhurst et al. 1998 divided MBL into two geological provinces, Ross Province in the west and Amundsen Province in the east, with the boundary at c. 140° W. The Amundsen Province is a Permian to Mesozoic Gondwana margin with a batholithic belt. To get a better geochronological and geochemical understanding about this remote and thus largely unsampled part of Antarctica, samples from the coastline of the Pine Island Bay, extending from eastern MBL to western Ellsworth Land, were investigated in terms of geochronology and geochemistry. $^{40}\text{Ar}/^{39}\text{Ar}$ dating yielded closure temperatures of c. 147 to 98 Ma for dioritic and granitic plutonic rocks and an age range of c. 97 to 95 Ma for granitoid and trachyandesitic dikes. Their major and trace element compositions show an I-type subduction-related chemistry. Therefore, the new data reveal that Mesozoic subduction-related magmatism occurred from 147–95 Ma in the Pine Island Bay region which is consistent with previously published U–Pb and K–Ar ages of I-type granitoids (Mukasa & Dalziel 2000). The oldest estimated oceanic age of easternmost MBL is c. 90 Ma (Eagles et al. 2004a). This means that the eastern MBL region experienced a short rift phase of less than 5–7 m.y., before the subduction arc of the hinterland was converted to a Late

Cretaceous passive margin. The change from subduction to rifting has been related to forces acting upon the plate margins by interaction of the palaeosubduction zone at the Zealandia/MBL margin of Gondwana with the Pacific-Phoenix spreading centre (e.g. Bradshaw 1989), the collision of the Hikurangi Plateau with Zealandia (e.g. Davy et al. 2008), and/or the activity of a mantle plume (Weaver et al. 1994, Storey et al. 1999, Hoernle et al. 2010). In contrast to Late Cretaceous mafic alkaline dikes of MBL studied by Storey et al. (1999), the Sr-Nd-Pb isotopic composition of the dikes investigated in this study does not reveal a HIMU component in the source of the melt but indicates an EM like mantle source. This could either reflect derivation from a metasomatized mantle wedge source (possibly by melts from subducted marine sediments), or contamination of mantle derived melts by continental crust during ascent and prolonged crustal residence.

The last chapter includes a major and trace element study of volcanics from another diffuse intraplate volcanic province in the northeastern Indian Ocean, the Christmas Island seamount province (CHRISP). This province extends in E-W direction and thus orthogonal to the NNE-direction of plate motion in the Wharton Basin, which provides clear indications that the seamount province cannot have formed over a stationary mantle plume (Wilson 1963). The purpose of this study was to use major and trace elements to elaborate whether the trace element composition of the CHRISP can be generated by shallow recycling of continental lithosphere at mid-ocean ridges following the model by Hoernle et al. (2011) which was based on radiogenic isotopes. Trace element data of the most mafic samples confirm that an enriched and a depleted endmember have contributed to the composition of the CHRISP. The enriched endmember, being most pronounced in the Christmas Island sub-province, is characterized by an increase in incompatible elements and LREE and thought to be related to lamproitic melts derived from subcontinental lithospheric mantle (SCLM). The depleted endmember is a MORB-like component, marked by depletion in incompatible elements. Mixing calculations indicate that the most primitive samples from Christmas Island can be generated by 25-30% lamproitic and 75-70% MORB melts. Despite the limited data set from unaltered mafic samples the trace element modeling suggest that the CHRISP volcanics can be generated by mixing of lamproitic and E-MORB melts and thus being consistent with the model of Hoernle et al. (2011).

REFERENCES:

Bradshaw, J.D., 1989. Cretaceous geotectonic pattern in the New Zealand region. *Tectonics* 8, 803–820.

Davy, B., Hoernle, K. and Werner, R., 2008. Hikurangi Plateau: crustal structure, rifted formation, and Gondwana subduction history. *Geochemistry Geophysics Geosystems* 9, 10.1029/2007GC001855.

Eagles, G., Gohl, K., Larter, R., 2004a. High-resolution animated tectonic reconstruction of the South Pacific and West Antarctic Margin. *Geochemistry, Geophysics, Geosystems* 5, Q07002.

Hoernle, K., Hauff, F., van den Bogaard, P., Werner, R., Mortimer, N., Geldmacher, J., Garbe-Schönberg, D. and Davy, B., 2010. Age and geochemistry of volcanic rocks from the Hikurangi and Manihiki oceanic plateaus. *Geochimica et Cosmochimica Acta*, 74, 7196–7219.

Hoernle, K., Hauff, F., Werner, R., van den Bogaard, P., Gibbons, A.D., S. Conrad and Müller R.D., 2011. Origin of Indian Ocean Seamount Province by shallow recycling of continental lithosphere. *Nature Geoscience* 4, 883-887.

Mukasa, S.B. and Dalziel, I.W.D., 2000. Marie Byrd Land, West Antarctica: evolution of the Gondwana's Pacific margin constrained by zircon U-Pb geochronology and feldspar common-Pb isotopic compositions. *Geological Society of America Bulletin* 112, 611–627.

Panter, K.S., Blusztajn, J., Hart, S.R., Kyle, P.R., Esser, R., McIntash, W.C., 2006. The origin of HIMU in the SW Pacific: evidence from intraplate volcanism in southern New Zealand and Subantarctic islands. *Journal of Petrology* 47, 1673–1704.

Pankhurst, R.J., Weaver, S.D., Bradshaw, J.D., Storey, B.C. and Irland, T.R., 1998. Geochronology and geochemistry of pre-Jurassic superterrane in Marie Byrd Land, Antarctica. *Journal of Geophysical Research* 103, 2529–2547.

Prestvik, T. and Duncan, R.A., 1991. The geology and age of Peter I Øy, Antarctica. *Polar Research* 9, 89-98.

Rocholl, A., Stein, M., Molzahn, M., Hart, S.R., Wörner, G., 1995. Geochemical evolution of rift magmas by progressive tapping of a stratified mantle source beneath the Ross Sea Rift, Northern Victoria Land, Antarctica. *Earth and Planetary Science Letters* 131, 207–224.

Storey, B.C., Leat, P.T., Weaver, S.D., Pankhurst, R.J., Bradshaw, J.D. and Kelly, S., 1999. Mantle plumes and Antarctica-New Zealand rifting: evidence from mid-Cretaceous mafic dykes. *Journal of the Geological Society* 156, 659–671.

Tappenden, V.E., 2003. Magmatic Response to the Evolving New Zealand Margin of Gondwana During the Mid–Late Cretaceous. (PhD thesis) University of Canterbury, Christchurch, New Zealand.

Weaver, S.D., Storey, B.C., Pankhurst, R.J., Mukasa, S.B., Divenere, V.J. and Bradshaw, J.D., 1994. Antarctica-New Zealand rifting and Marie Byrd Land lithospheric magmatism linked to ridge subduction and mantle plume activity. *Geology*, 22, 811–814.

Wilson, J.T., 1963. Evidence from islands on the spreading of the ocean floor. *Nature* 197, 536-538.

Wobbe, F., Gohl, K., Chambord, A., Sutherland, R., 2012. Structure and breakup history of the rifted margin of West Antarctica in relation to Cretaceous separation from Zealandia and Bellingshausen Plate motion. *Geochemistry, Geophysics, Geosystems* 13, Q04W12.

KURZFASSUNG:

In den Ozeanen der Erde sind die Hawaii-Emperor Seamountkette, der Walvis Rücken und die damit zusammenhängende Seamount Provinz, sowie der Ninetyeast Ridge und die Louisville Seamountkette gut begründete Beispiele für altersprogressiven Intraplattenvulkanismus bezüglich des aktiven Aufsteigens von heißen Mantelmateriale in einem stationären Plumes sensu Wilson (1963). Die Entstehung zahlreicher Seamounts im Südwestpazifik oder im nordöstlichen Indischen Ozean ist jedoch nicht konsistent mit der klassischen Mantelplumetheorie. Der Südwestpazifik, im Besonderen die Amundsen- und Bellingshausensee vor dem Schelf von Marie Byrd Land (Westantarktis), ist ein Gebiet mit zahlreichen magmatischen Ereignissen innerhalb einer Erdplatte, die sowohl die Marie Byrd Seamounts als auch Peter I Island und die De Gerlache Seamounts zu unterschiedlichen Zeitpunkten gebildet haben und nicht mit einem stationären Mantelplume erklärt werden können. Bathymetrische Daten der Marie Byrd Seamounts in der Amundsen- und Bellingshausensee haben gezeigt, dass diese Provinz aus 8 großen Vulkanen besteht und zusätzlich 30 kleinere vulkanische Strukturen (Rücken) existieren. Weiter östlich in der Bellingshausensee liegen die De Gerlache Seamounts und die große, aktive Vulkaninsel Peter I.

Eines der Hauptziele dieser Studie ist die Auswertung der bathymetrischen und vulkanologischen Daten, um einen Überblick über die morphologischen Charakteristika der Marie Byrd Seamounts und der Peter I Insel zu gewinnen. Mit einem hochqualitativen $^{40}\text{Ar}/^{39}\text{Ar}$ Datensatz an Mineralseparaten sollen die Alter der Marie Byrd Seamounts und der submarinen Basis von Peter I, sowie deren zeitliche und räumliche Entwicklung ermittelt werden. Weitere geochemische und petrologische Untersuchungen sollen helfen, die Geochemie der Mantelquellen zu charakterisieren und die Gründe für die Schmelzbildung zu verstehen, die zur Generierung der Marie Byrd Seamounts, Peter I Island und den De Gerlache Seamounts führten.

Das erste Kapitel dieser Studie beinhaltet neue $^{40}\text{Ar}/^{39}\text{Ar}$ Alter der Marie Byrd Seamounts. Diese liegen zwischen 65-56 Millionen Jahren und zeigen, dass die

Intraplattenvulkane nicht direkt auf eine Aktivität eines Mantelplumes schließen lassen, da sie keine räumliche Altersprogression aufweisen. Die neuen Alter der östlichen, submarinen Flanke von Peter I Island implizieren, dass die submarine Schildphase etwa 1.5 Millionen Jahre älter ist als der des subaerischen Vulkanismus, basierend auf früheren analysierten K-Ar Altern von Prestvik und Duncan 1991.

Zusätzlich wurden Haupt- und Spurenelemente sowie Sr-Nd-Hf-Pb (Doppel Spike) Isotopenmessungen an allen 3 Lokationen vorgenommen. Diese Daten zeigen für die Laven der Marie Byrd Seamounts, den De Gerlache Seamounts und Peter I Island eine Ozeaninselbasaltsignatur (OIB). Die isotopische Quellsignatur der Marie Byrd Seamounts und der De Gerlache Seamounts beinhaltet eine HIMU-Komponente ($\mu = \mu = {}^{238}\text{U}/{}^{204}\text{Pb}$) gemischt mit einer abgereicherten, wahrscheinlich pazifischen MORB Komponente. Die HIMU Komponente ist ähnlich zu den spätkretazisch-känozoischen Vulkanen der Hikurangi Seamounts vor Neuseeland (Hoernle et al. 2010), vulkanischen Intraplattenzentren auf Neuseeland (Tappenden 2003), den subantarktischen Inseln (Panter et al. 2006) und dem westantarktischen Riftsystem (WARS) (Rocholl et al. 1995). Diese Beobachtungen lassen auf eine gemeinsame Mantelquelle für diese Vulkanprovinzen schließen. Proben von Peter I Island hingegen spiegeln eine Affinität zu stark angereichertem Mantel (EM) wider, womöglich verursacht durch das Recyceln eines kontinentalen Fragments im flachen, oberen Mantel. Durch das Fehlen eines langlebigen Hotspots wird vermutet, dass im Vorstadium des Rifting zwischen Marie Byrd Land und Zealandia HIMU Material an die Basis der kontinentalen Lithosphäre akkretiert wurde und später reaktiviert wurde und zur Bildung der Marie Byrd Seamounts führte. Der „continental insulation flow“ nach King und Anderson (1989) wird als ein möglicher Mechanismus angesehen, um das subkontinental akkretierte Plumematerial in den oberen, ozeanischen Mantel lateral zu transportieren. Krustale Dehnungen im südlichen Bereich der Bellingshausenplatte könnten den adiabatischen Aufstieg des HIMU-Materials von der Basis Marie Byrd Lands ausgelöst haben. Die De Gerlache Seamounts sind höchstwahrscheinlich verbunden mit einer vorhandenen lithosphärischen Schwächezone, die unterhalb der De Gerlache Gravitations Anomalie zu finden ist.

Das zweite Kapitel dieser Studie befasst sich mit der Festlandsgeologie, der Westantarktis, insbesondere von Marie Byrd Land (MBL) und Ellsworth Land, um den Magmatismus zu beschreiben, der vor dem Einsetzen des Intraplattenvulkanismus in der Amundsen- und Bellingshausensee stattfand. Die westantarktische Küstenlinie stellt ein sehr schräges Querprofil durch einen mesozoischen-paläozoischen Gebirgsgürtel dar. Pankhurst et al.

(1998) unterteilen MBL in zwei geologische Provinzen, die Ross Provinz im Westen und die Amundsen Provinz im Osten, mit einer Grenze bei 140°W. Die Amundsen Provinz ist ein permischer bis mesozoischer Plattenrand von Gondwana mit einem batholitischen Gürtel. Um ein besseres geochronologisches und geochemisches Verständnis über diesen isolierten und kaum erprobten Teil der Antarktis zu erlangen, wurden Proben entlang der Küstenlinie der Pine Island Bay genommen, die sich vom östlichen Marie Land bis hin zum westlichen Ellsworth Land erstreckt und hinsichtlich ihrer Geochronologie und Geochemie untersucht wurden. $^{40}\text{Ar}/^{39}\text{Ar}$ Alter ergaben Schließungstemperaturen um etwa 147 bis 98 Millionen Jahre für die dioritischen und granitischen, plutonischen Gesteine und eine Altersspannbreite von etwa 97 bis 95 Ma für die granitoitischen und trachyandesitischen Gänge. Die Haupt- und Spurenelementzusammensetzung deutet auf eine I-type subduktionsbezogene Chemie hin. Die neuen Daten zeigen somit, dass mesozoischer subduktionsbezogener Magmatismus in der Pine Island Bay von etwa 147-95 Millionen Jahre auftrat, was konsistent ist mit bereits veröffentlichten U-Pb und K-Ar Altern von I-type Granitoiden aus diesem Gebiet (Mukasa und Dalziel 2000). Das älteste geschätzte Alter der Ozeankruste des östlichsten MBL ist circa 90 Millionen Jahre alt (Eagles et al. 2004a). Das bedeutet, dass die östliche Marie Byrd Land Region einer kurzen, weniger als 5-7 Millionen Jahren andauernden Riftphase unterlag, bevor der Subduktionsbogen des Hinterlandes umgewandelt wurde zu einem spätkretazischen passiven Plattenrand. Der Wechsel von Subduktion zum Rifting wird in Verbindung gebracht mit Kräften, die an Plattenrändern einwirken, wie durch das Zusammenspiel der Paläosubduktionszone am Rand von Zealandia/MBL dem Rand von Gondwana, mit dem Pazifik-Phoenix-Spreizungszentrum (Bradshaw 1989), der Kollision des Hikurangi Plateaus mit Zealandia (Davy et al. 2008) und/oder der Aktivität eines Mantelplumes (Weaver et al. 1994, Storey et al. 1999, Hoernle et al. 2010). Im Gegensatz zu den spätkretazischen, mafischen, alkalinen Gängen in Marie Byrd Land die von Storey et al. (1999) untersucht wurden, weisen die Gänge in dieser Studie keine HIMU Komponente in der Quelle auf, aber zeigen dafür eine EM ähnliche Mantelquelle. Diese kann entweder auf die Herkunft einer metasomatischen Mantelkeilquelle hindeuten (möglicherweise von Schmelzen subduzierter mariner Sedimente) oder durch Kontamination von Mantelschmelzen durch kontinentale Kruste während des Aufstiegs und während eines verlängerten krustalen Aufenthalts.

Das letzte Kapitel beinhaltet Haupt- und Spurenelemente der Vulkane einer weiteren diffusen Intraplattenvulkanprovinz im nordöstlichen Indischen Ozean, die Christmas Island Seamount Provinz (CHRISP). Diese Provinz erstreckt sich in Ost-West Ausdehnung und damit

orthogonal zu der Nord-Nord-Ost Plattenbewegungsrichtung im Wharton Becken. Das unterstützt die Hinweise, dass sich diese Seamount Provinz nicht über einen stationären Plume gebildet hat. Die Aufgabe dieser Studie war die Haupt- und Spurenelemente zu verwenden um zu zeigen, ob die Spurenelemente der CHRISP durch flaches recyceln von subkontinentalem lithosphärischem Mantel an mittelozeanischen Rücken generiert werden können, angelehnt an das Model von Hoernle et al. (2011) welches auf radiogenen Isotopendaten basiert. Spurenelementdaten der mafischsten Proben deuten darauf hin, dass ein angereichertes und ein verarmtes Endglied an der Zusammensetzung der CHRISP mitwirken. Die angereicherte Komponente ist am stärksten ausgeprägt in der Christmas Island Subprovinz und charakterisiert durch eine Anreicherung an inkompatiblen Elemente und LREE. Diese Komponente wird assoziiert mit lamproitischen Schmelzen, welche üblicherweise aus dem subkontinentalen lithosphärischem Mantel (SCLM) generiert werden. Das verarmte Endglied ist eine MORB Komponente, welche durch eine Abreicherung in inkompatiblen Elementen gekennzeichnet ist. Mischungsberechnungen implizieren, dass die primitivsten Proben von Christmas Island mit 25-30% lamproitischer und 75-70% MORB Schmelze generiert werden können. Trotz des limitierten Datensatzes an unalterierten, mafischen Proben, zeigt die Spurenelementmodellierung, dass die CHRISP Vulkane durch das Mischen von lamproitischen und E-MORB Schmelzen generiert werden können und sind damit konsistent mit dem Model von Hoernle et al. (2011).

REFERENCES:

Bradshaw, J.D., 1989. Cretaceous geotectonic pattern in the New Zealand region. *Tectonics* 8, 803–820.

Davy, B., Hoernle, K. and Werner, R., 2008. Hikurangi Plateau: crustal structure, rifted formation, and Gondwana subduction history. *Geochemistry Geophysics Geosystems* 9, 10.1029/2007GC001855.

Eagles, G., Gohl, K., Larter, R., 2004a. High-resolution animated tectonic reconstruction of the South Pacific and West Antarctic Margin. *Geochemistry, Geophysics, Geosystems* 5, Q07002.

Hoernle, K., Hauff, F., van den Bogaard, P., Werner, R., Mortimer, N., Geldmacher, J., Garbe-Schönberg, D. and Davy, B., 2010. Age and geochemistry of volcanic rocks from the Hikurangi

and Manihiki oceanic plateaus. *Geochimica et Cosmochimica Acta*, 74, 7196–7219.

Hoernle, K., Hauff, F., Werner, R., van den Bogaard, P., Gibbons, A.D., S. Conrad and Müller R.D., 2011. Origin of Indian Ocean Seamount Province by shallow recycling of continental lithosphere. *Nature Geoscience* 4, 883–887.

Mukasa, S.B. and Dalziel, I.W.D., 2000. Marie Byrd Land, West Antarctica: evolution of the Gondwana's Pacific margin constrained by zircon U-Pb geochronology and feldspar common-Pb isotopic compositions. *Geological Society of America Bulletin* 112, 611–627.

Panter, K.S., Blusztajn, J., Hart, S.R., Kyle, P.R., Esser, R., McIntash, W.C., 2006. The origin of HIMU in the SW Pacific: evidence from intraplate volcanism in southern New Zealand and Subantarctic islands. *Journal of Petrology* 47, 1673–1704.

Pankhurst, R.J., Weaver, S.D., Bradshaw, J.D., Storey, B.C. and Ireland, T.R., 1998. Geochronology and geochemistry of pre-Jurassic superterrane in Marie Byrd Land, Antarctica. *Journal of Geophysical Research* 103, 2529–2547.

Prestvik, T. and Duncan, R.A., 1991. The geology and age of Peter I Øy, Antarctica. *Polar Research* 9, 89–98.

Rocholl, A., Stein, M., Molzahn, M., Hart, S.R., Wörner, G., 1995. Geochemical evolution of rift magmas by progressive tapping of a stratified mantle source beneath the Ross Sea Rift, Northern Victoria Land, Antarctica. *Earth and Planetary Science Letters* 131, 207–224.

Storey, B.C., Leat, P.T., Weaver, S.D., Pankhurst, R.J., Bradshaw, J.D. and Kelly, S., 1999. Mantle plumes and Antarctica-New Zealand rifting: evidence from mid-Cretaceous mafic dykes. *Journal of the Geological Society* 156, 659–671.

Tappenden, V.E., 2003. Magmatic Response to the Evolving New Zealand Margin of Gondwana During the Mid–Late Cretaceous. (PhD thesis) University of Canterbury, Christchurch, New Zealand.

Weaver, S.D., Storey, B.C., Pankhurst, R.J., Mukasa, S.B., Divenere, V.J. and Bradshaw, J.D.,

1994. Antarctica-New Zealand rifting and Marie Byrd Land lithospheric magmatism linked to ridge subduction and mantle plume activity. *Geology*, 22, 811–814.

Wilson, J.T., 1963. Evidence from islands on the spreading of the ocean floor. *Nature* 197, 536-538.

Wobbe, F., Gohl, K., Chambord, A., Sutherland, R., 2012. Structure and breakup history of the rifted margin of West Antarctica in relation to Cretaceous separation from Zealandia and Bellingshausen Plate motion. *Geochemistry, Geophysics, Geosystems* 13, Q04W12.

DANKSAGUNG:

Die vorliegende Arbeit entstand im Rahmen der durch die Deutsche Forschungsgesellschaft (DFG) geförderten Projekte HO1833/15-1 und 15- 3 innerhalb des Schwerpunktprogrammes „Antarktisforschung“, und dem neuseeländischen Ministerium für Wissenschaft und Innovation. Das deutsche Ministerium für Bildung und Forschung (BMBF) förderte das SO199 CHRISP Projekt. Für die Ausarbeitung und das Stellen der Projektanträge möchte ich mich bei Prof. Dr. Kaj Hoernle, Dr. Folkmar Hauff und Dr. Reinhard Werner bedanken.

Mein Dank gilt meinem Betreuer Prof. Dr. Kaj Hoernle für die Vergabe dieser Arbeit, seine Diskussionsbereitschaft und konstruktiven Gespräche sowie die kritische Durchsicht meiner Manuskripte.

Des Weiteren bedanke ich mich bei Dr. Jörg Geldmacher für die Übernahme des zweiten Gutachtens.

Bedanken möchte ich mich auch bei Dr. Folkmar Hauff und Dr. Reinhard Werner für ihre Unterstützung bei der Auswertung und Interpretation meiner Daten sowie die kritische Durchsicht meiner Manuskripte. Dr. Folkmar Hauff und Silke Hauff danke ich zudem für die Durchführung der Isotopenanalysen.

Ein Dank geht an Dr. Paul van den Bogaard für die Durchführung der $^{40}\text{Ar}/^{39}\text{Ar}$ Altersdatierungen, an Nicholas Mortimer, Dr. Karsten Gohl, Dr. Doris Maicher und Dr. Andreas Klügel für die Beiträge zu den Manuskripten.

Weiterhin danken möchte ich Dagmar Rau für die RFA Analytik, Dieter Garbe-Schönberg und Dipl.-Ing. Ulrike Westernströer für die Unterstützung bei der Vorbereitung der Proben zur ICP-MS-Analytik.

Dr. Maxim Portnyagin und Dr. Thor Hansteen, Dr. Christian Timm und Dr. Ken Heydolph danke ich für ihre rege Diskussionsbereitschaft und Hilfsbereitschaft beim Mikroskopieren.

Meinen Freunden, Veronica, Vanessa, Nadine, Eileen, Tobias, Kathrin, Anke, Maren und Nina danke ich für ihre vielfältige und wertvolle Unterstützung in allen Lebenslagen.

Meiner Melli danke ich im Besonderen, da sie immer für mich da ist und auf der Zielgeraden dieser Arbeit noch viel Motivationsarbeit leistete.

Ein ganz spezieller Dank geht an meine schwarz-graue, vierbeinige Fellnase Monti. Der mich trotz meiner gelegentlichen Verstimmtheit in den letzten Wochen

unablässig mit seiner guten Laune bedrängte, auf den Spaziergängen stets sorgfältig darauf achtete, dass ich nie vom Weg abkam und mich immer wieder an der gleichen Haustür ablieferte.

Ein sehr großer Dank geht an meine Familie, meine Eltern und meine Schwester, die mich in den letzten Jahren tatkräftig unterstützt haben. Vielen Dank dafür!

Der größte Dank gebührt meinem Freund Wolfgang, für seine Geduld und Ausdauer in den ganzen letzten Jahren, und vor allem für den Glauben an mich und an das was ich tue.

INTRODUCTION:

On earth, the plate tectonic theory can well explain volcanism at mid oceanic ridge where new plates are created, and volcanism at continental margins and island arcs where oceanic plates are destroyed via subduction. While magma generation at mid ocean ridges is predominantly driven by adiabatic decompressional melting of passively upwelling, upper mantle melting in subduction zones is mainly caused by fluids added to the mantle wedge above the subducting plate by dehydration processes from the downgoing plate.

Intraplate volcanism on the other hand cannot straightforwardly be explained by plate tectonics. While continental rifts, sometimes leading to continental breakup, can explain volcanism by thinning of the lithosphere that leads to mantle upwelling and decompression melting, volcanism within plates away from lithospheric faulting is classically thought to be related to stationary and actively upwelling mantle diapirs that are not directly governed by plate tectonics. When Wilson in 1963 proposed that the distinctive linear shape of the Hawaiian Island-Emperor Seamounts chain resulted from the Pacific Plate moving over a deep, stationary hotspot in the mantle, located beneath the present-day position of the Island of Hawaii, it marked the beginning of the hotspot theory that has been applied to numerous volcanic chains in the world's oceans until present. The theory has been refined over the years by geochronology that proved age progressive volcanisms along these features, by geochemistry that provided evidence for a deep mantle origin and for recycling of subducting plates and material within mantle plumes. Finally, geophysical evidence by seismic tomography enabled mapping of plume structures at depth and showed that some root into the lower mantle. Still, there are many intraplate volcanic centers that cannot be explained by the hotspot theory sensu Wilson (1963) as for example in the southeastern Pacific, the Pukapuka ridges (Ballmer et al. 2007), on Zealandia (e.g. Hoernle et al. 2006) and Crary Mountains in Marie Byrd Land (Panter et al. 2000).

As a result, distinct plume models were developed, such as small plumes or plumelets (Duncan 1984, Holik et al. 1991, Geldmacher et al. 2000, 2001) and rising blobs (Hoernle und Schmincke 1993) or super plumes residing at depth and rise of smaller diapirs from there (Hoernle et al. 1995). Hence, some authors postulate that intraplate volcanism or hotspot volcanism in general is induced by shallow convectional processes in the upper mantle (King and Anderson 1998), melting along weak zones in the lithosphere (Smith 2003) or magmatism along fracture zones. The main motivation of this dissertation is to investigate enigmatic intraplate volcanism that cannot be explained by the hotspot theory by using geochronology and geochemistry of volcanics in conjunction with plate tectonic reconstruction from two areas: the Marie Byrd Seamounts off West Antarctica and the Christmas Island Seamount Province in the

Indian Ocean.

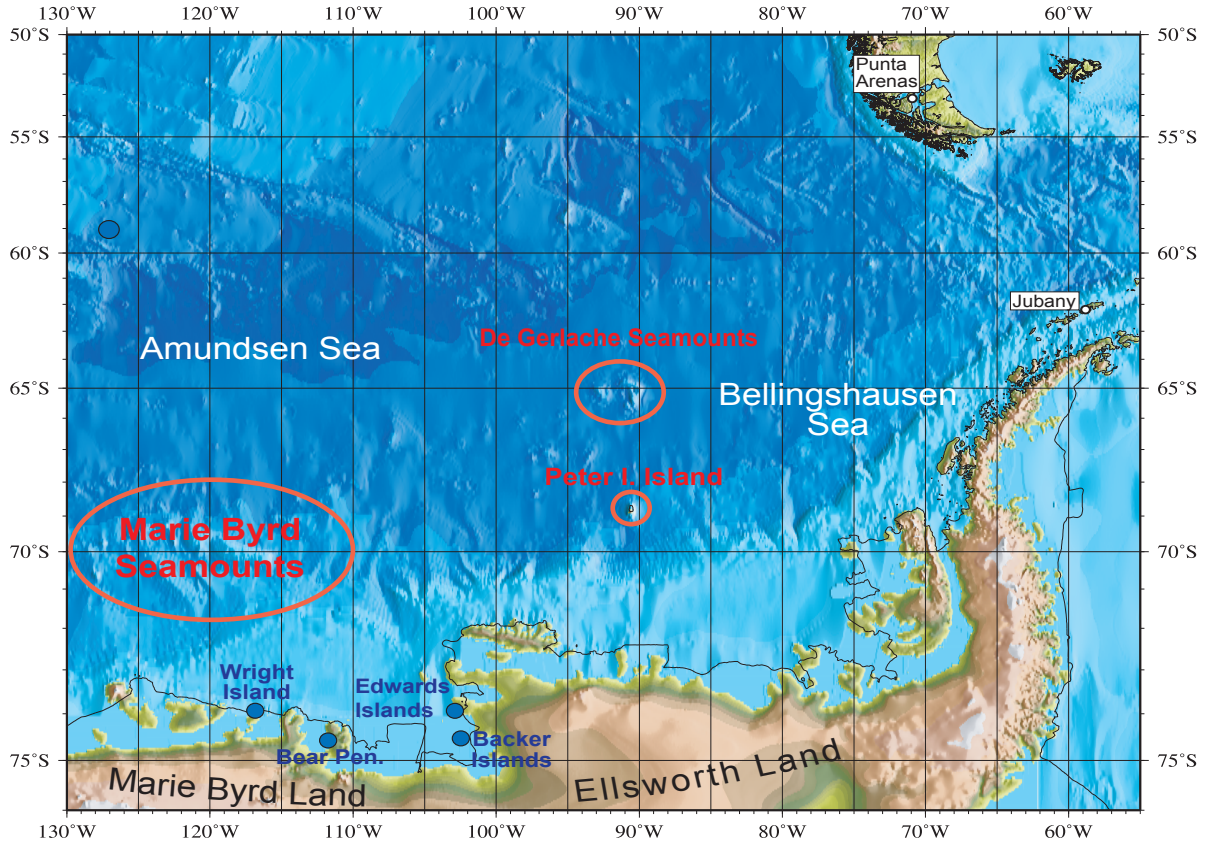


Fig. 1: Overview map of the South West Pacific in particular Amundsen Sea and Bellingshausen Sea. Red circles and blue circles sampling areas during Polarstern expedition ANT XXIII/4 except the De Gerlache Seamounts.

The focus area of investigation presented here are the shelf and ocean basins off Marie Byrd Land (Antarctica), namely the Pine Island Bay, the Amundsen and Bellingshausen Sea, respectively (see Fig. 1). This part of the world is not within easy reach due to its remote location, logistically difficult access and harsh weather conditions. Therefore, the rock samples obtained during R/V Polarstern expedition ANT XXIII/4 are a unique contribution to characterize the volcanism on eastern Marie Byrd Land and Pine Island Bay; a rifted Gondwana margin, along with oceanic intraplate volcanism at the Marie Byrd Seamounts, Peter I Island and the De Gerlache Seamounts. Because this area is a key location for continental break up between Antarctica and Zealandia, one of the overall aims was to test whether the Cretaceous break up of is documented in the tectonics and magmatic processes of this region. Furthermore, the absence of a long-lived hotspot in this region makes the Marie Byrd Seamounts, Peter I island and the Gerlache Seamounts part of the diffuse intraplate volcanic province proposed for the south west Pacific.

This dissertation includes $^{40}\text{Ar}/^{39}\text{Ar}$ ages and a detailed geochemical study (major and

trace elements and Sr-Nd-Hf-Pb double spike isotope data) of Marie Byrd Land, the Bellingshausen Sea and the Amundsen Sea. This includes data from granitoids of the Pine Island Bay and for the first time from the Marie Byrd Seamounts as well as the submarine base of Peter I Island and geochemical data for the Belgica Seamount (De Gerlache Seamount group). The samples were taken during Polarstern expedition ANT XXIII/4 in 2006 (Marie Byrd Land, Marie Byrd Seamounts, Peter I.) and ANTXII/4 (Belgica Seamount). Only two of the Marie Byrd seamounts were mapped by multi beam during on previous expeditions of R/C N.B Palmer in 1996 and Polarstern ANT-XI-3 in 1994 and ANT XVIII/5a in 2001, but no rock samples were taken. Thus neither age nor chemical data were yet available to decipher the origin and evolution of this 100,000 km² area that houses up to 3000 m high volcanic edifices. In detail a high quality laser step-heating ⁴⁰Ar/³⁹Ar geochronology was applied to verify whether the Marie Byrd Seamounts or the volcanism in the Pine Island Bay are of Cretaceous or Cenozoic and to test for possible connections to volcanic activity linked to the breakup of Gondwana or to the Cenozoic diffuse intraplate volcanism.

Additionally, the dissertation includes a major and trace element data set from the Christmas Island seamount province, which is another area of enigmatic intra plate volcanism in the Indian Ocean. The samples were taken during RV Sonne cruise SO199 CHRISP in 2008. 54 seamounts were partially mapped with the SIMRAD EM120 and 38 seamounts were sampled by dredging. This region is of great interest because these seamounts do not form a linear and continuous trail of volcanoes expected for a classical hotspot origin. A previous study by Hoernle et al. 2011 claims that these seamounts were formed in the vicinity of a paleo-spreading center where delaminated subcontinental lithospheric mantle (SCLM) was recycled by passive upwelling. The SCLM is thought to be initially transferred into the oceanic realm during the breakup of the northwestern continental margin of Australia. Two distinct chemical endmembers appear to have contributed to the composition of the CHRISP volcanics based on radiogenic isotopes (Hoernle et al. 2011). Namely these are SCLM and MORB. The aim of the study presented here was to test if this mixing scenario can be retraced with a new data set of major and trace elements.

The dissertation at hand comprises three independent chapters contributing to the above-mentioned objectives. The first chapter contains for the first time a comprehensive data set from the enigmatic Marie Byrd Seamount province including morphological, geochronological, and geochemical data, combined with additional data for the De Gerlache and Peter I Island volcanic complexes. The centerpiece of this study is the ⁴⁰Ar/³⁹Ar dating of 9 samples including the Marie Byrd Seamounts and the submarine base of Peter I Island. The age dating was carried out on

glass, feldspar and groundmass to identify the ages of the Marie Byrd Seamounts and the base of Peter I Island with published age data from Belgica Seamount, to give an overview of volcanism in these spatially confined area. The major aim was to verify whether the Marie Byrd Seamounts are of Cretaceous or Cenozoic origin and to test if the volcanic activity is linked to the breakup of Gondwana, and to determine the intervals of intraplate volcanism on Peter I Island and the De Gerlache Seamount to give a contribution to the hotly debated models on intraplate volcanism and to the plate tectonic reconstruction of the South West Pacific. Nineteen dredged samples from these localities were analyzed for major and trace elements, 23 for Sr-Nd-Pb isotope analyses and 9 samples for Hf-isotopes. These analyzes are of special interest to determine (1) the mantle endmembers; (2) to figure out if these volcanic edifices originate from a shallow asthenospheric source like the Cenozoic West Antarctic rift system, (3) or a deep mantle source like a plume (4) and especially if this plume is related to the mega plume or plumelets underneath Marie Byrd Land postulated after Weaver et al. 1994 and Storey et al. 1999, (5) or if there is a relation to the Cretaceous plume which may have induced the breakup of Gondwana. A further important point of this chapter is a comparison between similar HIMU- trace element and isotopic signatures and ages of volcanics on Zealandia, Marie Byrd Land and the Cenozoic intraplate volcanic province in the South West Pacific to decipher geochemical differences or similarities of their source regions.

The second chapter is focused on a geochronological and geochemical study presenting new $^{40}\text{Ar}/^{39}\text{Ar}$ age and XRF, ICPMS element concentration data, from recovered plutonic and dyke rocks of the Pine Island Bay region, Marie Byrd Land. This is a very important contribution to the spatial and temporal evolution of this part of the Antarctic margin, from which little is known so far. Previous studies by Storey et al. 1999 and Mukasa & Dalziel 2000 have shown that along the coast of Marie Byrd Land the former Gondwana margin, subduction ceased earlier in western Marie Byrd Land than in the east. This is reported in geochemical and geochronological studies of I-type volcanism, the following A-type volcanism indicated an abrupt change to rift related magmatism in western Marie Byrd Land and represents the breakup process between Marie Byrd Land and Zealandia. So until now, no A-type volcanism was ever found in the eastern Marie Byrd Land. To proof the temporal and tectonic evolution of this part of Antarctica and to confirm already existing studies, we analyzed 7 samples from the Pine Island Bay region.

The third chapter encompasses a major and trace element study on diffuse intraplate volcanism of the Christmas Island Seamount Province (CHRISP), situated in the northeastern Indian Ocean. The major aim of this study was the reconstruction of the spatial and temporal

evolution as well as the magmatic origin of this widely unexplored seamount province on the basis of major and trace elements and to test the model by Hoernle et al. (2011). This study contributes to the Great Plume Debate because the formation of the CHRISP seamounts cannot be well explained by conventional models for the origin of intraplate volcanism, and therefore, an alternative mechanism is required. Fiftytwo samples were analyzed for major and trace elements by XRF and ICP-MS to characterize the geochemical characteristics of the CHRISP. The trace element composition of the most primitive, unaltered samples was used to evaluate if the trace element composition of the CHRISP lavas can be generated by shallow recycling of continental lithosphere at mid-ocean ridges according to the model by Hoernle et al. (2011). A mixing model revealed that the trace element composition of the mafic CHRISP lavas can be generated by mixing of lamproitic and E-MORB melts, being consistent with the model of Hoernle et al. 2011.

REFERENCES:

Ballmer, M. D., J., van Hunen, G., Ito, P. J., Tackley, and T. A., Bianco, 2007. Non-hotspot volcano chains originating from small-scale sublithospheric convection. *Geophysical Research Letters* **34**. ISI:000251690300002.

Bradshaw, J.D., 1989. Cretaceous geotectonic pattern in the New Zealand region. *Tectonics* **8**, 803–820.

Davy, B., 1992. The influence of subducting plate buoyancy on subduction of the Hikurangi-Chatham Plateau beneath the North Island, New Zealand. In: *Geology and geophysics of continental margins*. Ed. J.S. Watkins, F. Zhiqiang, J.J. McMillan. AAPG memoir 53, 75-91.

Davy, B. and Wood, R., 1994. Gravity and magnetic modelling of the Hikurangi Plateau. *Marine Geology* **118**, 139-151.

DiVenere, V., Kent, D.V., 1999. Are the Pacific and Indo- Atlantic hotspot fixed? Testing the plate circuit trough Antarctica. *Earth and Planetary Science Letters* **170**, 105-117.

Duncan, R.A., 1984. Age-progressive volcanism in the New England seamounts and the opening of the central Atlantic Ocean, *Journal of Geophysical Research* **89**, 9980-9990.

Geldmacher, J., van den Bogaard, P., Hoernle, K., Schmincke H-U., 2000. Ar age dating of the Madeira Archipelago and hotspot track (eastern North Atlantic). *Geochemistry, Geophysics, Geosystems* 1, 1999GC000018.

Geldmacher, J., Hoernle, K., van den Bogaard, P., Zankl, G., Garbe-Schönberg, D., 2001. Earlier history of the C70-Ma-old Canary hotspot based on the temporal and geochemical evolution of the Selvagen archipelago and neighboring seamounts in the eastern north Atlantic. *Journal of Volcanology and Geothermal Research* 111, 55–87.

Hart, S.R., Blusztajn, J., Craddock, C., 1995. Cenozoic volcanism in Antarctica: Jones Mountains and Peter I Island. *Geochimica et Cosmochimica Acta* 59, 3379–3388.

Hart, S.R., Blusztajn, J., LeMasurier, W.E., Rex, D.C., 1997. Hobbs Coast Cenozoic volcanism, implications for the West Antarctic Rift System. *Chemical Geology* 139, 223–248.

Hole, M.J., LeMasurier, W.E., 1994. Tectonic controls on the geochemical composition of Cenozoic, mafic alkaline volcanic rocks from West Antarctica. *Contributions to Mineralogy and Petrology* 117, 187–202.

Holik, J.S., Rabinowitz, P.D. and Austin, J.A., 1991. Effects of Canary hotspot volcanism on structure of oceanic crust off Morocco. *Journal of Geophysical Research* 96-B7, 12.039-12.067.

Hoernle, K. and Schmincke, H.U., 1993. The role of partial melting in the 15-Ma geochemical evolution of Gran Canaria: A blob model for the Canary hotspot. *Journal of Petrology* 34(3), 599-626.

Hoernle, K., White, J.D.L., van den Bogaard, P., Hauff, F., Coombs, D.S., Werner, R., Timm, C., Garbe-Schoenberg, D., Reay, A., Cooper, A.F., 2006. Cenozoic intraplate volcanism on New Zealand: upwelling induced by lithospheric removal. *Earth and Planetary Science Letters* 248, 350–367.

Hoernle, K., Hauff, F., Werner, R., van den Bogaard, P., Gibbons, A.D., S. Conrad and Müller R.D., 2011. Origin of Indian Ocean Seamount Province by shallow recycling of continental lithosphere. *Nature Geoscience* 4, 883-887.

King, S.D., Anderson, D.L., 1998. Edge-driven convection. *Earth and Planetary Science Letters* 160, 289–296.

Luyendyk, B.P., 1995. Hypothesis for Cretaceous rifting of East Gondwana caused by subducted slap capture. *Geology* 23, 373–376.

Mukasa, S.B. and Dalziel, I.W.D., 2000. Marie Byrd Land, West Antarctica: evolution of the Gondwana's Pacific margin constrained by zircon U-Pb geochronology and feldspar common-Pb isotopic compositions. *Geological Society of America Bulletin* 112, 611–627.

Panter, K.S., Hart, S.R., Kyle, P., Blusztajn, J., Wilch, T., 2000. Geochemistry of Late Cenozoic basalts from the Crary Mountains: characterization of mantle sources in Marie Byrd Land, Antarctica. *Chemical Geology* 165, 215–241.

Rocholl, A., Stein, M., Molzahn, M., Hart, S.R., Wörner, G., 1995. Geochemical evolution of rift magmas by progressive tapping of a stratified mantle source beneath the Ross Sea Rift, Northern Victoria Land, Antarctica. *Earth and Planetary Science Letters* 131, 207–224.

Smith, A.D., 2003. A re-appraisal of stress field and convective roll models for the origin and distribution of Cretaceous to Recent intraplate volcanism in the Pacific basin, *International Geology Review*, 45.

Storey, B.C., Leat, P.T., Weaver, S.D., Pankhurst, R.J., Bradshaw, J.D. and Kelly, S., 1999. Mantle plumes and Antarctica-New Zealand rifting: evidence from mid-Cretaceous mafic dykes. *Journal of the Geological Society* 156, 659–671.

Weaver, S.D., Storey, B.C., Pankhurst, R.J., Mukasa, S.B., Divenere, V.J. and Bradshaw, J.D., 1994. Antarctica-New Zealand rifting and Marie Byrd Land lithospheric magmatism linked to ridge subduction and mantle plume activity. *Geology*, 22, 811–814.

Wilson, J.T., 1963. Evidence from islands on the spreading of the ocean floor. *Nature* 197, 536-538.

CONTENTS:

Abstract.....	I
Kurzfassung.....	VI
Danksagung.....	XII
Introduction.....	XIII

CHAPTER I

Seamounts off the West Antarctic margin: A case for non-hotspot driven intraplate volcanism

Abstract..	3
1. Introduction...	4
2. Tectonic and magmatic evolution of the SW-Pacific over the past 100 Ma.	7
3. Bathymetry and Morphology of Marie Byrd Seamounts and Peter I Island.....	9
4. Sample background.....	14
5. Petrography and rock classification.....	16
6. Analytical results.....	21
6.1 ⁴⁰ Ar/ ³⁹ Ar age dating.....	21
6.2 Major and trace elements.....	24
6.3 Sr-Nd-Pb-Hf isotopes.....	27
7. Discussion.....	33
7.1 Spatial distribution of Cenozoic volcanism in the Amundsen Sea and Bellingshausen Sea.....	33
7.2 Geochemical constraints on the origin of seamount magmatism.....	35
7.3 Origin of the HIMU component in non-hotspot related Southwest- Pacific and the Antarctic volcanic provinces.....	37
7.4 Model for the formation of the Marie Byrd Seamounts.....	42
8. Conclusions.....	44
Acknowledgments.....	45
References.....	46

CHAPTER II

Granitoids and dikes of the Pine Island Bay region, West Antarctica

Abstract.....	61
1. Introduction.....	62
2. Geological and tectonic setting.....	64
3. Sample background.....	65

4. Analytical methods.....	67
5. Results.....	69
5.1 Petrography and classification.....	69
5.2 Ar/Ar age dating.....	71
5.3 Geochemistry.....	75
6. Discussion.....	78
6.1 Petrogenesis.....	78
6.2 Age-composition patterns.....	79
6.3 Cretaceous geodynamics.....	82
Acknowledgments.....	83
References.....	84

CHAPTER III

Major and trace element composition of the Christmas Island Seamount Province: testing a two component mixing model

Abstract.....	89
1. Introduction.....	90
2. Geological setting and Morphology.....	91
3. Methods.....	93
4. Results: Major and trace elements.....	93
5. Discussion.....	110
5.1 Fractional crystallization and melting degree.....	110
5.2 Melting and source composition.....	116
5.3 Compositional range of the possible sources.....	119
5.4 Source rocks versus primitive Christmas Island (UVS) and eastern Wharton Basin Province (EWP).....	120
5.5 Two component mixing model.....	123
6. Conclusion.....	128
References.....	129
Appendices.....	134
Appendix I (CHAPTER I).....	134
Appendix II (CHAPTER II).....	159
Appendix III (CHAPTER III).....	172

CHAPTER I

Seamounts off the West Antarctic margin: A case for non-hotspot driven intraplate volcanism

A. Kipf^{a*}, F. Hauff^a, R. Werner^a, K. Gohl^b, P. van den Bogaard^a, K. Hoernle^a, D. Maicher^a, and A. Klügel^c

^a GEOMAR Helmholtz Centre for Ocean Research Kiel, Wischhofstr. 1-3, D-24148 Kiel, Germany

^b Alfred-Wegener-Institute for Polar and Marine Research, Postfach 120161, D-27515 Bremerhaven, Germany

^c University of Bremen, Postfach 330440, D-28334 Bremen, Germany

Published in Gondwana Research

ABSTRACT

New radiometric age and geochemical data of volcanic rocks from the guyot-type Marie Byrd Seamounts (MBS) and the De Gerlache Seamounts and Peter I Island (Amundsen Sea) are presented. $^{40}\text{Ar}/^{39}\text{Ar}$ ages of the shield phase of three MBS are Early Cenozoic (65 to 56 Ma) and indicate formation well after creation of the Pacific-Antarctic Ridge. A Pliocene age (3.0 Ma) documents a younger phase of volcanism at one MBS and a Pleistocene age (1.8 Ma) for the submarine base of Peter I Island. Together with published data, the new age data imply that Cenozoic intraplate magmatism occurred at distinct time intervals in spatially confined areas of the Amundsen Sea, excluding an origin through a fixed mantle plume. Peter I Island appears strongly influenced by an EMII type mantle component that may reflect shallow mantle recycling of a continental raft during the final breakup of Gondwana. By contrast the Sr-Nd-Pb-Hf isotopic compositions of the MBS display a strong affinity to a HIMU type mantle source. On

a regional scale the isotopic signatures overlap with those from volcanics related to the West Antarctic Rift System, and Cretaceous intraplate volcanics in and off New Zealand. We propose reactivation of the HIMU material, initially accreted to the base of continental lithosphere during the pre-rifting stage of Marie Byrd Land/Zealandia to explain intraplate volcanism in the Amundsen Sea in the absence of a long-lived hotspot. We propose continental insulation flow as the most plausible mechanism to transfer the sub-continental accreted plume material into the shallow oceanic mantle. Crustal extension at the southern boundary of the Bellingshausen Plate from about 74 to 62 Ma may have triggered adiabatic rise of the HIMU material from the base of Marie Byrd Land to form the MBS. The De Gerlache Seamounts are most likely related to a preserved zone of lithospheric weakness underneath the De Gerlache Gravity Anomaly.

1. INTRODUCTION

Seamounts are common bathymetric features on the seafloor and most are of volcanic origin. Although only a fraction of them have been mapped by ship-based echosounding, satellite altimetry has identified more than 13,000 seamounts taller than 1.5 km and predicts more than 100,000 seamounts higher than 1 km (e.g., Smith and Sandwell, 1997; Wessel et al., 2010). Seamounts are important probes of the composition and dynamics of the oceanic mantle and, if they form parts of hotspot tracks, they can also be important recorders of past plate motions (Hofmann, 2003; Tarduno et al., 2003; Koppers et al., 2012). They also form oases for marine life and biodiversity (e.g., Shank, 2010 for a recent review) and are significant components of hydrogeological systems focusing the exchange of heat and fluids between the oceanic lithosphere and the oceans (e.g., Fisher et al., 2003; Harris et al., 2004; Hutnak et al., 2008; Klügel et al., 2011). The latter processes can lead to the formation of economically important mineral deposits (e.g., Hein et al., 2010), which are, for example, commercially mined in some accreted seamount complexes (e.g., Safonova, 2009). Seamounts are also sites of geological hazards such as tsunamis through sector collapse during their growth stage (e.g., McMurtry et al., 2004). Upon subduction of the ocean floor, seamounts can also serve as prominent asperities generating earthquakes (e.g., Watts et al., 2010 for a recent review). As the subduction process can lead to crustal accretion of seamounts, they can be preserved in the accessible geological record, providing important insights from the evolution of hotspot tracks and continental margins to biological exchange between continents (e.g., Hoernle et al., 2002; Geldmacher et al., 2008; Portnyagin et al., 2008; Buchs et al., 2011; Safonova and Santosh, 2013). Despite the manifold contributions of seamounts to the dynamics of diverse earth

systems, their process of formation is still debated. Most commonly the occurrence of isolated volcanoes distant from plate boundaries is attributed to the upwelling of mantle plumes (e.g., Wilson, 1963; Morgan, 1971; Courtillot et al., 2003). The absence of linear volcanic chains and lack of spatially age progressive magmatism in many areas has stimulated a vigorous debate on the origin of intraplate volcanism (e.g., Anderson, 2000; Foulger and Natland, 2003; see also “Great Plume debate”, www.mantleplumes.org). Other important mechanisms of seamount formation include off-axis volcanism in the vicinity of spreading ridges by lateral expansion of the ridge melting regime (e.g., Batiza et al., 1990; Brandl et al., 2012 and references therein), recycling of delaminated continental lithosphere (Hoernle et al., 2011) and plate fracturing (e.g., Winterer and Sandwell, 1987; Natland and Winterer, 2005). In this paper, we report for the first time an integrated bathymetric, geochronological and geochemical data set from three seamount provinces off West Antarctica and show that these intraplate volcanoes are not directly linked to the activity of a mantle plume but rather reflect remobilization and transfer of fertile mantle from beneath West Antarctica.

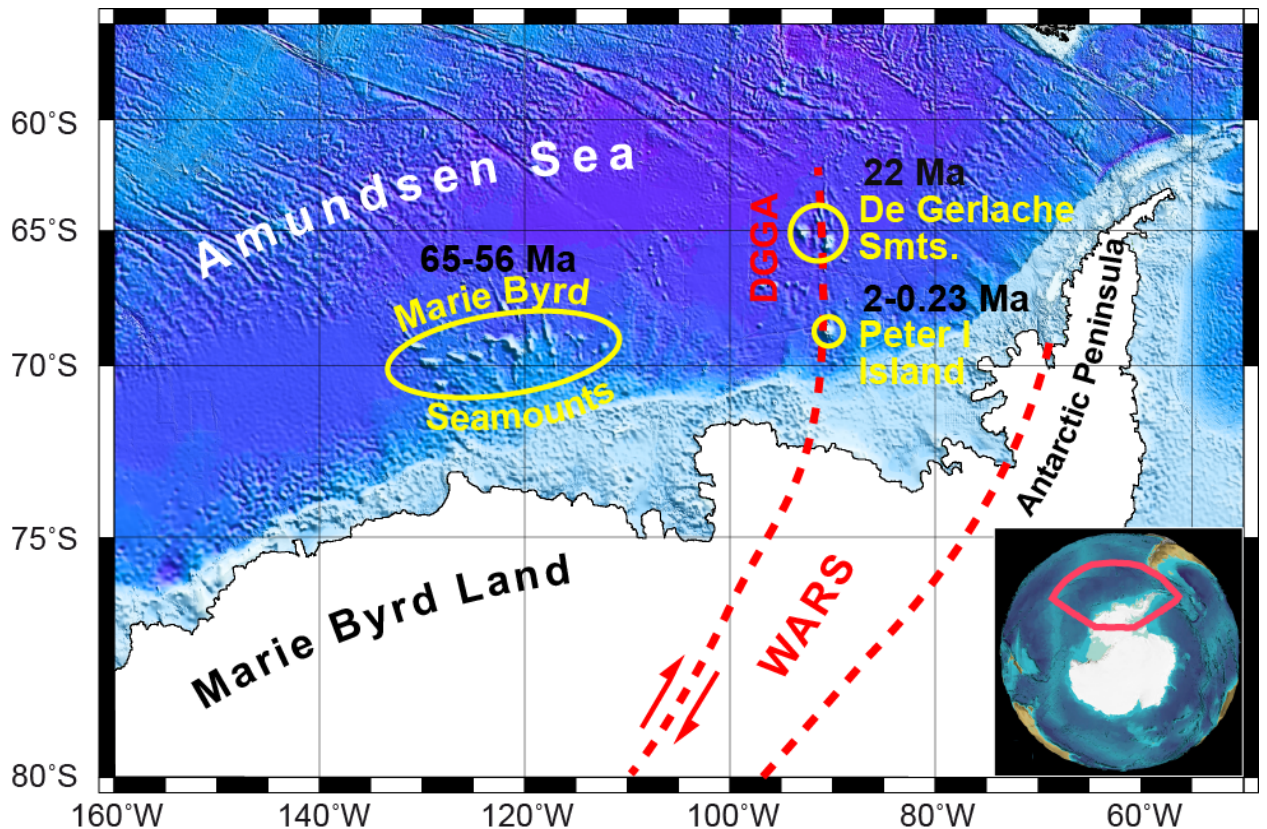


Fig. 1: Overview map of West Antarctica and the Amundsen Sea. The three seamount/ocean island volcanic provinces of the Amundsen Sea are marked by yellow circles. Dashed red lines indicate major tectonic lineaments (WARS - West Antarctic Rift System from Müller et al. (2007); DGGA - De Gerlache Gravity Anomaly). The map is based on the GEBCO_08 grid (version 20091120, <http://www.gebco.net>).

The Marie Byrd Seamounts (MBS), located in the western Amundsen Sea north of the continental shelf of Marie Byrd Land, West Antarctica (Fig. 1), are a good example of enigmatic intraplate volcanism. They are located on oceanic crust possibly older than 72 Ma (Heinemann et al., 1999; Eagles et al., 2004a,b) and form an elongated cluster of volcanic edifices, that extends for more than 800 km between $\sim 114^\circ$ and $\sim 131^\circ\text{W}$, and $\sim 68^\circ$ and $\sim 71^\circ\text{S}$. Based on rock fragments found in corers and dredges carried out at a single MBS (Hubert Miller Seamount), Udintsev et al. (2007) assumed that this structure represents a relict fragment of continental crust which was destructed and altered by a mantle plume. The authors, however, admit that the material recovered cannot unambiguously be interpreted as in situ rocks. Although the MBS form a vast seamount province covering over 200,000 km², their remote location made sampling difficult, inhibiting elucidation of their age, magma sources and volcanic evolution. Moreover, the relationship of the MBS to the magmatism associated with the final break-up of Gondwana and/or to the widespread but low volume intraplate volcanism in the SW Pacific region (e.g., Weaver et al., 1994; Storey et al., 1999; Rocchi et al., 2002a; Finn et al., 2005; Hoernle et al., 2006; Hoernle et al., 2010; Timm et al., 2010) was poorly constrained.

In 2006, the R/V POLARSTERN cruise ANT-XXIII/4 conducted a bathymetric mapping and dredge sampling survey of five MBS and associated structures. Samples from two other volcanic complexes in the Amundsen Sea, namely the previously studied ocean island volcano Peter I Island (e.g., Prestvik et al., 1990; Prestvik and Duncan, 1991; Hart et al., 1995) and the Belgica Seamount (De Gerlache Seamounts, Hagedorn et al., 2007) (Fig. 1), are included in our study to more fully characterize the sources and spatial evolution of intraplate magmatism in this region. Both Peter I Island and the De Gerlache Seamounts have been related to hotspot activity by most previous authors.

Here we present results of the bathymetric surveys together with $^{40}\text{Ar}/^{39}\text{Ar}$ ages and geochemical data (major and trace element and radiogenic Sr-Nd-Pb-Hf isotope ratios) of the recovered rocks. We show that magmatism in the Amundsen Sea occurred at distinct time intervals in spatially confined areas ruling out an origin through a single stationary hotspot. Notably this volcanism appears predominantly influenced by HIMU (high time-integrated $^{238}\text{U}/^{204}\text{Pb}$) type mantle, requiring emplacement and upwelling of such material in the depleted upper oceanic mantle well after the breakup of Zealandia from Antarctica. After briefly summarizing the tectonic and magmatic evolution affecting this part of the SW Pacific over the past 100 Ma, we discuss our results and evaluate processes, which may cause non-hotspot related HIMU-type intraplate volcanism in the Amundsen Sea.

2. TECTONIC AND MAGMATIC EVOLUTION OF THE SW-PACIFIC OVER THE PAST 100 MA

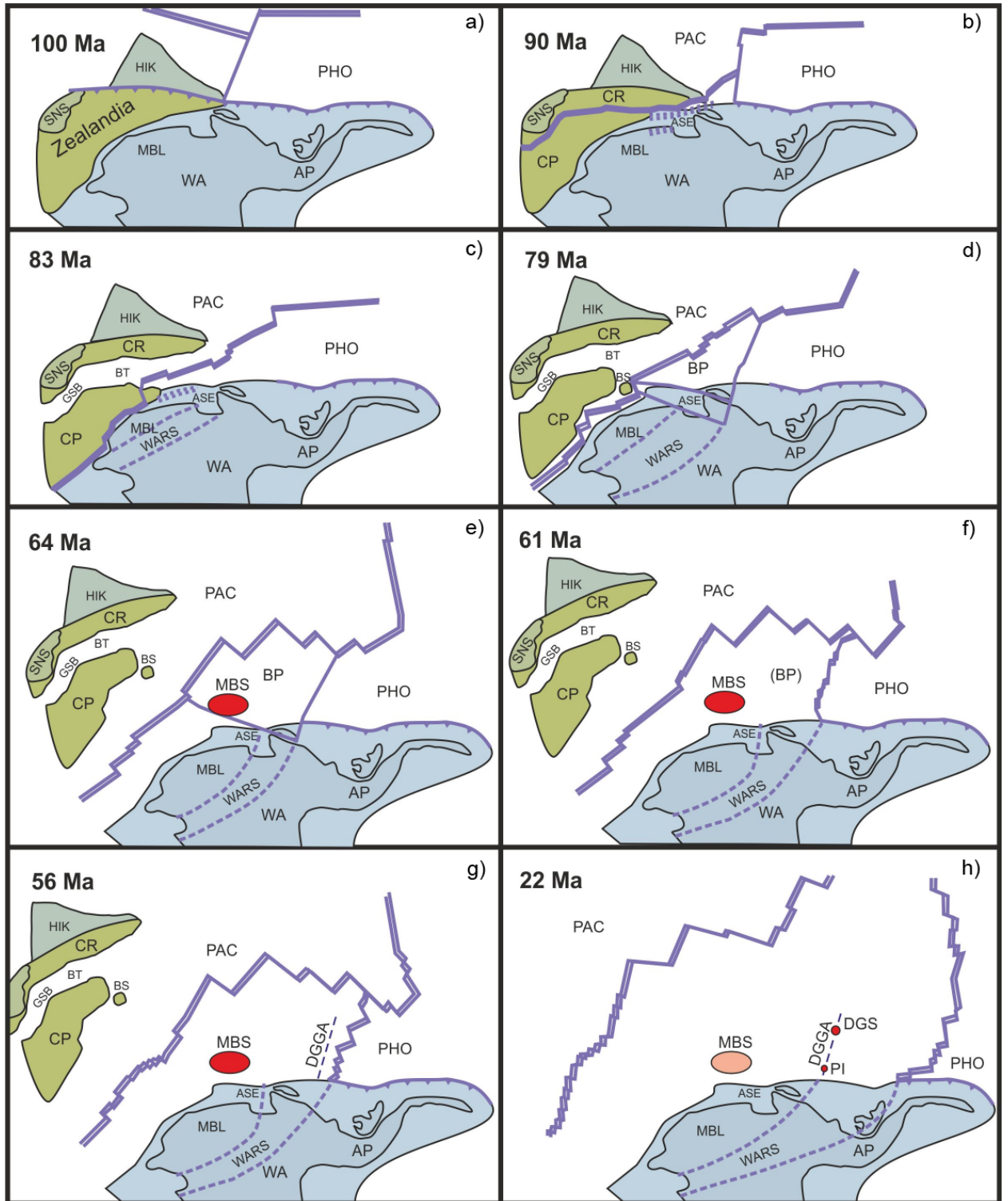


Fig. 2: Plate-tectonic reconstruction from 100 Ma to 22 Ma, using rotation parameters by Eagles et al. (2004a). Illustrated are the collision of Hikurangi Plateau with Zealandia at around 100 Ma, the breakup between Zealandia and West Antarctica at 90-80 Ma, the development of the Bellingshausen Plate and the subsequent volcanism along the West Antarctic margin. Double lines mark spreading ridge plate boundaries, single solid lines mark other

plate boundaries types, hashed lines in West Antarctica illustrate lineaments of the West Antarctic Rift System (Eagles et al., 2009; Gohl et al., 2013). Abbreviations are: SNS South Island New Zealand, HIK Hikurangi Plateau, CP Campbell Plateau, CR Chatham Rise, GSB Great South Basin, BS Bollons Seamount, BT Bounty Trough, WA West Antarctica, MBL Marie Byrd Land, AP Antarctic Peninsula, ASE Amundsen Sea Embayment, WARS West Antarctic Rift System, PAC Pacific Plate, PHO Phoenix Plate, BP Bellingshausen Plate, MBS Marie Byrd Seamounts (red area marks volcanic activity of the shield phase), DGS De Gerlache Seamounts, PI Peter I Island, DGGA De Gerlache Gravity Anomaly (suture of former PHO-BP ridge jump).

Plate-kinematic reconstructions (Fig. 2) demonstrate that Marie Byrd Land was attached to the southeastern margin of Zealandia prior to the final breakup of Gondwana (Fig. 2a; e.g., Eagles et al., 2004a). After the collision of the Hikurangi Plateau with the Gondwana margin (e.g., Davy et al., 2008; Hoernle et al., 2010) and cessation of subduction along the northern margin of Zealandia at c. 100 Ma (e.g., Weaver et al., 1994), extensional processes set in, causing Zealandia to rift from Marie Byrd Land (e.g., Larter et al., 2002; Eagles et al., 2004a; and Boger, 2011 for a recent review). The continental breakup initiated with the Chatham Rise separating from the Amundsen Sea Embayment sector during the Cretaceous Normal Polarity Superchron (CNS) at about 90 Ma (Fig. 2b). Thereafter the southwestward rift propagation jumped farther south and separated the Campbell Plateau from Marie Byrd Land just before chron C33 (83-79 Ma), leaving a rifted West Antarctic continental margin bordering the Amundsen Sea (Fig. 2c d; Larter et al., 2002; Eagles et al., 2004a).

During the late Cretaceous / Early Tertiary the southern Pacific region was sectioned into a minimum of three major tectonic plates (Bradshaw, 1989; Larter et al., 2002; Eagles et al., 2004a; Wobbe et al., 2012), the Pacific Plate, the Bellingshausen Plate, and the Phoenix or Aluk Plate adjacent to the Antarctic Plate (Fig. 2e). While the Phoenix Plate subducted beneath the eastern portion of the Antarctic Plate, the other plate boundaries were divergent or transform margins. During C27 (61 Ma) the Bellingshausen Plate ceased from being a separate plate and became incorporated into the Antarctic Plate (Fig. 2f; Eagles et al., 2004a, b; Wobbe et al., 2012). Heinemann et al. (1999) and Stock et al. (1997) suggest that the MBS province formed in the vicinity of the Antarctic-Pacific-Bellingshausen triple junction. Between C27 and C25/C24 (57 - 54 Ma), a substantial drop in spreading rate occurred at the Pacific-Antarctic Ridge, and together with a gradual rotation of the spreading direction (Müller et al., 2000), an increase in fracture zone density is notable (Eagles et al., 2004a). At the same time, the West Antarctic Rift System (WARS) continued its crustal extension in Marie Byrd Land and possibly into the Amundsen Sea Embayment just south of the MBS (Gohl et al., 2013). The De Gerlache Seamounts and Peter I Island are aligned along the so-called De Gerlache Gravity

Anomaly (DGGA) (Gohl et al., 1997a; McAdoo and Laxon, 1997; Hagedorn et al., 2007) (Fig. 2g+h) which was initially interpreted as a fracture zone of the earlier Phoenix-Antarctic Ridge (Hart et al., 1995). However, magnetic seafloor spreading data imply that this is a tectonic scar caused by a westward jump of the Pacific-Phoenix ridge at chron C27 (Larter et al., 2002; Eagles et al., 2004a). Müller et al. (2007) suggested that this zone of possible lithospheric weakness was reactivated by a northward extension of a later WARS branch (Figs. 1 and 2h).

The Late Cretaceous tectonic events were accompanied by intense volcanism in East Gondwana and Marie Byrd Land at c. 95-110 Ma (e.g., Hart et al., 1997; Storey et al., 1999). This magmatism has been related to large-scale mantle upwelling in conjunction with extension-induced rifting (Finn et al., 2005). Others assume an active mantle plume in the area of the Bellingshausen-Amundsen Sea or beneath East Gondwana (Hole and Le Masurier, 1994; Weaver et al., 1994; Rocholl et al., 1995; Hart et al., 1995, 1997; Panter et al., 2000; Hoernle et al., 2010; Sutherland et al., 2010), which may have caused the final break-up of Zealandia from Antarctica (e.g., Weaver et al., 1994; Storey et al., 1999; Hoernle et al., 2010). As the region underwent further plate reorganization, a second phase of volcanism occurred (Rocchi, 2002a,b; Nardini et al., 2009 and references therein, LeMasurier et al., 1990). This younger magmatism (30 - 25 Ma until recent) is mainly of alkaline nature and has been related to rifting and crustal extension associated with the WARS. Based on a HIMU (high time-integrated U/Pb) component found in many WARS volcanics, many authors suggest reactivation of old plume material embedded at the base of the continental lithosphere (e.g., Weaver et al., 1994) others favor a metasomatic origin (e.g., Nardini et al., 2009).

3. BATHYMETRY AND MORPHOLOGY OF MARIE BYRD SEAMOUNTS AND PETER I ISLAND

During cruise ANT-XXIII/4, the Atlas Hydrosweep DS-2 multi-beam echo-sounding system of onboard the R/V Polarstern was used to generate maps of five MBS (summarized in Table 1; Fig. 3a) and of the submarine base of Peter I Island (Gohl, 2007).

Table 1: Morphological features of the Marie Byrd Seamounts

	Seamount 6	Seamount 9	Haxby Seamount	Hubert Miller Seamount	Seamount C
Coordinates (centre)	69°47'S, 126°17'W	69°40'S, 124°45'W	69°07'S, 123°35'W	69°17'S, 121°20'W	69°12'S, 117°30'W
Shape	oval shaped guyot	oval shaped guyot	oval shaped guyot	oval shaped guyot	crudely circular guyot
Secondary features	small cones on flanks and plateau	small cones on flanks and plateau; WNW-ESE trending rift zone	small cones on flanks and plateau; WNW-ESE trending major rift zone, minor W-E and WSW-ENE rifts	small cones on flanks and plateau; several rift zones, most of them ~ SW-NE	small cones on flanks and plateau; rift zones mainly trending from SSW-NNE to SSE-NNW
Base level (m bsl)	3000-2800	3600-3400	4000	4000-3600	3500
Diameter at base (km)	80 x 20	long axis 25	30	75 x 50	17
Water depth of plateau (m bsl)	1600-1350	1600-1400	1800-1600	1600-1200	2400-2200
Edifice height (m)	~ 1650	~ 2200	~ 2400	~ 2800	~ 1300
Volume estimate (km³)	~ 2000	-	~ 1600	~ 8000	~ 200
Dredge samples^a	-	-	PS69/317-1	PS69/321-1 PS69/324-1 PS69/325-1	PS69/327-1

^a A detailed description of dredge operations and recovered material is provided in Gohl (2007).

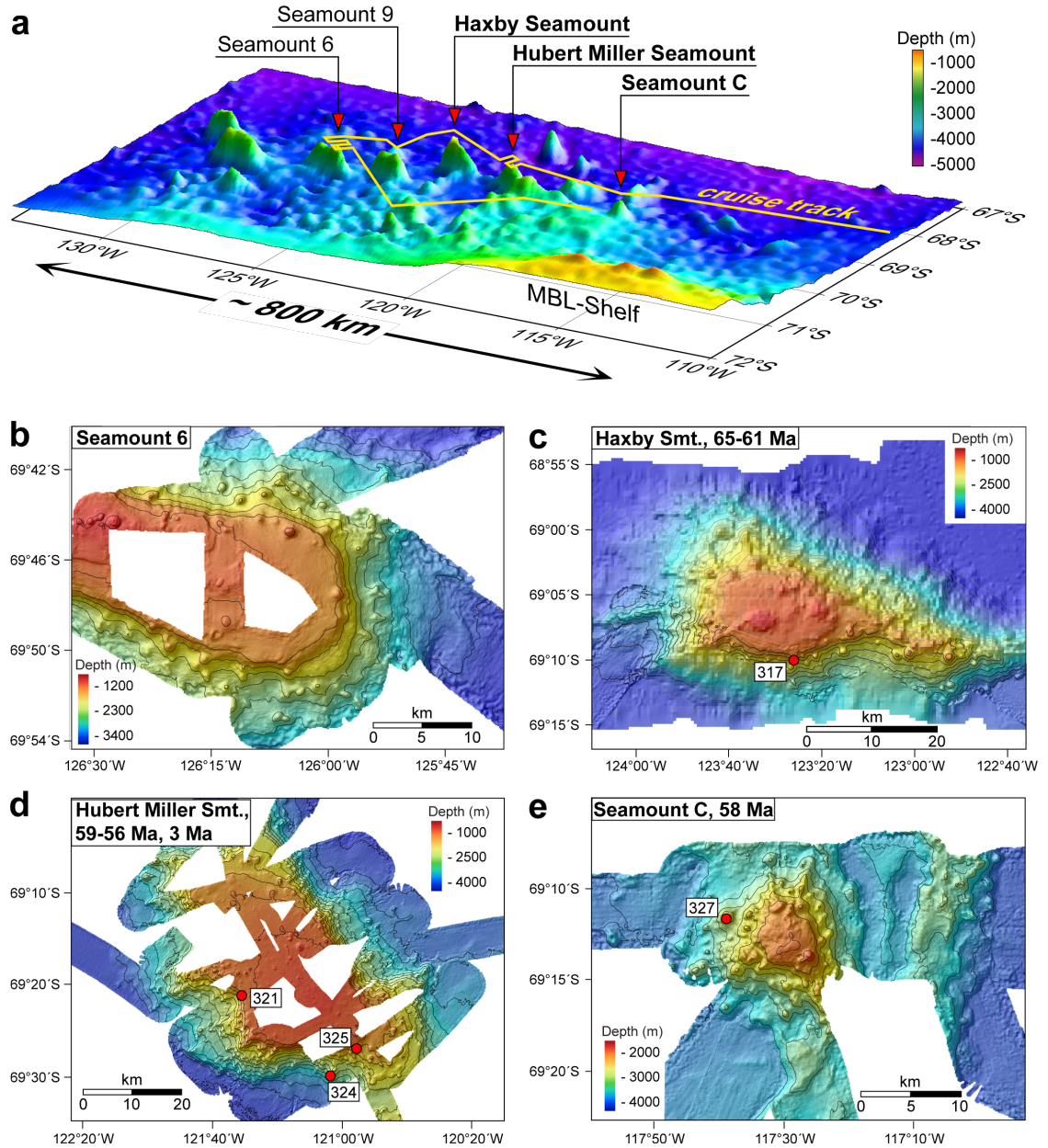


Fig. 3: (a) Overview of the Marie Byrd Seamount Province. Red arrows mark the MBS surveyed during R/V Polarstern cruise ANT-XXIII/4 in 2006, letters in bold signify those which have been successfully dredged. Predicted bathymetry after Smith and Sandwell (1997). **(b)** Multi-beam bathymetry of the eastern part of Seamount 6. This is the westernmost studied during ANT-XXIII/4 and has not been mapped before. It appears to be one of the largest MBS. **(c)** Haxby Seamount (named by the ANT-XIII/4 cruise participants) has completely been mapped on the R/V N.B. Palmer cruise in 1996 and morphologically studied in detail by Feldberg (1997). **(d)** Combined ANT-XVIII/5a (2001) and ANT-XXIII/4 multi-beam bathymetry of Hubert Miller Seamount. This Seamount is located ~40 nm ESE of Haxby and appears to be the largest of the MBS. **(e)** Combined ANT-XVI/3 (Miller and Grobe, 1996) and ANT-XXIII/4 multi-beam bathymetry of Seamount C. This seamount does not appear in the bathymetric maps derived from satellite gravity data. Note that Seamount C differs in size, high, and morphology from the other surveyed MBS guyots. The red dots with numbers mark dredge station of cruise ANT-XXIII/4 which yielded in situ volcanic rocks.

Combined with bathymetric data of previous cruises (RV Nathaniel B. Palmer in 1996, RV Polarstern ANT-XI/3 in 1994, and ANT-XVIII/5a in 2001; e.g., Miller and Grobe, 1996; Feldberg, 1997), these data reveal that the MBS are characterized by steep sides with relatively flat tops and additional small cones on the upper flanks and/or on the platforms. The guyot-like morphology of the main edifices is attributed to seamount growth above sea level to form ocean island volcanoes, which subsequently eroded to sea level and then subsided to their present position. The small cones must have formed after subsidence of the erosional platforms below wave base and therefore represent a late stage or post-erosional phase of volcanism.

The westernmost studied seamount, Seamount 6 (informal name), has an elongate WNW-ESE striking base (Fig. 3b). The steep-sided edifice is topped by a flat plateau, on which several well-preserved small volcanic cones are scattered, rising up to 200 m above the plateau. Seamount 9 (informal name) is located about 45 km east of Seamount 6. One track was surveyed across Seamount 9 (not shown in Fig. 3), which revealed an oval shaped guyot and a c. 10 km long WNW-ESE-trending ridge emanating from its western base. This ridge is composed of several aligned small volcanic cones and interpreted as volcanic rift zone. Haxby Seamount (named by the ANT-XIII/4 cruise participants) (Fig. 3c), which has been mapped previously on RV Nathaniel B. Palmer Cruise in 1996 (Feldberg, 1997), has a slightly curvilinear volcanic rift system with numerous cones on its top emanating from the eastern flank of the guyot and extending > 30 km to the east. Two less pronounced, c. 12 - 15 km long chains of cones and ridges emanating from the western flank may be the western continuation of the volcanic rift. Hubert Miller Seamount (Fig. 3d) is located ~ 75 km ESE of Haxby Seamount. This seamount is the largest MBS with frequent small cones and ridges scattered along its flanks but infrequent on the plateau. Several up to 8 km long volcanic rift zones extend from the base of Hubert Miller Seamount. The easternmost mapped seamount, Seamount C (informal name; Fig. 3e), is the smallest of the studied volcanoes. Its guyot-shaped edifice has a crudely circular base and a plateau of ~7 km diameter. Volcanic rifts extend from the base in northern and southern directions and NNE-SSW trending, curvilinear graben and ridge structures are adjacent to its eastern flank. The existence of further, most likely sediment covered, volcanic cones and ridge-like basement structures between the main MBS cluster and Marie Byrd Land are predicted from satellite gravity data (Smith and Sandwell, 1997) and observed in seismic data (Gohl et al., 1997b; Uenzelmann-Neben and Gohl, 2012). The original volume of MBS magmatism, however, remains unclear because of incomplete data and the largely unknown initial volume of the eroded islands. Based on the available bathymetric data (multi-beam and satellite gravity), the total volume of all present MBS can roughly be estimated to more than 20,000 km³. The

aerial extent of the former Marie Byrd islands were similar in size to Canary Islands, such as La Palma (compared to Hubert Miller Seamount) or El Hierro (compared to Seamount 6), which are believed to be the product of a mantle plume (e.g., Montelli et al., 2006).

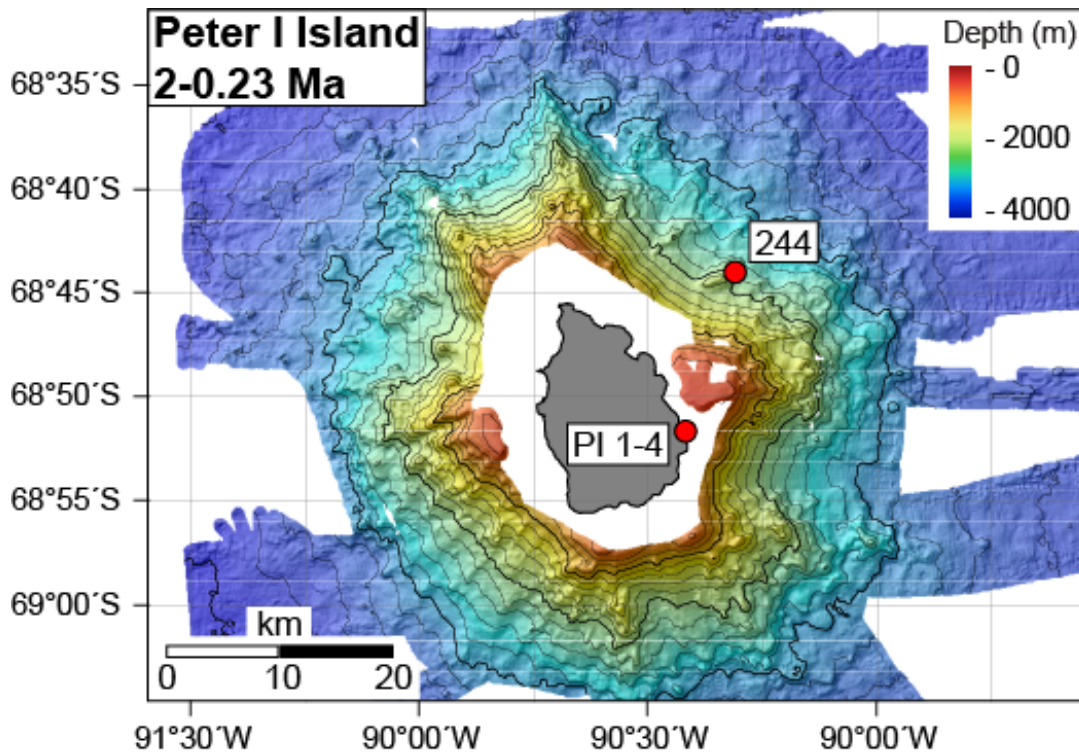


Fig. 4: Multi-beam bathymetry of the base of Peter I Island. The map reveals several small cone- and ridge-like structures on its flanks and a steep canyon at its eastern side which most likely has been formed by slope failure or sector collapse. The red dots indicate locations sampled during cruise during R/V Polarstern cruise ANT-XXIII/4 in 2006 (244 - dredge station at the eastern base of Peter I Island; PI 1-4 - subaerial samples taken on Michajlovodden peninsula).

The submarine base of Peter I Island was only partially surveyed prior to ANT-XXIII/4 and, except for dredge hauls directly off the coast of the island (Broch, 1927), unsampled (Fig. 4). The island is elongated in N-S direction and represents the top of a large volcano, which measures ~65 km in diameter at its base and rises from the abyssal plain at ~3,500 - 4,000 m to an elevation of 1,640 m above sea level. Volcanic rifts emanate from the submarine flank of the island mainly in northern and southern directions. A striking feature of Peter I Island is a c. 9 km wide depression in the eastern flank of its base, which most likely has been formed by a major slope failure or sector collapse.

4. SAMPLE BACKGROUND

Volcanic rocks were recovered at five dredge stations of the main MBS edifices and associated small cones (Fig. 3b-e). In addition a single dredge haul along the northeastern submarine flank of Peter I Island has been carried out (Fig. 4). At all dredge sites discussed here, the angular shape of the rocks, freshly broken surfaces and homogeneity of rock types within a single dredge were taken as evidence for an in-situ origin (and non-ice rafted) of the rocks. Our samples represent the first in-situ volcanic rocks recovered from the MBS. A detailed description of dredge operations and recovered material is provided in chapter 7 of Gohl (2007).

At Haxby Seamount, dredge haul PS69-317-1 from the upper southern slope beneath the plateau edge contained freshly broken carbonate cemented breccias, which consist of aphyric basaltic clasts up to 8 cm in size (Fig. 5a). At Hubert Miller Seamount, three dredges yielded mainly lava fragments; dredge PS69-321-1 along a steep slope below the SE plateau edge gave olivine (ol)-clinopyroxene (cpx)-phyric lava Fig. 5b, dredge PS69-324-1 at the lower SE slope beneath a cone like structure provided dense feldspar (fsp)-cpx-phyric basalt lava and (carbonate) cemented Mn-encrusted volcanic breccia, and dredge PS69-325-1 obtained vesicular fsp-phyric lava from the upper southern flank. At Seamount C, vesicular ol-fsp-phyric and dense fsp-phyric pillow fragments (Fig. 5c) were dredged from a cone on the lower western flank.

At Peter I Island, a 150 m high ridge located in ~ 1,800 m water depth on the NE slope of the volcano was dredged (PS69-244-1). The rocks are predominantly vesicular pillow and sheet flow lava fragments (Fig. 5d). Both are feldspar (fsp)-phyric and have up to 1 cm thick, fresh, glassy rims. Vesicles are generally unfilled and only a few glassy surfaces show early stages of palagonitization. The subaerial samples from Peter I Island were taken at the Michajlovodden peninsula (Fig. 4). They comprise vesicular lava (up to 15% vesicles; sample PI-1), aphyric agglutinates of a > 1.5 m thick, partially red oxidized layer outcropping in the northern part of the peninsula (sample PI-3), and part of a reddish volcanic bomb with 10- 20 % vesicles (sample PI-4).

Belgica Seamount is the easternmost edifice of the De Gerlache Seamount group. It is guyot-shaped and has a N-S elongated base diameter of c. 60 x 90 km with a flat-topped summit at c. 400 - 500 m below sea level. Belgica was dredge-sampled during Polarstern cruise ANTXXII-4 in 800 to 600 water depths (Hagedorn et al., 2007). Hagedorn et al. (2007) initially determined K-Ar ages and major and trace element geochemistry on the recovered samples. Here

we complement the existing data with Sr-Nd-Pb isotope data on a subset of newly prepared sample material.

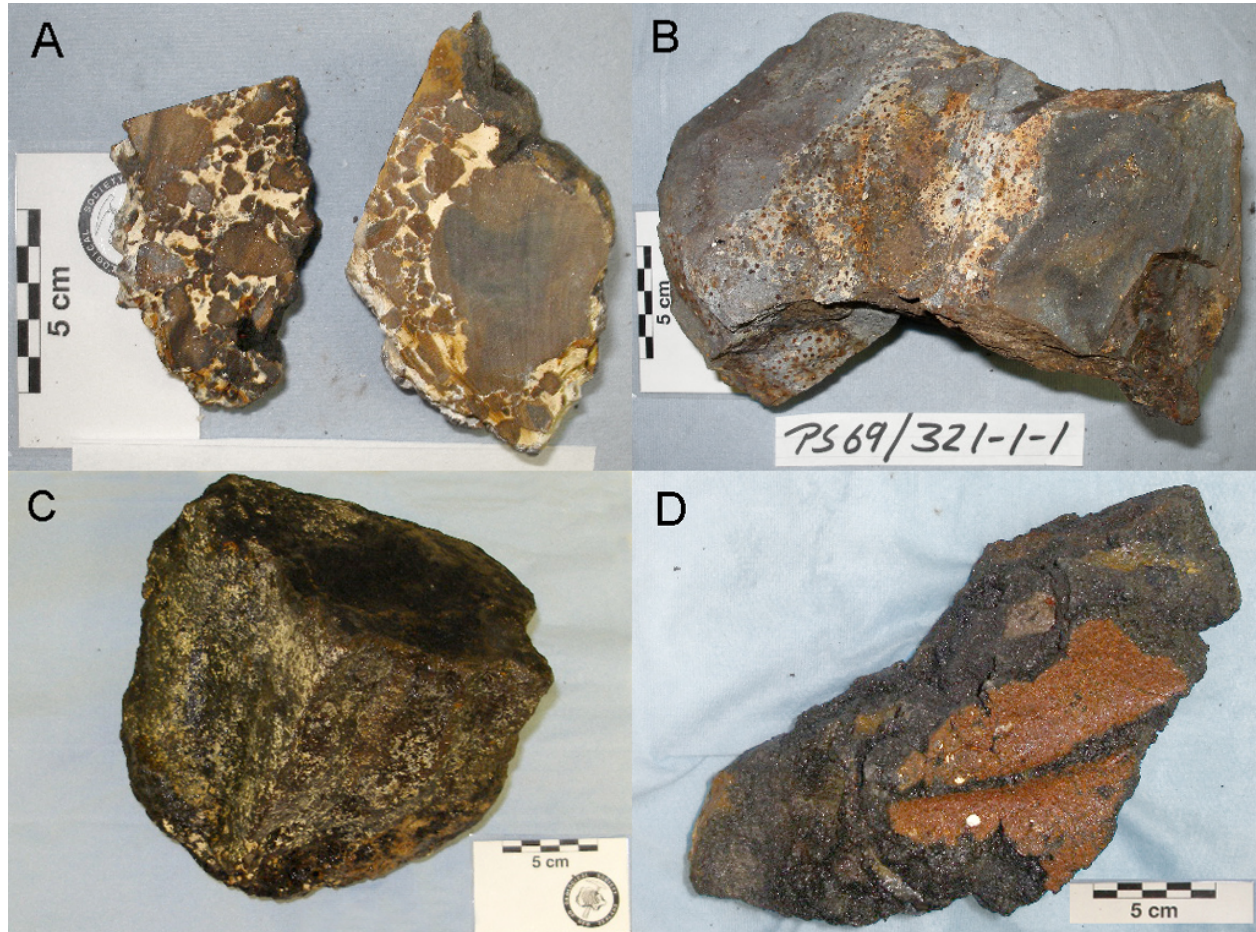


Fig. 5: Basaltic rocks dredged at the MBS and the submarine base of Peter I Island; **(a)** Typical monomict breccia from Haxby Seamount composed of dense, aphyric irregular-shaped and angular coarse lapilli set in a carbonaceous matrix (PS69/317-1); **(b)** dense ol-cpx-phyric basaltic lava fragment from Hubert Miller Seamount, note angularity and freshly broken surfaces of the sample (PS69/321-1); **(c)** dense fsp-phyric pillow fragment of Seamount C (PS69/327-1); **(d)** sheet lava flow fragment with fresh, 1 cm thick glassy rim from the submarine base of Peter I Island (PS69/244-1).

5. PETROGRAPHY AND ROCK CLASSIFICATION

The petrography of the MBS volcanics is quite uniform being slightly phyric with a few large phenocrysts of altered olivine and zoned plagioclase in a fine-grained groundmass of olivine, plagioclase and clinopyroxene. Occasionally, ilmenite and magnetite occur as accessory phases. Olivine is commonly altered to iddingsite and the latter is sometimes replaced by calcite. The groundmass is variably altered by low temperature processes ranging from hydrated glass at Haxby Seamount to replacement by secondary minerals such as zeolite and dolomite at Hubert Miller Seamount and Seamount C. The altered state of the MBS volcanic rocks is also manifested in elevated H₂O contents of up to 2 wt% in most samples, except that samples from Dredge 324 at Hubert Miller Seamount have <1 wt% H₂O and those from Seamount C have 3 wt% H₂O (Table 2). CO₂ contents are generally low (< 0.3 wt%) and only two samples show slightly elevated CO₂ > 0.5 wt%, due to secondary carbonate. Unusually high phosphorous contents were detected in 5 samples (marked with ^b in Table 2) and are interpreted to reflect the presence of secondary phosphate that is, however, not detected in thin section. Only samples with P₂O₅ ≤ 1 wt% are considered meaningful when treating the major element chemistry further below.

The submarine samples of Peter I Island are slightly porphyric with zoned plagioclase laths and small, homogeneously distributed clinopyroxene phenocrysts, set in a microcrystalline groundmass of clinopyroxene and plagioclase. Magnetite occurs as an accessory mineral and fresh glass is common. The subaerial volcanics of Peter I Island are more aphyric than those from the submarine flanks. The fine-grained crystalline groundmass of these samples contains pyroxene, plagioclase and possibly glass, and accessory minerals of magnetite, ilmenite and hematite. All samples from Peter I Island are generally very fresh as manifested by low H₂O (0.3-0.9 wt%) and CO₂ (< 0.06wt%) contents (Table 2).

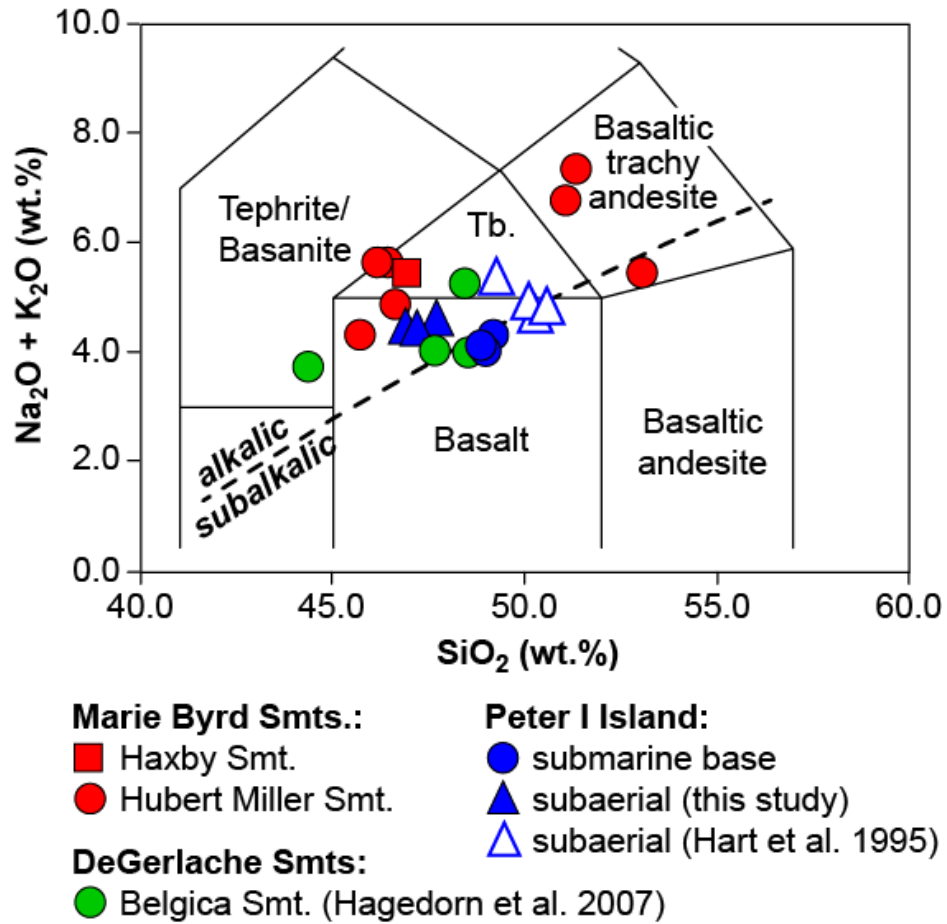


Fig. 6: Total alkali versus SiO_2 diagram illustrating the alkali basaltic to basaltic trachyandesitic composition of most samples from MBS, Peter I Island, and De Gerlache Seamounts. Subdivision between alkaline and subalkaline rock suites after Irvine and Baragar (1971). All data are normalized to a 100% volatile free basis. Samples displaying unusual high phosphor contents are not shown in this diagram (cf. Table 2). Tb - Trachybasalt.

The silica content of the entire sample suite ranges from 53.1 to 45.7 wt% SiO_2 . On a total alkali vs. silica diagram (TAS; Fig. 6), the majority of the samples plots above the alkaline – subalkaline division line and are classified as basalts, trachybasalts and basaltic trachyandesites. All but one of MBS samples lie along an alkali basaltic differentiation trend. The samples from the submarine flank of Peter I Island are tholeiitic basalts ($\text{SiO}_2 \sim 49$ wt%; $\text{Na}_2\text{O}+\text{K}_2\text{O}$ 4.1 - 4.3 wt%), whereas the subaerial samples are slightly more alkaline transitional tholeiites ($\text{SiO}_2 \sim 47$ wt%; $\text{Na}_2\text{O}+\text{K}_2\text{O}$ 4.3 - 4.5 wt%).

Table 2: Results of major and trace element analyses

	PS69/317 -1-1 Haxby Smt	PS69/317 -1-1 Replicate ICP-MS	PS69/317 -1-2 Haxby Smt	PS69/321 -1-2 Hubert Miller Smt	PS69/321 -1-4 Hubert Miller Smt	PS69/321 -1-5 Hubert Miller Smt	PS69/321 -1-12a Hubert Miller Smt
SiO ₂	46.13		42.03	50.22	46.23	45.95	50.19
TiO ₂	3.39		3.57	1.89	3.59	3.44	2.09
Al ₂ O ₃	16.33		18.2	17.15	17.59	16.62	18.46
Fe ₂ O ₃	14.81		15.91	11.49	14.19	13.95	11.09
MnO	0.21		0.21	0.22	0.19	0.22	0.17
MgO	3.46		3.41	2.58	2.85	3.96	2.07
CaO	7.72		9.02	6.39	8.84	8.44	6.76
Na ₂ O	3.82		3.51	4.57	3.54	3.53	4.53
K ₂ O	1.54		0.74	2.61	2.09	2.05	2.15
P ₂ O ₅	0.91		1.44 ^b	0.73	0.92	0.79	0.87
H ₂ O	1.91		2.38	2.23	1.80	1.86	2.10
CO ₂	0.06		0.17	0.30	0.08	0.07	0.07
TOTAL							
L	100.29		100.59	100.38	101.91	100.88	100.55
Rb	28.1	28.1	6.66	53.4	37.3	50.4	23.9
Ba	330	330	264	725	462	493	784
Th	4.79	4.72	4.60	6.89	4.57	4.43	7.31
U	1.52	1.52	0.427	1.75	0.816	0.695	0.296
Nb	70.3	70.6	68.1	123	78.5	77.2	119
Ta	4.21	4.18	4.27	6.60	4.59	4.45	6.97
La	49.6	48.9	64.4	76.8	52.4	51.4	65.9
Ce	106	106	114	154	106	103	146
Pb	2.75	2.35	2.41	3.81	2.44	2.65	3.37
Pr	13.1	13.1	14.4	17.0	12.2	11.6	16.1
Nd	55.6	55.2	57.6	63.2	46.0	44.3	61.6
Sr	760	756	1219	825	969	925	891
Sm	12.1	12.1	13.3	12.6	9.86	9.49	12.5
Hf	8.06	8.02	8.35	8.83	6.36	5.94	9.36
Zr	404	402	413	475	323	317	446
Eu	3.79	3.75	4.14	3.92	3.09	2.91	4.12
Gd	10.8	10.7	11.4	10.2	8.00	7.45	9.66
Tb	1.45	1.47	1.56	1.40	1.05	0.979	1.29
Dy	7.98	7.89	8.36	7.50	5.40	5.04	6.58
Ho	1.43	1.46	1.54	1.33	0.97	0.92	1.14
Y	42.3	42.0	51.6	43.6	32.5	31.5	35.5
Er	3.59	3.72	3.84	3.47	2.49	2.31	2.79
Tm	0.457	0.479	0.475	0.455	0.310	0.291	0.345
Yb	3.13	3.14	3.84	3.54	2.57	2.45	2.76
Lu	0.450	0.447	0.554	0.496	0.359	0.332	0.366

Table 2: continued

	PS69/324 -1-3 Hubert Miller Smt	PS69/324 -1-4 Hubert Miller Smt	PS69/324 -1-6 Hubert Miller Smt	PS69/325 -1-2a Hubert Miller Smt	PS69/325 -1-2b Hubert Miller Smt	PS69/327 -1-1 Seamount C	PS69/327 -1-2 Seamount C
SiO ₂	45.80	52.85	46.74	47.72	47.72	41.98	46.00
TiO ₂	2.60	0.85	3.26	2.52	2.49	2.26	2.70
Al ₂ O ₃	15.02	17.18	14.86	16.78	17.24	18.15	20.31
Fe ₂ O ₃	13.05	8.63	14.73	11.58	12.02	8.92	11.30
MnO	0.19	0.18	0.20	0.14	0.14	0.08	0.15
MgO	8.13	5.52	4.87	2.54	1.34	0.97	1.24
CaO	10.65	8.68	10.31	7.93	7.40	12.84	8.73
Na ₂ O	3.29	3.99	3.65	3.88	4.19	3.55	3.44
K ₂ O	1.04	1.45	1.24	2.74	3.24	1.74	1.38
P ₂ O ₅	0.48	0.21	0.54	1.69 ^b	2.12 ^b	5.02 ^b	1.62 ^b
H ₂ O	0.74	0.98	0.82	2.12	2.13	2.92	3.03
CO ₂	0.13	0.07	0.08	0.59	0.18	0.56	0.24
TOTAL	101.12	100.59	101.30	100.23	100.21	98.99	100.14
Rb	24.1	35.8	28.0	90.1	57.3	27.2	21.5
Ba	311	455	320	469	480	404	427
Th	2.99	4.72	3.91	6.93	7.02	5.21	5.06
U	0.743	0.819	0.982	1.34	1.33	1.78	1.43
Nb	46.0	78.5	56.6	95.6	96.8	55.6	58.7
Ta	2.78	4.60	3.39	5.38	5.44	3.48	3.58
La	32.1	53.1	38.3	73.5	73.8	66.2	44.6
Ce	66.2	107	78.4	141	144	80.4	84.5
Pb	2.47	2.30	1.89	3.38	3.21	3.07	2.24
Pr	7.74	12.3	8.98	16.3	16.3	10.4	9.36
Nd	30.1	46.5	35.5	62.4	62.3	39.0	35.6
Sr	626	967	568	674	717	811	843
Sm	6.69	9.97	8.08	12.9	13.3	8.09	7.89
Hf	4.30	6.35	5.55	7.99	8.02	4.99	5.37
Zr	205	321	261	412	417	250	258
Eu	2.19	3.04	2.49	3.59	3.56	2.45	2.49
Gd	5.89	8.10	7.17	10.9	10.9	7.78	6.87
Tb	0.814	1.02	1.02	1.48	1.41	1.07	0.957
Dy	4.38	5.49	5.74	7.39	7.51	6.32	5.30
Ho	0.787	0.971	1.02	1.35	1.36	1.33	0.979
Y	25.2	31.6	31.8	48.7	46.1	66.5	32.0
Er	2.07	2.50	2.66	3.50	3.52	3.71	2.70
Tm	0.261	0.325	0.350	0.458	0.449	0.509	0.349
Yb	2.08	2.49	2.65	3.63	3.54	4.21	2.72
Lu	0.278	0.350	0.364	0.515	0.506	0.674	0.377

Table 2: continued

	PS69/244 -1-1		PS69/244 -1-3		PS69/244 -1-5		PS69/ PI-1		PS69/ PI-3		PS69/ PI-4	
	Peter	I	Peter	I	Peter	I	Peter	I	Peter	I	Peter	I
	submarine		submarine		submarine		subaerial		subaerial		subaerial	
SiO ₂	49.48		49.09		49.26		47.79		47.26		48.15	
TiO ₂	2.79		2.74		2.75		3.53		3.48		3.46	
Al ₂ O ₃	13.68		13.26		13.61		12.79		12.52		12.73	
Fe ₂ O ₃	12.58		12.55		12.85		13.48		13.36		13.03	
MnO	0.14		0.15		0.14		0.15		0.15		0.14	
MgO	8.18		9.2		8.55		9.64		9.86		9.42	
CaO	9.00		8.68		8.91		9.03		8.83		8.67	
Na ₂ O	3.17		3.03		3.00		3.07		3.03		3.17	
K ₂ O	1.16		1.08		1.15		1.37		1.42		1.47	
P ₂ O ₅	0.50		0.51		0.48		0.64		0.69		0.78	
H ₂ O	0.86		0.87		0.94		0.28		0.45		0.38	
CO ₂	0.05		0.05		0.06		0.04		0.04		0.04	
TOTAL	101.59		101.21		101.70		101.81		101.09		101.44	
Rb	20.3		19.8		19.2		23.9		26.5		26.3	
Ba	240		228		226		308		315		332	
Th	2.85		2.68		2.57		3.53		3.74		3.78	
U	0.887		0.725		0.704		0.920		0.984		1.02	
Nb	30.2		29.4		28.9		48.5		48.7		50.6	
Ta	1.88		1.83		1.76		2.82		2.89		2.90	
La	27.2		26.7		26.1		38.0		40.3		43.1	
Ce	58.5		57.1		55.6		80.9		85.2		92.4	
Pb	2.30		2.26		2.22		2.26		2.46		2.31	
Pr	7.49		7.20		6.95		10.2		10.4		11.4	
Nd	32.7		30.8		29.2		43.1		43.6		48.5	
Sr	624		622		632		797		804		871	
Sm	7.57		7.54		7.48		9.80		10.2		11.0	
Hf	5.22		5.19		5.03		7.03		7.42		7.59	
Zr	233		230		227		315		326		344	
Eu	2.43		2.48		2.39		3.14		3.21		3.52	
Gd	6.78		6.55		6.38		8.50		8.63		9.61	
Tb	0.874		0.882		0.854		1.14		1.13		1.19	
Dy	4.69		4.54		4.40		5.70		5.52		5.85	
Ho	0.792		0.737		0.706		0.924		0.894		0.963	
Y	22.5		21.6		21.6		24.9		24.9		25.7	
Er	1.83		1.72		1.73		2.14		2.05		2.14	
Tm	0.226		0.207		0.204		0.255		0.246		0.256	
Yb	1.53		1.50		1.49		1.58		1.54		1.56	
Lu	0.192		0.193		0.186		0.206		0.209		0.203	

^b Results with unusual high values not shown in Fig. 6

6. ANALYTICAL RESULTS

6.1 $^{40}\text{Ar}/^{39}\text{Ar}$ age dating

Table 3: $^{40}\text{Ar}/^{39}\text{Ar}$ step heating analyses results.

Seamount	Sample ID	Analysis ID	Dated material	Plateau age (Ma)	\pm 2Sigma	^{39}Ar fraction	MSWD	Probability
Haxby	317-1-1	gls	glass	64.7	\pm 0.8	63.1	0.95	0.46
	317-1-2	gls	glass	62.3	\pm 0.4	56.8	0.99	0.44
	317-1-2	gl2	glass	61.2	\pm 0.5	72.9	1.19	0.27
Hubert Miller	321-1-2	fss	plag	56.7	\pm 1.9	73.9	0.61	0.72
	321-1-2	mx2	matrix	58.9	\pm 0.6	95.6	1.10	0.34
	321-1-5	fss	plag	57.0	\pm 0.9	58.4	1.30	0.23
	321-1-5	mx2	matrix	55.7	\pm 0.5	63.5	0.78	0.45
	325-1-2B	fss	plag	56.5	\pm 0.6	61.1	1.20	0.30
	324-1-3	mxs	matrix	3.0	\pm 0.5	84.6	1.30	0.21
"C"	327-1-2	mx2	matrix	58.7	\pm 0.8	55.7	1.90	0.04
Peter I^c	244-1-1	gls	glass	1.9	\pm 0.3	83.8	1.03	0.41
	244-1-3	gl2	glass	1.7	\pm 0.3	96.4	0.58	0.87

^c dated samples from Peter I Island are dredge samples from its submarine base

The $^{40}\text{Ar}/^{39}\text{Ar}$ age dating results are summarized in Table 3. Age and alteration index spectra (based on the measured $^{36}\text{Ar}/^{37}\text{Ar}$ ratios after Baksi, 2007) are shown in Figure 7. A detailed description of the methods and the full analytical data are provided in Appendix 1.

Glasses from two hyaloclastite breccia samples at Haxby Seamount yield plateau ages of 64.2 ± 0.9 Ma (317-1-1gls) and of 62.3 ± 0.4 (317-1-2gls) and 61.2 ± 0.5 Ma (317-1-2gl2), slightly outside of the two sigma analytical errors. Alteration indices are relatively high even in the plateau sections (0.001 to 0.01), reflecting partial hydration of the basalt glass and uptake of atmospheric ^{36}Ar .

Three samples of porphyric lava from Hubert Miller Seamount yield plagioclase step-heating plateau ages of 56.7 ± 1.9 Ma (321-1-2), 56.5 ± 0.6 Ma (325-1-2B) and 57.0 ± 0.9 Ma (321-1-5). Alteration indices are high in the low-temperature heating steps indicating partial alteration of the feldspars, but systematically low in the plateau steps (< 0.0002) indicating

degassing from little or un-altered sites. Matrix step-heating analyses from the same rock samples yield plateau age results within error of the feldspar step-heating results (321-1-2: 58.9 ± 0.6 Ma; 321-1-5: 55.7 ± 0.5 Ma), but are considered inferior with respect to scatter and alteration effects.

The matrix step-heating analysis of aphyric basalt lava sample 324-1-3, in contrast, yields a plateau age of 3.0 ± 0.5 Ma. Alteration indices are high in the plateau section (0.003 to 0.01), possibly indicating a partial loss of radiogenic ^{40}Ar . Nevertheless, the analysis shows that Hubert Miller Seamount comprises both Paleocene and Pliocene lavas.

The least-altered aphyric lava sample from Seamount “C” (327-1-2) yields a low-probability plateau age of 58.7 ± 0.8 Ma, with intermediate plateau-step alteration indices (0.002 to 0.008). Fresh basaltic glass from Peter I Seamount yields plateau steps alteration indices <0.0009 (244-1-1) and <0.0001 (244-1-3), and plateau ages of 1.9 ± 0.3 Ma, 1.7 ± 0.3 Ma respectively.

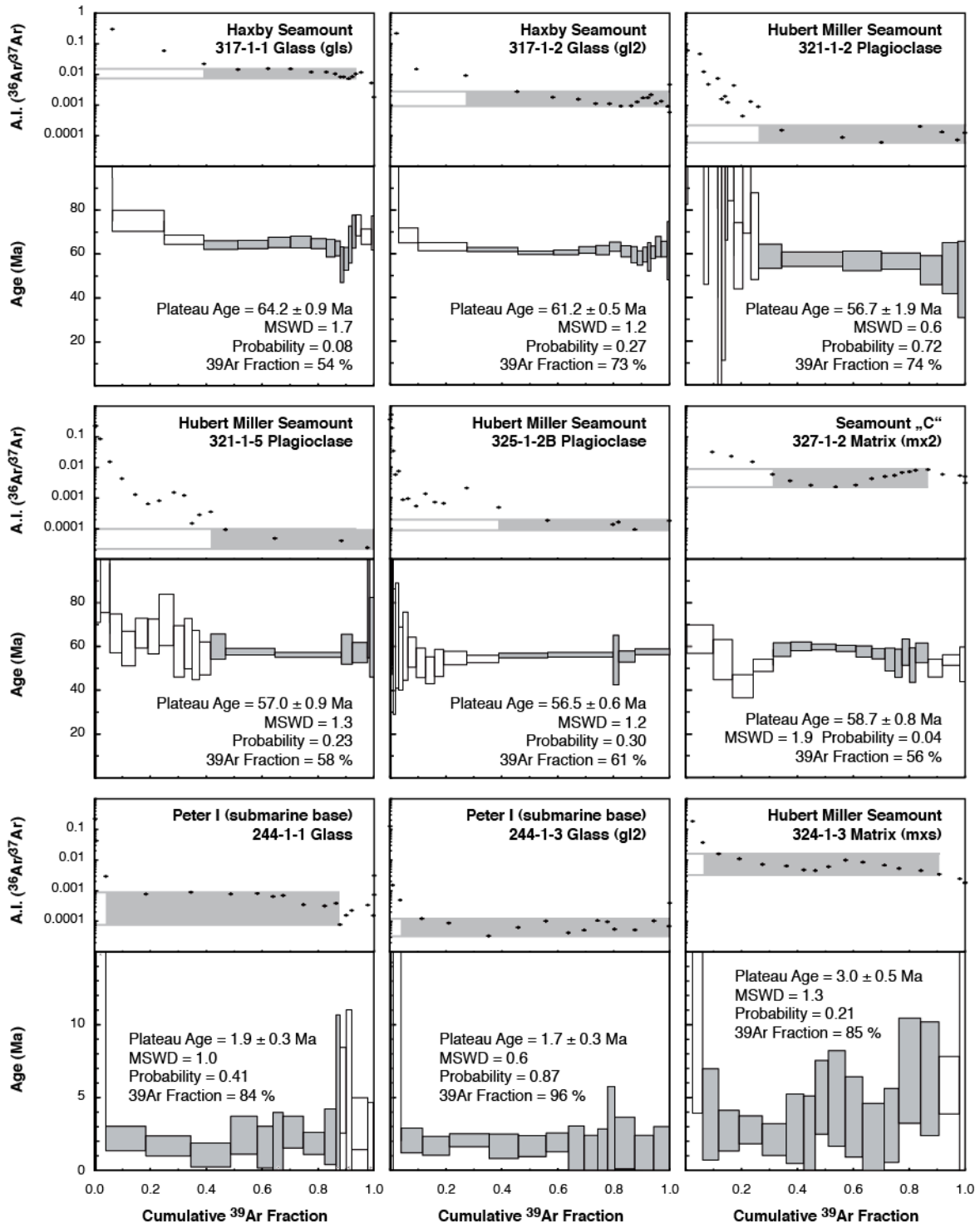


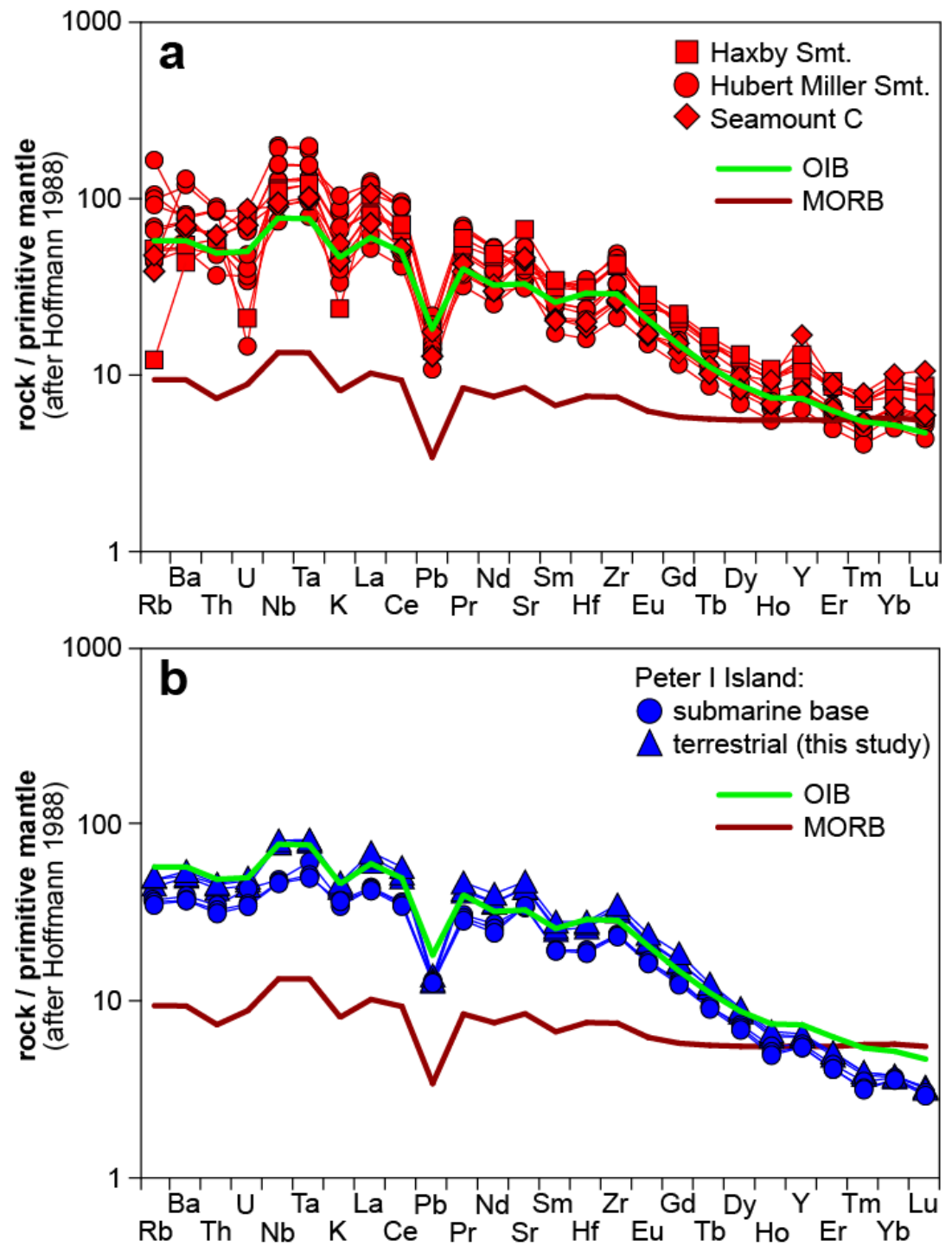
Fig. 7: Age spectra and alteration indices (A.I.) from $^{40}\text{Ar}/^{39}\text{Ar}$ laser step-heating experiments. Plateau steps and corresponding range of alteration index values are accentuated by grey shading. Stated errors are $\pm 2\sigma$.

6.2 Major and trace elements

A total of 19 samples from the MBS and Peter I Island were analyzed for major and trace elements compositions and the results are shown in Table 2. Descriptions of methods and uncertainties are given in Appendix 1. A full table with sample locations, radiometric ages and geochemical data is provided in Table A4 of the Appendix 1. The majority of MBS samples are fairly evolved (8 to 2 wt% MgO), whereas samples from Peter I Island are more primitive and cluster between 8 and 10 wt% MgO. Al_2O_3 shows a good negative correlation with decreasing MgO, suggesting fractionation of pyroxene and olivine. In the most evolved MBS lavas (<3 wt% MgO), FeOt and TiO_2 significantly decrease which may reflect fractionation of ilmenite in late stage melts. Subaerial and submarine samples of Peter I Island exhibit small compositional differences. The submarine samples have higher SiO_2 and Al_2O_3 and slightly lower MgO, FeOt and TiO_2 contents than the subaerial samples.

Trace elements patterns of the MBS are typical for ocean islands basalts (OIB; Fig. 8a) with characteristic troughs for Pb and K and strong enrichments for Nb and Ta relative to primitive mantle. The Nb and Ta enrichments are most pronounced in samples from Hubert Miller Seamount while Haxby Seamount and Seamount C are less enriched in the most incompatible elements (Rb, Ba and Th). All MBS samples show strong enrichment of the light REE (LREE) relative to the heavy REE (HREE) (see Fig 8c), suggesting small degrees of partial melting while differentiation of the HREE indicates melting within the garnet stability field (>70 – 80 km).

The new trace element data from Peter I Island also display trace element patterns similar to OIB (Fig. 8b) that compares well with the data of Prestvik et al. (1990) and Hart et al. (1995). Overall the subaerial samples are slightly more enriched in incompatible elements than the submarine sample but show similar HREE abundances (Fig. 8d), which is consistent with lower degrees of melting for the subaerial lavas. In contrast to the MBS, Peter I Island samples are slightly less enriched in LREE and the most incompatible elements (Rb through Ta) and show lower La/Sm ratios (Fig. 9a), indicating higher degrees of partial melting than observed for the MBS. Notably the LREE are more strongly enriched relative to the HREE through a more pronounced HREE depletion. The higher (Sm/Yb)_n ratios of the Peter I Island melts suggest that their source had a higher garnet content (Fig. 9b).



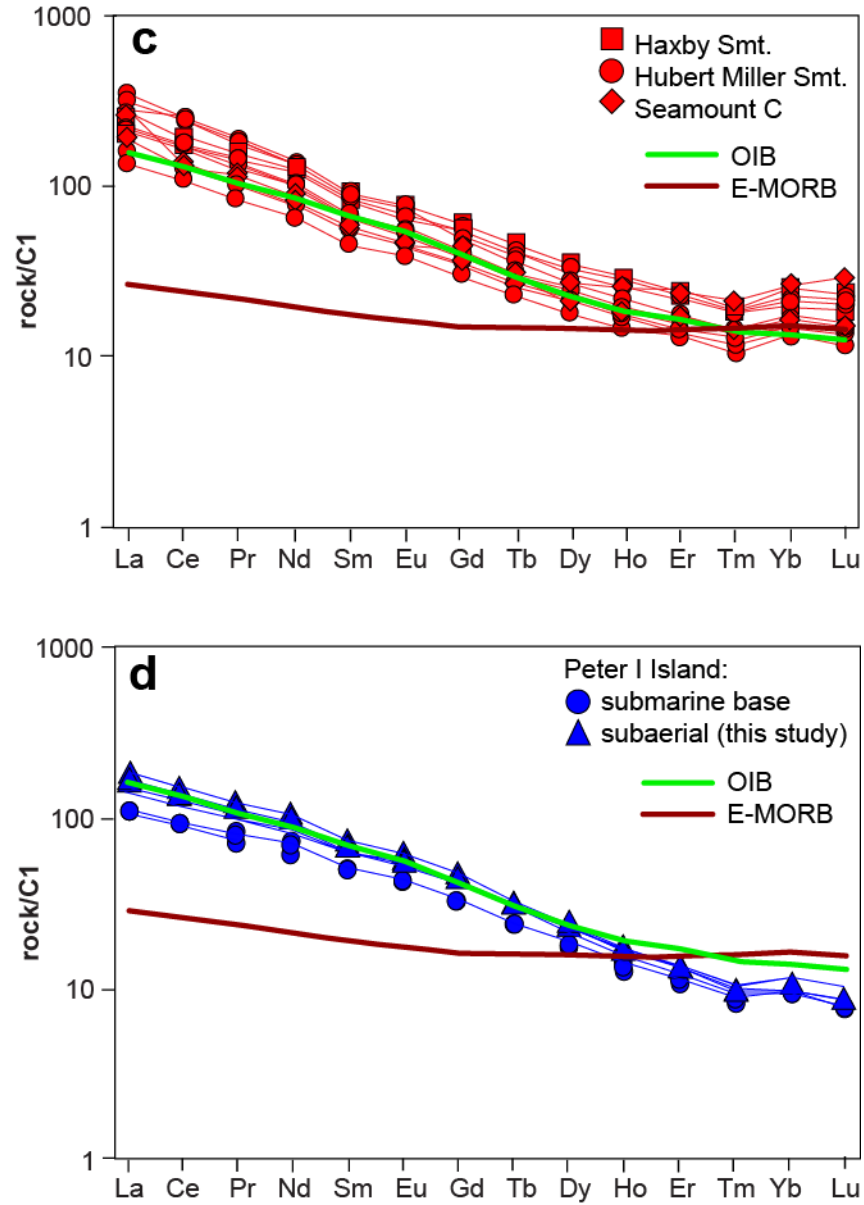


Fig. 8: Multi-element diagram normalized to primitive mantle after Hofmann (1988) for **(a)** MBS and **(b)** Peter I Island samples. The trace elements patterns of the all samples are similar to those of ocean islands basalts (OIB). OIB and E-MORB pattern after Sun and McDonough (1989). REE diagrams normalized to C1 after McDonough and Sun (1995) for **(c)** MBS and **(d)** Peter I Island samples.

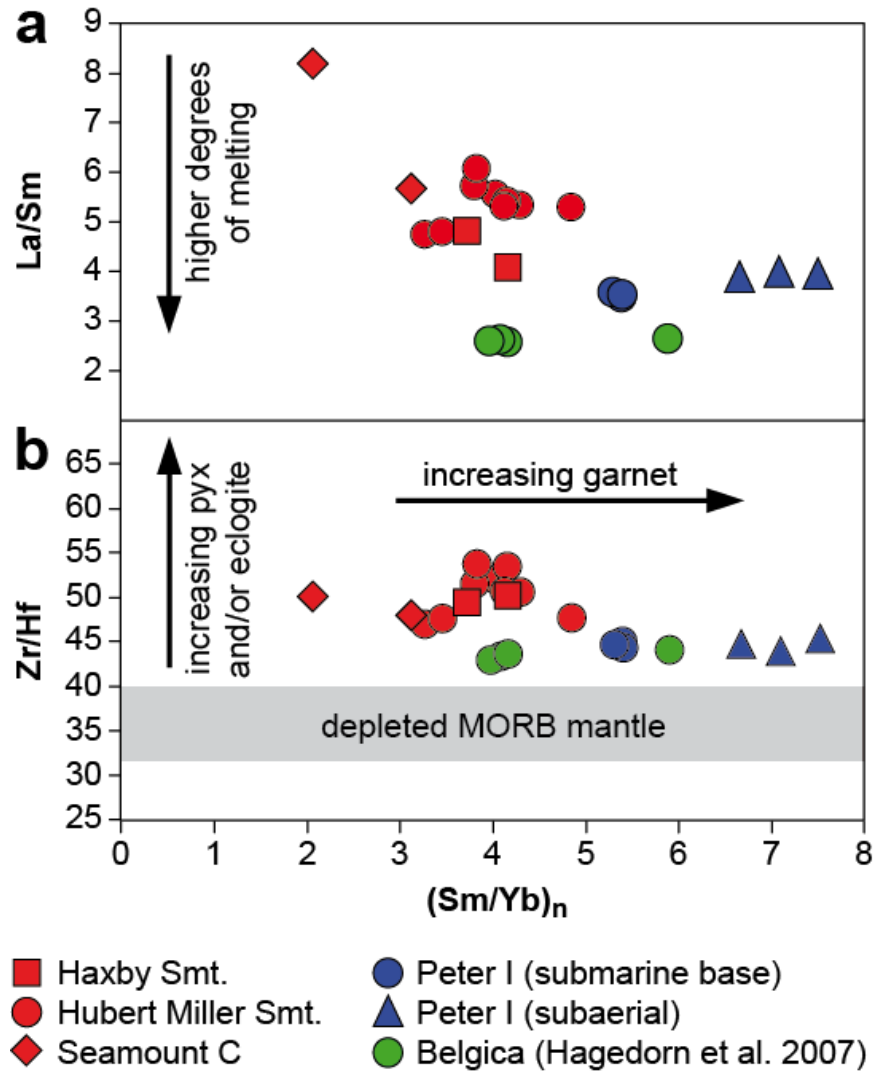


Fig. 9: $(\text{Sm}/\text{Yb})_n$ (n = normalized to primitive mantle after Hofmann, 1988) versus (a) La/Sm and (b) Zr/Hf ratios. Lower La/Sm ratios indicate slightly higher degrees of partial melting for Peter I Island and Belgica Seamount than for MBS. Residual garnet and pyroxene and/or eclogite in the magma source is indicated by high $(\text{Sm}/\text{Yb})_n$ ratios of 2 to 8 and relatively high Zr/Hf ratios (> 40), respectively. Zr/Hf ratios for depleted MORB mantle (32 - 40) after Salters and Stracke (2004) and Workman and Hart (2005).

6.3 Sr-Nd-Pb-Hf isotopes

Sr-Nd-Pb-Hf isotopic ratios of representative samples from the MBS, Belgica Seamount, and Peter I Island are shown in Table 4. Descriptions of analytical methods and accuracy along with initial isotopic ratios are given in Appendix 1 and Table A4. Figures 10 and 11 compare the new MBS, Peter I Island and Belgica Seamount isotope data with data of West Antarctic volcanic rocks, related to the WARS (for data sources see figure captions) and the Hikurangi Seamounts (Hoernle et al., 2010). Excluding two samples with anomalously high

$^{87}\text{Sr}/^{86}\text{Sr}$ isotope ratios that may have been affected by seawater alteration, the MBS samples form a crude negative array on the Sr-Nd isotope diagram (Fig. 10). The samples from Seamount C have the most radiogenic Nd and least radiogenic Sr isotope ratios and fall between Pacific MORB and the high $^{238}\text{U}/^{204}\text{Pb}$ (HIMU) mantle endmember. Samples from Hubert Miller Seamount have the least radiogenic Nd isotope ratios and trend vaguely towards an enriched mantle (EM) type component (Fig. 10). The Belgica samples plot within the Pacific MORB field and the Peter I Island samples lie within the published field for this island (Prestvik et al., 1990; Hart et al., 1995) and are displaced to slightly more radiogenic Sr and less radiogenic Nd isotope ratios i.e. to faintly more EM flavored compositions than the majority of Hubert Miller Seamount samples. In Pb-Pb isotope space (Fig. 11a), the MBS volcanic rocks do not form a simple two component mixing array as the majority of samples extends from a HIMU-type component with radiogenic Pb towards enriched mantle one (EMI) while two samples having significantly lower $^{207}\text{Pb}/^{204}\text{Pb}$ which displaces them towards the extension of the Pacific MORB field. Sample 324-1-4 from Hubert Miller Seamount has the least radiogenic Pb composition of all MBS and plots above the Pacific MORB field away from the main MBS array while samples from Haxby Seamount possess the most radiogenic Pb composition. The Belgica Seamount samples plot near the unradiogenic end of the main MBS field in Pb-Pb isotope space (Fig. 11a) but possess more radiogenic $^{143}\text{Nd}/^{144}\text{Nd}$ compositions than the MBS (Fig. 11b). The majority of MBS samples and all Belgica Seamount samples largely overlap with the fields of the West Antarctic volcanics and the Hikurangi Seamounts (Fig. 11). The Peter I Island samples overlap the published data from this island and have Pb isotope compositions near the enriched mantle two (EMII) component.

The above mixing relations are also seen in co-variations of $^{206}\text{Pb}/^{204}\text{Pb}$ versus $^{143}\text{Nd}/^{144}\text{Nd}$ (Fig. 11b) and eNd versus eHf (Fig. 12). On the Pb vs Nd isotope diagram, it is clear that at least three distinct components are required in the source of the MBS seamounts. Haxby Seamount has radiogenic Pb and intermediate Nd isotope ratios, similar to the HIMU mantle endmember. Seamount C and two Hubert Miller Seamount samples have less radiogenic Pb and intermediate Nd, trending toward Pacific MORB (or depleted mantle = DM). The remaining Hubert Miller seamount samples except sample 324-1-4 have radiogenic Pb but the least radiogenic Nd, so that they are somewhat displaced toward EM like compositions. On the Nd-Hf isotope diagram, the MBS seamounts show a relatively restricted range in Nd but a large range in Hf isotope ratios that fall between Pacific MORB (DM) and the HIMU and EM mantle endmembers. The Belgica Seamount samples have the most MORB-like compositions in Nd, but their $^{206}\text{Pb}/^{204}\text{Pb}$ isotopic compositions are more radiogenic than commonly found in MORB.

The Peter I Island samples have a clear EMII-type isotope signal with respect to Pb while Sr, Nd and Hf isotopes are just EM indicative.

Table 4: Sr-Nd-Pb-Hf-Isotope analyses.

	⁸⁷ Sr/ ⁸⁶ Sr	2 sigma	¹⁴³ Nd/ ¹⁴⁴ Nd	2 sigma	²⁰⁶ Pb/ ²⁰⁴ Pb	2 sigma	²⁰⁷ Pb/ ²⁰⁴ Pb	2 sigma	²⁰⁸ Pb/ ²⁰⁴ Pb	2 sigma	¹⁷⁶ Hf/ ¹⁷⁷ Hf	2 sigma
Marie Byrd Smts.												
PS69/317-1-1	0.703093	0.000003	0.512885	0.000003	20.7725	0.0015	15.7739	0.0016	40.1472	0.0056	0.282871	0.000005
PS69/317-1-2	0.704186	0.000003	0.512881	0.000003	20.4116	0.0020	15.7561	0.0022	39.9679	0.0075	0.282875	0.000004
PS69/321-1-2	0.703384	0.000003	0.512798	0.000003	20.2467	0.0016	15.7229	0.0017	40.0393	0.0057	0.282879	0.000003
PS69/321-1-4	0.703277	0.000002	0.512806	0.000002	20.1075	0.0006	15.7153	0.0006	39.9521	0.0018	0.282880	0.000004
PS69/321-1-5	0.703335	0.000002	0.512816	0.000003	20.1005	0.0008	15.7160	0.0008	39.9815	0.0028		
PS69/321-1-12a	0.703230	0.000003	0.512811	0.000003	19.9595	0.0008	15.7082	0.0009	39.9274	0.0028	0.282875	0.000004
PS69/324-1-3	0.703094	0.000003	0.512906	0.000003	19.6713	0.0011	15.6140	0.0013	39.5216	0.0044	0.282787	0.000007
PS69/324-1-4	0.704027	0.000003	0.512881	0.000003	18.7063	0.0006	15.6189	0.0007	38.4900	0.0020	0.282877	0.000004
PS69/324-1-4 ^d	0.704043	0.000003	0.512870	0.000003	18.7110	0.0006	15.6184	0.0007	38.4973	0.0019		
PS69/324-1-6	0.703108	0.000003	0.512899	0.000003	19.8645	0.0009	15.6339	0.0009	39.7163	0.0027	0.283003	0.000004
PS69/324-1-6 ^d					19.8661	0.0013	15.6331	0.0014	39.7173	0.0048		
PS69/325-1-2a	0.703502	0.000003	0.512809	0.000003	20.1218	0.0008	15.7193	0.0006	39.9100	0.0016	0.282862	0.000004
PS69/325-1-2b	0.703417	0.000002	0.512817	0.000003	20.0871	0.0008	15.7180	0.0006	39.8863	0.0017		
PS69/327-1-1	0.702888	0.000003	0.512913	0.000006	19.8152	0.0010	15.6835	0.0010	39.2970	0.0031	0.282927	0.000004
PS69/327-1-2	0.702805	0.000003	0.512918	0.000009	19.8530	0.0008	15.6903	0.0008	39.3447	0.0024		
PS69/327-1-2 ^d	0.702831	0.000003	0.512927	0.000004								
De Gerlache Smts.												
PS-2693-1_(1) ^e	0.703015	0.000005	0.512967	0.000002	19.8515	0.0021	15.6878	0.0018	39.5057	0.0049		
PS-2693-1_(2) ^e	0.703023	0.000005	0.512966	0.000003	19.8376	0.0025	15.6795	0.0021	39.4705	0.0056		
PS-2693-1_(3) ^e	0.703029	0.000005	0.512966	0.000003	19.8278	0.0032	15.6804	0.0027	39.4777	0.0063		
PS-2693-1_(4) ^e	0.703029	0.000004	0.512957	0.000003	19.9238	0.0037	15.6834	0.0030	39.4845	0.0081		
PS-2693-1_(5) ^e	0.702998	0.000005	0.512983	0.000004	19.7441	0.0025	15.6641	0.0024	39.3550	0.0069		
PS-2693-1_(6) ^e	0.702994	0.000005	0.512975	0.000003	19.7447	0.0016	15.6601	0.0012	39.3438	0.0032		
Peter I Island												
PS69/244-1-1	0.703748	0.000003	0.512759	0.000002	19.2360	0.0015	15.7437	0.0017	39.3779	0.0056	0.282798	0.000003
PS69/244-1-3	0.703752	0.000003	0.512750	0.000003	19.2517	0.0006	15.7520	0.0006	39.4162	0.0019		
PS69/PI-1 ^f	0.703759	0.000005	0.512805	0.000002	19.3013	0.0012	15.7216	0.0010	39.3230	0.0026		
PS69/PI-3	0.703837	0.000002	0.512782	0.000002	19.3015	0.0007	15.7409	0.0006	39.3865	0.0015		
PS69/PI-4	0.703871	0.000002	0.512775	0.000003	19.3244	0.0007	15.7456	0.0006	39.4265	0.0014		

^d Replicate analyses^e ⁸⁷Sr/⁸⁶Sr determined on MAT262 TIMS^f Pb isotope ratios without Pb DS

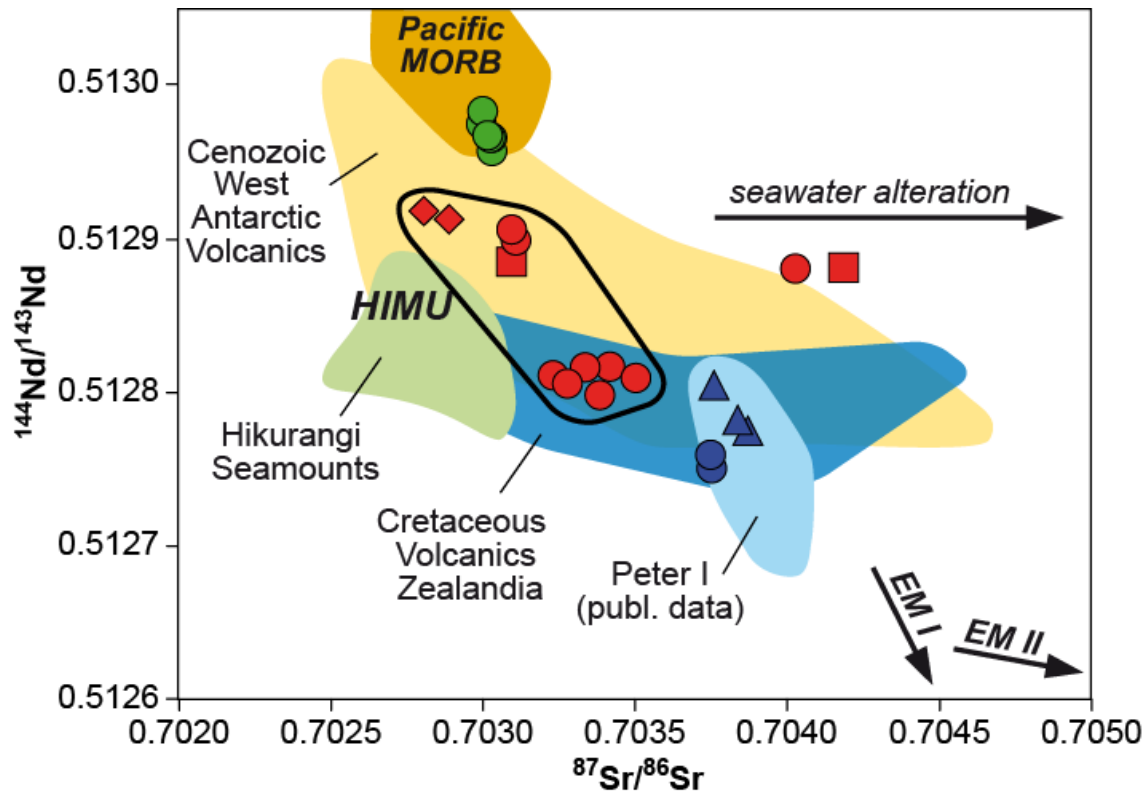


Fig. 10: $^{87}\text{Sr}/^{86}\text{Sr}$ versus $^{143}\text{Nd}/^{144}\text{Nd}$ isotope correlation diagram for MBS, Peter I Island, and Belgica Seamount samples. The field for West Antarctic volcanics is defined by data of the WARS (Rocholl et al., 1995; Rocchi et al., 2002a), the Jones Mountains in Ellsworth Land (Hart et al., 1995), and the Marie Byrd Land Volcanic Province (Hart et al., 1997; Panter et al., 1997, 2000), which extends along the Pacific margin of Marie Byrd Land. Most authors consider the volcanism at the Marie Byrd Land Volcanic Province and Jones Mountains as related to the WARS (e.g., Hart et al., 1995, 1997; Panter et al., 2000). The field for the Hikurangi Seamounts is based on data by Hoernle et al. (2010), published data for Peter I Island comprise analyses of subaerial basaltic lavas from Prestvik et al. (1990) and Hart et al. (1995). The field for Cretaceous volcanics of New Zealand are based on Tappenden (2003); Panter et al. (2006) and McCoy-West et al. (2010). HIMU, EM I, and EM II after Zindler and Hart (1986) and Hart et al. (1992). Fields for Pacific MORB are from PetDB (<http://www.earthchem.org/petdb>) based on analyses of fresh glass.

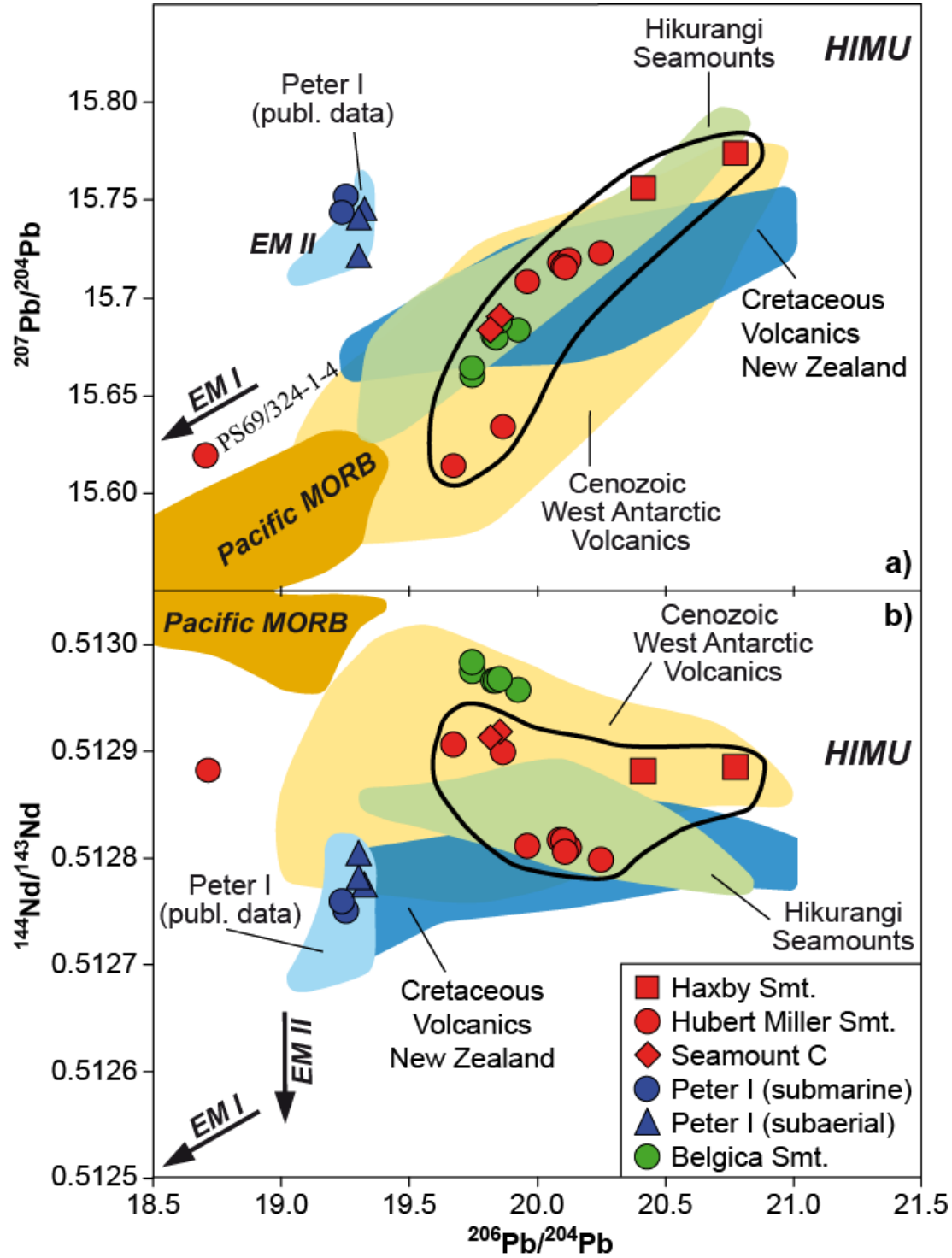


Fig. 11: (a) $^{206}\text{Pb}/^{204}\text{Pb}$ versus $^{207}\text{Pb}/^{204}\text{Pb}$, and (b) $^{143}\text{Nd}/^{144}\text{Nd}$ isotope correlation diagrams for MBS, Peter I Island, and Belgica Seamount samples. Symbols and data sources as in Figure 10.

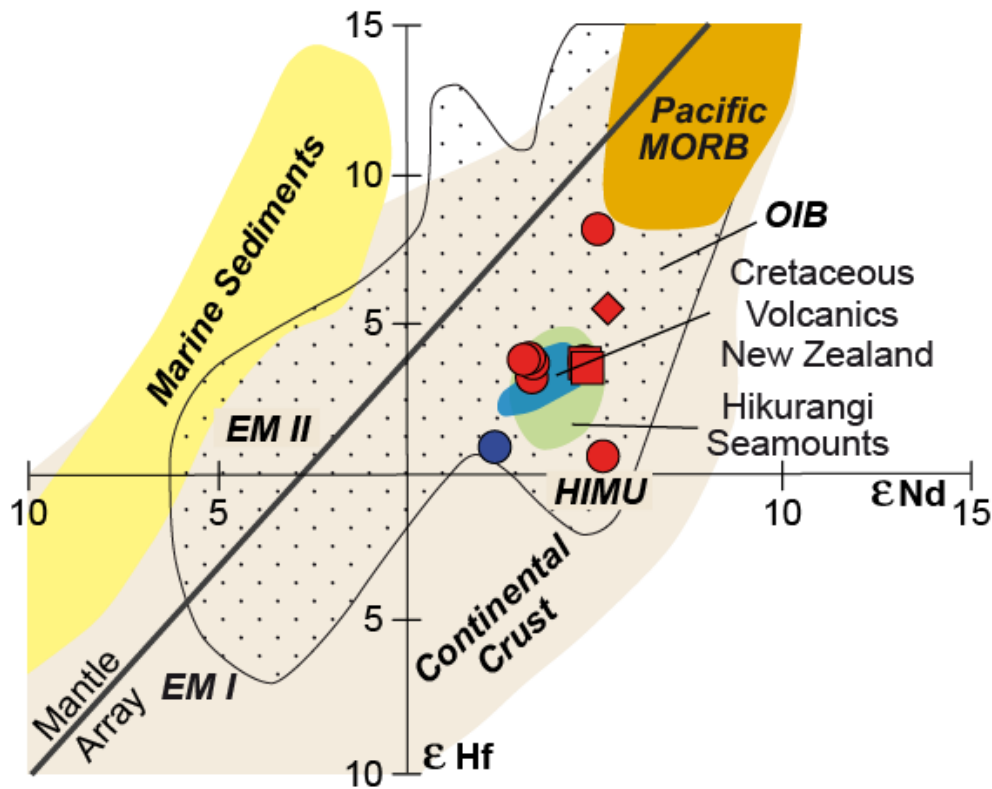


Fig. 12: eNd versus eHf isotope correlation diagram for MBS and Peter I Island samples. Figure modified after Geldmacher et al. (2003), symbols and data sources for Hikurangi Seamounts and Pacific MORB as in Figure 10. The New Zealand Cretaceous field includes Nd values by Tappenden (2003) and Hf values analyzed by Timm et al. (2010) for the Mandamus Complex, as well as data from McCoy-West et al. (2010) for Lookout Volcanics.

7. DISCUSSION

7.1 Spatial distribution of Cenozoic volcanism in the Amundsen Sea and Bellingshausen Sea

$^{40}\text{Ar}/^{39}\text{Ar}$ dating of six samples from the MBS yielded Early Cenozoic ages ranging from 64 to 57 Ma. A clear spatial age progression between the three dated MBS is not observed. The oldest ages are from Haxby Seamount in the west (64-61 Ma) and clearly younger ages are from Hubert Miller Seamount to the east (57 Ma, three feldspar ages). Seamount C, the easternmost seamount, yielded an intermediate age (59 Ma), but this matrix age with a very low probability should be treated with caution. The Pliocene age of 3.0 ± 0.5 Ma determined for sample 324-1-3 was collected right beneath a small volcanic cone along the upper slope of Hubert Miller Seamount (Fig. 3d) and most likely represents the age of this cone. Similar cones are scattered on the plateau and slopes of all mapped MBS (cf. Fig. 3), indicating widespread

and possibly long-lasting low volume post-erosional volcanism, as has been observed at other seamount provinces worldwide (e.g., Geldmacher et al., 2005; Hoernle et al., 2004, 2010).

Assuming that the $^{40}\text{Ar}/^{39}\text{Ar}$ ages obtained at the three MBS are close (within a few million years) to the time when these islands were eroded and submerged below sea-level, a minimum subsidence rate can be calculated for each seamount taking the age and present water depth of the plateau of the seamount into account. Seamount C, the smallest and deepest edifice, displays the highest subsidence rate of ~ 41 m/Ma if it is actually a guyot. In contrast, the larger Haxby and Hubert Miller Seamounts both yield minimum subsidence rates of ~ 28 m/Ma despite their apparent age difference of ~ 5 Ma. We note that the plateau edges of the westernmost Seamounts 6 and 9 lie at roughly similar water depth (1,600 – 1,350 m, Tab. 1) as observed for Haxby and Hubert Miller Seamounts (1,800 – 1,200 m), which in turn may indicate a comparable subsidence history provided similarities in lithospheric age and structure west of Haxby Seamount as well as analogous formation ages of 60 ± 5 Ma.

The new ages (1.9 ± 0.3 Ma to 1.7 ± 0.3 Ma) for samples from the eastern submarine flank of Peter I Island are significantly older than earlier published K-Ar ages (327 ± 88 ka to 111 ± 36 ka [1 sigma errors], Prestvik and Duncan, 1991) obtained on subaerial samples, which suggests that the fresh pillow glasses belong to an earlier submarine phase of this volcano.

Together with published Upper Miocene K-Ar ages for the Belgica Seamount (20 - 23 Ma, Hagedorn et al., 2007), the three seamount / ocean island volcanic provinces of the Amundsen and Bellingshausen Sea appear to have formed at distinct age intervals of 64 - 57 Ma for the MBS, at ~ 22 Ma for the De Gerlache Seamounts and at least since ~ 2 Ma at Peter I Island. The three seamount / ocean island groups are spatially arranged in a highly elongated triangle with the MBS lying at its western tip and the De Gerlache Seamounts and Peter I Island forming the eastern limit (Fig. 1). The age distribution neither shows a correlation with spatial distribution nor a correlation with the age of the underlying ocean crust (e.g., Eagles et al., 2004a). A relationship between ages and plate motion cannot be observed, because neither the relative motion between the Bellingshausen Plate and the Antarctic Plate nor the absolute plate motion of the Antarctic Plate was significant for this time period (Eagles et al., 2004a, b; Wobbe et al., 2012; Doubrovine et al., 2012).

Therefore the irregular spatial distribution of seamount ages in the Amundsen Sea and Bellingshausen Sea indicates that this magmatism occurred at distinct time intervals in spatially confined areas. This observation excludes an origin through a single stationary hotspot

sensu Morgan (1971). Instead this regional age pattern of intraplate volcanism favors the presence of three melting anomalies independent in space and time. Before we explore possibilities of non-plume related intraplate volcanism, we will first briefly reiterate geochemical constraints on the origin of the magma sources.

7.2 Geochemical constraints on the origin of seamount magmatism

Lavas of all three seamount provinces (MBS, De Gerlache and Peter I Island) display a strong enrichment of the LREE relative to the HREE (Fig. 8c+d), clearly indicating partial melting in the presence of garnet. Likewise $(\text{Sm/Yb})_N$, $(\text{Gd/Yb})_N$ and $(\text{Dy/Yb})_N$ are all > 1 which, is consistent with residual garnet in the source (cf. Fig. 9b). Furthermore, the slight enrichment of Zr relative to Hf on the mantle-normalized plot (Fig. 8a + b) is also consistent with residual garnet (Hauri et al., 1994). Consequently melt segregation in all three areas must have occurred in the garnet stability field $> 60 - 80$ km or $40-50$ km if garnet pyroxenite was in the source (Hirschmann and Stolper, 1996). High Zr/Hf (43 - 54, (Fig. 9b), Nb/Ta (16 - 19) and low Zr/Sm (31 - 38) provide additional support for partial melting of eclogite/garnet pyroxenite (i.e. recycled ocean crust), rather than garnet peridotite, consistent with a HIMU component in the mantle source.

The isotopic signatures of MBS volcanic rocks are consistent with the presence of a HIMU-type mantle component in the source of these rocks (Figs. 10 - 12). The extremely radiogenic $^{206}\text{Pb}/^{204}\text{Pb}$ of the HIMU-endmember requires a high $^{238}\text{U}/^{204}\text{Pb}$ in the source; a component unlikely to develop in significant amounts within the convecting upper oceanic mantle without crustal recycling (see Stracke, 2012 for a recent review). HIMU is classically thought to reflect deep mantle recycling of oceanic crust by mantle plumes, ascending from deep in the mantle (Hofmann and White, 1982; White, 2010), however, from the lack of clear indications for the long-term existence of a classical mantle plume in the Amundsen Sea it is clear that alternative mechanisms are required to explain the occurrence of HIMU type intraplate volcanism in this area, as has also been proposed for HIMU-type volcanic rocks in New Zealand (Hoernle et al., 2006).

Subaerial and submarine samples of Peter I Island exhibit small compositional differences with the submarine samples having higher SiO_2 and Al_2O_3 and slightly lower MgO , FeO_t and TiO_2 contents than the subaerial samples. The slight differences in MgO , FeO_t , Al_2O_3 and TiO_2 between submarine and subaerial lavas could be related through fractionation of olivine, pyroxene and possibly ilmenite from a subaerial melt composition, but this scenario

cannot explain the higher incompatible element abundances in the subaerial lavas. Along with the slightly more alkaline character of the subaerial lavas in our sample set, the data indicates that the subaerial lavas could reflect slightly lower degrees of mantle melting, which would also explain their higher incompatible element abundances. Variations in the extent of partial melting are common during the life cycle of ocean island volcanoes with more alkaline compositions of lavas during the subaerial stage compared to less alkaline (tholeiitic) compositions during the submarine shield stage (e.g., Frey et al., 1990). Even during the submarine stage, short-term variations in the degree of partial melting have been observed at Loihi Seamount in the Hawaiian Islands (Garcia et al., 1993).

The Pb isotopic composition of lavas from Peter I Island carry a clear EM II source signal (Fig. 11a) that is commonly thought to reflect contributions from pelagic sediments or upper continental crust (e.g., Zindler and Hart, 1986; Willbold and Stracke, 2010). The mafic composition of Peter I Island lavas, negative Pb anomalies and high Ce/Pb (~25 in submarine samples, 34-40 in subaerial samples) argue against shallow AFC processes such as sediment assimilation or preferential leaching of sedimentary Pb. This conclusion is similar to that of Hart et al. (1995), who explain the high $^{207}\text{Pb}/^{204}\text{Pb}$ signature of Peter I Island melts as evidence for the involvement of a mantle plume with EM II characteristics. We also note that the majority of global pelagic sediments have lower $^{206}\text{Pb}/^{204}\text{Pb}$ and $^{207}\text{Pb}/^{204}\text{Pb}$ ratios than observed in the Peter I Island lavas and thus involvement of modern pelagic sediment seems less likely. This is consistent with the Hf-Nd isotope ratios, which show that marine sediments did not influence the submarine sample of Peter I Island (Fig. 12). Ce/Pb lying within (or slightly above) the canonical array of 25 ± 5 for global OIB and MORB (after Hofmann et al., 1986) provides additional evidence for derivation from oceanic mantle rather than involvement of continental crust, which has Ce/Pb of 3-5. The solitary location of Peter I Island suggests that magmatism is related to a localized upwelling of EMII-like mantle but it is unclear whether this is connected to a blob rising from a thermal boundary such as the SW Pacific superswell or melting of a continental raft that drifted into the oceanic upper mantle during the final Gondwana breakup.

In summary, Cenozoic intraplate volcanism in the Amundsen Sea and Bellingshausen Sea requires involvement of depleted MORB mantle in the source with significant contributions of enriched components of HIMU and EM affinity. Due to the lack of clear evidence for the existence of a mantle plume in this region, a model is needed to explain the evidence for enriched (“plume like”) components in the source of Amundsen Sea intraplate volcanism and a non-plume related process to accomplish adiabatic mantle melting in an intraplate environment.

7.3 Origin of the HIMU component in non-hotspot related Southwest-Pacific and Antarctic volcanic provinces

Alkalic volcanism with HIMU-like incompatible-element and isotopic signatures, similar to the samples from MBS, is reported from numerous locations throughout the SW Pacific and West Antarctica. These include the Chatham Rise, Hikurangi Seamounts, intraplate volcanic fields in New Zealand, sub-Antarctic islands and West Antarctica (e.g., Baker et al., 1994; Hart, 1997; Weaver and Pankhurst, 1991; Weaver et al., 1994; Rocholl et al., 1995; Tappenden, 2003; Panter et al., 2000, 2006; Nardini et al., 2009; Hoernle et al., 2010). In all these localities, volcanic centers are diffusely distributed and do not show any age progression relative to plate motion. Most commonly, models suggest localized extension/upwelling of asthenosphere that induces melting of metasomatized lithosphere in thin spots to produce the diffuse alkaline magmatism.

Finn et al. (2005) postulate a “diffuse alkaline magmatic province (DAMP)”, which formed without any rifting or plume upwelling. They temporally extend the DAMP into the Cenozoic and explain this magmatism by detachment of subducted slabs from the base of Gondwana lithosphere in the late Cretaceous. The sinking of material into the mantle is thought to have introduced Rayleigh Taylor instabilities along the Gondwana margin and activated lateral and vertical flow of warm Pacific mantle. After Finn et al. (2005) the interaction of the warm mantle with metasomatized lithosphere generated the HIMU geochemical characteristics of the DAMP. A shortcoming of this model is, however, that Finn et al. (2005) had to focus their study on old, continental fragments of East Gondwana, and could not include oceanic occurrences like the MBS, the De Gerlache Seamounts or the Hikurangi Seamounts which are situated on top of Hikurangi Plateau off New Zealand. An important difference between the seamounts and the continental alkaline provinces is that the majority of seamount provinces formed on relatively young oceanic crust. While HIMU signatures can be found in old continental terranes, HIMU-type volcanism in the oceans either requires rise of HIMU material from depth or some sort of refertilization of the upper mantle, especially when required shortly after ocean crust formation. No doubt, small-scale heterogeneities exist in the upper mantle away from mantle plumes as is evident from small off-axis seamounts that often have more enriched element and isotopic signatures than associated MORB (e.g., Brandl et al., 2012 and references therein). It seems, however, unlikely that such small-scale heterogeneities are present shortly

after formation of the ocean crust to an extent that can explain the c. 1000-8000 km³ of enriched melt required to form individual MBS (see Table 1 for volume estimates). In other words, even if Raleigh Taylor instabilities affected the Gondwana margin it seems unlikely that upwelling of regular Pacific upper mantle that underwent high degrees of melting shortly before can serve as the source of the HIMU-type compositions without refertilization.

Alternatively the superplume beneath the SW-Pacific could have supplied a dense swarm of widely distributed and contemporaneously active secondary plumes causing diffuse alkaline volcanism (Suetsugu et al., 2009). Since it is in principle possible that secondary plumelets or blobs are continuously rising from the SW Pacific superswell (presumed to have stalled at the 660 km transition zone; Courtillot et al., 2003) they may also serve as the cause of volcanism forming the MBS and De Gerlache Seamounts. The age-distance relationship between MBS and the much further north located Pacific Superswell is, however, unclear. Alternatively Timm et al. (2010 and references therein) identify a low velocity anomaly extending from Chatham Rise off New Zealand to western Antarctica in at 600 - 1500km depth and suggest that this could be the HIMU source polluting the upper mantle in this area since Cretaceous. Still it appears accidental that only the Marie Byrd Land margin was hit by a short-lived swarm of plumelets and no other oceanic region above this low velocity zone. Therefore we explore an alternative scenario for the oceanic seamount provinces off Marie Byrd Land based on reactivation of (HIMU) material, added to the base of continental lithosphere by plume activity during the pre-rifting stage of Marie Byrd Land/Zealandia.

On a regional scale, the MBS and Belgica Seamount data overlap with the data field of the Hikurangi Seamounts (Hoernle et al., 2010) in most isotope correlation diagrams (Fig. 10 - 12). A similar HIMU signature of Cretaceous rocks is also found at the Mandamus complex, the Lookout Volcanics in southern New Zealand, and the Chatham Islands (Weaver and Pankhurst, 1991; Tappenden, 2003; Panter et al., 2006; McCoy-West et al., 2010). During the Cretaceous these localities were assembled adjacent to Marie Byrd Land. It has been proposed that a HIMU type plume or plume head may have caused breakup of the Gondwana margin in this region (e.g., Weaver et al., 1994; Hart et al., 1997; Storey et al., 1999; Hoernle et al., 2010). This plume event may have also influenced the source characteristics of the Hikurangi Seamounts (Hoernle et al., 2010) and may have been accompanied by large scale underplating of the Zealandia continental lithosphere by HIMU material (e.g. Weaver et al., 1994; Hart et al., 1997; Panter et al., 2000) (Fig. 13). During the mid Cretaceous the plume head expanded and thus forced rifting and the breakup of Gondwana as it impacted at the base of the continental lithosphere (Weaver et al., 1994). We note, however, that in contrast to other continental breakup

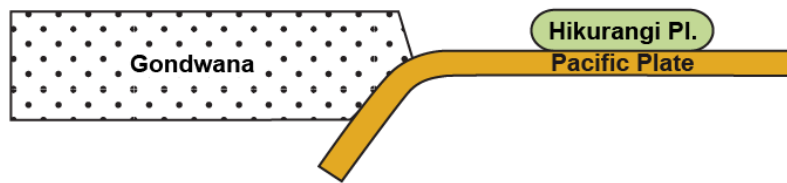
related mantle plumes such as the Tristan-Gough in the South-Atlantic (and related Paraná and Etendeka continental flood basalts), a flood basalt event is absent on Zealandia and West Antarctica, possibly reflecting the convergent margin setting and associated thick continental lithosphere along the Gondwana margin. Together with the observation that the Cretaceous HIMU volcanism occurred only locally and was of relatively low volume, it seems likely that unmelted HIMU-mantle got attached at the base the Gondwana lithosphere, which underwent extension and rifting during that period. The proposed large-scale underplating of HIMU material beneath East Gondwana is consistent with the HIMU signature of many Cenozoic continental volcanics from West Antarctica (e.g., Hobbs Coast, Marie Byrd Land Volcanic Province, WARS; cf. Figs. 10 and 11). Accordingly, many authors relate the Cenozoic HIMU similarities in West Antarctica to the reactivation of HIMU material, added to the base of the continental lithosphere during the earliest pre-rifting stage of the Marie Byrd Land through plume activity (e.g., Weaver et al., 1994; Rocholl et al., 1995; Hart et al., 1997; Panter et al., 2000). Alternatively Nardini et al. (2009 and references therein) call upon a late Cretaceous metasomatic event that caused variable elevation of U/Pb ratios in the sublithospheric mantle to an extent that explains the high $^{206}\text{Pb}/^{204}\text{Pb}$ of < 20Ma WARS volcanics and generation of their HIMU isotopic source signatures through radiogenic ingrowth over extremely short time scales. The regional context, however, requires the presence of a HIMU component that is already present in the Cretaceous, so that the metasomatic model of Nardini et al. (2009) for the formation of HIMU appears less likely.

Notably, the field for continental volcanic rocks of West Antarctica overlaps the data of the oceanic seamount provinces (Hikurangi Seamounts, MBS, De Gerlache) (Figs. 10 and 11), which have been formed close to the East Gondwana and West Antarctic margin, respectively. The samples also fall within the range of Cretaceous volcanic rocks of southern New Zealand, suggesting that all the above-mentioned volcanic suites originate from a similar HIMU source. This material may therefore also represent reactivation of fossil Cretaceous plume material that was originally attached to the base of the continental lithosphere during Marie Byrd Land/Zealandia break up. In contrast to the above mentioned onshore occurrences of Cenozoic HIMU volcanism, an additional transport mechanism and mode of reactivation is required to explain the marine equivalents of HIMU volcanism, because this material needs first of all be transferred into the oceanic mantle beneath the newly formed ocean basins of the Amundsen / Bellingshausen Sea followed by decompression melting (see section 7.4 for details).

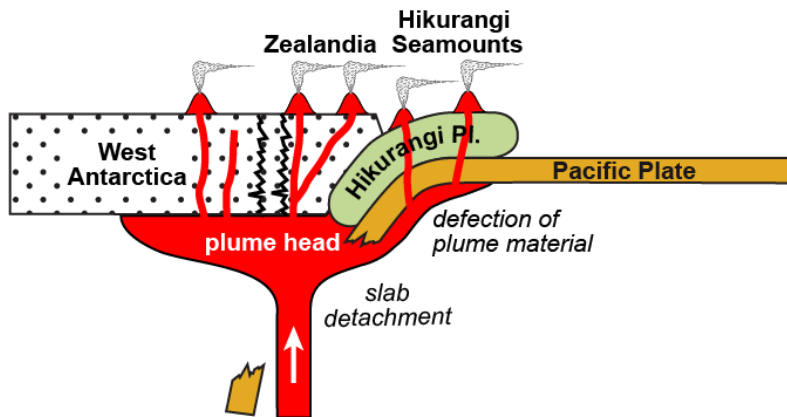
Admittedly the arguments for an initial upwelling of plume-like material and storage at the base of the Gondwana lithosphere are solely based on geochemistry, which points to a HIMU

like mantle. Such a source is unlikely to develop in situ in a mantle region affected by long-term subduction zone volcanism and small scale convection cells operating within the mantle wedge both leading to continuous depletion and replenishment of the arc mantle. On the other hand, upwelling of refertilized subcontinental lithospheric mantle (SCLM), isolated from mantle circulation for several billion years, can lead to the formation of EM type melts (e.g., Rudnick, 1995; Griffin et al., 2009; Hoernle et al., 2011; Soager et al., 2013). Ancient SCLM, however, features low $^{206}\text{Pb}/^{204}\text{Pb}$ and $^{143}\text{Nd}/^{144}\text{Nd}$ along with high $^{207}\text{Pb}/^{204}\text{Pb}$ and $^{87}\text{Sr}/^{86}\text{Sr}$ ratios, reflecting an ancient source that evolved with low U/Pb, Sm/Nd but high Rb/Sr (see Tang et al., 2013 for a recent review). Mantle regions that underwent such a fractionation and/or metasomatic event early in the earth's history are commonly thought to be involved in the formation of the early continental crust, having resided thereafter in the roots of stable Achaean cratons. In conclusion, SCLM seems to be a very unlikely candidate as source of the Cretaceous HIMU type intraplate volcanism due the conflicting isotopic composition of SCLM (EM-like) and the long-term subduction zone setting of this area. Therefore our preferred model for the origin of the HIMU component in the MBS and De Gerlache lavas is reactivation of fossil Cretaceous plume material, which was attached and stored at the base of the West Antarctic continental lithosphere during East Gondwana breakup.

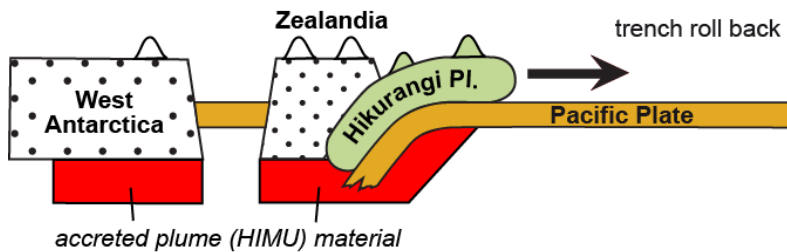
a) Early Cretaceous subduction at East Gondwana margin



b) Cessation of subduction at ~100 Ma and plume event



c) Break up at ~90 Ma and subsequent rifting



d) Formation of the MBS at ~65 - 55 Ma

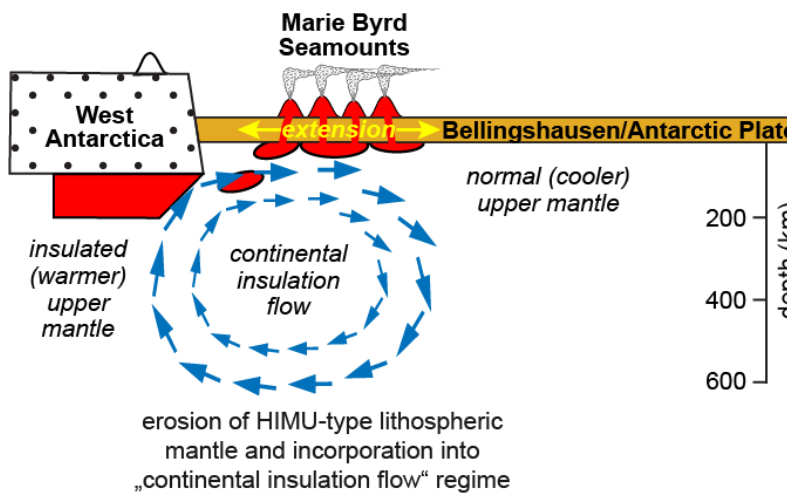


Fig. 13: Schematic sketch placing the origin of the MBS in a regional geodynamic context. **(a)** During the final stage of subduction of the Pacific Plate beneath the Zealandia/West Antarctic Gondwana margin, the Hikurangi

Plateau approaches the subduction zone. **(b)** Forces acting upon the plate margin as, for example, the collision of the Hikurangi Plateau with Zealandia (e.g., Bradshaw, 1989, Davy et al., 2008) cause cessation of subduction and slab detachment. The impact of a plumehead at that time was accompanied by large scale underplating of HIMU material beneath East Gondwana (e.g., Weaver et al., 1994; Hart et al., 1997) and the Hikurangi Plateau (possibly by deflection of the plume material by the subducting plate; Hoernle et al., 2010), triggering volcanism on West Antarctica and Zealandia and the formation of the Hikurangi Seamounts. **(c)** After subduction ended extensional processes set in, causing the break-up of Zealandia from Marie Byrd Land at ~90 Ma and subsequent rifting, forming the oceanic crust of the Amundsen Sea (Eagles et al., 2004a). **(d)** Lateral temperature differences between warm mantle beneath the continental lithosphere and normal upper mantle drove continental-insulation flow (model modified after King and Anderson, 1995), allowing sub-continental mantle material to rise into the upper mantle beneath the adjacent oceanic lithosphere. At the Cretaceous/Tertiary boundary lithospheric extension at the southern margin of the Bellingshausen Plate (e.g., Wobbe et al., 2012) formed deep reaching faults that allowed rise of plume type melts and formation of the MBS from a magma source similar to that of the Hikurangi Seamounts and the West-Antarctic/Zealandia volcanoes. For further details and references see text.

7.4 Model for the formation of the Marie Byrd Seamounts

In the case of the West Antarctic volcanoes, underplated HIMU material may have been reactivated and caused to upwell during the WARS extension (e.g., Hart et al., 1997). For the formation of the c. 99 to 67 Ma Hikurangi Seamounts, Hoernle et al. (2010) propose the rise of HIMU-type material directly beneath the Hikurangi Plateau - a ~118 Ma oceanic LIP (Hoernle et al., 2010) that formed in connection with the Manihiki (Timm et al., 2011) and possibly the Ontong Java plateaus (Taylor, 2006), through deflection of rising plume material beneath Zealandia by the subducting plate towards the Hikurangi plateau, which was about to collide with the Zealandia margin at that time (Fig. 13a+b). For the MBS and De Gerlache Seamounts, however, a mechanism is required that enables lateral transport of the earlier emplaced HIMU material under Marie Byrd Land beneath the newly formed bordering oceanic lithosphere.

When the new oceanic crust of the Amundsen Sea formed, Zealandia (including the Hikurangi plateau) rifted away from Marie Byrd Land in a northward direction (Fig. 13c), whereas the West Antarctic continental margin remained more or less fixed and developed as a relatively stable passive margin thereafter (e.g., Eagles et al. 2004a; Wobbe et al., 2012). Mutter et al. (1988) proposed a transition zone directly at the edge of thicker to thinner lithosphere where small convective flow is focused. In case of the MBS and De Gerlache Seamounts, the transition zone lies at the edge of the Antarctic continental

lithosphere and the beginning of the adjacent oceanic crust. Several mechanisms such as edge-driven convection (EDC), small-scale convection (SSC) or shear-driven upwelling (SDU) have been suggested to explain edge-driven buoyant flow between young, thin and old, thicker lithosphere (e.g., King and Anderson, 1995, 1998; King and Ritsema, 2000; Huang et al., 2003; Dumoulin et al., 2008; Conrad et al., 2010 and references therein). For example, (super-) continents may effectively insulate the upper mantle, leading to a buildup of heat (Gurnis et al., 1998; Anderson, 1994; Lowman and Jarvis, 1995, 1996). These lateral temperature differences between the warm mantle beneath the continental lithosphere and normal upper mantle can drive an upper mantle convective flow pattern that leads to upwelling beneath the continent-ocean transition zone (Fig. 13d), the so-called “continental-insulation flow” (e.g., King and Anderson, 1995, 1998). From numerical modeling, King and Anderson (1998) suggest that lateral variations in temperature of at least 30°C are required for continental insulation flow to significantly modify or even shut off the normal, downwelling EDC flow. Higher temperature anomalies (150 - 200°C) would drive major upper mantle convection cells. In case of the Cretaceous East Gondwana lithosphere, the impact of the hot plume head may have caused additional heating of the mantle beneath the continental lithosphere and therefore reinforced the lateral variations in mantle temperature and consequently mantle convection. Notably, the pattern of flow resulting from continental insulation is opposite to that of normal EDC flow (King and Anderson, 1995, 1998). At the initial stages of rifting of a continent, upwelling should occur as warm mantle from beneath the continent that occupies the space created by spreading between the continental masses. At the Late Cretaceous Marie Byrd Land margin, this process would transfer mantle material directly from beneath the continent into the upper mantle under the adjacent oceanic lithosphere on which the MBS started to form at that time (Fig. 13d). Therefore we consider continental insulation flow as the most plausible mechanism to bring the HIMU plume-like material previously attached beneath Marie Byrd Land upwards beneath the adjacent oceanic lithosphere of the Bellingshausen / Antarctic plate.

As the HIMU material was transported upwards beneath the newly formed oceanic lithosphere from beneath the thick Antarctica continental crust, the material will melt by decompression. The volcanism forming the De Gerlache Seamounts at ~22 Ma and the Pleistocene activity of Peter I Island, on the other hand, was most likely related to the De Gerlache Gravity Anomaly (Figs. 1 and 2), which represents a zone of lithospheric weakness resulting from a presumed WARS activity in this region (Müller et al., 2007), where pre-

existing N-S striking faults allowed rise (and decompression melting) of HIMU type material brought up beneath the oceanic lithosphere by mantle convection. The formation of the MBS may therefore have been triggered by a complex sequence of plate reorganization events that affected the West Antarctic margin and the Bellingshausen Plate in Late Cretaceous and Early Cenozoic (e.g., Eagles et al., 2004a; Wobbe et al., 2012). Shortly before the Bellingshausen Plate became incorporated into the Antarctic Plate at 61 Ma (Eagles et al., 2004a, b; Wobbe et al., 2012), a change in rotation of the Bellingshausen Plate from counterclockwise to clockwise was accompanied by lithospheric extension on its southern margin between 74 and 62 Ma (Wobbe et al., 2012). Contemporaneously the MBS started to form in that area (Fig. 2) (Fig 13 d), suggesting that lithospheric extension lead to upwelling of sublithosphericly attached HIMU material and deep reaching faults that allowed rise of the HIMU type melts and formation of large volcanic islands (Fig. 13d).

8. CONCLUSIONS

Our new morphological, geochronological, and geochemical data for the MBS combined with additional data for the De Gerlache and Peter I Island volcanic complexes (complementing previously published data) permit for the first time a comprehensive reconstruction of the origin and evolution of Cenozoic intraplate volcanism in the Amundsen Sea. The most important results are:

- (1) Intraplate volcanism occurred during the entire Cenozoic at distinct time intervals in spatially confined areas in the Amundsen Sea, excluding an origin of this volcanism by a single stationary hotspot.
- (2) The MBS and De Gerlache Seamount lavas show OIB signatures and posses a distinct HIMU component in their magma source similar to Late Cretaceous – Cenozoic volcanics of the Hikurangi Seamounts off New Zealand, intraplate volcanic fields in New Zealand, sub Antarctic islands and the WARS, suggesting a common mantle source for these volcanic provinces.
- (3) Peter I Island displays a strong EM affinity probably caused by shallow mantle recycling of a continental fragment.

Consequently, the formation of the MBS and De Gerlache Seamounts intraplate volcanism requires an alternative, non-hotspot scenario, which takes distinct melting anomalies independent in space and time and a non-hotspot related HIMU source into account.

Placing the morphological, geochronological, and geochemical data in a regional plate tectonic context, we conclude that the most plausible explanation for the HIMU type intraplate volcanism in the Amundsen Sea is reactivation of HIMU-material, added to the base of the Antarctic lithosphere by a Late Cretaceous plume event. Major tectonic events, namely the separation of Zealandia from Antarctica during the final stage of the Gondwana break-up and subsequent formation of ocean crust give way for transport of the sublithospheric HIMU material beneath the Amundsen Sea oceanic crust by continental insulation flow. Extension caused by plate tectonic reorganization (MBS) and/or lithospheric weakening underneath the De Gerlache Gravity Anomaly (De Gerlache, Peter I Island) allow rise and adiabatic melting of the HIMU material resulting in the formation of these volcanic edifices. Reactivation of the MBS magmatism resulting in Pliocene low volume volcanism and the Pleistocene formation of Peter I Island document ongoing magmatism in the Amundsen Sea.

The new model for the Amundsen Sea volcanism presented here adds to case examples for non-hotspot intraplate volcanism and provides additional evidence that HIMU-type intraplate volcanism is not necessarily a direct consequence of an actively upwelling, stationary mantle plume or hotspot.

ACKNOWLEDGMENTS

We are grateful to Captain Pahl, the crew, and shipboard scientific party for their excellent support during RV Polarstern cruise ANT-XXIII/4. R. Gersonde (AWI) kindly provided the dredge samples from Belgica Seamount. D. Rau, S. Hauff, J. Sticklus (GEOMAR) and H. Anders (Uni-Bremen) are thanked for technical assistance during lab work and S. Gauger for help with processing of the bathymetric data. Discussions with Maxim Portnyagin, Jan Grobys, Graeme Eagles, and Christian Timm significantly helped to develop this paper. Furthermore we are grateful for the constructive reviews of John Gamble and Tsuyoshi Komiya that helped to improve an earlier version of the manuscript. We thank Inna Yu Safonova for editorial handling and useful comments that helped to emphasize the

importance of seamount formation. The German Research Foundation (DFG; Grants HO1833/15-1 to –3 to KH and FH) funded this research.

REFERENCES

Anderson, D.L., 1994. Superplumes or supercontinents? *Geology* 22, 39–42, doi:10.1130/0091-7613(1994)022<0039:SOS>2.3.CO;2.

Anderson, D.L., 2000. The thermal state of the upper mantle; No role for mantle plumes. *Geophysical Research Letters* 27(22), 3623–3626, doi:10.1029/2000GL011533.

Baker, I.A., Gamble, J.A. and Graham I.J., 1994. The age, geology, and geochemistry of the Tapuaenuku Igneous Complex, Marlborough, New Zealand. *New Zealand Journal of Geology and Geophysics* 37, 249–268, doi:10.1080/00288306.1994.9514620.

Baksi, A. K., 2007. A quantitative tool for detecting alteration in undisturbed rocks and minerals–I: Water, chemical weathering, and atmospheric argon. *Special Paper of the Geological Society of America* 430, 1197, 285–303, doi:10.1130/2007.2430(16).

Batiza, R., Niu, Y., Zayac, W.C., 1990. Chemistry of seamounts near the East Pacific Rise: Implications for the geometry of subaxial mantle flow. *Geology* 18, 1122–1125, doi:10.1130/0091-7613(1990)018<1122:COSENTE>2.3.CO;2.

Boger, S.D., 2011. Antarctica- Before and after Gondwana. *Gondwana Research* 19 (2), 335–371, <http://dx.doi.org/10.1016/j.gr.2010.09.003>.

Bradshaw, J.D., 1989. Cretaceous geotectonic patterns in the New Zealand region. *Tectonics* 8, 803–820, doi:10.1029/TC008i004p00803.

Brandl, P.A., Beier, C., Regelous, M., Abouchami, W., Haase, K.M., Garbe-Schönberg, D.,

Galer, S.J.G., 2012. Volcanism on the flanks of the East Pacific Rise: Quantitative constraints on mantle heterogeneity and melting processes. *Chemical Geology* 298-299, 41-56, <http://dx.doi.org/10.1016/j.chemgeo.2011.12.015>.

Broch, O.A., 1927. Gesteine von der Peter I.-Insel, West Antarktis. *Avhandlinger / Det Norske Videnskaps-Akademi, I, Matematisk-Naturvidenskapelig Oslo KL.* 9, 1-41.

Buchs, D.M., Arculus, R.J., Baumgartner, P.O., Ulianov, A., 2011. Oceanic intraplate volcanoes exposed: Example from seamounts accreted in Panama. *Geology* 39, 335-338, doi:10.1130/G31703.1.

Conrad, C.P. and Behn, M.D., 2010. Constraints on lithosphere net rotation and asthenospheric viscosity from global mantle flow models and seismic anisotropy. *Geochemistry Geophysics Geosystems* 11, Q05W05, doi:10.1029/2009GC002970.

Courtillot, V., Davaille, A., Besse, J., Stock, J., 2003. Three distinct types of hotspots in the Earth's mantle. *Earth and Planetary Science Letters* 205, 295-308, [http://dx.doi.org/10.1016/S0012-821X\(02\)01048-8](http://dx.doi.org/10.1016/S0012-821X(02)01048-8).

Davy, B.W., Hoernle, K., Werner R., 2008. Hikurangi Plateau: crustal structure, rifted formation, and Gondwana subduction history. *Geochemistry Geophysics Geosystems* 9, Q07004, doi:10.1029/2007GC001855.

Dobrovine, P.V., Steinberger, B. and Torsvik, T.H., 2012. Absolute plate motions in a reference frame defined by moving hot spots in the Pacific, Atlantic, and Indian oceans. *Journal of Geophysical Research* 117, B09101, doi:10.1029/2011JB009072.

Dumoulin, C., Choblet, G. and Doin, M.P., 2008. Convective interactions between oceanic lithosphere and asthenosphere: Influence of a transform fault. *Earth and Planetary Science Letters* 274, 301-309, <http://dx.doi.org/10.1016/j.epsl.2008.07.017>.

Eagles, G., Gohl, K. and Larter R., 2004a. High-resolution animated tectonic reconstruction

of the South Pacific and West Antarctic Margin. *Geochemistry Geophysics Geosystems* 5, Q07002, doi:10.1029/2003GC000657.

Eagles, G., Gohl, K., Larter, R., 2004b. Life of the Bellingshausen plate. *Geophysical Research Letters* 31, L07603, <http://dx.doi.org/10.1029/2003GL019127>.

Eagles, G., Larter, R., Gohl, K., and Vaughan, A.P.M., 2009. West Antarctic Rift System in the Antarctic Peninsula. *Geophysical Research Letters* 36, L21305, <http://dx.doi.org/10.1029/2009GL040721>.

Feldberg, M.J., 1997. A geophysical study of seamount E, Bellingshausen Sea, Antarctica. Diploma Degree of Bachelor of Arts, Wesleyan University, USA.

Finn, C. A., Müller, R.D. and Panter K.S., 2005. A Cenozoic diffuse alkaline magmatic province in the SW Pacific without rift or plume origin. *Geochemistry Geophysics Geosystems* 6, Q02005, doi:10.1029/2004GC000723.

Fisher, A.T., Davis, E.E., Hutnak, M., Spiess, V., Zühlsdorff, L., Cherkaoui, A., Christiansen, L., Edwards, K., Macdonald, R., Villinger, H., Mottl, M.J., Wheat, C.G., Becker, K., 2003. Hydrothermal recharge and discharge across 50 km guided by seamounts on a young ridge flank. *Nature* 421, 618-621, doi:10.1038/nature01352.

Foulger, G.R., Natland, J.H., 2003. Is "Hotspot" Volcanism a Consequence of Plate Tectonics? *Science* 300, 921-922, doi:10.1126/science.1083376.

Frey, F.A., Wise, W.S., Garcia, M.O., West, H., Kwon, S.-T., Kennedy, A., 1990. Evolution of Mauna Kea Volcano, Hawaii: petrologic and geochemical constraints on postshield volcanism. *Journal of Geophysical Research* 95(B2), 1271–1300, <http://dx.doi.org/10.1029/JB095iB02p01271>.

Garcia, M.O., Jorgenson, B.A., Mahoney, J.J., Ito, E., Irving, A.J., 1993. An evaluation of temporal geochemical evolution of Loihi Summit Lavas: Results from Alvin submersible

dives. Journal of Geophysical Research 98(B1), 537-550,
<http://dx.doi.org/10.1029/92JB01707>.

Geldmacher, J., Hoernle K., van den Bogaard, P., Duggen, S. and Werner R., 2005. New $^{40}\text{Ar}/^{39}\text{Ar}$ age and geochemical data from seamounts in the Canary and Madeira volcanic provinces: support for the mantle plume hypothesis. *Earth and Planetary Science Letters* 237, 85-101, doi:10.1016/j.epsl.2005.04.037.

Geldmacher, J., Hanan, B. B., Blichert-Toft, J., Harpp, K., Hoernle, K., Hauff, F., Werner, R. und Kerr, A. (2003). Hf isotopic variations in volcanic rocks from the Caribbean Large Igneous Province and Galápagos hotspot tracks. *Geochemistry Geophysics Geosystems*, 422(7), doi:10.1029/2002GC000477.

Geldmacher, J., Hoernle, K., van den Bogaard, P., Hauff, F., Klügel, A., 2008. Age and Geochemistry of the Central American Forearc Basement (DSDP Leg 67 and 84): Insights into Mesozoic Arc Volcanism and Seamount Accretion on the Fringe of the Caribbean LIP. *Journal of Petrology* 49, 1781-1815, doi:10.1093/petrology/egn046.

Gohl, K., Nitsche, F.O. and Miller H., 1997a. Seismic and gravity data reveal Tertiary interplate subduction in the Bellingshausen Sea southeast Pacific. *Geology* 25, 371–374, doi: 10.1130/0091-7613(1997) 025<0371:SAGDRT> 2.3.CO;2.

Gohl, K., Nitsche, F., Vanneste, K., Miller, H., Fechner, N., Oszko, L., Hübscher, C., Weigelt,

E. and Lambrecht, A., 1997b. Tectonic and sedimentary architecture of the Bellingshausen and Amundsen Sea Basins, SE Pacific, by seismic profiling, in: *The Antarctic Region: Geological Evolution and Processes*, by Ricci, C.A. (ed.), p. 719-723, Terra Antartica Publication, Siena.

Gohl, K., 2007. The Expedition ANTARKTIS-XXIII/4 of the Research Vessel Polarstern in 2006. *Berichte zur Polar- und Meeresforschung (Reports on Polar and Marine Research)*, Bremerhaven, Alfred Wegener Institute for Polar and Marine Research, No. 557, 166 pp.

<http://epic.awi.de/26756/>.

Gohl, K., Denk, A., Wobbe, F., Eagles G., 2013. Deciphering tectonic phases of the Amundsen Sea Embayment shelf, West Antarctica, from a magnetic anomaly grid. *Tectonophysics* 585, 113-123, doi:10.1016/j.tecto.2012.06.036.

Griffin, W.L., O'Reilly, S.Y., Afonso, J.C., Begg, G.C., 2009. The Composition and Evolution of Lithospheric Mantle: a Re-evaluation and its Tectonic Implications. *Journal of Petrology* 50, 1185-1204, doi:10.1093/petrology/egn033.

Gurnis, M., Mueller, R.D. and L. Moresi, L., 1998. Dynamics of Cretaceous vertical motion of Australia and the Australian-Antarctic discordance. *Science* 279, 1499-1504, doi: 10.1126/science.279.5356.1499.

Hagedorn, B., Gersonde, R., Gohl, K., Hubberten, H-W., 2007. Petrology, Geochemistry and K-Ar Age Constraints of the Eastern De Gerlache Seamount Alkaline Basalts (Bellingshausen Sea, Southeast Pacific). *Polarforschung* 76(3), 87 – 94, <http://epic.28876.d001>.

Harris, R.N., Fisher, A.T., Chapman, D.S., 2004. Fluid flow through seamounts and implications for global mass fluxes. *Geology* 32, 725-728, doi:10.1130/G20387.1.

Hart, S.R., Hauri, E.H., Oschmann, L.A. and Whitehead, J.A., 1992. Mantle plumes and entrainment: Isotopic evidence. *Science* 256, 517–520, doi:10.1126/science.256.5056.517.

Hart, S.R., Blusztajn, J. and Craddock, C., 1995. Cenozoic volcanism in Antarctica: Jones Mountains and Peter I Island. *Geochimica et Cosmochimica Acta* 59, 3379-3388, [http://dx.doi.org/10.1016/0016-7037\(95\)00212-I](http://dx.doi.org/10.1016/0016-7037(95)00212-I).

Hart, S. R., Blusztajn, J., LeMasurier, W.E., Rex, D.C., 1997. Hobbs Coast Cenozoic volcanism, implications for the West Antarctic rift system. *Chemical Geology* 139, 223–248, [http://dx.doi.org/10.1016/S0009-2541\(97\)00037-5](http://dx.doi.org/10.1016/S0009-2541(97)00037-5).

Hauri, E. H., Whitehead, J.A. and Hart, S.A., 1994. Fluid dynamic and geochemical aspects of entrainment in mantle plumes. *Journal of Geophysical Research* 99(B12), 24275-24300, <http://dx.doi.org/10.1029/94JB01257>.

Hein, J.R., Conrad, T.A., Staudigel, H., 2010. Seamount Mineral Deposits: A Source of Rare Metals for High-Technology Industries. *Oceanography* 23, 184–189, <http://dx.doi.org/10.5670/oceanog.2010.70>.

Heinemann, J., Stock, J., Clayton, R., Hafner, K., Cande, S. and Raymond, C., 1999. Constraints on the proposed Marie Byrd Land-Bellingshausen plate boundary from seismic reflection data. *Journal of Geophysical Research* 104(B11), 25321–25330, doi:10.1029/1998JB900079.

Hirschmann, M.M. and Stolper, E.M., 1996. A possible role for garnet pyroxenite in the origin of the "garnet signature" in MORB. *Contributions Mineralogy Petrology* 124, 185-208, doi:10.1007/s004100050184.

Hoernle, K., van den Bogaard, P., Werner, R., Lissina, B., Hauff, F., Alvarado, G., Garbe-Schönberg, D., 2002. Missing history (16-71 Ma) of the Galápagos Hotspot: Implications for the tectonic and biological evolution of the Americas. *Geology* 30, 795-798, doi:10.1130/0091-7613(2002)030<0795:mhmotg>2.0.co;2.

Hoernle K., Hauff, F., Werner, R., Mortimer, N., 2004. New Insights into the Origin and Evolution of the Hikurangi Oceanic Plateau (Southwest Pacific) from Multi-beam Mapping and Sampling. *EOS Transactions American Geophysical Union* 85(41), 401-408, <http://dx.doi.org/10.1029/2004EO410001>.

Hoernle, K., White, J.D.L., van den Bogaard, P., Hauff, F., Coombs, D.S., Werner, R., Timm, C., Garbe-Schoenberg, D., Reay, A. and Cooper, A.F., 2006. Cenozoic intraplate volcanism on New Zealand: upwelling induced by lithospheric removal. *Earth and Planetary Science Letters* 248, 350-367, <http://dx.doi.org/10.1016/j.epsl.2006.06.001>.

Hoernle, K., Hauff, F., van den Bogaard, P., Werner, R., Mortimer, N., Geldmacher, J., Garbe-Schoenberg, D., Davy, B., 2010. Age and Geochemistry of Volcanic Rocks from the Hikurangi and Manihiki Oceanic Plateaus. *Geochimica et Cosmochimica Acta* 74(24), 7196-7219, doi:10.1016/j.gca.2010.09.030.

Hoernle, K., Hauff, F., Werner, R., van den Bogaard, P., Gibbons, A.D., Conrad, S., Müller, R.D., 2011. Origin of Indian Ocean Seamount Province by shallow recycling of continental lithosphere. *Nature Geoscience* 4, 883-887, doi:10.1038/ngeo1331.

Hofmann, A.W. and White, W.M., 1982. Mantle plumes from ancient oceanic crust. *Earth and Planetary Science Letters* 57, 421-436, [http://dx.doi.org/10.1016/0012-821X\(82\)90161-3](http://dx.doi.org/10.1016/0012-821X(82)90161-3).

Hofmann, A.W., Jochum, K-P., Seufert, M. and White, W.M., 1986. Nb and Pb in oceanic basalts: new constraints on mantle evolution. *Earth and Planetary Science Letters* 79, 33-45, doi: 10.1016/0012-821X(86)90038-5.

Hofmann, A.W., 1988. Chemical differentiation of the Earth: the relationship between mantle, continental and oceanic crust. *Earth and Planetary Science Letters* 90, 297-314, doi: 10.1016/0012-821X(88)90132-X.

Hofmann, A.W., 2003. Sampling mantle heterogeneity through oceanic basalts: isotopes and trace elements, In: Carlson, R.W. (Ed.), *The Mantle and Core*. Elsevier, Amsterdam, pp. 61-101, <http://dx.doi.org/10.1016/B0-08-043751-6/02123-X>.

Hole, M.J. and LeMasurier, W.E., 1994. Tectonic controls on the geochemical composition of Cenozoic, mafic alkaline volcanic rocks from West Antarctica. *Contributions to Mineralogy and Petrology* 117, 187-202, doi:10.1007/BF00286842.

Huang, J., Zhong, S. and van Hunen, J., 2003. Controls on sub-lithospheric small-scale convection. *Journal of Geophysical Research* 108(B8), 2405, doi:10.1029/2003JB002456.

Hutnak, M., Fisher, A.T., Harris, R., Stein, C., Wang, K., Spinelli, G., Schindler, M., Villinger, H., Silver, E., 2008. Large heat and fluid fluxes driven through mid-plate outcrops

on ocean crust. *Nature Geoscience* 1, 611-614, doi:10.1038/ngeo264.

Irvine, T.N. and Baragar, W.R.A., 1971. A guide to the chemical classification of the common volcanic rocks. *Canadian Journal of Earth Sciences* 8, 523-548, doi:10.1139/e71-055.

King, S.D. and Anderson, D.L., 1995. An alternative mechanism to flood basalt formation. *Earth and Planetary Science Letters* 136, 269-279, [http://dx.doi.org/10.1016/0012-821X\(95\)00205-Q](http://dx.doi.org/10.1016/0012-821X(95)00205-Q).

King, S.D. and Anderson, D.L., 1998. Edge-Driven Convection. *Earth Planetary Science Letters* 160, 289-296, [http://dx.doi.org/10.1016/S0012-821X\(98\)00089-2](http://dx.doi.org/10.1016/S0012-821X(98)00089-2).

King, S.D. and Ritsema, J., 2000. African hotspot volcanism: small-scale convection in the upper mantle beneath cratons. *Science* 290, 1137-1140, doi:10.1126/science.290.5494.1137.

Klügel, A., Hansteen, T.H., van den Bogaard, P., Strauss, H., Hauff, F., 2011. Holocene fluid venting at an extinct Cretaceous seamount, Canary archipelago. *Geology* 39, 855–858, doi:10.1130/G32006.1.

Koppers, A.A.P., Yamazaki, T., Geldmacher, J., Gee, J.S., Pressling, N. and IODP Expedition 330 Scientific Party, 2012. Limited latitudinal mantle plume motion for the Louisville hotspot. *Nature Geoscience* 5, 911-917, doi:10.1038/ngeo1638.

Larter, R.D., Cunningham, A.P., Barker, P.F., Gohl, K. and Nitsche, F.O., 2002. Tectonic evolution of the Pacific margin of Antarctica – 1. Late Cretaceous tectonic reconstructions. *Journal of Geophysical Research* 107(B12), 2345, doi:10.1029/2000JB000052.

LeMasurier, W.E., Thomson, J.W., Baker, P., Kyle, P., Rowley, P., Smellie, J. and W. Verwoerd (Eds.) 1990. *Volcanoes of the Antarctic Plate and Southern Oceans*. Antarctic Research Series 48, pp. 487, AGU, Washington, D. C. doi:10.1029/AR048.

Lowman, J.P. and Jarvis, G.T., 1995. Mantle convection models of continental collision and

breakup incorporating finite thickness plates. *Physics of the Earth and Planetary Interiors* 88, 53-68, [http://dx.doi.org/10.1016/0031-9201\(94\)05076-A](http://dx.doi.org/10.1016/0031-9201(94)05076-A).

Lowman, J.P. and Jarvis, G.T., 1996. Continental collisions in wide aspect ratio and high Rayleigh number two-dimensional mantle convection models. *Journal of Geophysical Research* 101(B11), 25485-25497, <http://dx.doi.org/10.1029/96JB02568>.

McAdoo, D.C. and Laxon, S., 1997. Antarctic tectonics: constraints from an ERS-1 satellite marine gravity field. *Science* 276, 556-560, doi:10.1126/science.276.5312.556.

McCoy-West, A.J., Baker, J.A., Faure, K. and Wysoczanski, R., 2010. Petrogenesis and origins of mid-Cretaceous continental intraplate volcanism in Marlborough, New Zealand: implications for the long-lived HIMU magmatic mega-province of the SW Pacific. *Journal of Petrology* 51, 2003-2045, doi:10.1093/petrology/egq046.

McDonough, W.F., Sun, S.-s., 1995. The composition of the earth. *Chemical Geology* 120, 223-253, doi:10.1016/0009-2541(94)00140-4.

McMurtry, G.M., Fryer, G.J., Tappin, D.R., Wilkinson, I.P., Williams, M., Fietzke, J., Garbe-Schönberg, D., Watts, P., 2004. Megatsunami deposits on Kohala volcano, Hawaii, from flank collapse of Mauna Loa. *Geology* 32, 741-744, doi: 10.1130/G20642.1.

Miller, H., Grobe, H., 1996. The expedition ANTARKTIS-XI/3 of RV 'Polarstern' in 1994. *Berichte zur Polarforschung*, No. 188, [http:// epic.10189.d001](http://epic.10189.d001).

Montelli, R., Nolet, G., Dahlen, F.A., Masters, G., 2006. A catalogue of deep mantle plumes: New results from finite-frequency tomography. *Geochemistry, Geophysics, Geosystems* 7, Q11007, <http://dx.doi.org/10.1029/2006GC001248>.

Morgan, W.J., 1971. Convection plumes in the lower mantle. *Nature* 230, 42-43, doi:10.1038/230042a0.

Müller, R.D., Gaina, C., Tikku, A., Mihut, D., Cande, S.C. and Stock, J.M., 2000.

Mesozoic/Cenozoic tectonic events around Australia. *Geophysical Monograph* 121, 161-188, doi:10.1029/GM121p0161.

Müller, R.D., Gohl, K., Cande, S.C., Goncharov, A. and Golynsky, A.V., 2007. Eocene to Miocene geometry of the West Antarctic Rift System. *Australian Journal of Earth Sciences* 54, 1033–1045, doi:10.1080/08120090701615691.

Mutter, J.C., Buck, W.R. and Zehnder, C.M., 1988. Convective partial melting 1. A model for the formation of thick basaltic sequences during the initiation of spreading. *Journal of Geophysical Research* 93(B2), 1031–1048, <http://dx.doi.org/10.1029/JB093iB02p01031>.

Nardini, I., Armienti, P., Rocchi, S., Dallai, L., Harrison, D., 2009. Sr-Nd-Pb-He-O Isotope and Geochemical Constraints on the Genesis of Cenozoic Magmas from the West Antarctic Rift. *Journal of Petrology* 50(7), 1359-1375, doi:10.1093/petrology/egn082.

Natland, J.H., Winterer, E.L., 2005. Fissure control on volcanic action in the Pacific, In: Foulger, G.R., Natland, J.H., Presnall, D.C., Anderson, D.L. (Eds.), *Plumes, Plates and Paradigms*. Geological Society of America, Boulder CO, pp. 687-710, doi: 10.1130/0-8137-2388-4.687.

Panter, K.S., Kyle, P.R. and Smellie, J.L., 1997. Petrogenesis of a Phonolite-Trachyte Succession at Mount Sidley, Marie Byrd Land, Antarctica. *Journal of Petrology* 38(9), 1225-1253, doi:10.1093/petroj/38.9.1225.

Panter, K.S., Hart, S.R., Kyle, P., Blusztajn, J., Wilch, T., 2000. Geochemistry of Late Cenozoic basalts from the Crary Mountains: characterization of mantle sources in Marie Byrd Land, Antarctica. *Chemical Geology* 165, 215–241, [http://dx.doi.org/10.1016/S0009-2541\(99\)00171-0](http://dx.doi.org/10.1016/S0009-2541(99)00171-0).

Panter, K.S., Blusztajn, J., Hart, S.R., Kyle, P.R., Esser, R. and McIntosh W.C., 2006. The origin of HIMU in the SW Pacific: evidence from intraplate volcanism in southern New Zealand and Subantarctic islands. *Journal of Petrology* 47, 1673-1704, doi:10.1093/petrology/egl024.

Portnyagin, M., Savelyev, D., Hoernle, K., Hauff, F., Garbe-Schönberg, D., 2008. Mid-Cretaceous Hawaiian tholeiites preserved in Kamchatka. *Geology* 36, 903-906, doi:10.1130/g25171a.1.

Prestvik, T., Barnes, C.G., Sundvoll, B. and Duncan, R.A., 1990. Petrology of Peter I Øy (Peter I Island), West Antarctica. *Journal of Volcanology and Geothermal Research* 44, 315-338, [http://dx.doi.org/10.1016/0377-0273\(90\)90025-B](http://dx.doi.org/10.1016/0377-0273(90)90025-B).

Prestvik, T., and Duncan, R.A., 1991. The geology and age of Peter I Øy, Antarctica. *Polar Research* 9, 89-98, doi:10.1111/j.1751-8369.1991.tb00404.x.

Rocchi, S., Armienti, P., D'Orazio, M., Tonarini, S., Wijbrans, J., Di Vincenzo, G., 2002a. Cenozoic magmatism in the western Ross Embayment: role of mantle plume versus plate dynamics in the development of the West Antarctic Rift System. *Journal of Geophysical Research* 107(B9), 2195, <http://dx.doi.org/10.1029/2001JB000515>.

Rocchi, S., LeMasurier, W.E. and Di Vincenzo, G., 2002b. Uplift and erosion history in Marie Byrd Land as a key to possible mid-Cenozoic plate motion between East and West Antarctica. *Geological Society of America Abstract Programs* 34(6), 238.

Rocholl, A., Stein, M., Molzahn, M., Hart, S.R., Wörner G., 1995. Geochemical evolution of rift magmas by progressive tapping of a stratified mantle source beneath the Ross Sea Rift, Northern Victoria Land, Antarctica. *Earth and Planetary Science Letters* 131, 207-224, [http://dx.doi.org/10.1016/0012-821X\(95\)00024-7](http://dx.doi.org/10.1016/0012-821X(95)00024-7).

Rudnick, R.L., 1995. Making continental crust. *Nature* 378, 571-578, doi:10.1038/378571a0.

Safonova, I.Y., 2009. Intraplate magmatism and oceanic plate stratigraphy of the Paleo-Asian and Paleo-Pacific Oceans from 600 to 140 Ma. *Ore Geology Reviews* 35, 137-154, doi:10.1016/j.oregeorev.2008.09.002.

Safonova, I.Y., Santosh, M., in press. Accretionary complexes in the Asia-Pacific region:

Tracing archives of ocean plate stratigraphy and tracking mantle plumes. *Gondwana Research*, doi:10.1016/j.gr.2012.10.008.

Salters, V.J.M. and Stracke A., 2004. Composition of the depleted mantle. *Geochemistry Geophysics Geosystems* 5, Q05B07, doi:10.1029/2003GC000597.

Shank, T.M., 2010. Seamounts: Deep-Ocean Laboratories of Faunal Connectivity, Evolution, and Endemism. *Oceanography* 23, 108–122, <http://dx.doi.org/10.5670/oceanog.2010.65>.

Smith, W.H.F. and Sandwell, D.T, 1997. Global sea floor topography from satellite altimetry and ship depth soundings. *Science* 277, 1956–1962, doi:10.1126/science.277.5334.1956.

Soager, N., Holm, P.M., Llambias, E.J., 2013. Payenia volcanic province, southern Mendoza, Argentina: OIB mantle upwelling in a backarc environment. *Chem Geol* 349-350, 36-53, <http://dx.doi.org/10.1016/j.chemgeo.2013.04.007>.

Stock, J.M., 1997. Geophysical Secrets Beneath Antarctic Waters. *Engineering Sciences* 60 (3),18-27.

Storey, B.C., Leat, P.T., Weaver, S.D., Pankhurst, R.J., Bradshaw, J.D. and Kelley, S., 1999. Mantle plumes and Antarctica–New Zealand rifting; evidence from Mid-Cretaceous mafic dykes. *Journal of the Geological Society* 156, 659–671, <http://dx.doi.org/10.1144/gsjgs.156.4.0659>.

Stracke, A., 2012. Earth's heterogeneous mantle: A product of convection-driven interaction between crust and mantle. *Chemical Geology* 330-331, 274-299, <http://dx.doi.org/10.1016/j.chemgeo.2012.08.007>.

Suetsugu D., Isse, T., Tanaka, S., Obayashi, M., Shiobara, H., Sugioka, H., Kanazawa, T., Fukao, Y., Barruol, G. and Reymond, D., 2009. South Pacific mantle plumes imaged by seismic observation on islands and seafloor. *Geochemistry Geophysics Geosystems* 10, Q11014. doi:10.1029/2009GC002533.

Sun, S. S. and McDonough, W.F., 1989. Chemical and isotopic systematics of oceanic basalts: implications for mantle composition and processes. In: Saunders, A. D. & Norry, M. J. (eds) *Magmatism in the Ocean Basins*. Geological Society Special Publications 42, 313-345, doi:10.1144/GSL.SP.1989.042.01.19.

Sutherland, R., Spasojevic, S., Gurnis, M., 2010. Mantle upwelling after Gondwana subduction death explains anomalous topography and subsidence history of eastern New Zealand and West Antarctic. *Geology* 38, 155–158, doi:10.1130/G30613.1.

Tang, Y.-J., Zhang, H.-F., Ying, J.-F., Su, B.-X., 2013. Widespread refertilization of cratonic and circum-cratonic lithospheric mantle. *Earth-Science Reviews* 118, 45-68, <http://dx.doi.org/10.1016/j.earscirev.2013.01.004>.

Tappenden, V.E., 2003. Magmatic response to the evolving New Zealand margin of Gondwana during the Mid-Late Cretaceous. PhD thesis, University of Canterbury, Christchurch, New Zealand.

Tarduno, J.A., Duncan, R.A., Scholl, D.W., Cottrell, R.D., Steinberger, B., Thordason, T., Kerr, B.C., Neal, C.R., Frey, F.A., Torii, M., Carvallo, C., 2003. The Emperor seamounts: Southward motion of the Hawaiian hotspot plume in earth's mantle. *Science* 301, 1064-1069, doi:10.1126/science.1086442.

Taylor, B., 2006. The single largest oceanic plateau: Ontong Java-Manihiki-Hikurangi. *Earth and Planetary Science Letters* 241, 372-380, doi:10.1016/j.epsl.2005.11.049.

Timm, C., Hoernle, K., Werner, R., Hauff, F., van den Bogaard, P., White, J., Mortimer, N., Garbe-Schoenberg, D., 2010. Temporal and geochemical evolution of the Cenozoic intraplate volcanism of Zealandia. *Earth-Science Reviews* 98, 38-64, doi:10.1016/j.earscirev.2009.10.002.

Timm, C., Hoernle, K., Werner, R., Hauff, F., van den Bogaard, P., Michael, P., Coffin, M. and Koppers, A., 2011. *Age and geochemistry of the oceanic Manihiki Plateau, SW Pacific:*

new evidence for a plume origin. Earth and Planetary Science Letters 304 (1-2), 135-146, doi: 10.1016/j.epsl.2011.01.025.

Udintsev, G.B., Kurentsova, N.A., Teterin, D.E. and Roshchina, I.A., 2007. Petrology of the Hubert Miller Seamount, Marie Byrd Seamounts Province, West Antarctic, Southern Ocean. Doklady Earth Sciences 415A 6, 895-900, doi:10.1134/S1028334X07060141.

Uenzelmann-Neben, G. and Gohl, K., 2012. Amundsen Sea sediment drifts: Archives of modifications in oceanographic and climatic conditions, Marine Geology, 299-302, 51-62 doi:10.1016/j.margeo.2011.12.007.

Watts, A.B., Koppers, A.A.P., Robinson, D.P., 2010. Seamount Subduction and Earthquakes. Oceanography 23(1), 166–173, <http://dx.doi.org/10.5670/oceanog.2010.68#sthash.6fn0xSSg.dpuf>.

Weaver, S.D. and Pankhurst, R.J. 1991. A precise Rb-Sr age for the Mandamus Igneous Complex, North Canterbury, and regional tectonic implications. New Zealand Journal of Geology and Geophysics 34, 341-345, doi:10.1080/00288306.1991.9514472.

Weaver, S.D., Storey, B.C., Pankhurst, R.J., Mukasa, S.B., DiVenere, V.J., and Bradshaw, J.D., 1994. Antarctica-New Zealand rifting and Marie Byrd Land lithospheric magmatism linked to ridge subduction and mantle plume activity. Geology 22, 811-814, doi:10.1130/0091-7613(1994)022<0811:ANZRAM>2.3.CO;2.

Wessel, P., Sandwell, D.T., Kim, S.-S., 2010. The global seamount census. Oceanography 23, 24–33, <http://dx.doi.org/10.5670/oceanog.2010.60>.

White, W.M., 2010. Oceanic Island Basalts and Mantle Plumes: The Geochemical Perspective. Annual Review of Earth and Planetary Sciences 38, 133-160, doi:10.1146/annurev-earth-040809-152450.

Willbold, M., Stracke, A., 2010. Formation of enriched mantle components by recycling of upper and lower continental crust. Chemical Geology 276, 188-197,

<http://dx.doi.org/10.1016/j.chemgeo.2010.06.005>.

Wilson, J.T., 1963. Evidence from islands on the spreading of the ocean floor. *Nature* 197, 536-538, doi:10.1038/197536a0.

Winterer, E.L., Sandwell, D.T., 1987. Evidence from en-echelon cross-grain ridges for tensional cracks in the Pacific plate. *Nature* 329, 534-537, doi:10.1038/329534a0.

Wobbe, F., Gohl, K., Chambord, A., Sutherland, R., 2012. Structure and breakup history of the rifted margin of West Antarctica in relation to Cretaceous separation from Zealandia and Bellingshausen plate motion. *Geochemistry Geophysics Geosystems* 13, Q04W12, doi:10.1029/2011GC003742.

Workman, R. K. and Hart, S.R., 2005. Major and trace element composition of the depleted MORB mantle (DMM). *Earth Planetary Science Letters* 231, 53-72, <http://dx.doi.org/10.1016/j.epsl.2004.12.005>.

Zindler, A., and Hart, S.R., 1986. Chemical Geodynamics. *Annual Review of Earth and Planetary Sciences* 14, 493-571, <http://dx.doi.org/10.1146/annurev.ea.14.050186.002425>.

CHAPTER II

Granitoids and dikes of the Pine Island Bay region, West Antarctica

Andrea Kipf¹, Nicholas Mortimer², Reinhard Werner^{1*}, Karsten Gohl³, Paul van den Bogaard¹, Folkmar Hauff¹, Kaj Hoernle¹

¹ Helmholtz-Zentrum für Ozeanforschung Kiel (GEOMAR), Wischhofstr. 1-3, D-24148 Kiel, Germany

² GNS Science, Private Bag 1930, Dunedin, New Zealand

³ Alfred-Wegener-Institut für Polar- und Meeresforschung, Postfach 120161, D-27515 Bremerhaven, Germany

Published in Antarctic Science

ABSTRACT

We present geochronological and geochemical data for eight plutonic rocks from five locations in the Pine Island Bay area of West Antarctica, collected during R/V Polarstern expedition ANT-XXIII/4. Ar/Ar dating yielded closure temperatures of c. 147 to 98 Ma for dioritic and granitic plutonic rocks and an age range of c. 97 to 95 Ma for granitoid and trachyandesitic dikes. Major and trace element compositions indicate that all rocks have an I-type subduction-related chemistry. There are no A-type granitic rocks in our dataset, and none are yet reported from the Pine Island Bay area. Our results confirm earlier models of post-100 Ma subduction on this part of the Gondwana margin.

1. INTRODUCTION

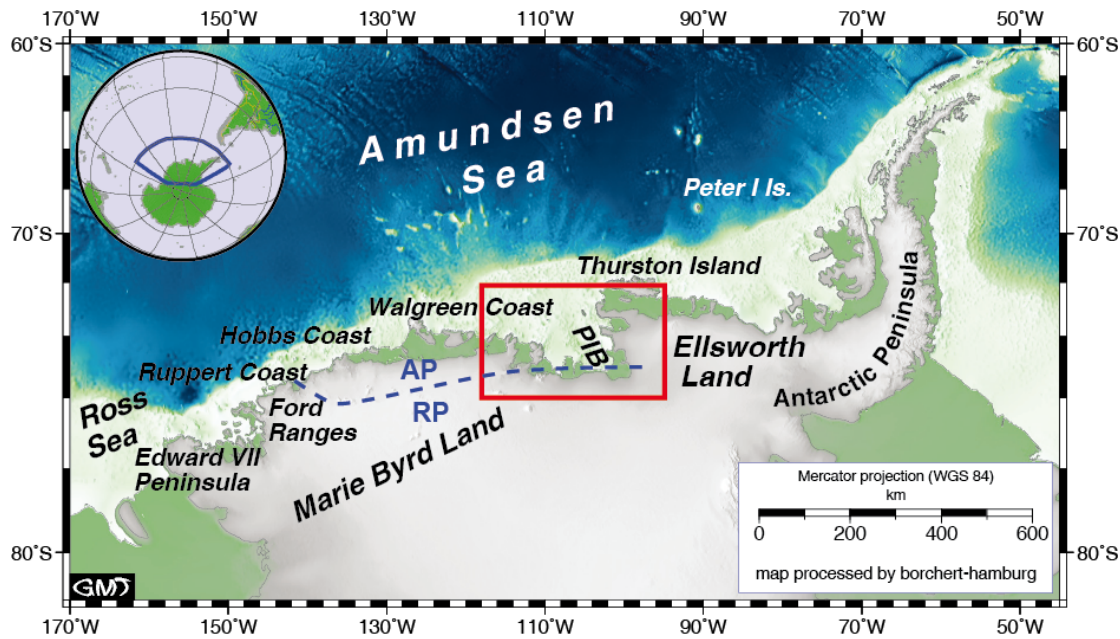


Fig. 1. Overview map of West Antarctica. The red box indicates the map area shown in Fig. 2, the dashed blue line marks the boundary between Amundsen (AP) and Ross Provinces (RP) after Pankhurst *et al.* (1998). Map based on ETOPO 1-minute grid (Smith & Sandwell 1997). PIB=Pine Island Bay.

Coastal West Antarctica (Fig. 1) consists of three major crustal blocks, Marie Byrd Land (MBL), Thurston Island and the Antarctic Peninsula (e.g. Vaughan & Storey 2000). The Thurston Island block is separated from the MBL block by Pine Island Bay, and from the Antarctic Peninsula block by Eltanin Bay and Ronne Entrance. Whether the deep glacial troughs of both embayments follow the block boundaries, is still unknown. Until 90-83 Ma, West Antarctica formed part of the Gondwana supercontinent along with Zealandia and Australia. The conjugate margins of West Antarctica and Zealandia are key locations for understanding processes that cause supercontinent breakup. Whereas reasonably comprehensive Cretaceous geological datasets and syntheses exist for Zealandia (e.g. Tulloch & Kimbrough 2003, Tulloch *et al.* 2009), Marie Byrd Land (e.g. Weaver *et al.* 1992, 1994, Pankhurst *et al.* 1998, Storey *et al.* 1999, Mukasa & Dalziel 2000) and the Antarctic Peninsula (e.g. Leat *et al.* 1995, Wareham *et al.* 1997, Vaughan & Storey 2000), much less is known about the Thurston Island block because of more remote access and greater ice-sheet coverage.

During R/V Polarstern expedition ANT-XXIII/4 to the Amundsen Sea embayment in 2006, several ice-free basement outcrops were visited along the coast of easternmost MBL and on small islands in Pine Island Bay that are part of the Thurston Island block (Fig. 2).

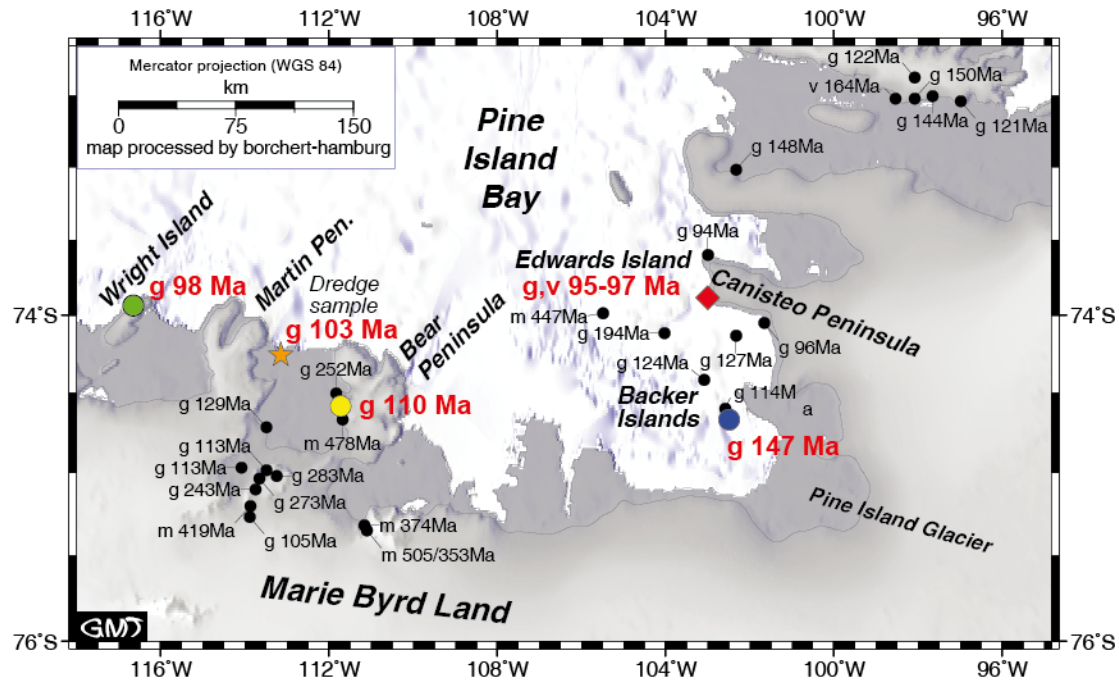


Fig. 2. Overview map of the Walgreen Coast and Pine Island Bay area. R/V Polarstern expedition ANT-XXIII/4 sampling sites of the igneous basement are marked by coloured symbols (the same coloured symbols are used in subsequent figures). Bold red numbers indicate Ar/Ar ages presented in this study, small black numbers published age data from Pankhurst *et al.* (1993, 1998) and Mukasa & Dalziel (2000). U-Pb ages are marked by black squares. Letters indicate rock types which have been dated (g = granitoids, m = metamorphic rocks, v = volcanic rocks). Map based on ETOPO 1-minute grid (Smith & Sandwell 1997).

In the course of this expedition, four of these outcrops were surveyed and sampled using small boat and helicopter support. Subsequently dredge material from a fifth location was obtained. In this paper, we report results of Ar-Ar radiometric dating and geochemical analyses of the recovered plutonic and dike rocks. The data and results presented in this study contribute to the small but growing geological understanding of this part of the Antarctic margin.

2. GEOLOGICAL AND TECTONIC SETTING

Geological knowledge of the Pine Island Bay area (Fig. 2) is based on early reconnaissance mapping along the coast by, for example, Craddock *et al.* (1964) and later geochronological and geochemical sampling by Leat *et al.* (1993), Pankhurst *et al.* (1993, 1998) and Mukasa & Dalziel (2000). This work has shown that episodic I-type subduction-related plutonism and volcanism occurred from the Permian to the Early Cretaceous throughout the Pine Island Bay-Thurston Island area, and that minor older gneissic basement is also present. The West Antarctica coastline provides a very oblique cross section across the Mesozoic-Paleozoic orogenic belts of Gondwana. Pankhurst *et al.* (1998) divided MBL into two geological provinces, Ross Province in the west and Amundsen Province in the east, with the boundary approximately at longitude 140°W (Fig. 1). The Amundsen Province (which includes Pine Island Bay), is a Permian to Mesozoic Gondwana-margin batholithic belt that is spatially continuous with the Pacific Margin Magnetic Anomaly of Maslanyj & Storey (1990), the Antarctic Peninsula batholith of Leat *et al.* (1995) and the Central Domain of Vaughan and Storey (2000). Prior to Gondwana breakup the batholith also continued into the Median Batholith of New Zealand (Pankhurst *et al.* 1998).

Several studies have addressed the age of cessation of subduction-related magmatism in West Antarctica. In MBL, a 124-108 Ma suite of calc-alkalic, metaluminous I-type granitoids reflects the final stage of subduction prior to its cessation beneath the Zealandia/West Antarctic Gondwana margin (e.g. Bradshaw 1989, Weaver *et al.* 1994). According to Weaver *et al.* (1994), subduction ceased at 105 Ma in western MBL (Ruppert and Hobbs Coast). The onset of intracontinental rifting in western MBL is clearly indicated by 102-95 Ma alkalic, metaluminous to peralkaline A-type granitoids, which make up about 75% of the exposed rocks at the Ruppert-Hobbs coast (e.g. Weaver *et al.* 1994). These interpretations were supported by the western MBL U-Pb study of Mukasa and Dalziel (2000) who reported their youngest dated subduction-related I-type pluton to be 110 Ma, A-type plutons to range from 102-98 Ma and rift-related mafic and intermediate dikes to be 101±1 Ma. Siddoway *et al.* (2004) interpreted mylonitic gneisses and granites to be an indication of crustal extension in western MBL at 98-95 Ma.

In eastern MBL (Walgreen Coast to western Pine Island Bay, Fig. 1), which had Chatham Rise between it and the subducting margin, subduction-related I-type magmatism occurred at

least until 94 ± 3 Ma (U-Pb zircon date), the implication being that, in MBL, subduction ceased earlier in the west than in the east (Mukasa & Dalziel, 2000). The change from subduction to rifting has been related to forces acting upon the plate margins by interaction of the paleo-subduction zone at the Zealandia/MBL margin of Gondwana with (1) the Pacific-Phoenix spreading centre (e.g., Bradshaw 1989, Luyendyk 1995, Mukasa & Dalziel 2000), (2) the collision of the Hikurangi Plateau with Zealandia (e.g., Bradshaw 1989, Davy *et al.* 2008), and/or (3) the activity of a mantle plume (e.g., Weaver *et al.* 1994, Storey *et al.* 1999, Hoernle *et al.* 2010). Storey *et al.* (1999), for example, claim to have identified HIMU Pb-isotope signatures (high time-integrated U/Pb-ratios in the source region) in Late Cretaceous mafic alkaline dikes of MBL, which may indicate the involvement of a mantle plume in the final breakup.

3. SAMPLE BACKGROUND

Rock sampling was conducted on Wright Island and Bear Peninsula along the Walgreen Coast and on two islands within Pine Island Bay, an area that has been sampled by earlier expeditions (Fig. 2, Table 1). Additionally, a granitic sample (DR 193.1, kindly provided by R. D. Larter, British Antarctic Survey) dredged c. 40 km west of Bear Peninsula at c. 600 m water depth during R/V James C. Ross cruise JR141 has been dated for this study, but not geochemically analysed because of the small sample size.

At the north-western coast of Wright Island of Walgreen Coast, huge cliffs expose outcrops of relatively fine-grained crystalline basement (Fig. 3A, samples PS69/277-1 and 7), cut by several (inaccessible) dikes. Dark biotite-rich inclusions and dikes a few cm wide are common at the sampling site. On Bear Peninsula, relatively homogeneous, coarse-grained granitic rocks outcrop ~490 m above sea level on top of a smooth hill (sample PS69/BI-5). A weakly developed foliation in the granitic rocks, the common occurrence of dark xenoliths (most likely meta-sediment) and intercalated siliceous layers may indicate that this outcrop represents the edge (or roof) of a pluton, probably intruding the gneissic rocks reported and dated by Pankhurst *et al.* (1998).

Table 1: Sample locations.

No. PS69-	Location Name	Sample Type	Latitude deg_min	Longitude deg_min	Elevation a.s.l.
277-1	Wright Island	granodiorite	73°57.72'S	116°52.38'W	3 m
277-7	Wright Island	syeno-diorite	73°57.72'S	116°52.38'W	3 m
BI-5	Bear Peninsula	granite	74°34.74'S	111°53.38'W	470-490 m
PIB-1	Backer Islands	granite	74°30.66'S	102°26.36'W	6 m
LI-1	Edwards Island	trachyandesitic dike	73°51.17'S	102°59.33'W	10 m
LI-2	Edwards Island	alkali-granitic	73°51.17'S	102°59.33'W	2 m
LI-3	Edwards Island	alkali-granitic	73°51.17'S	102°59.33'W	5 m
DR193.1	c. 20 nm W off Bear Peninsula	granite	74°09.30'S	112°50.8'W	600 m b.s.l.

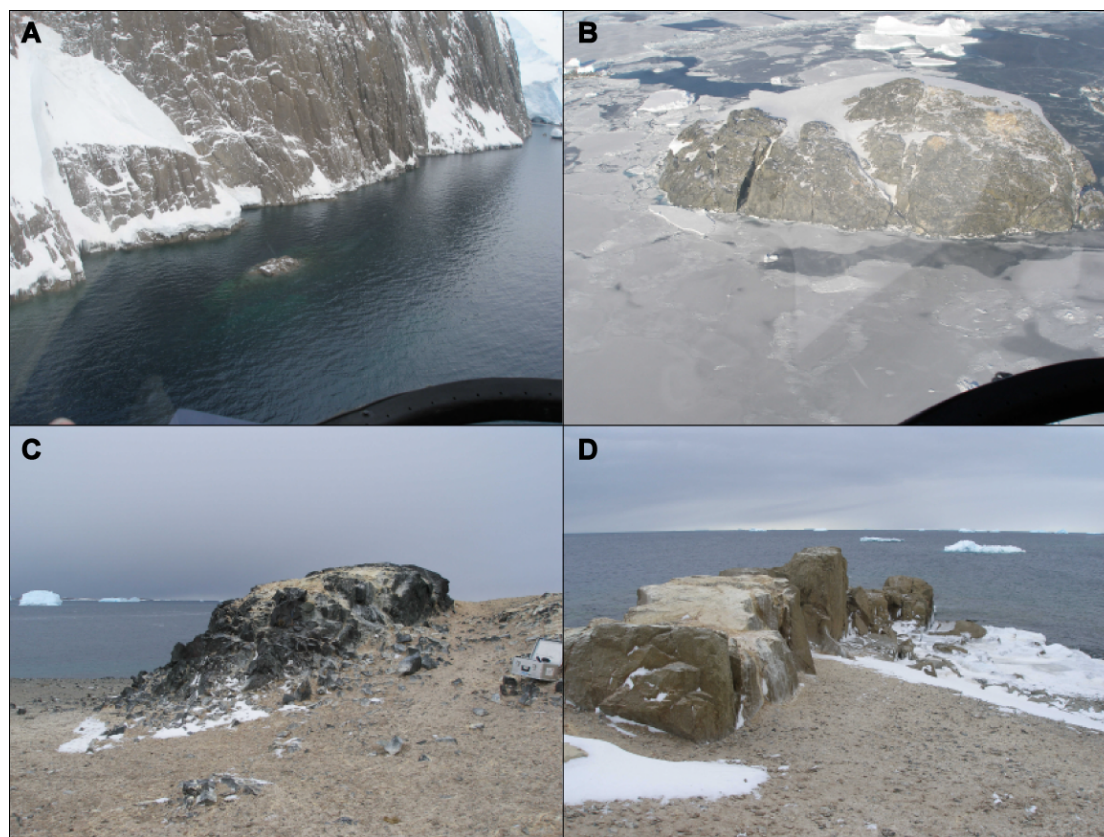


Fig. 3. Outcrops in the Walgreen Coast - Pine Island Bay area. A: Huge cliffs expose crystalline basement at the north-western coast of Wright Island. Samples PS69/277-1 and -7 were taken from the small island in front of the cliffs. B: Most islands surveyed on cruise ANTXXIII/4 in the Pine Island Bay consist mainly of granitic rocks. C: A porphyritic dike (sample PS69/LI-1) and D: granitic rocks (samples PS69/LI-2 and -3) on Edwards Island. Note the dike-like structure of the granitic outcrop.

In Pine Island Bay, Backer Islands (sample PS69/PIB-1) are part of a prominent southeast-northwest striking island chain, which extends from Ellsworth Land (“Evans Knoll”) beneath the ice-shelf north of the Pine Island Glacier. These islands mainly consist of granitic rocks and our sample was taken from the southern part of the island chain (Fig. 3B; cf. Mukasa & Dalziel 2000). In contrast, an island group west of Canisteo Peninsula is marked by a succession of east-west striking dikes, up to a few meters wide. Our field observations on Edwards Island revealed black porphyritic dikes (Fig. 3C; sample PS69/LI-1) alternating with light, holocrystalline granitic rocks (samples PS69/LI-2 to 3). The granitic rocks also show a dike-like morphology (Fig. 3D), but it is not evident from field observations whether the trachyandesitic dikes intruded into a granitic host rock or all the rocks exposed on Edwards Island are dikes. Radiometric dating (see below) indicates, however, that formation and cooling of the granitic rocks occurred at the same time and after the emplacement of the trachyandesitic dikes. Therefore Edwards Island most likely consists of a succession of trachyandesitic and granitic dikes as suggested by the structure of the outcrops.

4. ANALYTICAL METHODS

Samples selected for geochemistry were first crushed, then repeatedly washed in deionised water and thereafter carefully handpicked under a binocular microscope. Major and trace element data were analyzed at SARM laboratories (Service d'Analyse des Roches et des Mineraux) in France. Major elements were determined using an ICP-OES IRIS Advantage ERS – ThermoFisher, trace elements using an ICP-MS X7 – ThermoFisher. Standards BR, DR-N, UB-N, AN-G and GH were used for calibration. For a more detailed description of methods and reference materials see Carignan *et al.* (2001). The Sr-Nd-Pb isotopic composition of sample PS69/LI-1 was determined at Helmholtz Centre for Ocean Research Kiel (GEOMAR) by thermal ionisation mass spectrometry (TIMS) following the methods outlined in Hoernle *et al.* (2010). Measured and initial isotopic ratios along with standard values are shown in Table 2.

$^{40}\text{Ar}/^{39}\text{Ar}$ analyses were conducted on biotite and feldspar phenocrysts at the GEOMAR Geochronology Laboratory. The crystals were handpicked from crushed and sieved splits. Feldspar phenocrysts were etched in diluted hydrofluoric acid. All separates were cleaned using an ultrasonic disintegrator.

Minerals were irradiated in aluminium trays with a cadmium lining at the 5MW reactor of the Helmholtz-Zentrum Geesthacht, Centre of Materials and Coastal Research (GKSS). The neutron flux was monitored using Taylor Creek Rhyolite sanidine (TCR-2: 27.87 ± 0.04 Ma; Lanphere & Dalrymple 2000). $^{40}\text{Ar}/^{39}\text{Ar}$ laser step-heating analyses were carried out with a 20W SpectraPhysics Argon-Ion laser and an MAP 216 series noble gas mass spectrometer. Ar isotope ratios were corrected for mass discrimination, background and blank values, J-value gradients, and interfering neutron reactions on Ca and K.

Table 2: Sr-Nd-Pb isotope ratios of sample PS69/LI-1

Sample	PS69/LI-1
Age(My)	97.1
$^{87}\text{Sr}/^{86}\text{Sr}$	0.705455
2 SE(M)	0.000005
Rb (ppm)	56.3
Sr (ppm)	693
$^{87}\text{Rb}/^{86}\text{Sr}$	0.235
$^{87}\text{Sr}/^{86}\text{Sr}_i$	0.705131
$^{143}\text{Nd}/^{144}\text{Nd}$	0.512596
2 SE(M)	0.000002
eNd	-0.81
Sm (ppm)	5.26
Nd (ppm)	28.2
$^{147}\text{Sm}/^{144}\text{Nd}$	0.112
$^{143}\text{Nd}/^{144}\text{Nd}_i$	0.512525
eNd _i	0.23
$^{206}\text{Pb}/^{204}\text{Pb}$	18.8452
2 SE(M)	0.0006
$^{207}\text{Pb}/^{204}\text{Pb}$	15.6396
2 SE(M)	0.0005
$^{208}\text{Pb}/^{204}\text{Pb}$	38.6728
2 SE(M)	0.0015
Pb (ppm)	12.3
U (ppm)	1.82
Th (ppm)	8.16
$^{238}\text{U}/^{204}\text{Pb}$	9.48
$^{232}\text{Th}/^{204}\text{Pb}$	43.9
$^{206}\text{Pb}/^{204}\text{Pb}_i$	18.70
$^{207}\text{Pb}/^{204}\text{Pb}_i$	15.63
$^{208}\text{Pb}/^{204}\text{Pb}_i$	38.46

Standards measured along with the sample were normalized and gave $^{87}\text{Sr}/^{86}\text{Sr} = 0.710250 \pm 10$ (n=10, 2s external) for NBS987 on the MAT262 and $^{143}\text{Nd}/^{144}\text{Nd} = 0.511850 \pm 8$ (n=13, 2s external) for La Jolla on the TRITON. Pb double-spike corrected values for NBS981 are $^{206}\text{Pb}/^{204}\text{Pb} = 16.9416 \pm 21$, $^{207}\text{Pb}/^{204}\text{Pb} = 15.4996 \pm 20$ and $^{208}\text{Pb}/^{204}\text{Pb} = 36.7231 \pm 52$ (n=45; 2σ external) on the MAT262

during the time period 2006-2008 when the data for this sample was acquired. All errors refer to the last significant digit. $2\text{ SE (M)} = 2\text{ sigma error of the mean}$; $_i$ = initial isotopic ratio using the age (Table 2) and the trace element concentrations (Table 3) of the sample.

Step-heating results are plotted in age spectra (apparent age and error vs. cumulative ^{39}Ar). Statistical plateaus are defined as more than 3 consecutive steps comprising $>50\%$ of the ^{39}Ar released, with ages overlapping within 2σ errors.

$^{36}\text{Ar}/^{39}\text{Ar}$ ratios (biotite, K-feldspar) and $^{36}\text{Ar}/^{37}\text{Ar}$ ratios (plagioclase), both corrected for neutron reactions on Ca and normalized to $J=0.01$, are monitored to assess the variable degree of alteration of the samples (Baksi 2007) and heating steps with excessively high alteration indices are excluded from plateau age calculations. Plateau ages represent the inverse-variance weighted mean of the (accepted) plateau steps ages and errors (2σ). Statistical robustness of plateaus and plateau ages are tested by the MSWD (mean square weighted deviates) and probability of fit (which should be >0.05 at $2s/95\%$ confidence levels) (Baksi 2007 and references therein).

5. RESULTS

5.1 Petrography and Classification

All sampled plutonic rocks are coarse-grained, (equi-) granular, holocrystalline, leucocratic granitoids. They range from medium-K syeno-diorites and high-K granodiorites on Wright Island to subalkaline (medium-K) granites on Bear Peninsula and Backer Islands (Fig. 4).

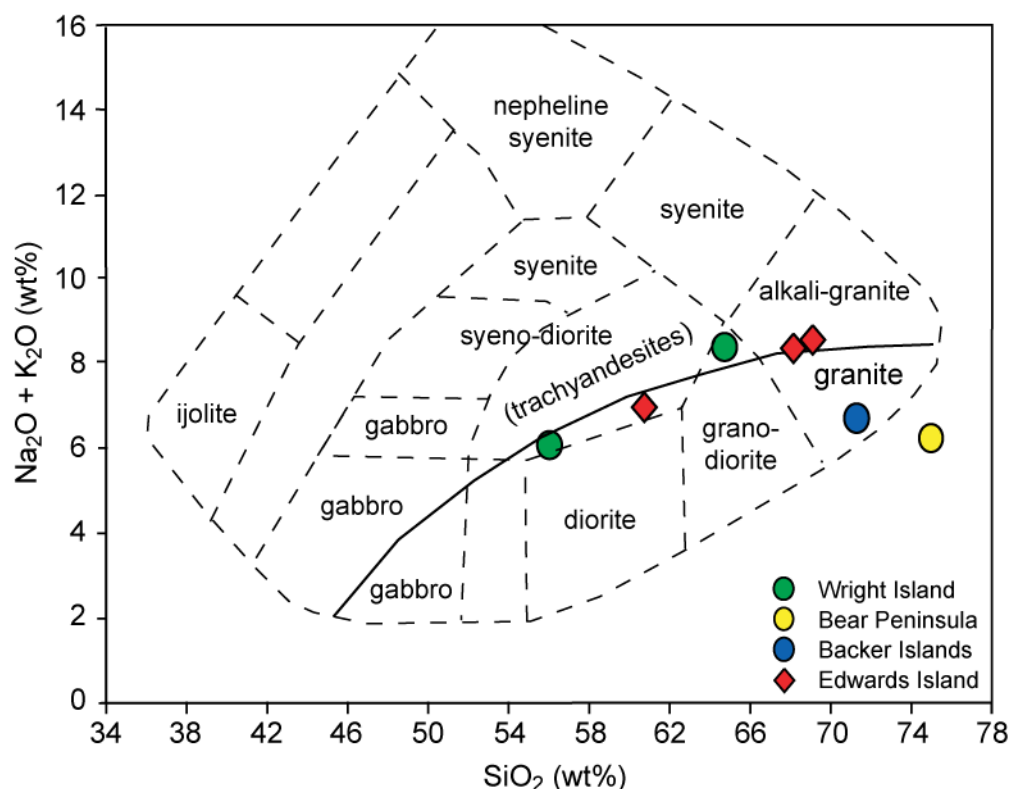


Fig. 4. Classification of the samples from Walgreen Coast and Pine Island Bay. The solid line marks the subdivision between alkalic and subalkalic rocks. All samples show evolved subalkalic or slightly alkalic compositions. The porphyritic dike rock sampled on Edwards Island falls into the field for trachyandesites. All analyses have been normalized to a volatile free total of 100%.

Major constituents are quartz, alkali feldspar and zoned plagioclase. Other common mineral phases are hornblende, apatite, titanomagnetite, and biotite, while muscovite occurs rarely. Amphibole is restricted to the granites. The porphyritic dike sample PS69/LI-1 from Edwards Island is a trachyandesite (micro-syenodiorite) with a glomerophyric texture. Large feldspar phenocrysts (up to 5 mm) occur in a fine-grained matrix, which mainly consists of plagioclase, hornblende, and titanomagnetite. The other rocks sampled on Edwards Island are evolved, holocrystalline alkali-granitic rocks. Major mineral phases are quartz, sanidine, plagioclase and biotite. Hornblende, muscovite, nepheline, apatite, and titanomagnetite are minor components.

The samples from Wright Island and Bear Peninsula do not show any signs of alteration, whereas the granitic rocks from Backer and Edwards Islands show minor alteration of feldspars to secondary calcite and chlorite. The trachyandesite from Edwards Island is slightly altered (minor calcite replacement of some phenocrysts).

5.2 Ar/Ar Age Dating

$^{40}\text{Ar}/^{39}\text{Ar}$ step-heating results are summarized in Table 3, age, alteration index spectra are shown in Figure 5, and full analytical data are given in Table S1.

Two biotite step-heating analyses from Wright Island granodiorite sample 277–1 yield plateau ages of 98.4 ± 0.3 Ma and 98.3 ± 0.4 Ma. $^{36}\text{Ar}/^{39}\text{Ar}$ alteration indices are reasonably low in the high-temperature plateau sections (0.002 to 0.007), but up to three orders of magnitude higher in the low-temperature heating steps (excluded from plateau). Plateau age results are identical within error, thus a weighted mean age of 98.3 ± 0.2 Ma (2s; MSWD = 0.22; Probability = 0.64) was calculated for sample 277-1.

Table 3: Results of step-heating $^{40}\text{Ar}/^{39}\text{Ar}$ analyses. † = weighted mean of plateau ages. †† = weighted mean of “best step” averages.

Sample ID	Locality	Plateau age (Ma)	2s	MSWD	Pro-bability	% ^{39}Ar in plateau	Dated material
PS69-							
277-1bts	Wright Island	98.4	± 0.3	0.50	0.89	58	biotite
277-1bt2	Wright Island	98.3	± 0.4	0.15	0.99	58	biotite
		98.3 †	± 0.2	0.22	0.64		
277-7bts	Wright Island	97.9	± 0.4	0.24	1.00	82	biotite
LI-1fss	Edwards Island	97.1	± 0.5	1.08	0.37	88	plagioclase
LI-2fs2	Edwards Island	97.1	± 0.7	1.50	0.12	92	plagioclase
LI-3fss	Edwards Island	95.2	± 0.7	1.20	0.29	74	K-feldspar
PIB-1bt3	Backer Island	147.0	± 0.6	1.30	0.23	61	biotite
PIB-1bt4	Backer Island	147.3	± 0.6	1.18	0.31	50	biotite
		147.2 †	± 0.4	0.46	0.50		
PIB-1bt6	Backer Island	151.9	± 0.4	1.30	0.26	63	biotite
BI-5bts, bt3, bt6	Bear Peninsula	109.8 ††	± 1.3	0.53	0.59		biotite
DR193.1	c. 20 nm W off Bear Peninsula	103.5	± 0.3	1.80	0.13	66	plagioclase

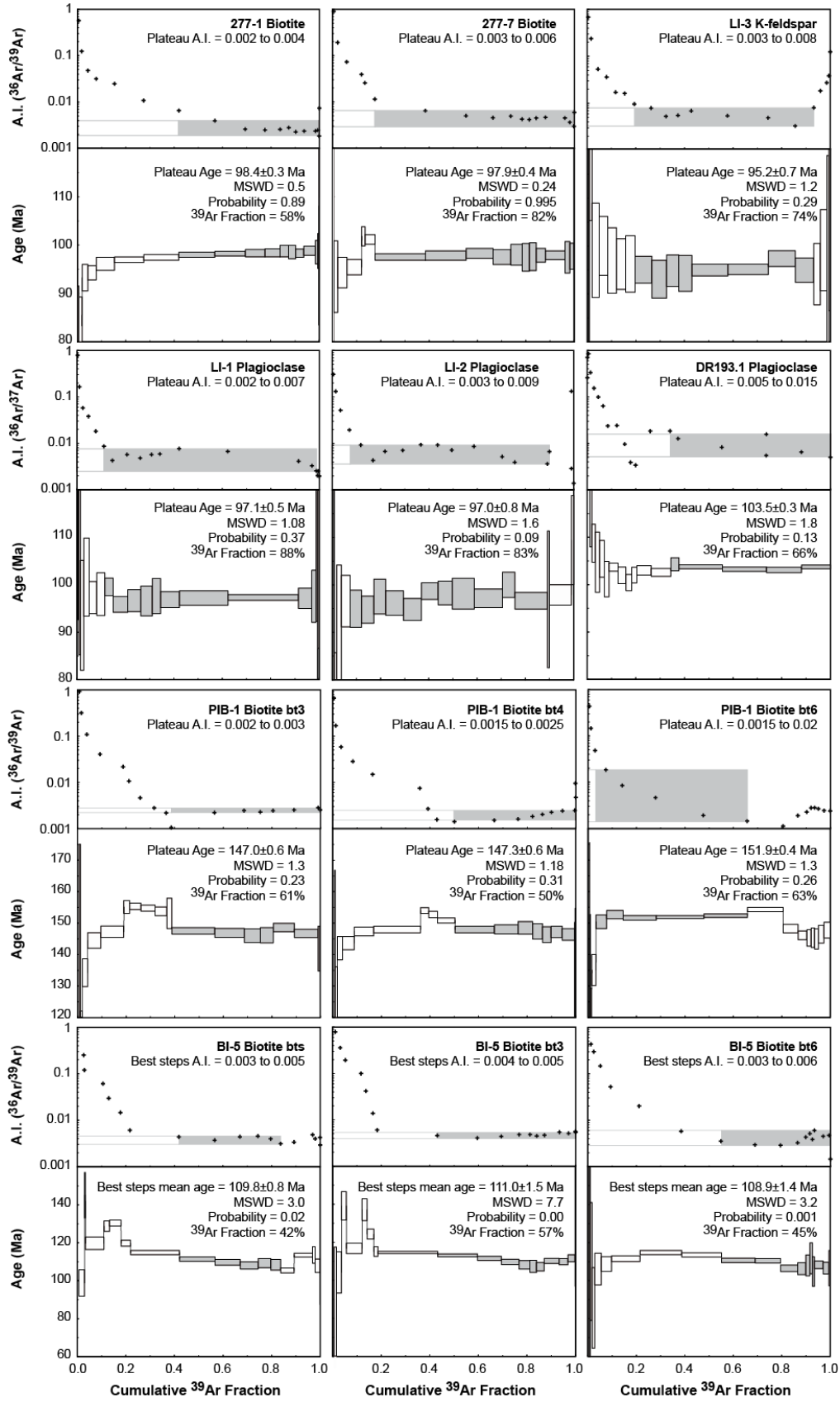


Fig. 5. Age spectra and alteration indices (A.I.) from $^{40}\text{Ar}/^{39}\text{Ar}$ laser step-heating experiments. Plateau steps and corresponding range of alteration index values are accentuated by grey shading. Error bars are $\pm 2\sigma$.

Biotite step-heating of Wright Island syeno-diorite sample 277-7 yields a slightly younger plateau age of 97.9 ± 0.4 Ma. Plateau step alteration indices indicate degassing from little-altered sites ($^{36}\text{Ar}/^{39}\text{Ar} = 0.003$ to 0.006). Small low-temperature fractions ($<18\%$ ^{39}Ar) yield higher alteration indices (0.01 to 10) and lower apparent ages due to a loss of radiogenic ^{40}Ar during alteration.

Plagioclase feldspar step-heating of Edwards Island trachyandesite dike LI-1 yields a plateau age of 97.1 ± 0.5 Ma. $^{36}\text{Ar}/^{37}\text{Ar}$ ratios are reasonably low in the high-temperature plateau section (0.002 to 0.007), but gradually higher in the lower temperature heating steps (0.01 - 1.7) indicating partial alteration (steps 1 to 7, excluded from plateau).

Plagioclase from Edwards Island alkali-granitic rock sample LI-2 yields similar results. Alteration is low in the plateau steps ($^{36}\text{Ar}/^{37}\text{Ar} = 0.003$ - 0.009), which yield a plateau age of 97.1 ± 0.7 Ma. Lower temperature steps degassed more altered sites ($^{36}\text{Ar}/^{37}\text{Ar} = 0.02$ - 2.4), and thus are rejected from the plateau. K-feldspar (anorthoclase?) step-heating of Edwards Island alkali-granite sample LI-3 yields a plateau age of 95.2 ± 0.7 Ma ($^{36}\text{Ar}/^{39}\text{Ar} = 0.003$ to 0.008). Both the lowest and highest temperature steps show significantly higher alteration ($^{36}\text{Ar}/^{39}\text{Ar} = 0.01$ to 2.2) and are rejected from the plateau age calculation.

Six step-heating analyses were carried out on biotite from Backer Islands granite sample PIB-1, three of which yielded disturbed spectra without significant ($>50\%$ ^{39}Ar) plateaus. Two analyses yield high-temperature plateaus at 147.0 ± 0.6 Ma (PIB-1bt3) and 147.3 ± 0.6 Ma (PIB-1bt4) with acceptable alteration indices in the plateau steps (0.002 to 0.003). Significant alteration in the low-temperature spectrum result in apparent ages significantly lower (due to radiogenic ^{40}Ar loss?) and apparent ages significantly higher (due to recoil ^{39}Ar loss?) than the plateau ages.

Analysis PIB-1bt6 yields a low-temperature plateau at 151.9 ± 0.4 Ma, but alteration indices up to 0.02 clearly show that this plateau includes degassing from altered sites. Seven high-temperature steps with low alteration indices (0.002 to 0.003) yield apparent ages around 147 Ma again. This indicates that the low-temperature plateau is in fact a pseudo-plateau possibly derived from a “balanced” loss of radiogenic ^{40}Ar and recoiled ^{39}Ar . The biotite $^{40}\text{Ar}/^{39}\text{Ar}$ age

of granite PIB-1 is determined as 147.2 ± 0.4 Ma (MSWD = 0.46, Probability = 0.5) from the weighted mean of the bt3 and bt4 plateau age results.

Three step-heating analyses of biotite from Bear Peninsula granite sample BI-5 (bts, bt3, bt6) yield disturbed spectra. None of the analyses shows a significant plateau ($>50\%$ ^{39}Ar). All show effects of significant alteration, such as high $^{37}\text{Ar}/^{39}\text{Ar}$ ratios >0.02 indicating the presence of alteration products (chlorite, epidote) in the biotite crystals (Baksi 2007), and high $^{36}\text{Ar}/^{39}\text{Ar}$ ratios indicating substantial uptake of ^{36}Ar , likely loss of radiogenic ^{40}Ar during alteration, and possible recoil loss of ^{39}Ar during irradiation. The least altered high-temperature degassing steps show acceptable alteration indices ranging from 0.003 to 0.006, comprise only 42% (bts), 57% (bt3), and 45% (bt6) of the ^{39}Ar released, and yield mean ages identical within 2σ uncertainties/95% confidence levels (109.8 ± 0.8 Ma, 111.0 ± 1.5 Ma, 108.9 ± 1.4 Ma). High MSWD (≥ 3) and low Probability (< 0.05) indicate excess scatter and presence of geological error. The weighted mean of these three “best steps averages” is 109.8 ± 1.3 Ma (MSWD = 0.53; Probability = 0.59) and considered our best estimate for the biotite $^{40}\text{Ar}/^{39}\text{Ar}$ age of Bear Peninsula granite BI-5.

Plagioclase step-heating of granite sample DR193.1, dredged c. 40 km west of Bear Peninsula, yields a high-temperature plateau at 103.5 ± 0.3 Ma. $^{36}\text{Ar}/^{37}\text{Ar}$ ratios of the low-temperature heating steps (0.01-1.0) and plateau steps (0.005-0.02) indicate partial alteration of the plagioclase crystals. The sample may have experienced minor loss of radiogenic ^{40}Ar , and its age estimate may therefore be a few percent too low.

The biotite and plagioclase $^{40}\text{Ar}/^{39}\text{Ar}$ ages of the Pine Island Bay granites and diorites (277-1, 277-7, PIB-1, BI-5, DR193.1) approximate the time that passed since cooling below closure temperatures (ca 300-200 °C; McDougall and Harrison, 1999; Cassata et al., 2009), and may post-date the time of emplacement and crystallization by several million years. We note, however, that there is a reasonable match between our $^{40}\text{Ar}/^{39}\text{Ar}$ ages and the published U-Pb ages (see discussion chapter), indicating that the $^{40}\text{Ar}/^{39}\text{Ar}$ ages approximate to intrusion ages and are not just a spread of cooling ages. In case of the more rapidly cooled Pine Island Bay trachyandesitic and granitoid dikes (LI-1, LI-2, LI-3), the plagioclase and K-feldspar $^{40}\text{Ar}/^{39}\text{Ar}$ ages closely reflect the time of cooling and emplacement.

5.3 Geochemistry

Major and trace element data of all studied samples (except DR193-1) are given in Table 4. The samples from Backer Islands and Bear Peninsula are highly fractionated with $\text{SiO}_2 = 71\text{--}75$ wt.% and $\text{Fe}_2\text{O}_3 = 2\text{--}3$ wt.%, whereas the Wright Island samples show more intermediate compositions with $\text{SiO}_2 = 56\text{--}64$ wt.% and $\text{Fe}_2\text{O}_3 = 5\text{--}8$ wt.%. The granitic Edwards Island dikes show evolved compositions with $\text{SiO}_2 = 68.7$ wt.% and 68.6 wt.%, the trachyandesitic dike has $\text{SiO}_2 = 59.6$ wt.% and $\text{MgO} = 2.6$ wt.%. All samples are metaluminous.

All analyzed samples display multi-element patterns similar to I-type subduction-related rocks with the characteristic depletion in Nb and Ta and enrichment in fluid-mobile elements Rb, Ba, U, Pb, Sr and K (Fig. 6A). The high concentrations in incompatible elements and the pronounced depletion in Ti reflect the evolved nature of the rocks. Negative anomalies of Nb, Ta, and in part in Ti may be caused by residual rutile during melting. The decrease in Fe_2O_3 and TiO_2 with increasing SiO_2 in the samples, however, also indicates fractionation of Fe-Ti oxides. The negative P anomaly indicates fractionation of apatite. Their rare earth element patterns (Fig. 6B) reveal enrichment in light rare earth element (LREE) and relatively flat heavy rare earth element (HREE) patterns. The slight concave shape in the HREE patterns with relative depletion in Dy, Ho, Er, Tm relative to Yb, Lu, Tb and lighter REEs could reflect amphibole and/or apatite fractionation. A distinct negative Eu anomaly, as is commonly observed for evolved plutonic rocks from Marie Byrd Land and Ellsworth Land (e.g. Weaver *et al.* 1992) reflecting plagioclase fractionation, does not appear in the multi-element patterns of the MBL samples analyzed in this study. A lack of a significant negative Eu anomaly in arc rocks is considered to be a characteristic feature of adakites (Defant & Drummond 1990). Several further geochemical features of most of our samples may point to a weakly adakitic composition as, for example, high SiO_2 (≥ 56 w.%) and Al_2O_3 (≥ 15 wt.%), low $<3\%$ MgO (Fig. 6), low Nb and Ta (Fig. 6a), and low HREE (e.g., Y and Yb, Figs. 6, 7). We note, however, that most of these features could also be caused by plagioclase accumulation which is common in arc magmas.

Table 4: Results of major and trace element analyses

	PS69/ 277-1-1 Wright Island	PS69/ 277-1-7 Wright Island	PS69/ BI-5 Bear Penin.	PS69/ PIB-1 Backer Islands	PS69/ LI-1 Edwards Island	PS69/ LI-2 Edwards Island	PS69/ LI-3 Edwards Island
SiO ₂	63.40	55.40	73.77	70.54	58.50	66.39	67.01
TiO ₂	0.52	1.29	0.27	0.33	0.80	0.46	0.41
Al ₂ O ₃	17.23	18.32	12.83	14.48	16.67	15.63	15.36
Fe ₂ O ₃	4.66	7.48	2.18	2.97	5.93	2.85	2.55
MnO	0.06	0.13	0.05	0.05	0.08	0.08	0.07
MgO	1.10	2.77	0.59	0.63	2.56	1.09	0.84
CaO	3.14	7.24	2.10	2.89	4.89	2.31	2.02
Na ₂ O	4.77	4.82	4.05	4.09	3.95	4.12	4.12
K ₂ O	2.93	0.93	1.79	2.20	2.31	3.55	3.72
P ₂ O ₅	0.15	0.42	0.06	0.11	0.31	0.17	0.14
H ₂ O	0.78	0.79	0.90	0.48	1.61	1.27	1.15
CO ₂	0.02	0.10	0.04	0.02	0.88	0.14	0.37
Total	98.75	99.66	98.64	98.79	98.48	98.06	97.78
Rb	87.9	84.9	54.7	87.0	56.3	128	136
Ba	1018	995	527	853	749	877	941
Th	7.69	8.10	5.31	4.52	8.16	16.0	17.0
U	1.46	1.55	1.54	1.20	1.82	4.03	4.00
Nb	7.01	6.73	4.02	4.76	6.91	9.40	9.57
Ta	0.64	0.64	0.43	0.46	0.56	0.88	0.90
La	35.4	34.3	15.0	18.4	27.4	35.0	35.4
Ce	67.4	65.9	30.6	39.5	58.9	69.6	69.1
Pb	15.3	15.6	7.2	18.7	12.3	16.4	17.2
Pr	7.20	7.15	3.59	4.35	7.14	7.76	7.54
Nd	25.1	25.1	14.4	16.2	28.2	28.0	27.0
Sr	479	464	150	384	693	442	345
Sm	3.91	3.83	3.20	3.10	5.26	4.80	4.54
Hf	7.06	6.88	3.58	4.00	4.93	6.30	6.47
Zr	299	289	127	163	197	258	267
Eu	1.54	1.48	0.78	1.10	1.39	1.16	1.10
Gd	2.98	2.79	3.16	2.30	3.93	3.56	3.32
Tb	0.39	0.38	0.55	0.34	0.55	0.53	0.49
Dy	2.17	2.15	3.62	1.92	3.06	3.00	2.87
Ho	0.42	0.40	0.79	0.39	0.58	0.60	0.57
Y	12.4	12.4	23.7	11.6	16.2	17.9	17.0
Er	1.20	1.20	2.41	1.18	1.58	1.79	1.71
Tm	0.19	0.19	0.38	0.18	0.23	0.28	0.27
Yb	1.30	1.31	2.78	1.25	1.56	2.05	2.00
Lu	0.21	0.22	0.46	0.21	0.24	0.34	0.33

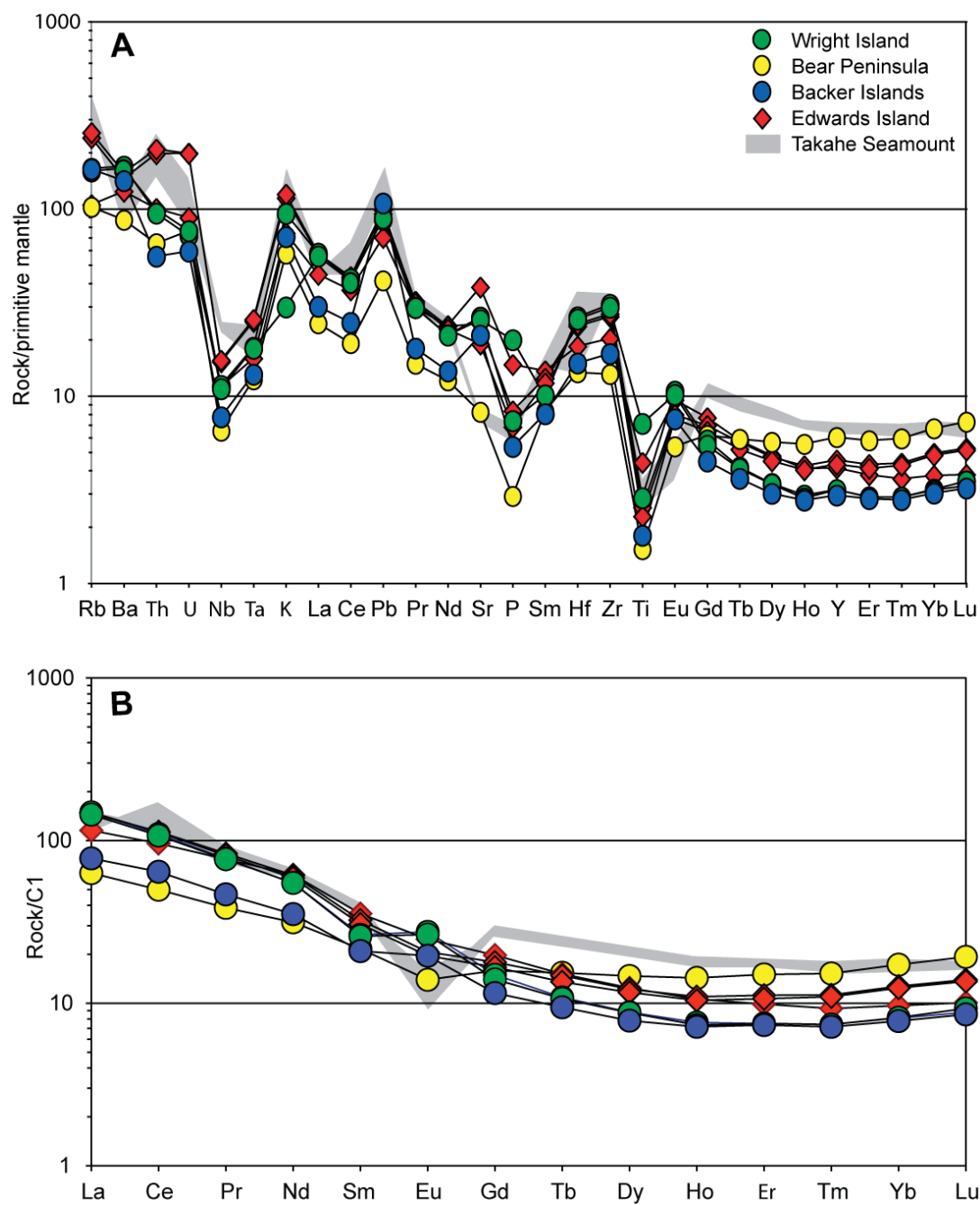


Fig. 6. Multi-element diagram normalized to primitive mantle (after Hofmann 1988) and rare earth element (REE) diagram normalized to chondrites (after McDonough & Sun 1995) for the Walgreen Coast and Pine Island Bay rocks. The 97 Ma granites of Takahe Seamount (Mortimer *et al.* 2006) are shown for reference; note the distinct Eu anomaly for the A-type Takahe granites.

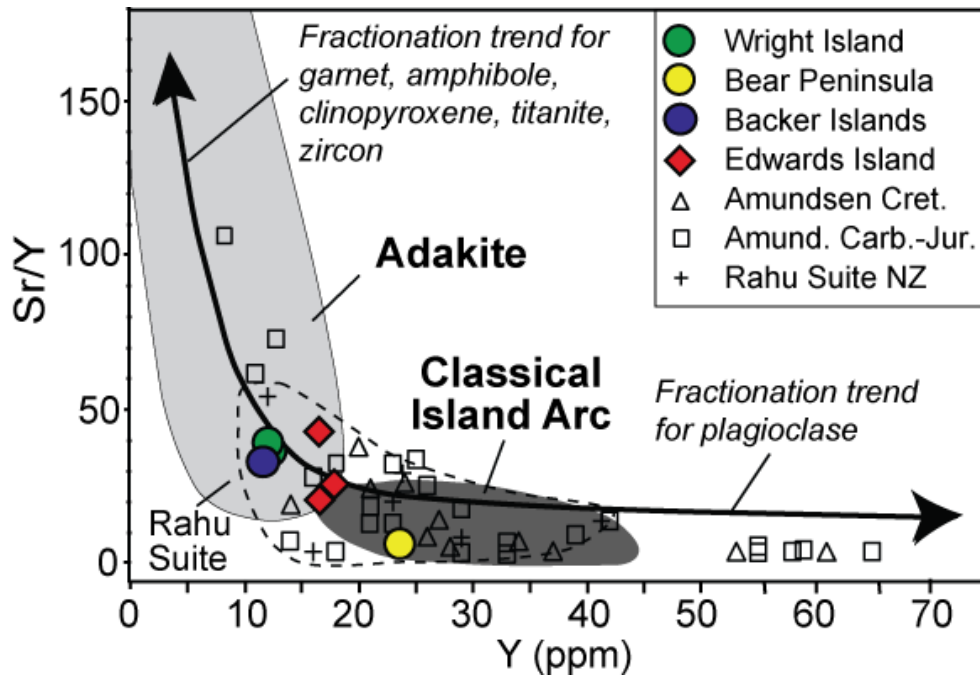


Fig. 7. Y versus Sr/Y discrimination diagram after Defant & Drummond (1990) reveals an weak adakitic composition of most Walgreen coast and Pine Island Bay samples. Only the granite sampled on Bear Peninsula falls into the fields for “classical” arc compositions. Previously published data from Cretaceous granitoids from the Amundsen suite (Pankhurst *et al.* 1993, 1998), the Cretaceous New Zealand Rahu Suite (Tulloch & Kimbrough 2003) and Cretaceous sodic granites from the Antarctic Peninsula (Wareham *et al.* 1997) are shown for reference. Field for adakites and fractionation trends after Richards & Kerrick (2007).

6. DISCUSSION

6.1 Petrogenesis

The range of rock types, along with major and trace element contents and ratios, support an origin for our analysed Pine Island Bay granitoids in a subduction-related setting (Fig. 8).

Except for the granite from Bear Peninsula, all of our samples show slightly elevated high Sr/Y ratios (Fig. 7). In this regard they are similar to the moderate Sr/Y 105-120 Ma Rahu Suite granites of New Zealand and also to sodic Cretaceous granites from the Antarctic Peninsula batholith (Wareham *et al.* 1997). It is noteworthy that the entire MBL to Antarctic Peninsula part of the Cretaceous Gondwana margin lacks true adakitic and/or high Sr/Y

suites such as those that dominate Zealandia's Median Batholith in the time interval 105-130 Ma (Tulloch & Kimbrough 2003).

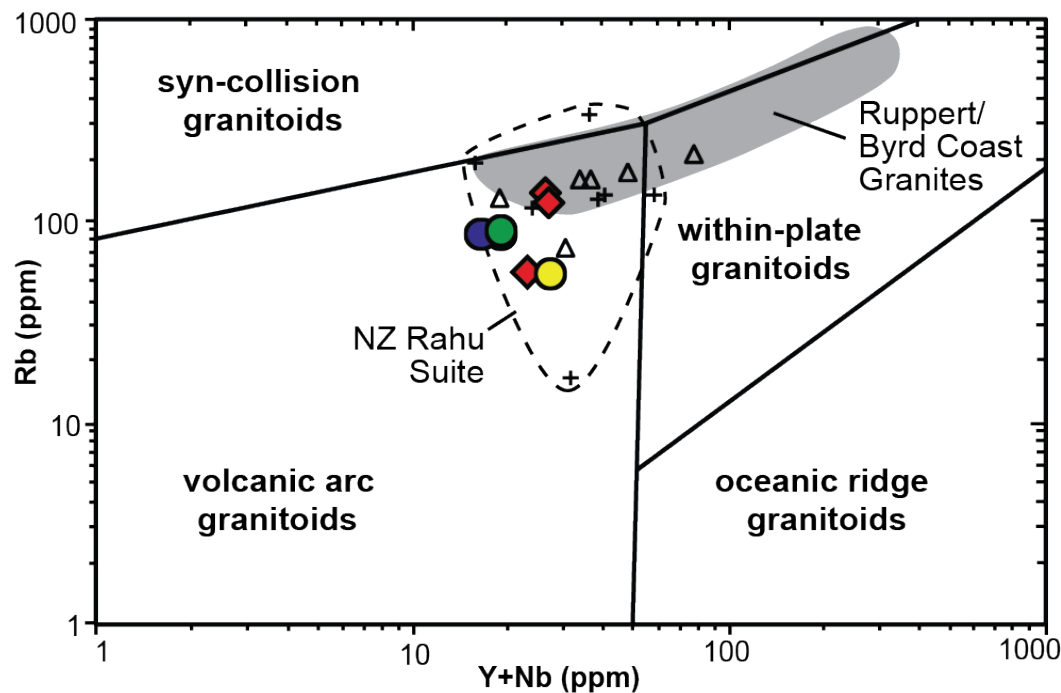


Fig. 8. Y+Nb versus Rb tectonic discrimination diagram for granitoids after Pearce *et al.* (1984). The basement samples yielded on R/V Polarstern ANT XXIII/4 cruise fall into the field for volcanic arc granitoids, consistent with a subduction setting for these rocks. Field for granites from Edward VII Peninsula and Ruppert Coast is based on published data from Weaver *et al.* 1992 and Pankhurst *et al.* 1998. Symbols as in Figure 7.

The moderately enriched Sr-Nd-Pb isotopic composition of the 97 Ma trachyandesite dike sample PS69/LI-1 from Edwards Island (Table 2) could either reflect derivation from a metasomatized mantle wedge source (possibly by melts from subducted marine sediments), or contamination of mantle derived melts by continental crust during ascent and prolonged crustal residence. In either case no evidence is found for the presence of a high μ ($\mu = {}^{238}\text{U}/{}^{204}\text{Pb}$) (HIMU) (or plume) component in the source of the melt, as reported for Late Cretaceous mafic dikes in MBL by Storey *et al.* (1999).

6.2 Age-composition patterns

Our combined age and geochemical data indicate that Mesozoic continental arc magmatism occurred at least from c. 150 Ma until 95 Ma along the Walgreen Coast and in

the Pine Island Bay area, consistent with previously published U-Pb and K-Ar ages of I-type granitoids (Fig. 9; Mukasa & Dalziel 2000).

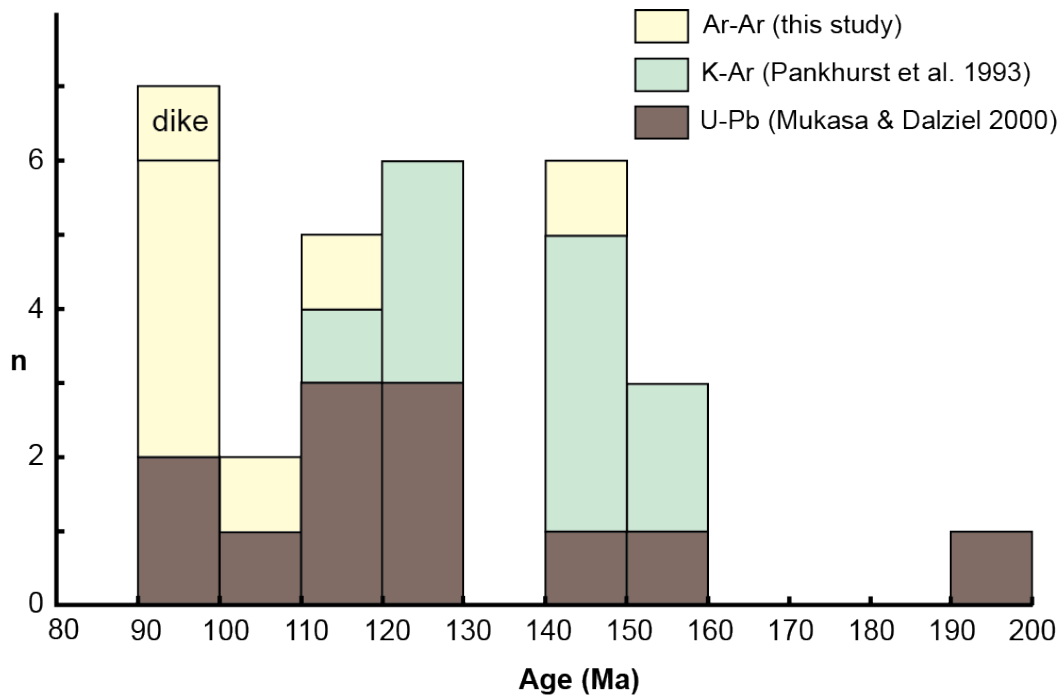


Fig. 9. Histogram comparing ages of Jurassic and Cretaceous I-type plutons in the Thurston Island-Pine Island Bay area. The youngest dated Mesozoic rock in the Pine Island Bay area (Fig. 2) is 94 Ma (U-Pb zircon by Mukasa & Dalziel 2000).

Notably, there seems to be a peak in magmatic activity between c. 100 and 95 Ma, indicated by the closure temperatures of biotites from granitoids on Wright Island (98 Ma), U-Pb ages of granitoids from McKenzie Island (96 Ma) and Lindsey Island (94 Ma) (Mukasa & Dalziel 2000), and the rapidly cooled dikes on Edwards Islands (95 and 97 Ma, respectively). Interestingly, this peak is within the age range of the Lassiter Coast Intrusive Suite in the southern Antarctic Peninsula (Flowerdew et al. 2005). We cannot exclude, however, the possibility that this peak reflects a sampling and/or cooling bias of this poorly-mapped and lightly-sampled area.

The persistence of I-type magmatism to c. 95 Ma differs significantly from the seemingly abrupt change from I-type to A-type magmatism at 107-101 Ma along the Ruppert Coast of western MBL (Storey *et al.* 1999, Mukasa & Dalziel 2000). It also differs from the situation in Zealandia where three pulses of I/A-type volcanism occurred at c. 101, c. 97

and c. 85 Ma with A-type character increasing with time (Tulloch *et al.* 2009). Tulloch *et al.* (2009) interpret the onset of the earliest A-type magmatism at 101 Ma to indicate the initial absence of a slab beneath Zealandia, and relate the decreasing degree of I-type geochemical characteristics in the younger suites to decreasing crustal contamination due to progressive crustal thinning. While no Cretaceous A-type igneous rocks have thus far been reported from sites east of Ruppert Coast, we note that the 97 Ma Takahe A-type granite reconstructs to a position close to the western tip of Thurston Island (Fig. 10) (Mortimer *et al.* 2006). In the Antarctic Peninsula batholith, Leat *et al.* (1995) note that the most intense period of intermediate composition I- and IS-type magmatism was 142-97 Ma. They allude to the existence of some <97 Ma alkaline igneous complexes but, unlike for Zealandia (Tulloch *et al.* 2009), these have not been interpreted as having any major regional tectonic significance for Gondwana margin tectonics.

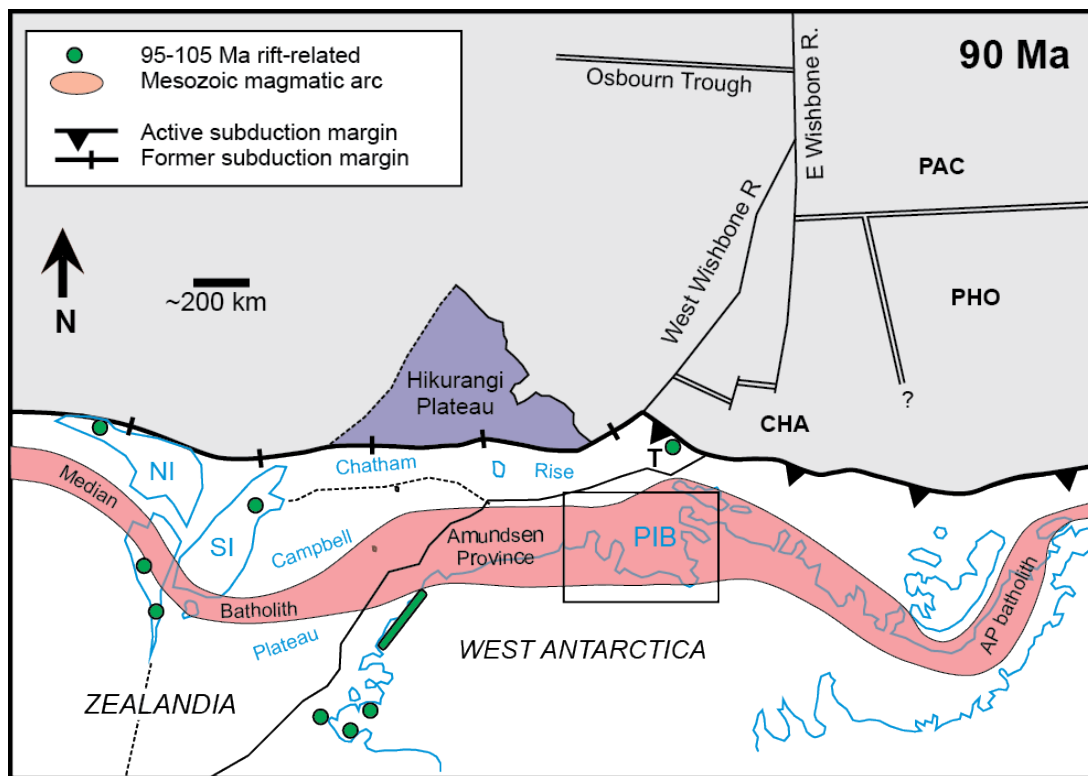


Fig. 10. Reconstruction of Zealandia and West Antarctica at 90 Ma, combining features from Eagles *et al.* (2004), and Mortimer *et al.* (2006). Note the wide zone of the magmatic arc in eastern MBL, possibly due to crustal extension after the Hikurangi Plateau-Chatham Rise collision and cessation of the subduction. The rectangle indicates the map area of Fig. 2 (NI – North Island of New Zealand, SI – Southern Island, T – Takahe Seamount, PIB – Pine Island Bay, PAC – Pacific plate, PHO – Phoenix Plate, CHA – Charcot Plate).

6.3 Cretaceous geodynamics

The subduction-related I-type granitoids of Pine Island Bay are approximately 500 km south of the present day continent-ocean margin. No arc-trench gaps of this size exist today (Jarrard 1986). Between 100-200 km of this distance can be accounted for by post-subduction stretching of West Antarctica crust (Eagles *et al.* 2004). Arc-trench gaps of c. 300 km are observed in many modern day continental arcs (Jarrard 1986), and flat-slab subduction models have been proposed for the Early Cretaceous Gondwana margin (Tulloch & Kimbrough 2003).

Metamorphic core complexes and A-type granites developed in Zealandia and western MBL in the interval 100-85 Ma (Siddoway *et al.* 2004, Tulloch *et al.* 2009 and references therein). According to Eagles *et al.* (2004), a first phase of extension in the Zealandia/MBL region can be related to the establishment of a proto-Pacific-Antarctic plate boundary in the Bounty Trough and Great South Basin east and southeast of New Zealand South Island, resulting in considerable thinning of the continental lithosphere (Grobys *et al.* 2009 and references therein). This rift-phase led to the separation of the Chatham Rise from eastern MBL just after 90 Ma (Eagles *et al.* 2004). At c. 84 Ma the locus of rifting shifted to the boundary between the southeast margin of Campbell Plateau and the MBL margin, followed by seafloor spreading along the Pacific-Antarctic Ridge and the ultimate separation of Zealandia from Antarctica (Eagles *et al.* 2004). Evidence for crustal extension on the eastern MBL side can be found on the broad continental shelf of the Amundsen Sea embayment where geophysical data reveal a 22-24 km thin crust, and dominant magnetic lineaments are interpreted as rift-related mafic intrusions, parallel to the Pacific-Antarctic spreading axis (Gohl *et al.* 2007, Gohl *in press*). It is possible that continental rifting, which is associated with the West Antarctic Rift System, not only played a role in Ellsworth Land and its continental margin (Müller *et al.* 2007) but also affected the eastern MBL and Amundsen Sea Embayment region (Jordan *et al.* 2010; Gohl *in press*).

The role of the Hikurangi Plateau in all this remains uncertain. The time of collision of the plateau with the Gondwana margin cannot be independently established but can only be inferred to be in the range of 105-65 Ma from continental geology (Mortimer *et al.* 2006); this leads to circular arguments about cause and effect. The presence of alkalic HIMU-type volcanism on the Hikurangi Plateau and on the South Island of New Zealand beginning

between at 100-95 Ma ago, however, suggests that the Hikurangi Plateau had already collided or was close to Zealandia by this time (Hoernle *et al.* 2010). Many aspects of the geology of the Gondwana margin (cessation of subduction, inception of rifting, slab windows) can equally be explained by subduction of a spreading ridge (Bradshaw 1989, Tulloch *et al.* 2009).

The present day continental margin of the Amundsen Sea Embayment and off the Walgreen Coast is not the old Gondwana subduction zone, but a Cretaceous rift margin, facing the currently active Pacific-Antarctic Ridge (Eagles *et al.* 2004, Gohl *et al.* 2007, Gohl in press). The extrapolation of oceanic crustal age from observed spreading anomalies 34y (83 Ma) in the south-eastern Amundsen Sea towards the continent-ocean boundary of easternmost MBL results in an oldest estimated oceanic age of c. 90 Ma (Eagles *et al.* 2004). This means that the eastern MBL region experienced a short rift phase of less than 5-7 m.y., before the subduction arc of the hinterland was converted to a Late Cretaceous passive margin.

ACKNOWLEDGMENTS

We are grateful to Captain Pahl, the ship and helicopter crews, and shipboard scientific party for their excellent support during RV Polarstern cruise ANT-XXIII/4. S. Hauff and J. Sticklus are thanked for technical assistance, and W. Borchert for creating Figures 1 and 2. Robert D. Larter kindly provided the dredge sample DR193.1. Discussions with Maxim Portnyagin, Jan Grobys, Graeme Eagles, Andreas Veit, and Christian Timm helped significantly to develop this paper. Comments on earlier versions of the manuscript by Phil Leat, Christine Siddoway, Alan Vaughan and an anonymous reviewer are appreciated. The German Research Foundation (DFG; Grants HO1833/15-1 to -3 to KH and FH) and the New Zealand Ministry of Science and Innovation funded this research.

REFERENCES

- BAKSI, A.K. 2007. A quantitative tool for detecting alteration in undisturbed rocks and minerals - I: Water, chemical weathering, and atmospheric argon. *Geological Society of America Special Paper*, 430, 285-303.
- BRADSHAW, J.D. 1989. Cretaceous geotectonic pattern in the New Zealand region. *Tectonics*, 8, 803-820.
- CARIGNAN, J., HILD, P., MEVELLE, G., MOREL, J., & YEGHICHEYAN, D. 2001. Routine analyses of trace elements in geological samples using flow, injection and low pressure on-line liquid chromatography coupled to ICP-MS : a study of reference materials BR, DR-N, UB-N, AN-G and GH. *Geotandards Newsletter*, 25 (2-3), 187-198.
- CASSATA, W.S., RENNE, P.R. & SHUSTER, D.L. 2009. Argon diffusion in plagioclase and implications for thermochronometry: A case study from the Bushveld Complex, South Africa. *Geochimica et Cosmochimica Acta* 73, 6600–6612
- CRADDOCK, C., BASTIEN, T.W., & RUTFORD, R.H. 1964. Geology of the Jones Mountains area. In ADIE R.J., ed. *Antarctic Geology*. Amsterdam: North Holland Publishing Co, 171-187.
- DAVY, B., HOERNLE, K., & WERNER, R. 2008. Hikurangi Plateau: Crustal structure, rifted formation, and Gondwana subduction history. *Geochemistry Geophysics Geosystems*, 9, Q07004, doi:10.1029/2007GC001855
- DEFANT, M.J., & DRUMMOND, M.S. 1990. Derivation of some modern arc magmas by partial melting of young subducted lithosphere. *Nature*, 347, 662-665.
- EAGLES, G., GOHL, K., & LARTER, R.D. 2004. High-resolution animated tectonic reconstruction of the South Pacific and West Antarctic margin. *Geochemistry, Geophysics, Geosystems*, 5, doi:10.1029/2003GC000657.

FLOWERDEW, M.J., MILLAR, I.L., VAUGHAN, A.P.M. AND PANKHURST, R.J. 2005. Age and tectonic significance of the Lassiter Coast intrusive suite, Eastern Ellsworth Land, Antarctic Peninsula. *Antarctic Science*, 17, 443-452.

GOHL, K. In press. Basement control on past ice sheet dynamics in the Amundsen Sea Embayment, West Antarctica. *Palaeogeography, Palaeoclimatology, Palaeoecology*, doi:10.1016/j.palaeo.2011.02.022.

GOHL, K., TETERIN, D., EAGLES, G., NETZEBAND, G., GROBYS, J., PARSIEGLA, N., SCHLÜTER, P., LEINWEBER, V., LARTER, R.D., UENZELMANN-NEBEN, G., & UDINTSEV, G.B. 2007. Geophysical survey reveals tectonic structures in the Amundsen Sea embayment, West Antarctica. In Cooper, A.K., C.R. Raymond, et al., eds. *Proceedings of the 10th Int. Symposium of Antarctic Earth Sciences*, USGS Open-File Report 2007-1047, doi:10.3133/of2007-1047.srp047.

GROBYS, J.W.D., GOHL, K., & UENZELMANN-NEBEN, G. 2009. Extensional and magmatic nature of the Campbell Plateau and Great South Basin from deep crustal studies. *Tectonophysics*, 472, 213-225, doi:10.1016/j.tecto.2008.05.003.

HOERNLE, K., HAUFF, F., VAN DEN BOGAARD, P., WERNER, R., MORTIMER, N., GELDMACHER, J., GARBE-SCHÖNBERG, D., & DAVY, B. 2010. Age and Geochemistry of Volcanic Rocks from the Hikurangi and Manihiki Oceanic Plateaus. *Geochimica et Cosmochimica Acta*, 74, 7196-7219 doi:10.1016/j.gca.2010.09.030.

HOFMANN, A.W. 1988. Chemical differentiation of the earth: The relationship between mantle, continental crust, and oceanic crust. *Earth Planetary Science Letters*, 90, 297-314.

JARRARD, R.D. 1986. Relations among subduction parameters. *Reviews of Geophysics*, 24, 217-284.

JORDAN, T.A., FERRACCIOLI, F., VAUGHAN, D.G., HOLT, J.W., CORR, H., BLANKENSHIP, D.D. & DIEHL, T.M., 2010. Aerogravity evidence for major crustal thinning under the Pine Island

Glacier region (West Antarctica). *Geological Society of America Bulletin*, 122, 714–726.
doi:10.1130/B26417.1.

LANPHERE, M.A., & DALRYMPLE, G.B. 2000. First-principles calibration of ^{38}Ar tracers: Implications for the ages of $^{40}\text{Ar}/^{39}\text{Ar}$ fluence monitors. *U.S. Geological Survey Professional Paper*, 1621, 1-10.

LEAT, P.T., SCARROW, J.H., & MILLAR, I.L. 1995. On the Antarctic Peninsula batholith. *Geological Magazine*, 132, 399-412.

LEAT, P.T., STOREY, B.C., & PANKHURST, R.J. 1993. Geochemistry of Palaeozoic-Mesozoic Pacific rim orogenic magmatism, Thurston Island area, West Antarctica. *Antarctic Science*, 5, 281-296.

LUYENDYK, B.P. 1995. Hypothesis for cretaceous rifting of East Gondwana caused by subducted slab capture. *Geology*, 23, 373-376.

MASLANYJ, M., & STOREY, B.C. 1990. Regional aeromagnetic anomalies in Ellsworth Land: crustal structure and Mesozoic microplate boundaries within West Antarctica. *Tectonics*, 9, 1515-1532.

MCDONOUGH, W.F., & SUN, S.-S. 1995. The composition of the Earth. *Chemical Geology*, 120, 223-253.

MCDUGALL, I. & HARRISON, T.M. 1999. Geochronology and Thermochronology by the $^{40}\text{Ar}/^{39}\text{Ar}$ Method. 2nd ed., Oxford University Press, 269 pp.

MORTIMER, N., HOERNLE, K., HAUFF, F., PALIN, J.M., DUNLOP, W.J., WERNER, R., & FAURE, K. 2006. New constraints on the age and evolution of the Wishbone Ridge, southwest Pacific Cretaceous microplates, and Zealandia-West Antarctica breakup. *Geology*, 34, 185-188.

-
- MUKASA, S.B., & DAZIEL, I.W.D. 2000. Marie Byrd Land, West Antarctica: Evolution of the Gondwana's Pacific margin constrained by zircon U-Pb geochronology and feldspar common-Pb isotopic compositions. *Geological Society of America Bulletin*, 112 (4), 611-627.
- MÜLLER, R.D., GOHL, K., CANDE, S.C., GONCHAROV, A. & GOLYNSKY, A.V. 2007. Eocene to Miocene geometry of the West Antarctic rift system. *Australian Journal of Earth Sciences*, 54, 1033-1045, doi:10.1080/08120090701615691.
- PANKHURST, R.J., MILLAR, I.L., GRUNOW, A.M., & STOREY, B.C. 1993. The pre-Cenozoic magmatic history of the Thurston Island crustal block, West Antarctica. *Journal of Geophysical Research*, 98 (B7), 11835-11849.
- PANKHURST, R.J., WEAVER, S.D., BRADSHAW, J.D., STOREY, B.C., & IRELAND, T.R. 1998. Geochronology and geochemistry of pre-Jurassic superterranes in Marie Byrd Land, Antarctica. *Journal of Geophysical Research*, 103 (B2), 2529-2547.
- PEARCE, J.A., HARRIS, N.B.W., & TINDLE, A. 1984. Trace element discrimination diagrams for the tectonic interpretation of granitic rocks. *Journal of Petrology*, 25 (4), 956-983.
- RICHARDS, J.P., & KERRICK, R. 2007. Adakite-like rocks: Their diverse origins and questionable role in metallogenesis. Special Paper, *Economic Geology*, 102, 537-576.
- SIDDOWAY, C.S., BALDWIN, S., FITZGERALD, P.G., FANNING, C.M., AND LUYEDNDYK, B.P. 2004. Ross Sea mylonites and the timing of intracontinental extension within the West Antarctic rift system. *Geology*, 32 (1), 57-60.
- SMITH, W.H.F., & SANDWELL, D.T. 1997. Global seafloor topography from satellite altimetry and ship depth soundings. *Science*, 277, 1956-1962.
- STOREY, B.C., LEAT, P.T., WEAVER, S.D., PANKHURST, R.J., BRADSHAW, J.D., & KELLEY, S. 1999. Mantle plumes and Antarctica-New Zealand rifting: evidence from mid-Cretaceous mafic dykes. *Journal of the Geological Society London*, 156, 659-671.

TULLOCH, A. J., & KIMBROUGH, D. L. 2003. Paired plutonic belts in convergent margins and the development of high Sr/Y magmatism: Peninsular Ranges batholith of Baja-California and Median batholith of New Zealand. *Geological Society of America Special Paper*, 374, 275–295.

TULLOCH, A.J., RAMEZANI, J., MORTIMER, N., MORTENSEN, J., VAN DEN BOGAARD, P., & MAAS, R. 2009. Cretaceous felsic volcanism in New Zealand and Lord Howe Rise (Zealandia) as a precursor to final Gondwana break-up. *In* Ring, U. & Wernicke, B., eds. *Extending a continent: architecture, rheology and heat budget*. Geological Society of London Special Publication, 321, 89-118.

VAUGHAN, A.P.M., & STOREY, B.C. 2000. The eastern Palmer Land shear zone: a new terrane accretion model for the Mesozoic development of the Antarctic Peninsula. *Journal of the Geological Society, London*, 157, 1243-1256.

WAREHAM, C.D., MILLAR, I.L., & VAUGHAN, A.P.M. 1997. The generation of sodic granite magmas. Western Palmer Land, Antarctic Peninsula. *Contributions to Mineralogy and Petrology*, 128, 81-96.

WEAVER, S.D., ADAMS, C.J., PANKHURST, R.J., & GIBSON, I.L. 1992. Granites of the Edward VII Peninsula, Marie Byrd Land: anorogenic magmatism related to Antarctic - New Zealand rifting. *Transactions of the Royal Society of Edinburgh, Earth Sciences*, 83, 281-290.

WEAVER, S.D., STOREY, B.C., PANKHURST, R.J., MUKASA, S.B., DiVENERE, V.J., & BRADSHAW, J.D. 1994. Antarctica-New Zealand rifting and Marie Byrd Land lithospheric magmatism linked to ridge subduction and mantle plume activity. *Geology*, 22, 811-814.

CHAPTER III

Major and trace element composition of the Christmas Island Seamount Province: testing a two component mixing model

A. Kipf, F. Hauff, R. Werner, K. Hoernle

in preparation

ABSTRACT

This study presents new major and trace element data of volcanic rocks from the Christmas Island Seamount Province (CHRISP) in the SE-Indian Ocean. Sr-Nd-Pb-Hf isotope data from these samples were presented in Hoernle et al. (2011). Here we evaluate if the trace element composition of the CHRISP samples can be generated by shallow recycling of continental lithosphere at mid-ocean ridges according to the model by Hoernle et al. (2011). The new data show, however, that the majority of the seamount samples are fairly evolved, affected by alteration, crystal fractionation and/or assimilation. Trace element data of unaltered, mafic samples (MgO >12 wt. %) confirm, that an enriched and a depleted endmember have affected the composition of the CHRISP. The enriched endmember, being most pronounced in the Christmas Island sub-province, is characterized by an increase in incompatible elements and LREE and thought to be lamproites derived from subcontinental lithospheric mantle (SCLM). The depleted endmember is a MORB-like component marked by depletion in incompatible elements and an increase in REE compared to primitive mantle. Mixing calculations indicate that the most primitive samples from Christmas Island can be generated by 25-30 % lamproitic and 75-70% MORB melts. Only a minor lamproitic component of 2-3%, however, is required to generate the most primitive sample of the Eastern Wharton Basin Province. Basically, the limited data set from unaltered, mafic samples suggest that the trace element chemistry of the CHRISP rocks can be generated by mixing of lamproitic and E-MORB melts, being consistent with the model of Hoernle et al. (2011).

1. INTRODUCTION

Seamounts are widely distributed on the ocean floor. Some are arranged in chains and others diffusely scattered. Seamounts and aseismic ridges forming linear, age progressive chains are commonly thought to originate from relatively stationary mantle upwellings (e.g. Lonsdale 1988, Royer et al. 1991, O'Connor et al 2013, Rohde et al 2013 and references therein) that are usually referred to as mantle plumes or hot spots (Wilson 1963, Morgan 1971). The most prominent example of such intraplate volcanoes are the Hawaiian Islands and related Hawaiian and Emperor seamount chains that show a systematic increase of volcanic ages towards the northwest which is away from the region of today's active plume upwelling and thus overall consistent with a relatively fixed hot spot underneath the moving Pacific lithosphere (Tarduno et al. 2003, Steinberger et al 2004, Lei et al. 2006, O'Connor et al. 2013). On the other hand, other seamount regions are more irregularly distributed, appear unrelated to plate motion and often display no clear spatial age progression of volcanism. The Marie Byrd Seamounts off the shelf of West-Antarctica are a good example of such a seamount province (Kipf et al., 2014). Although arranged in a broad morphological chain, their alignment appears devoid of plate motion and they exhibit no clear spatial age progression. Formation of this seamount province is thought to reflect outflow of fossil HIMU material by continental insulation, that was initially accreted to the base of the West-Antarctic lithosphere during a Cretaceous plume event.

Another very large region of diffuse intra-plate volcanism is the Christmas Island Seamount Province (CHRISP) in the northeastern Indian Ocean (Werner et al. 2009). This province extends in an E-W direction and thus orthogonal to the NNE-direction of plate motion in the Wharton Basin, which provides clear indications that the seamount province can not have formed over a "classical", fixed mantle plume. It is also unlikely that volcanism forming the seamounts is controlled by lithospheric cracks since faults and fracture zones in this area (e.g., Investigator Ridge) predominantly strike N-S. Hoernle et al. (2011) explain the origin of this volcanism through delamination of subcontinental lithospheric mantle (SCLM) during continental breakup and rifting of the West Burma block from Australia followed by shallow recycling and upwelling in connection with the Wharton basin spreading center. Based on radiogenic Sr-Nd-Pb-Hf isotope compositions it is evident that the CHRISP volcanism requires mixing of isotopically enriched SCLM with depleted mid ocean ridge basalt (MORB) sources. The occurrence of SCLM sources within the oceans is, however, rather

unusual as it requires transport of such material into the oceanic mantle by delamination during continental rifting or subduction erosion and resurfacing by deep mantle plumes. In cratonic environments, SCLM is more frequently tapped as for example by low degree melting (possibly related to deep reaching crustal extension) leading to the formation of lamproites, which after all are volumetrically very minor on Earth (Mitchell and Bergmann 1991). Since the SCLM mixing endmember of the CHRISP sensu Hoernle et al. (2011) appears isotopically as a mixture of SCLM found in NW Australian lamproites (Fraser et al. 1985) and the NW Australian mafic-ultramafic layered Millindinna complex (Korsch and Gulson 1986), the study presented here aims to evaluate if the trace element chemistry of the CHRISP volcanics can also be generated through mixing of lamproitic SCLM melts with MORB.

2. GEOLOGICAL SETTING AND MORPHOLOGY

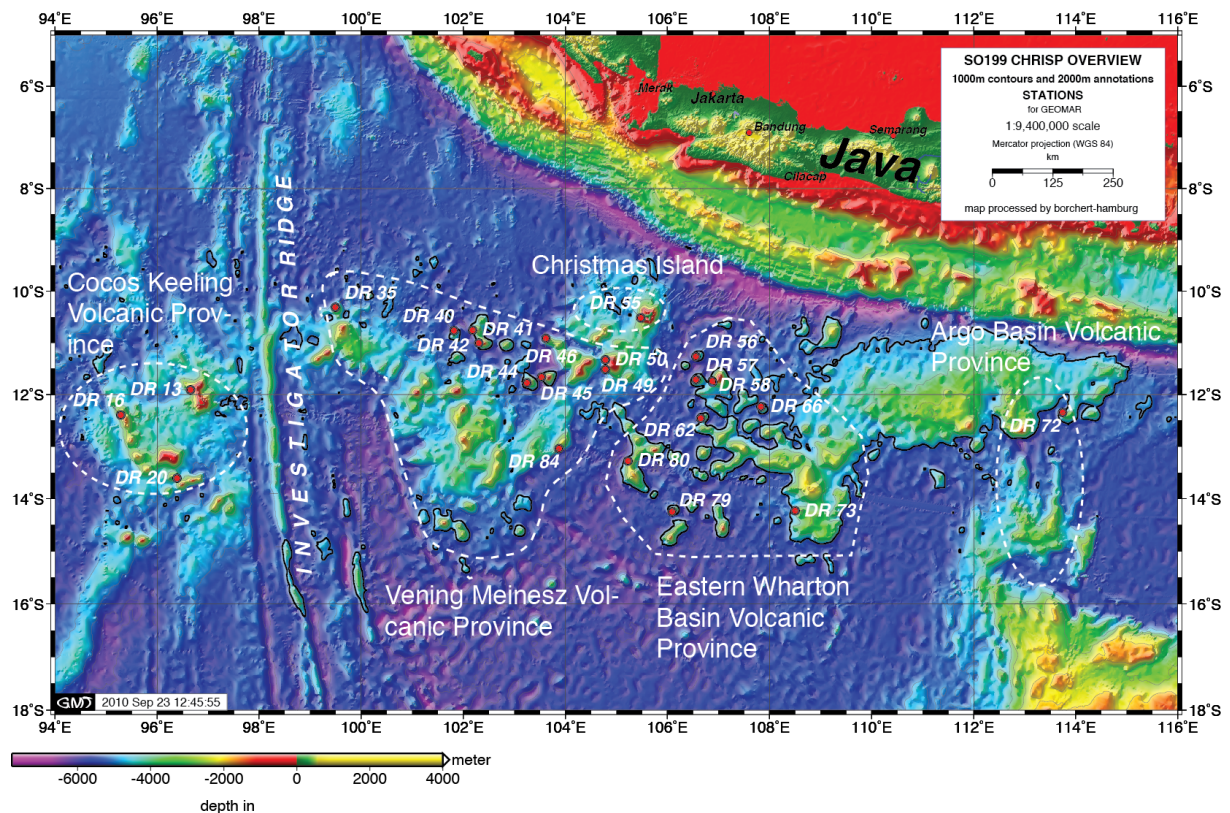


Fig. 1: Overview map of the Christmas Island Seamount Province (CHRISP) in the northeast Indian Ocean. The white cycles imply the subprovinces of CHRISP, Cocos Keeling Volcanic Province, the Vening Meinesz Volcanic Province, Christmas Island, the eastern Wharton Volcanic Province and the Argo Province. The map is based on the GEBCO_08 grid (version 20091120, <http://www.gebco.net>).

The “Christmas Island Seamount Province” (CHRISP) is located between $\sim 10^{\circ}\text{S}$ and $\sim 15^{\circ}\text{S}$ and $\sim 95^{\circ}\text{E}$ and $\sim 109^{\circ}\text{E}$ and covers $\sim 1,000,000$ square kilometers (approximately three times the area of Germany) in the southeast Indian Ocean (Fig. 1). The seamount province extends in E-W length of 1,800 km and its N-S elongation is about 600 km. This area is characterized by approximately 54 large, up to $> 4,500$ m high seamounts and is divided into four sub-provinces. The westernmost part forms the Cocos/Keeling Atolls, the Muirfield Seamount and submarine volcanic and tectonic features (Cocos-Keeling Volcanic Province, CKP). All seamounts of the CKP are located in a water depth of c. 3,800 m and range in age from 47 to 56 Ma (Hoernle et al. 2011). The 1,800 km long, N-S striking Investigator Ridge fracture zone divides the CKP in the west from a discontinuous chain of seamounts in the east, called the Vening Meinesz Seamount province (VMP) that covers the westernmost part of the Wharton Basin and includes Christmas Island near the Java Trench (Hoernle et al., 2011). The VMP seamounts reveal several guyot-type seamounts, which represent former ocean island volcanoes and range in age from 64 to 95 Ma (Hoernle et al. 2011). The variable depths of their erosional platforms imply different ages of these volcanoes and/or non-uniform subsidence of $\sim 2,500 - 1,200$ m since their erosion. Uneroded volcanic cones on the guyot platforms as well as seamounts with uneroded tops at shallower water depths than the guyots indicate revival of volcanic activity after subsidence of the guyots below sea level. Evidence for rejuvenated volcanism comes from the c. 4 Ma upper volcanic series (UVS) on Christmas Island that appears related to lithospheric bending along the outer rise of the Java trench (Woodroffe 1988).

The eastern Wharton Basin Volcanic Province (EWP) lies east of the Vening Meinesz Seamount Province with some seamounts showing a guyot-like morphology. The present water depth of the erosional platforms varies between $\sim 3,000$ m and $\sim 2,000$ m with the surrounding ocean floor at 5,000-6,000 m water depth. These observations also indicate different ages of the volcanoes and/or non-uniform subsidence rates. The other seamounts in this area do not show any clear evidence for wave erosion of their top areas. However, they partly possess a somewhat untypical morphology resembling tilted blocks rather than volcanoes (Werner et al. 2009). Age determinations range from 94 to 119 Ma for this sub province (Hoernle et al. 2011). One sample from a seamount of the Argo Basin Province with an age of 136 Ma is included in the major element analyzes, but is not taken into further consideration in this study because of its low <2 wt% MgO value.

3. METHODS

Samples selected for geochemistry were first crushed to small pieces in a steel jaw crusher, then repeatedly washed in deionized water until a clear solution was obtained and then carefully hand-picked under a binocular microscope. Sample powders were prepared in an agate mortar and agate swing mill.

Major element analyses were determined using by a Phillips X'Unique PW 1480 X-ray fluorescence spectrometer using a Rh-tube at GEOMAR and by ICP-ES at the Acme Analytical Laboratories Ltd. in Vancouver. Eight international rock standards were measured along with the samples (JA-2, JB-2, JB-3, JR-1, AGV-2, BIR-1, BHVO-2, BCR-2, and AGV). Information about data quality is presented in appendix 3 tables 1-3.

Trace element analyses were carried out on an AGILENT 7500cs inductively coupled plasma mass spectrometer at the Institute of Geosciences at the Christian-Albrechts University of Kiel after the methods of Garbe-Schönberg (1993) and at the Acme Analytical Laboratories Ltd. in Vancouver by inductively coupled plasma mass spectrometry (ICP-MS) subsequent to a lithium metaborate/tetraborate fusion and nitric acid as well as an Aqua Regia digestion. BIR-1, BHVO-2, BCR-2 and AGV-2 were analyzed as geochemical reference materials. Information about data quality is given in appendix 3 tables 3-4.

The geochemical mixing model was generated with standard spreadsheet software. At first the Indian lamproites and the Leucite Hills (Leucite Hills lamproites) were mixed to form a hybrid lamproitic endmember. For this purpose only samples with complete trace elements data sets, excluding those with unusual Pb anomalies, were taken from the literature (Chalapathi et al. 2004 for the Indian lamproites and Mirnejad et al. 2006 for Leucite Hills Lamproites). Values for enriched mid-ocean ridge basalt (E-MORB) were taken from Sun and McDonough 1989. Different proportions of lamproite and MORB were mixed for each trace element to evaluate if the Christmas seamount province basalt trace element contents could be generated through mixing.

4. RESULTS: MAJOR AND TRACE ELEMENTS

A total of 68 samples from all CHRISP sub-provinces were analyzed for major- and trace elements. Only samples with ≤ 2.5 wt% P_2O_5 and ≤ 5 wt% volatiles ($CO_2 + H_2O$) were considered to provide useable petrologic information and were cleared for further analysis of

trace element concentrations. CO₂ contents range from 0.03-0.7- wt% in most samples but two samples have extreme values up to 1.66 wt%. H₂O values range from 0.27-3.15- wt%, with only one sample having very high contents of 4.92 wt%. Based on the volatile contents and petrographic observations, the rock samples are considered to cover a wide range in the degree of alteration that ranges from slightly to strongly altered with the majority being moderately altered. Sample locations and geochemical data are given in tables 1 and 2.

Samples from the CHRISP range from ultrabasic to acidic (42-69 wt% SiO₂) and are classified as basanites/tephrites, phonotephrites (trachy-) basalts (basaltic-) trachyandesite and trachytes composition in the total alkali silica (TAS) diagram (Fig. 2). The majority of the samples are alkaline (12.7- 4.3 wt% Na₂O+K₂O) and only few samples, mainly from the EWP, are slightly tholeiitic. The TAS-diagram suggests variable melt evolution trends of the VMP, EWP and CKP sub-provinces. Here even the „primitive“ samples of VMP are significantly more alkalic than those of EWP and CKP. The latter form a mildly alkalic differentiation trend with the more primitive samples of EWP plotting in the basalt field (alkaline and tholeiitic).

Samples from Christmas Island are divided into a lower volcanic series (LVS, \approx 40 Ma) and an upper volcanic series (UVS \approx 4 Ma). In general the Christmas Island lavas are less enriched in SiO₂, TiO₂, K₂O, CaO, P₂O₅, FeOt and Na₂O than the remainder of the CHRISP. For clarity reasons the CHRISP data are shown in Fig. 3a-h while those from Christmas Island in Fig. 4a-h. The majority are basanites which mainly belong to UVS (MgO 15.5 wt% , SiO₂ 42 wt%, Na₂O+K₂O 3.4 wt%) and alkali basalts along with a few more evolved trachytes (LVS) (MgO = 4 wt%, SiO₂ = 60.5 wt.%, Na₂O+K₂O = 11.3 wt.%). LVS samples form the base of Christmas Island and are slightly more alkaline than the subaerial UVS samples.

Except for Christmas Island samples, CHRISP samples are generally fairly evolved and range from 5.7- 0.18 wt.% MgO with the most “mafic” samples occurring within the EWP (Figs. 3a-h and 4a-h). Major element variations versus MgO show for all sub-provinces (excluding Christmas Island) overlapping fields and vague trends for some elements. With decreasing MgO, K₂O, Na₂O and SiO₂ increase while CaO, decrease. Two trends for TiO₂ and FeOt are observed for VMP and EWP samples. Between 4-5 wt.% MgO values indicate decrease and increase of TiO₂ and FeOt. Consideration of trace element concentrations to reveal source characteristics is limited to samples with \geq 2 wt% MgO. Multi element or spider diagrams of primitive mantle normalized incompatible element show patterns resembling ocean island

basalts (OIB) for the CKP and VMP, whereas the subalkalic EWP ranges between OIB and enriched (E)-MORB (Fig. 5a-d). All provinces show typical troughs in Pb, Ti and enrichments in Nb and Ta relative to primitive mantle. K-troughs that are typical for OIB occur in CKP and VMP and nearly all samples from Christmas Island while K, Rb, and Ba peaks are abundant in the EWP and are attributed to more advanced stages of alteration / weathering of these samples.

CHRISP samples show positive as well as negative P anomalies (mostly EWP samples) in spider diagrams. As usual in ocean island basalts Ni and Cr are quite depleted. The values for Ni and Cr in the sub-provinces CKP, VMP, EWP and AP range from 80-0.5 ppm for Ni and for Cr 226-6 ppm. Volcanics from all provinces are enriched in light rare earth elements (LREE) relative to the heavy REE (HREE, Fig. 6a-6d). Petrologically significant anomalies are absent in nearly all sub-provinces. Subdued positive inflection of Eu is apparent in 4 subalkaline samples from the EWP with relatively high MgO 5.73-3.92 wt%.

Table 1: Sample location of the recovered dredged rocks

Dredge SO199-	Dredge No.	Location name	Sample type	on bottom lat °S	on bottom lat°S	on bottom long °E	off bottom lat°S	off bottom long°E	water depth (m) max.- min
DR13 DR13	-1 -12c	Cocos/Keeling Island	trachyandesit e trachyandesit e	11.906	11.901	96.651	11.901	96.659	2402- 1880
DR16	-1c	Muirfield Seamount	trachybasalt	12.394	12.394	95.288	12.394	95.290	2883-2676
DR20	-6	Muirfield Seamount	trachyandesit e	13.606	13.603	96.389	13.603	96.397	3140-2819
DR35	-1A	Vening Meinesz Seamounts W	basalt	10.312	10.312	99.491	10.312	99.492	3084-3060
DR40 DR40 DR40	-1 -2 -3	Vening Meinesz Seamounts C	phonotephrite trachybasalt trachybasalt	10.765	10.765	101.812	10.765	101.821	4306-3791
DR41	-1	Vening Meinesz Seamounts C	tehphrite	10.759	10.761	102.176	10.761	102.192	3754-3282
DR42 DR42	-1 -3	Vening Meinesz Seamounts C	phonotephrite phonotephrite	11.030	11.026	102.304	11.026	102.312	3963-3441
DR44	-1	Vening Meinesz Seamounts E	trachybasalt	11.775	11.775	103.241	11.775	103.251	2525-2036
DR45	-1	Vening Meinesz Seamounts E	trachyte	11.663	11.659	103.534	11.659	103.543	3746-3277
DR46	-1	Vening Meinesz Seamounts E	trachybasalt	10.915	10.922	103.617	10.922	103.624	4361-3769

Table 1: continued

Dredge SO199-	Dredge No.	Location name	Sample type	on bottom lat °S	on bottom lat°S	on bottom long °E	off bottom lat°S	off bottom long°E	water depth (m) max.- min
DR49 DR49 DR49	-1 -8 -14	Vening Meinesz Seamounts E	basaltic trachyandesite trachyte trachyte	11.512	11.517	104.783	11.517	104.792	4582-4050
DR50	-2	Vening Meinesz Seamounts E	trachyte	11.331	11.330	104.783	11.330	104.800	3125-3022
DR55	-1	Christmas Island (UVS)	tephrite	10.514	10.516	105.474	10.516	105.480	1891-1427
DR56 DR56 DR56	-1 -4 -6	Seamount group SE of Christmas Island	basalt trachyandesite trachyte	11.263	11.267	106.555	11.267	106.562	3997-3338
DR57	-1	Seamount group SE of Christmas Island	basalt	11.710	11.712	106.554	11.712	106.564	3501-3050
DR58	-1	Seamount group SE of Christmas Island	basaltic trachyandesite	11.737	11.740	106.880	11.740	106.889	2609-3113
DR62	-1	Seamount group SE of Christmas Island	trachybasalt	12.457	12.460	106.650	12.460	106.661	3477-2898
DR66 DR66 DR66	-1 -2 -5	Seamount group SE of Christmas Island	trachybasalt basalt basalt	12.230	12.236	107.826	12.236	107.835	3907-3381
DR72	-1	Seamounts on W-margin of Argo Basin	basalt	12.347	12.352	113.779	12.352	113.785	4398-3914

Table 1: continued

Dredge S0199-	Dredge No.	Location name	Sample type	on bottom lat °S	on bottom lat°S	on bottom long °E	off bottom lat°S	off bottom long°E	water depth (m) max.- min
DR73 DR73	-1 -11c	Southeastern Christmas Is. Prov. Smts.	basaltic trachyandesit e trachyte	14.230	14.225	108.496	14.225	108.504	4331-3983
DR79 DR79 DR79	-1 -3 -4	Southeastern Christmas Is. Prov. Smts.	basaltic trachyandesit e trachyte trachyte	14.249	14.250	106.090	14.250	106.091	3787-3820
DR80	-1	Southeastern Christmas Is. Prov. Smts.	trachyte	13.274	13.279	105.225	13.279	105.232	3220-2707
DR84	-2	Southeastern Christmas Is. Prov. Smts.	basalt	13.036	13.032	103.875	13.032	103.882	3542-3239

Table 2: Results of major and trace element analyses (IFG and Acme Lab*) of Cocos Keeling Island volcanic province (CKP). Vening Meinesz volcanic province (VMP). eastern Wharton volcanic province (EWP). Argo Basin volcanic province (AP) and Christmas Island (LVS and UVS)

	SO199- DR13-1 (CKP)	SO199- DR13- 12C* (CKP)	SO199- DR16-1C (CKP)	SO199- DR20-6 (CKP)	SO199- DR35-1A (VMP)	SO199- DR40-1 (VMP)	SO199- DR40-2 (VMP)
	Cocos Keeling Island	Cocos Keeling Island	Noel Seamount	Klaus Seamount	Rudolf Seamount	Gringe Seamount	Gringe Seamount
SiO ₂	54.6	55.64	45.11	58.69	48.51	45.03	43.62
TiO ₂	1.62	1.62	2.49	0.66	2.49	3.49	3.58
Al ₂ O ₃	18.74	17.54	19.84	17.44	14.97	18.85	19.46
Fe ₂ O ₃	7.79	6.78	11.43	8.19	13.94	13.01	13.65
MnO	0.10	0.09	0.19	0.11	0.16	0.12	0.09
MgO	1.89	1.60	4.33	0.83	4.34	1.14	1.58
CaO	5.17	5.02	5.87	2.55	10.14	7.44	7.75
Na ₂ O	5.22	5.36	3.43	5.74	3.32	3.39	3.23
K ₂ O	2.65	3.33	2.12	3.68	0.95	2.88	1.86
P ₂ O ₅	0.63	0.66	0.89	0.15	0.45	2.06	2.01
H ₂ O	1.39	1.67	4.92	1.53	1.25	2.19	2.87
CO ₂	0.03	0.33	0.06	0.03	0.05	0.17	0.15
TOTAL	99.83	98.01	100.68	99.60	100.57	99.77	99.85
Rb	32.0	50.7	424	31.6	18.8	35.0	28.0
Ba	600	575	600	1256	123	567	557
Th	10.2	11.7	18.2	11.6	1.80	5.13	5.20
U	1.05	0.70	2.26	0.31	0.51	1.51	1.48
Nb	104	96.7	114	88.5	20.7	62.6	63.3
Ta	5.85	6.20	7.08	5.44	1.26	3.84	3.94
La	62.2	65.5	88.8	66.8	15.4	51.1	54.6
Ce	132	136	132	107	34.7	102	102
Pb	4.50	3.10	9.50	4.80	1.10	3.32	3.25
Pr	14.6	15.2	15.1	15.7	4.74	12.4	13.1
Nd	57.3	58.7	54.4	63.0	21.9	51.8	54.3
Sr	425	384	761	214	247	897	1024
Sm	11.4	10.8	9.44	14.2	5.86	10.4	10.9
Hf	11.0	11.5	11.3	17.7	4.19	6.98	7.09
Zr	513	412	568	727	170	308	310
Eu	3.55	3.25	2.82	4.94	2.01	3.48	3.66
Gd	10.8	10.1	8.68	14.4	6.77	9.91	10.4
Tb	1.64	1.64	1.22	2.33	1.14	1.41	1.49
Dy	8.96	9.14	6.43	13.5	7.01	7.45	7.92
Ho	1.67	1.71	1.19	2.58	1.41	1.34	1.45
Y	44.4	46.0	34.1	65.2	38.1	38.1	42.3
Er	4.38	4.53	3.18	6.74	3.77	3.38	3.68
Tm	0.61	0.65	0.46	0.94	0.55	0.45	0.49
Yb	3.90	4.01	3.02	6.06	3.52	2.81	3.08
Lu	0.55	0.60	0.45	0.87	0.51	0.40	0.44

Table 2: continued

	SO199- DR40-3 (VMP)	SO199- DR41-1 (VMP)	SO199- DR42-1* (VMP)	SO199- DR42-3 (VMP)	SO199- DR44-1 (VMP)	SO199- DR45-1 (VMP)	SO199- DR46-1 (VMP)
	Gringe Seamount	Mt. Melchior Seamount	Lucia Seamount	Lucia Seamount	Attention Seamount	Glögg Seamount	Halley Seamount
SiO ₂	49.86	45.17	48.20	48.10	48.09	62.02	47.35
TiO ₂	1.98	3.37	3.52	3.20	3.01	0.29	2.36
Al ₂ O ₃	17.56	16.66	17.50	18.12	17.33	17.72	19.59
Fe ₂ O ₃	11.10	12.22	11.80	11.46	11.78	5.17	12.59
MnO	0.11	0.22	0.15	0.11	0.12	0.17	0.08
MgO	0.74	1.98	0.99	0.87	3.01	0.27	1.33
CaO	5.93	8.46	5.45	6.71	6.89	1.43	6.82
Na ₂ O	4.66	3.63	3.68	3.85	4.02	6.02	3.66
K ₂ O	4.01	2.35	4.21	3.96	2.88	6.14	2.33
P ₂ O ₅	2.14	2.50	1.00	1.88	0.99	0.10	1.00
H ₂ O	1.54	3.00	2.85	1.81	2.11	0.27	3.05
CO ₂	0.07	0.23	0.15	0.11	0.26	0.01	0.10
TOTAL	99.70	99.77	96.65	100.18	100.49	99.79	100.23
Rb	57.4	34.0	56.5	56.1	47.6	124	31.9
Ba	745	839	581	545	831	47.9	480
Th	6.72	4.56	4.50	4.29	5.17	22.4	4.30
U	1.78	1.65	1.40	1.34	1.26	1.31	1.34
Nb	75.5	55.2	56.6	54.6	69.5	151	46.7
Ta	4.80	3.53	3.40	3.29	4.01	9.83	2.71
La	75.9	44.0	48.3	43.3	61.5	124	46.3
Ce	143	84.0	97.1	90.2	122	248	68.0
Pb	4.68	3.43	3.40	3.61	4.87	13.2	3.38
Pr	18.4	10.1	11.7	10.7	14.1	22.9	9.50
Nd	73.7	42.1	47.2	44.9	55.9	75.1	37.8
Sr	759	960	677	669	960	22.3	706
Sm	13.8	9.09	9.67	9.31	10.1	10.8	7.52
Hf	8.96	5.84	7.30	6.71	8.39	21.5	5.10
Zr	413	245	298	297.5	377	822	228
Eu	4.41	3.09	3.28	3.14	3.32	0.85	2.55
Gd	12.6	8.56	8.90	8.86	9.03	8.79	7.61
Tb	1.73	1.21	1.36	1.28	1.21	1.20	1.11
Dy	9.00	6.26	7.51	6.83	5.90	5.90	6.21
Ho	1.65	1.11	1.36	1.26	1.00	1.08	1.20
Y	48.8	30.2	41.0	33.9	27.1	28.7	37.4
Er	4.20	2.70	3.84	3.19	2.41	2.98	3.16
Tm	0.55	0.35	0.53	0.43	0.30	0.44	0.44
Yb	3.43	2.10	3.04	2.70	1.77	3.01	2.74
Lu	0.49	0.29	0.47	0.38	0.24	0.45	0.39

Table 2: continued

	SO199- DR49-1 (VMP)	SO199- DR49-8 (VMP)	SO199- DR49-14 (VMP)	SO199- DR50-2 (VMP)	SO199- DR84-2* (VMP)	SO199- DR56-1 (EWP)	SO199- DR56-1 (EWP)	SO199- DR56-4 (EWP)
	Apollo 8 Seamount	Apollo 8 Seamount	Apollo 8 Seamount	Apollo 8 Seamount	Ulrike Seamount	Royal Mary Seamount	Replicate ICP-MS	Royal Mary Seamount
SiO ₂	52.38	61.24	63.20	59.03	47.51	48.10		52.35
TiO ₂	3.10	0.32	0.36	0.68	4.45	1.28		3.34
Al ₂ O ₃	17.09	17.28	17.59	18.76	14.04	23.97		17.53
Fe ₂ O ₃	8.47	6.95	4.51	5.09	13.50	4.72		10.08
MnO	0.08	0.09	0.07	0.10	0.16	0.05		0.06
MgO	1.80	0.18	0.31	1.04	3.97	1.49		1.23
CaO	6.04	1.07	1.22	1.98	9.09	13.84		4.62
Na ₂ O	4.17	6.20	6.37	4.90	3.43	3.07		4.36
K ₂ O	4.16	5.95	6.16	6.48	0.83	1.19		3.57
P ₂ O ₅	1.00	0.09	0.08	0.21	0.56	0.3		1.00
H ₂ O	1.12	0.69	0.40	2.06	2.03	0.56		1.50
CO ₂	0.07	0.02	0.01	0.04	0.07	1.66		0.06
TOTAL	99.48	100.08	100.28	100.37	97.61	100.23		99.79
Rb	58.4	194	139	114	12.9	11.5	11.5	56.0
Ba	703	15.0	7.34	125	178	301	307	776
Th	6.12	19.9	15.5	12.2	2.80	1.49	1.50	4.68
U	1.29	0.79	0.47	2.50	0.40	1.10	1.10	2.32
Nb	72.4	209	82.9	135	31.1	18.5	18.5	55.4
Ta	4.2	11.0	10.1	7.36	2.20	1.09	1.12	3.35
La	60.0	153	132	94.9	23.6	16.9	17.0	60.8
Ce	121	257	200	183	59.1	33.6	33.8	106
Pb	5.85	14.0	6.82	14.5	1.30	1.95	1.96	4.86
Pr	14.2	32.2	30.5	19.6	7.15	3.97	4.02	13.4
Nd	56.4	116	109	69.6	31.4	16.1	16.1	53.9
Sr	768	14.8	12.9	102	283	747	757	518
Sm	10.3	20.2	17.4	11.3	7.82	3.16	3.20	10.4
Hf	10.0	35.1	17.9	22.1	6.20	2.70	2.71	8.54
Zr	454	1629	449	1012	240	116	115	372
Eu	3.22	1.07	0.56	2.00	2.60	1.25	1.26	3.16
Gd	9.10	17.1	12.6	9.55	8.88	3.06	3.06	10.6
Tb	1.25	2.52	1.60	1.36	1.55	0.45	0.45	1.64
Dy	6.31	13.6	6.80	7.09	8.47	2.45	2.46	9.88
Ho	1.13	2.60	1.08	1.31	1.72	0.47	0.47	2.07
Y	31.2	71.1	25.1	35.7	47.9	12.7	12.7	60.6
Er	2.84	7.17	2.64	3.55	4.59	1.23	1.24	5.69
Tm	0.38	1.05	0.33	0.51	0.69	0.17	0.17	0.82
Yb	2.36	6.97	2.12	3.34	4.02	1.08	1.08	5.34
Lu	0.33	1.02	0.31	0.49	0.62	0.16	0.16	0.77

Table 2: continued

	SO199- DR56-6 (EWP)	SO199- DR57-1 (EWP)	SO199- DR58-1 (EWP)	SO199- DR62-1 (EWP)	SO199- DR66-1 (EWP)	SO199- DR66-2 (EWP)	SO199- DR66-5* (EWP)
	Royal Mary Seamount	Elena Seamount	Max Seamount	Janne Seamount	Finn Seamount	Finn Seamount	Finn Seamount
SiO ₂	62.42	50.52	50.16	46.56	50.81	50.15	50.62
TiO ₂	0.50	2.85	2.76	3.01	1.45	1.47	1.63
Al ₂ O ₃	18.08	14.61	17.74	18.94	19.92	18.02	15.96
Fe ₂ O ₃	3.99	13.26	10.64	14.39	8.84	8.85	9.80
MnO	0.09	0.19	0.08	0.10	0.06	0.09	0.13
MgO	0.72	4.04	2.63	1.82	3.84	5.66	4.99
CaO	1.55	8.84	5.81	6.74	7.64	10.14	10.62
Na ₂ O	5.38	3.73	3.69	3.49	3.39	3.30	3.03
K ₂ O	5.98	1.21	2.05	1.40	1.68	0.87	0.78
P ₂ O ₅	0.11	0.40	1.00	0.50	0.32	0.18	1.00
H ₂ O	0.97	1.16	2.74	2.83	2.19	1.74	1.74
CO ₂	0.02	0.03	0.08	0.06	0.03	0.01	0.26
TOTAL	99.81	100.74	99.38	99.84	100.26	100.48	98.82
Rb	51.2	25.1	41.00	30.2	29.4	13.5	14.9
Ba	1292	337	378	261	144	143	83.0
Th	12.3	3.53	2.65	2.80	1.14	1.08	0.80
U	0.36	0.79	0.78	0.71	0.53	0.29	0.40
Nb	84.6	43.2	34.7	39.0	13.0	12.4	9.50
Ta	6.31	2.50	2.70	2.26	0.77	0.74	0.60
La	85.0	32.4	32.4	26.5	14.3	9.15	8.30
Ce	153.1	65.5	62.8	51.4	24.7	21.4	21.5
Pb	7.25	2.64	3.55	2.29	1.27	1.48	0.90
Pr	17.9	7.85	8.41	6.75	3.72	2.86	2.89
Nd	65.2	32.3	37.0	28.2	16.6	13.1	14.4
Sr	86.4	329	528	429	374	362	376
Sm	11.6	7.14	8.41	6.41	4.05	3.42	4.04
Hf	19.4	5.35	6.00	4.94	2.88	2.76	3.50
Zr	734	223	252	208	121	115	114
Eu	2.48	2.34	2.74	2.14	1.53	1.34	1.62
Gd	10.5	7.70	8.15	6.69	4.60	3.82	4.93
Tb	1.61	1.23	1.20	1.06	0.75	0.63	0.83
Dy	9.05	7.26	6.51	7.09	4.59	3.79	4.58
Ho	1.78	1.44	1.21	1.31	0.92	0.75	0.91
Y	44.8	39.0	34.4	35.7	26.5	19.8	25.2
Er	4.97	3.88	3.09	3.55	2.46	1.99	2.71
Tm	0.76	0.56	0.43	0.51	0.35	0.28	0.73
Yb	5.37	3.61	2.65	3.34	2.24	1.84	2.21
Lu	0.80	0.53	0.38	0.49	0.32	0.27	0.34

Table 2: continued

	SO199- DR73-1 (EWP)	SO199- DR73-11C (EWP)	SO199- DR79-1 (EWP)	SO199- DR79-3 (EWP)	SO199- DR79-4 (EWP)	SO199- DR80-1* (EWP)	SO199- DR72-1 (AP)
	Annegret Seamount	Annegret Seamount	Bente Seamount	Bente Seamount	Bente Seamount	Clara- Marie Seamount	Iris Seamount
SiO ₂	49.86	65.20	48.70	62.26	61.12	68.3	50.16
TiO ₂	2.82	0.23	2.99	0.43	0.49	0.27	2.53
Al ₂ O ₃	15.56	15.80	17.51	17.97	18.02	14.15	19.00
Fe ₂ O ₃	14.79	4.02	9.78	4.61	5.51	4.33	12.18
MnO	0.08	0.03	0.12	0.10	0.08	0.05	0.08
MgO	2.35	0.34	1.46	0.54	0.68	0.18	1.77
CaO	4.16	0.15	7.89	1.68	1.73	0.37	7.20
Na ₂ O	3.49	5.66	3.63	5.22	5.08	5.69	3.33
K ₂ O	3.06	6.82	3.42	6.14	5.70	5.38	1.59
P ₂ O ₅	0.91	0.03	1.00	0.09	0.17	0.04	0.43
H ₂ O	3.15		1.83	1.05	1.33	0.02	2.09
CO ₂	0.08	0.07	1.62	0.02	0.03	0.07	0.03
TOTAL	100.31	98.35	99.95	100.11	100.00	98.83	100.39
Rb	62.5	147	78.6	46.6	42.0	194	40.9
Ba	438	9.00	394	403.0	624	5.00	51.0
Th	4.33	27.5	3.35	9.03	8.11	20.8	1.17
U	0.71	0.20	0.89	0.37	0.21	1.20	0.61
Nb	25.1	59.6	33.4	52.6	53.2	144	18.0
Ta	1.68	6.70	2.12	3.76	3.48	10.0	1.09
La	33.9	145	37.6	26.5	76.9	136	13.7
Ce	68.4	202	66.2	75.6	112	260	30.3
Pb	4.15	11.6	3.91	6.20	5.32	6.50	0.63
Pr	9.03	33.3	8.66	18.3	17.9	29.4	4.37
Nd	37.8	124	36.0	70.2	69.2	111	20.5
Sr	368	15.1	459	56.5	86.6	11.5	197
Sm	8.29	22.1	7.69	13.6	13.4	20.5	5.67
Hf	5.96	23.7	5.62	18.4	16.6	35.1	3.98
Zr	238	608	251	844	791	1485	149
Eu	2.62	0.74	2.51	2.31	2.82	1.13	1.99
Gd	8.24	17.8	7.83	12.2	12.4	16.9	6.81
Tb	1.25	3.00	1.18	1.90	1.91	2.92	1.18
Dy	7.21	15.7	6.66	10.7	10.5	16.0	7.43
Ho	1.38	2.60	1.30	2.07	1.98	2.97	1.52
Y	37.8	55.7	39.1	50.6	48.8	63.3	41.0
Er	3.63	6.67	3.41	5.80	5.20	8.65	4.08
Tm	0.50	0.93	0.48	0.88	0.74	1.40	0.60
Yb	3.21	5.25	3.01	6.28	4.79	9.28	3.80
Lu	0.46	0.74	0.43	0.97	0.70	1.44	0.56

Table 2: continued

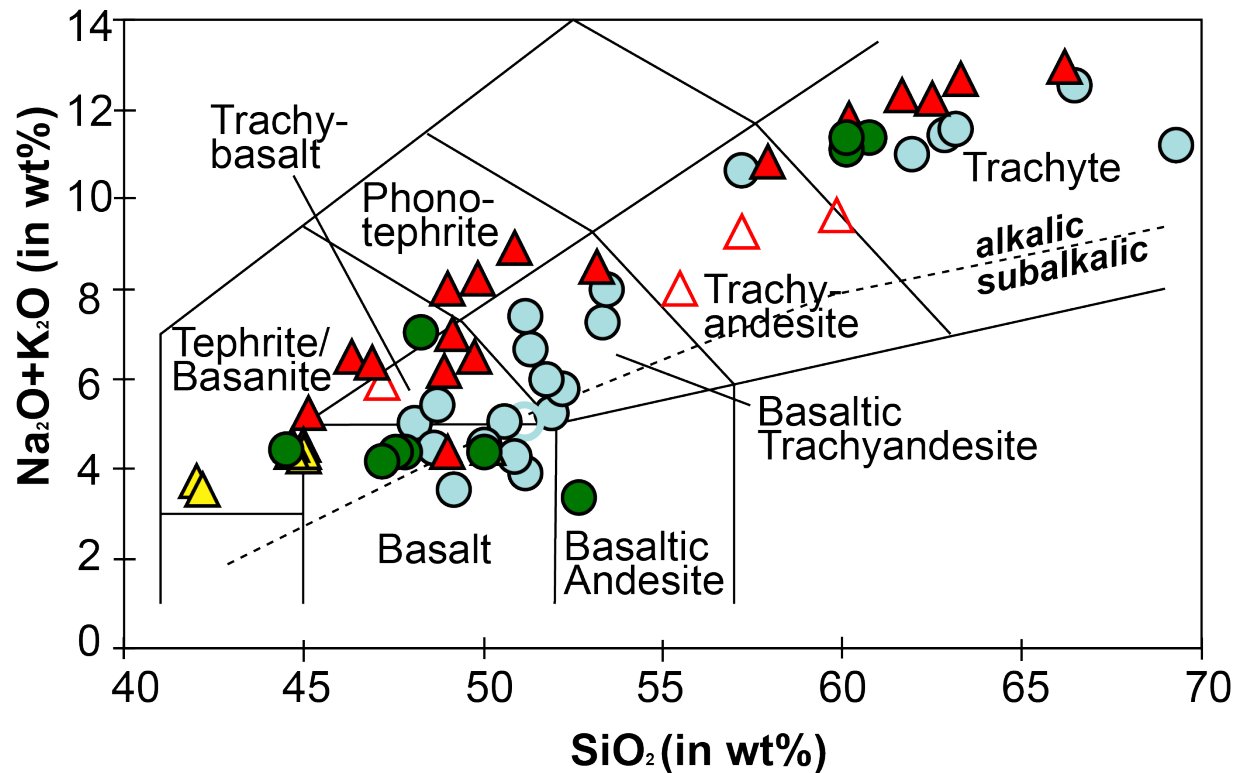
	SO199- DR55-1 (LVS)	CH1A* (UVS)	CH1B* (UVS)	CH2* (UVS)	CH3* (UVS)	CH4* (UVS)	CH5* (LVS)
	Christmas Island	Christmas Island	Christmas Island	Christmas Island	Christmas Island	Christmas Island	Christmas Island
SiO ₂	47.50	43.48	43.06	43.07	43.35	42.90	58.50
TiO ₂	3.2	1.92	1.93	1.87	1.89	1.90	0.35
Al ₂ O ₃	15.80	12.21	12.22	11.81	11.94	12.18	17.10
Fe ₂ O ₃	12.37	10.95	10.97	10.84	10.98	11.00	7.19
MnO	0.17	0.18	0.18	0.17	0.18	0.18	0.22
MgO	2.45	11.03	11.25	11.89	11.76	11.42	0.94
CaO	8.07	12.24	12.39	12.30	12.28	12.31	2.23
Na ₂ O	4.57	1.88	1.79	1.79	1.79	1.82	5.08
K ₂ O	2.37	2.47	2.40	2.23	2.17	2.27	5.85
P ₂ O ₅	1.94	0.58	0.55	0.54	0.53	0.54	0.09
H ₂ O	1.06	2.23	2.49	2.55	2.19	2.52	2.09
CO ₂	0.10	0.07	0.01	0.15	0.11	0.18	0.11
TOTAL	99.60	99.35	99.36	99.35	99.33	99.35	99.73
Rb	32.8	53.0	51.7	49.1	48.4	49.9	131.2
Ba	471	1275	1227	1192	1485	1304	215
Th	7.09	7.70	8.10	7.90	8.30	8.10	15.3
U	1.64	1.70	1.70	1.70	1.70	1.80	3.40
Nb	104	54.7	54.1	51.7	53.5	51.5	163
Ta	6.20	3.30	3.20	3.20	3.20	2.90	9.40
La	77.8	56.0	55.7	54.0	55.2	53.7	108
Ce	166	122	119	120	121	117	231
Pb	3.62	9.60	9.70	9.40	9.10	9.30	4.00
Pr	20.0	13.6	13.6	13.3	13.4	13.1	23.5
Nd	82.3	54.1	54.1	53.0	53.4	54.8	85.0
Sr	1064	1321	1276	1239	1268	1261	31.6
Sm	15.7	9.52	9.45	9.08	9.27	9.16	13.9
Hf	12.1	6.10	5.80	6.10	6.20	5.30	19.9
Zr	567	251	249	244	245	240.3	758
Eu	4.80	2.87	2.91	2.75	2.83	2.75	2.85
Gd	13.6	6.93	6.93	6.61	6.69	6.86	10.2
Tb	1.81	1.01	0.99	0.96	0.97	0.95	1.75
Dy	8.50	4.75	4.47	4.44	4.60	4.38	9.05
Ho	1.38	0.77	0.78	0.73	0.77	0.76	1.66
Y	36.8	22.7	21.8	21.5	21.9	20.9	46.0
Er	3.18	1.85	1.91	1.81	1.82	1.81	4.41
Tm	0.37	0.25	0.25	0.25	0.26	0.25	0.62
Yb	2.15	1.47	1.53	1.37	1.39	1.44	3.78
Lu	0.29	0.22	0.21	0.22	0.21	0.20	0.55

Table 2: continued

	CH5B* (LVS)	CH6* (LVS)	CH7A* (UVS)	CH7B* (UVS)	CH8* (LVS)	CH9 * (LVS)	CH10* (LVS)
	Christmas Island	Christmas Island	Christmas Island	Christmas Island	Christmas Island	Christmas Island	Christmas Island
SiO ₂	58.71	58.90	40.54	40.71	51.17	43.08	49.35
TiO ₂	0.35	0.26	2.20	2.20	0.99	3.51	2.62
Al ₂ O ₃	17.03	17.25	10.75	10.52	19.93	11.52	13.79
Fe ₂ O ₃	7.25	6.77	11.93	12.01	9.04	13.01	12.29
MnO	0.23	0.18	0.18	0.18	0.15	0.16	0.16
MgO	0.84	0.40	14.67	14.91	3.23	10.49	7.33
CaO	2.27	2.25	12.28	12.26	9.45	9.19	8.09
Na ₂ O	5.08	5.33	1.70	1.59	2.90	2.25	3.37
K ₂ O	5.81	5.67	1.74	1.66	0.36	1.95	1.04
P ₂ O ₅	0.09	0.05	0.54	0.55	0.11	1.00	0.51
H ₂ O	2.09	2.69	2.49	2.49	2.35	3.19	1.09
CO ₂	0.01	0.01	0.11	0.01	0.15	0.01	0.01
TOTAL	99.71	99.70	99.30	99.31	99.79	99.47	99.65
Rb	131	129	37.5	36.8	6.90	31.8	17.3
Ba	225	58.0	1149	1263	109	561	298
Th	16.5	19.7	8.50	9.00	0.30	4.20	2.90
U	3.30	4.80	1.80	1.80	0.10	1.10	1.00
Nb	171.0	202	53.6	53.7	1.70	73.7	38.1
Ta	10.0	11.5	3.30	3.00	0.20	4.30	2.30
La	77.8	129	54.4	53.7	3.50	47.7	26.5
Ce	112.1	273	115	115	10.0	108	59.3
Pb	4.40	8.10	9.70	9.20	1.60	1.60	0.50
Pr	24.3	28.1	13.0	13.0	1.44	12.6	7.02
Nd	90.9	104	52.7	51.2	7.40	54.1	31.5
Sr	62.1	94.6	1364	1258	330	1052	470
Sm	14.3	16.4	8.83	8.84	2.38	9.96	6.45
Hf	19.5	22.8	5.10	5.00	1.60	6.50	6.70
Zr	780	940	197	193	46.5	259	252
Eu	2.87	2.49	2.68	2.65	0.89	3.38	2.19
Gd	10.4	12.2	6.36	6.27	3.01	9.07	6.35
Tb	1.83	2.09	0.92	0.91	0.55	1.29	0.99
Dy	9.42	10.7	4.16	4.16	3.18	5.96	5.05
Ho	1.69	2.03	0.71	0.69	0.70	0.96	0.91
Y	46.1	55.3	19.5	19.2	19.5	27.5	25.0
Er	4.56	5.19	1.78	1.61	2.02	2.22	2.28
Tm	0.64	0.75	0.23	0.23	0.30	0.29	0.30
Yb	3.86	4.48	1.28	1.25	1.93	1.62	1.81
Lu	0.56	0.66	0.18	0.18	0.30	0.21	0.25

Table 2: continued

	CH11* (LVS)	CH12* (LVS)	CH13* (LVS)
	Christmas Island	Christmas Island	Christmas Island
SiO ₂	46.28	45.70	46.46
TiO ₂	3.16	3.36	3.24
Al ₂ O ₃	12.35	12.69	12.64
Fe ₂ O ₃	12.42	12.36	12.22
MnO	0.16	0.19	0.16
MgO	9.95	8.40	8.97
CaO	8.92	8.94	9.23
Na ₂ O	2.69	2.65	2.74
K ₂ O	1.52	1.74	1.58
P ₂ O ₅	0.52	0.72	0.54
H ₂ O	1.21	2.10	1.08
CO ₂	0.29	0.70	0.62
TOTAL	99.56	99.53	99.57
Rb	29.5	31.9	28.8
Ba	403	569	396
Th	5.50	7.40	5.10
U	1.30	1.60	1.30
Nb	55.3	65	56.9
Ta	3.40	3.90	3.30
La	43.7	54.9	43.3
Ce	92.3	119	91.0
Pb	2.10	2.90	2.30
Pr	10.3	12.9	10.1
Nd	42.2	50.9	40.9
Sr	602	866	637.8
Sm	7.79	8.21	7.69
Hf	6.70	8.50	6.50
Zr	257	330	253.4
Eu	2.41	2.69	2.41
Gd	6.82	6.69	6.64
Tb	1.06	1.06	1.02
Dy	5.15	4.84	5.18
Ho	0.97	0.89	0.95
Y	25.6	25.1	25.2
Er	2.26	2.18	2.41
Tm	0.31	0.31	0.32
Yb	1.84	1.89	1.81
Lu	0.25	0.25	0.26



Christmas Island Seamount Province:

- △ CKP- Cocos Keeling Island Volcanic Province
- ▲ VMP- Vening Meinesz Volcanic Province
- EWP-Eastern Wharton Basin Volcanic Province
- AP- Argo Basin Volcanic Province
- Christmas Island:
- ▲ (UVS) upper volcanic section
- (LVS) lower volcanic section

Fig. 2: Total alkali versus SiO_2 diagram illustrating the dominantly alkaline composition of the CHRISP ranging from tephrites and basalts over (trachy-)andesites to trachytes. The following abbreviations were used for each subprovince: Cocos Keeling Volcanic Province (CKP), the Vening Meinesz Volcanic Province (VMP), Christmas Island (UVS= upper volcanic section, and LVS= lower volcanic section), the eastern Wharton Volcanic Province (EWP), and the Argo Province (AP). Symbols in all diagrams are always the same: unfilled red triangle (CKP), filled red triangle (VMP), blue filled circle (EWP) blue unfilled circle (AP), Christmas Island (UVS) yellow filled triangle and Christmas Island (LVS) green filled circle. Subdivision between alkaline and subalkaline rock suites after Irvine and Baragar (1971). All data are normalized to a 100% volatile free basis.

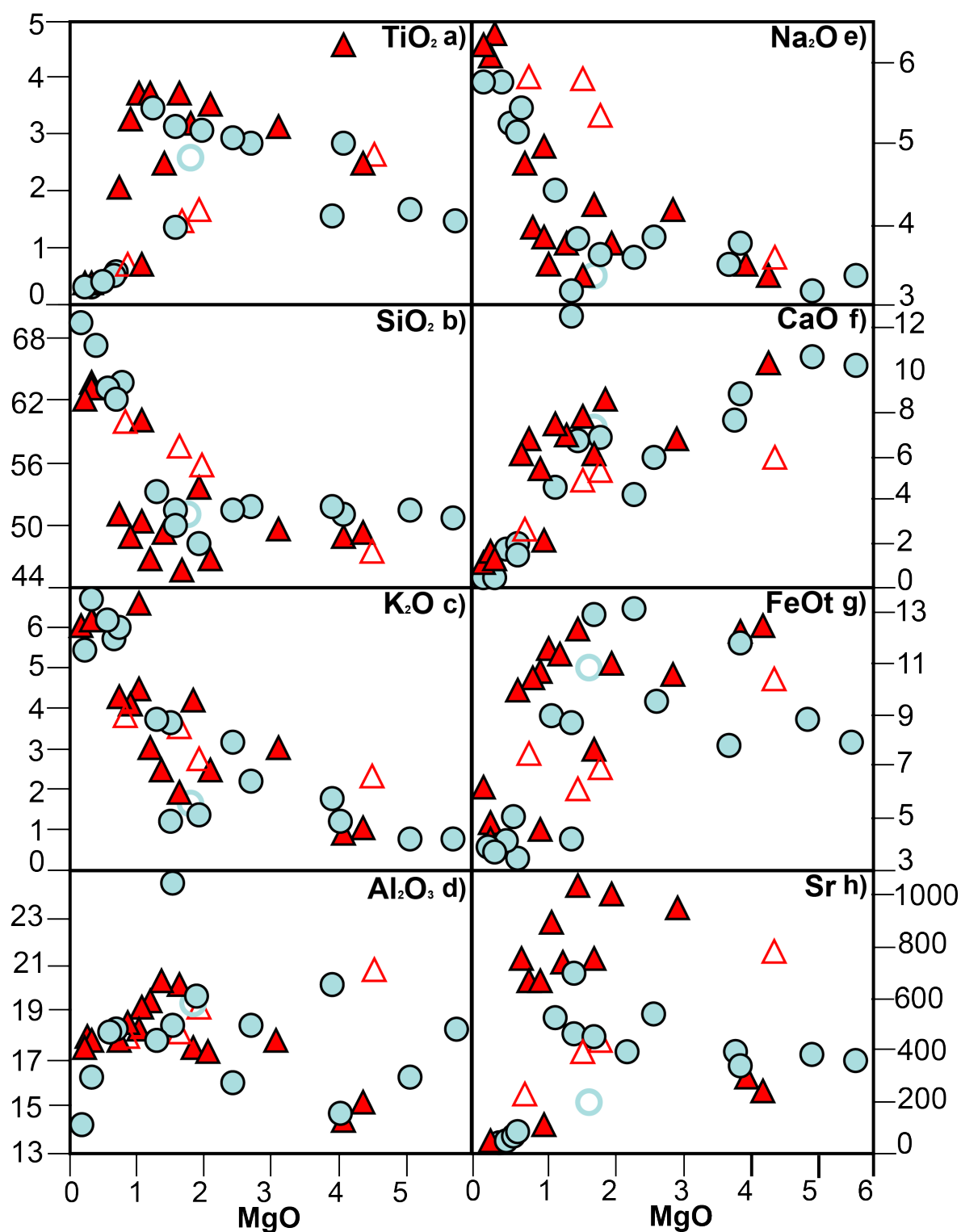


Fig. 3a-h: Selected major and trace elements versus MgO of the CHRISP subprovinces, CKP, VMP, EWP and AP. The major element diagrams show that most of the samples are affected by fractionation and/or alteration. Major element variations in sub-provinces CKP, VMP and EWP are controlled by clinopyroxene, plagioclase, k-feldspar, magnetite, and amphibole. Symbols as in figure 2.

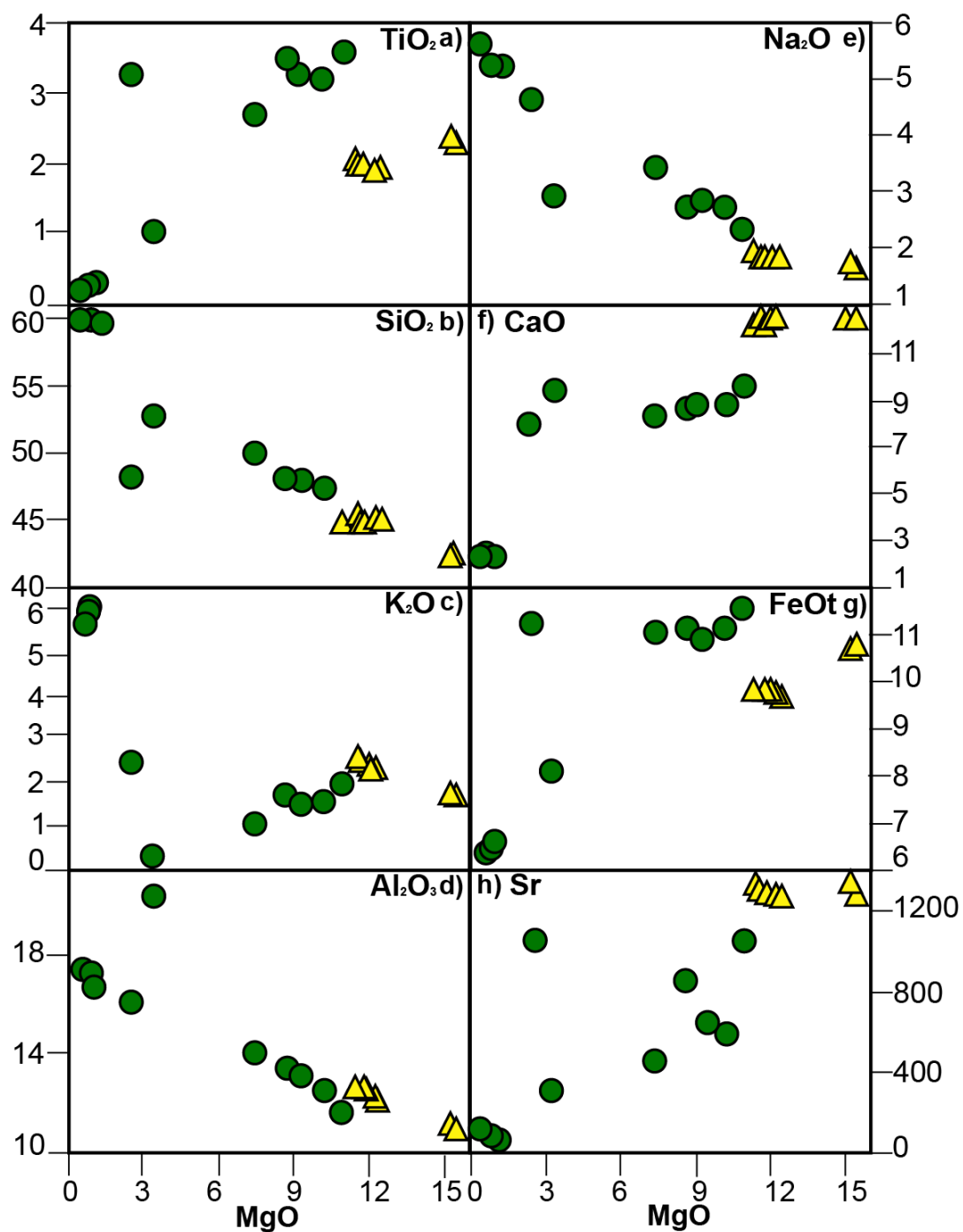


Fig. 4a-h: Selected major and trace elements versus MgO of Christmas Island. Christmas Island samples are consistent with fractionation of olivine, pyroxene, ilmenite and apatite. Symbols as in figure 2.

5. DISCUSSION

5.1 Fractional crystallization and partial melting degree

Samples of the CHRISP comprise a broad variety of rock types. The great range of rock samples within each sub-province is probably due to crystal fractionation or accumulation of minerals at relatively shallow levels. The sub-provinces CKP, VMP and EWP follow almost the same fractionation trends of minerals in their group. Samples from Christmas Island differ slightly in their mineral fractionation trends from the other sub-provinces (see Fig. 3a-h and 4 a-h).

Major element variations in sub-provinces CKP, VMP and EWP are controlled by clinopyroxene, plagioclase, k-feldspar, magnetite, and amphibole. A strong decrease in CaO (5-6 wt%) and Al₂O₃ (1.37 wt%) as well as depletion in Cr with decreasing MgO suggests fractionation of plagioclase and clinopyroxene in these samples. A similar decrease in TiO₂ and FeO_t below 1 wt% MgO implies fractionation of Fe-Ti oxides such as magnetite or ilmenite oxides being consistent with thin section observation. Additionally Sr can be a useful indicator for plagioclase crystallization at shallow depths. Therefore the decreasing effect of Sr with MgO might reflect plagioclase as a fractional phase in the sub-provinces EWP, CKP and VMP (Fig. 3h). The high variability of Sr at 2 wt.% MgO suggests variable assemblages of plagioclases as thin sections confirm. Additionally Sr shows a very different behavior from Al₂O₃ and therefore apatite fractionation/accumulation must also play a role. Samples of Christmas Island display well-constrained fractionation trends reflecting consideration of a single volcanic system that differs sharply with respect to the incompatible behavior of Al₂O₃ and compatible behavior of K₂O during melt differentiation in comparison with the remainder of the CHRISP (see Fig 3a-h and 4a-h). In detail the most primitive UVS samples have 15.5 wt.% MgO and are considered near primary melts (Fig. 4a-h). Like in all other sub-provinces CaO decreases with decreasing MgO but the above mentioned increase in Al₂O₃ (best represented in LVS) points to pyroxene as the sole Ca fractionating mineral phase, so that plagioclase fractionation seems absent in the LVS. Other elements such as TiO₂, CaO, FeO_t, P₂O₅ and Sr decrease with a decrease in MgO at Christmas Island consistent with fractionation of olivine, pyroxene, ilmenite and apatite over the course of magma evolution. The relatively strong enrichment in the transitional metals Ni and Cr

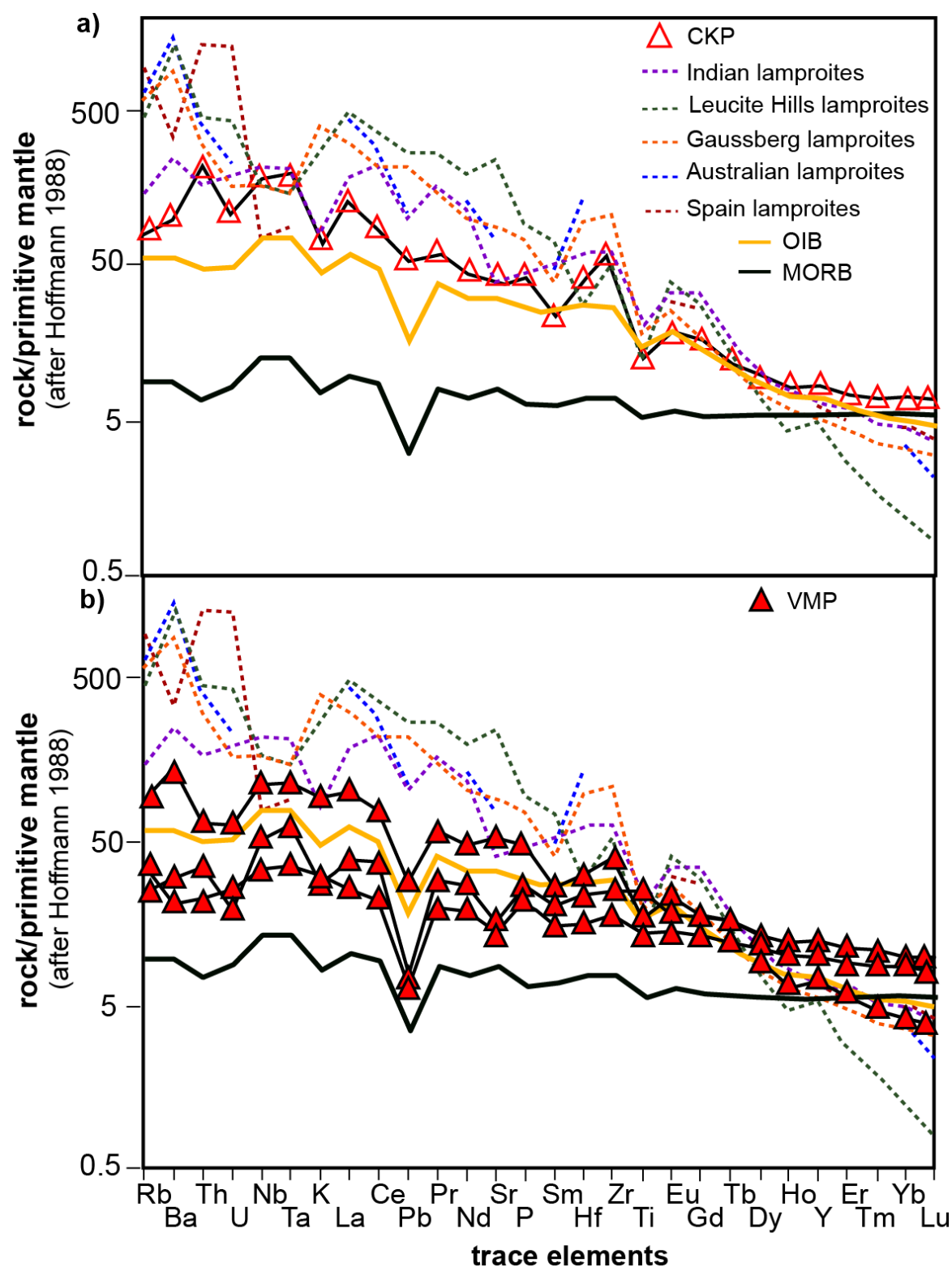
compared to the other sub-provinces, implies that olivine started to fractionate Ni at 200 ppm and Cr >1200 ppm levels.

The absence of plagioclase on the liquidus and olivine + pyroxene \pm Cr-spinel as main fractionation phases indicate a deep magma reservoir (>5 kb; Albarede and Tamagnan 1988) for the UVS beneath Christmas Island. The unusual compatible behavior of K₂O in comparison to CHRISP indicates fractionation of a K-rich phase such as amphibole and/or phlogopite. In the most evolved LVS samples the strong enrichment in K₂O probably reflects K-feldspar accumulation.

The negative slope within the HREE ((Sm/Yb)_n, (Gd/Yb)_n and (Dy/Yb)_n > 1) indicates that garnet was a residual source phase over the entire CHRISP (Fig. 6a-d). Other minor fractional phases are shown in a slight positive inflection of Eu in 4 subalkaline samples from EWP which are interpreted to result from plagioclase accumulation as shown in thin sections (Fig. 5c).

To distinguish between different degrees of partial melting in all subprovinces, concentration of incompatible trace elements were used which are particularly sensitive to partial melting degree. In combination with SiO₂ content, incompatible trace element ratios such as e.g. (La/Yb)_n, (La/Sm)_n, Nb/Y and Ta/Yb show that the degree of melting is low in all subprovinces but small differences exist between them as is already evident from their strong alkalinity (Fig. 2). EWP lavas have been generated by the lowest melting degree as indicated by a high SiO₂ saturation (48.05-69.21 wt%) and low incompatible trace element ratios (La/Yb)_n (2.43-18.68), (La/Sm)_n (1.29-4.61), (Nb/Y) (0.38-2.29), and Ta/Yb (0.27-1.28) (Fig. 6a-d). In contrast to the EWP subprovince, Christmas Island reveals higher ratios of (La/Yb)_n (1.22-29.88), (La/Sm)_n (0.92-4.96), Nb/Y (0.09-3.71), and Ta/Yb (1.22-10) and lower SiO₂ saturation of 42.05-60.69 wt. %, which likely indicates a higher partial melting degree. Samples from the VMP and CKP subprovinces show similar trace element ratios and SiO₂ values compared to Christmas Island and may therefore also generated by higher degrees of partial melting than the EWP lavas (Fig. 6a-d).

The major conclusion of this chapter is that the majority of the CHRISP samples are strongly affected by fractionation and that most samples were probably generated by slightly varying but generally low partial melting degrees.



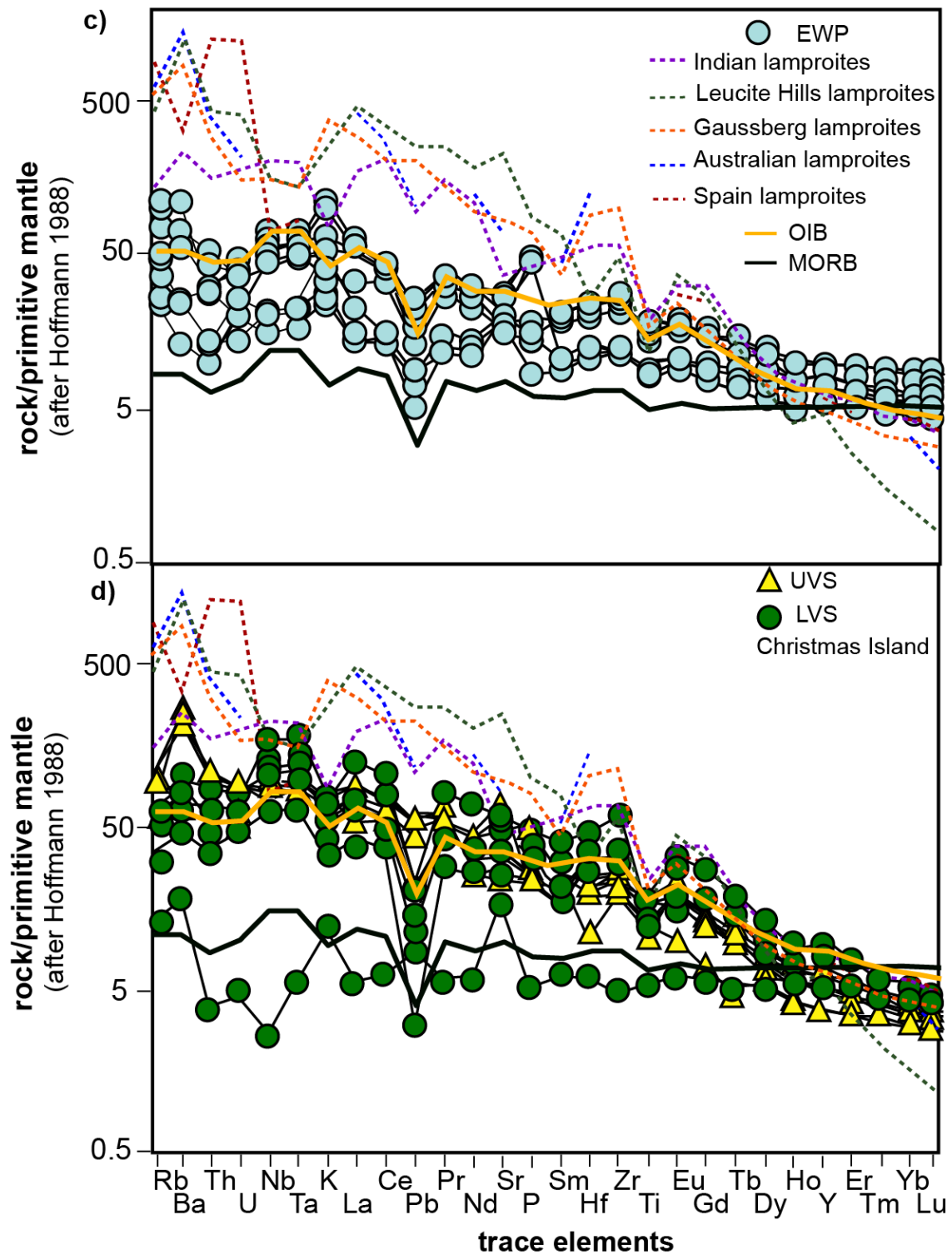
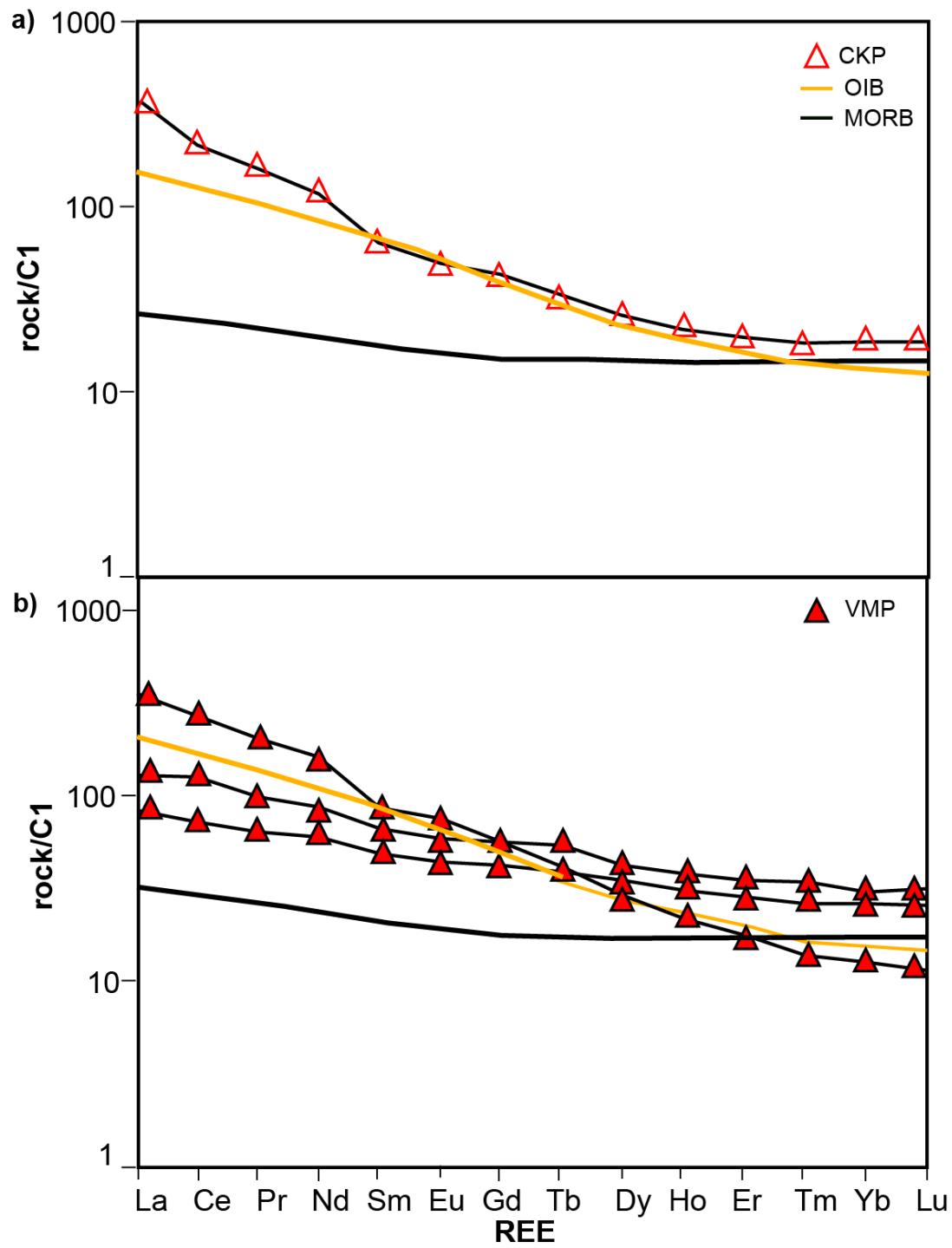


Fig. 5a-d: Multi-element diagram normalized to primitive mantle after Hofmann (1988) for (a) CKP (b) VMP (c) EWP and (d) Christmas Island (UVS and LVS). The trace elements patterns of the CKP, VMP and Christmas Island UVS and LVS are similar to those of ocean islands basalts (OIB), whereas EWP ranges between OIB and E-MORB. OIB and E-MORB pattern after Sun and McDonough (1989). Symbols as in figure 2. Additionally for comparison in all multi element diagrams were plotted data from lamproites of Leucite Hills

=dashed orange line, Indian Lamproites =dashed purple line, Gaussberg Lamproite = dashed green line, Spain lamproites= dashed red line and Australian lamproites= dashed blue line.



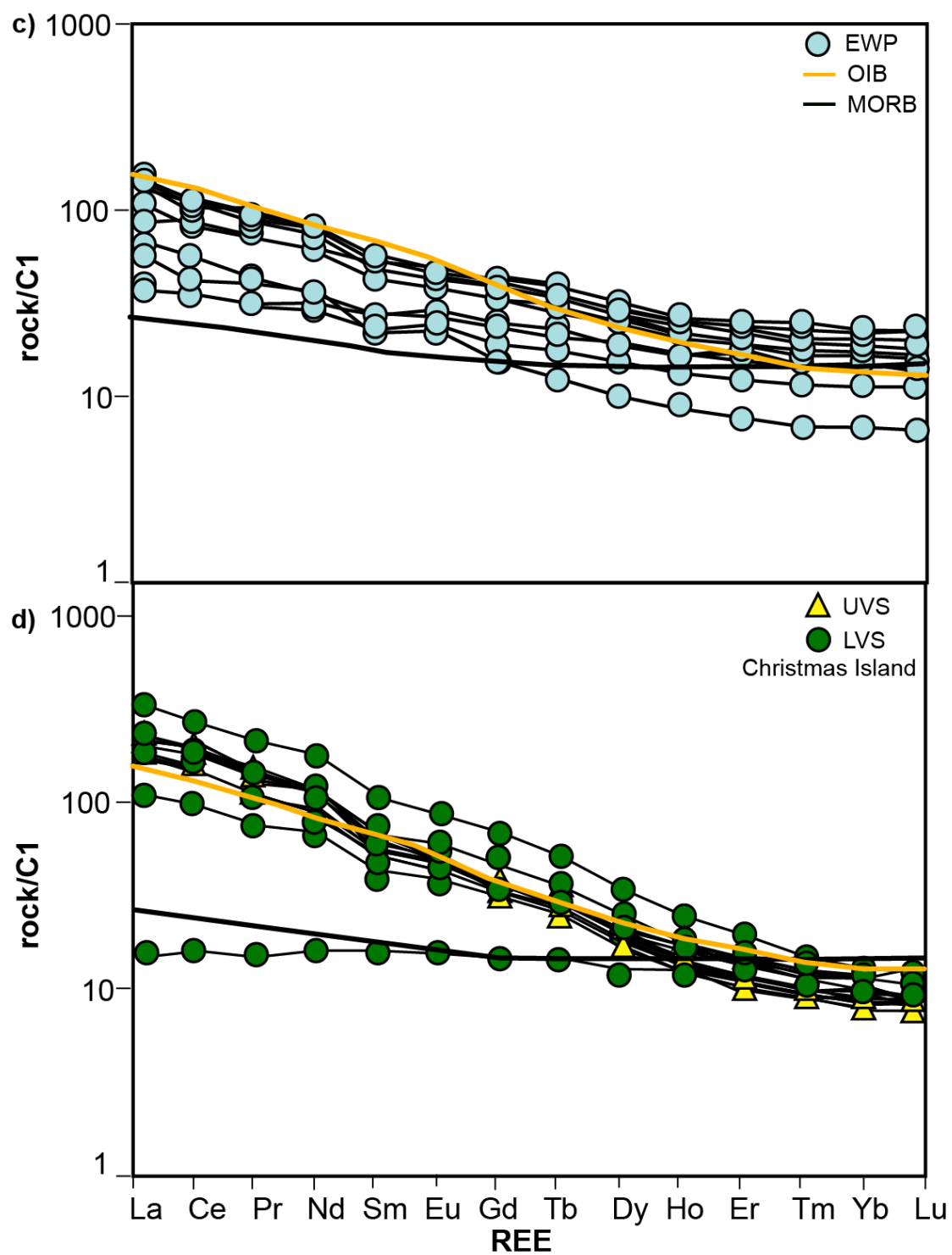


Fig. 6a-d: REE diagrams normalized to C1 after McDonough and Sun (1995) for (a) CKP (b) VMP (c) EWP and (d) UVS and LVS Christmas Island samples. Symbols as in figure 2.

5.2 Melting and source composition

In order to explore the trace element composition of the magma sources, it is necessary to only consider samples, which are least affected by melt differentiation processes. Because melts that have undergone differentiation processes such as crystal fractionation, become enriched in incompatible elements and depleted in compatible elements, they do not reflect the melt composition in equilibrium with the source region. For that reason samples from the CKP, VMP and EWP with less than 4 wt% MgO are eliminated from further consideration. Hence only one sample of CKP and VMP and 4 samples of EWP will be considered further. Seven samples from Christmas Island (UVS) >11 wt% MgO appear largely unaffected by crystal fractionation and are probably closest to a primary melt and thus are the best approximation of the enriched source component.

In principle the enrichment in major elements and trace elements of the CHRISP volcanics could result from low degrees of partial melting and or melting of a source enriched in incompatible elements. The multi element diagrams imply clearly strong enrichment in incompatible elements, especially the large ion lithophile elements (LIL) Rb, Ba, K, Sr (see Fig. 5a-d) which probably indicates melting of a source enriched in LIL for the CHRISP, in particular for UVS, VMP, and CKP. In contrast the REE diagrams show that differences in the degree of melting exist between the sub-provinces (as discussed above). While the CKP and Christmas Island (UVS) display strong enrichments in light rare earth elements (LREE) over the heavy rare earth elements (HREE) compared to average global OIB, this enrichment is significantly less pronounced for the EWP, VMP and AP. To distinguish the effects of melting from source composition on element enrichment, it is common practice to plot incompatible element ratios of elements with similar melt-mineral distribution coefficients (K_D) as such ratios closest fingerprint the source. Incompatible element ratios of pairs with different K_D mirror the effects of melting more strongly. The high field strengths elements (HFS; e.g. Th, Ta, Nb Hf, Pb and Zr) and the rare earth elements (REE) can be used for discrimination between the tectonic settings of igneous rocks. Due to the altered status of the samples only immobile elements such as Th, Nb, Ta, Zr, Hf and Yb were used (Fig. 7a-b) for discrimination.

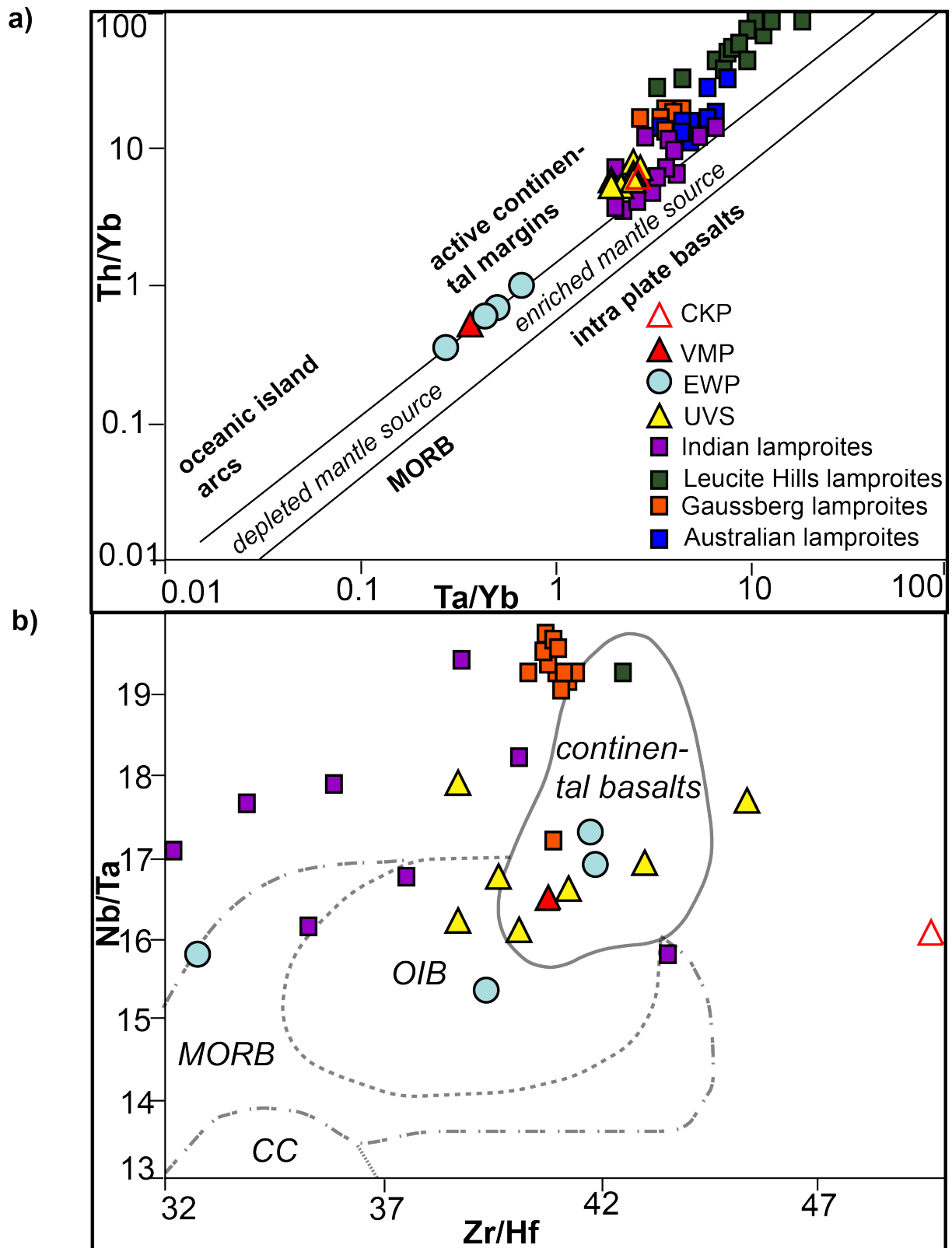


Fig. 7: Selected trace element ratios of a) Ta/Yb versus Th/Yb and b) Zr/Hf versus Nb/Ta. a) Ta/Yb versus Th/Yb diagram shows that samples of CHRISP range between an enriched and a depleted mantle component. b) Zr/Hf versus Nb/Ta indicate that most samples are more enriched than OIB and range into the field for continental basalts indicating a source which is enriched in Nb/Ta and Zr/Hf. The low Nb/Ta and Zr/Hf values

may imply a source with low HFS. Abbreviations: CC= continental crust, OIB= ocean island basalt, MORB= mid oceanic ridge basalt.

On a plot of Ta/Yb versus Th/Yb (Fig. 7a) the samples plot on the boundary (EWP and VMP) or slightly above the mantle mid-ocean ridge basalt (MORB) - ocean island basalt (OIB) array and range between an enriched mantle component and a depleted component (MORB). It should be noted that the UVS of Christmas Island show a clear affinity towards an enriched mantle component with high values for Th/Yb and relatively high Ta/Yb ratio. In addition they partially lie outside the oceanic basalt field and plot towards active continental margins. Samples from sub-provinces VMP and EWP seem more influenced by a depleted component displayed in lower Th/Yb and Ta/Yb ratios, but also trend towards an enriched component. The Zr/Hf versus Nb/Ta diagram (Fig. 7b) indicates that the many of the samples are noticeably more enriched than OIB. Some of the samples plot within the field for continental basalts. The trace element data imply that the source from which the samples were derived must be enriched in Nb/Ta with a relatively high enrichment in Zr/Hf. In summary, the major and trace element composition of the CHRISP rocks suggests derivation from a source with at least two different components, one of them enriched in LIL (Rb, Ba, K, Pb), HFS and LREE and the other one lowering the values for MREE and HREE compared to average OIB.

According to the model of Hoernle et al. (2011) the CHRISP formed near the spreading center where the West Burma block separated from Australia and India about 150 Ma ago. They explain the isotopic composition of the CHRISP through mixing of subcontinental lithospheric mantle (SCLM) with MORB type mantle.

In their model Hoernle et al. (2011) propose shallow recycling of (Archaean) continental lithosphere and mixing with MORB to generate the CHRISP. Archaean continental lithosphere can be found for instance in lamproites from NW- Australia (Fraser et al. 1985), India (Chalapathi et al. 2004 and Chakrabati et al. 2007), Antarctica (Murphy et al. 2002) or North America (Mirnejad and Bell 2006). Lamproites are small degree melts and are derived from subcontinental lithospheric mantle (SCLM enriched in H₂O and CO₂) that has undergone (ancient) metasomatism. During the rifting process the metasomatized SCLM (increased density by the presence of garnet pyroxenite and eclogite possibly) was delaminated into the convecting mantle. Heating and stirring of cold SCLM can induce dismemberment of this material and lower its density. Then it can rise up and mix with young oceanic crust formed at the W. Burma/Australian MOR (Korenaga 2005) by decompressional melting and could have generated the CHRISP by off-axis volcanism. In contrast volcanism at Christmas Island (LVS = ~44 Ma and UVS = ~4 Ma) occurred further away from the MOR in

an intraplate setting beneath older and thicker lithosphere tapping unmelted SCLM that did not intersect the solidus at the MOR due to horizontal deflection within the MOR flow regime.

Since Hoernle et al. 2011 base their model exclusively on radiogenic isotope data, we will now test if the model of SCLM-MORB mixing also works for the trace elements using the most primitive CHRISP samples from the eastern Wharton Basin (SO199 DR66-2) and Christmas Island UVS (CH7A and CH7B).

5.3 Compositional range of the possible sources

Hoernle et al. 2011 based their model on metasomatized SCLM, which is more commonly envisioned as the source of continental lamproites. These rocks mostly formed during Proterozoic to Quaternary and occur as dykes, flows, diatremes, cinder cones, pyroclastic deposits or pipes (Davies et al. 2006). Lamproites are often connected to post-orogenic magmatism and occur within plates or in a collisional environment (Kononova et al. 2011). In general lamproites are characterized by low CaO, Al₂O₃ and Na₂O contents but high K₂O/Al₂O₃ and relatively high Mg content (Foley et al. 1987). Trace elements concentrations (Fig. 5a-d) imply extreme source enrichments, specifically in the most highly incompatible elements (Foley et al. 1987). Nevertheless lamproites display variable source characteristics that presumably depend on their tectonic setting. Leucite Hills lamproites (Leucite Hills lamproites) in North America have negative Nb-Ta and Ti anomalies, which suggest relation to subducted material metasomatizing the arc mantle and they also show strong enrichment in LIL (Ba, K, Eu and Sr) (Mirnejad and Bell 2006). Lamproite samples from Australia analyzed by Fraser et al. (1985) and Graham et al. (1999) and those from southern Spain (Venturelli et al. 1984a, Nelson et al. 1986; average line of Spain lamproites and Australian lamproites see (Fig. 5a-d) seem to have similar trace element patterns as Leucite Hills lamproites and therefore may be influenced by similar metasomatic process. By contrast, the Gaussberg lamproites in Antarctica show pronounced troughs in elements like Th, U, Nb-Ta, Sm and Ti, but similar enrichments in Ba, K and Eu as Leucite Hills lamproites and additionally strong positive Zr and Hf peaks (Murphy et al. 2002). Fairly different from these localities are the Proterozoic lamproites from southern India. Compared to Leucite Hills lamproites and Gaussberg lamproites, these rocks are significantly less enriched in incompatible elements and do not show any Nb-Ta trough (Chalapathi et al. 2004). This is explained by a

metasomatic enrichment event in the sub-continental lithospheric mantle, which was affected by the migration of low-temperature, small-fraction, melts from the convecting mantle (McKenzie 1989). Compared to the other localities, there is a depletion in K, Sr and Ti. A general observation is that the source of lamproites has always undergone metasomatic enrichment process with variable involvement of sediments, fluids or silicate melts and caused source enrichment in major and trace elements. With the exception of the Indian lamproites almost all lamproites show an influence of an ancient subduction process (see average lamproites of Leucite Hills lamproites, Gausberg Lamproites and Indian lamproites in (Fig 5a-d). Nevertheless, since India was attached to Australia and close to the location where the CHRISP seamounts were ultimately formed, they, together with the Australian lamproites, are the most relevant for this study.

MORB mantle and/or recycled oceanic crust is invoked by Hoernle et al. (2011) to represent the depleted component in the CHRISP volcanics. Trace elements in MORB are generally characterized by very low LIL, HFS and low LREE but relatively high HREE compared to primitive mantle (Sun and McDonough 1989). The differences in MORBs are explained by their diverse modes of generation. Normal MORB seems derived by partial melting of a chemically fairly homogenous, well-mixed upper mantle reservoir, while the enriched MORB is thought to reflect a more heterogeneous reservoir with enriched and depleted components (le Roex et al. 1992, Workman and Hart 2005). With respect to CHRISP it is likely that Indian MORB, enriched in comparison to Pacific and North Atlantic MORB, is the most useful representative for depleted component. Indian and South Atlantic MORB are part of the so called DUPAL anomaly. The DUPAL anomaly is characterized by high $^{208}\text{Pb}/^{204}\text{Pb}$ and $^{207}\text{Pb}/^{204}\text{Pb}$ for a given $^{206}\text{Pb}/^{204}\text{Pb}$ relative to the Northern Hemisphere Reference Line (NHRL) as well as elevated $^{87}\text{Sr}/^{86}\text{Sr}$ and lower $^{143}\text{Nd}/^{144}\text{Nd}$ (Hart, 1984).

5.4 Source rocks versus primitive Christmas Island (UVS) and eastern Wharton Basin Volcanic Province (EWP)

This section attempts to compare the average source rock composition of the envisioned enriched (lamproites) and depleted (Indian MORB) components with the most mafic samples from Christmas Island (CH7A and CH7B) and the EWP (SO199 DR66-2). For this purpose representative lamproites from Spain, Australia, North America, Antarctica and India as well

as E-MORB are displayed along with Christmas Island (UVS) and EWP data (Fig 7). All lamproites are more enriched in LIL and LREE and similar or more strongly depleted in HREE than UVS. Although UVS reveals element patterns similar to OIB, it cannot be ruled out that this lava series has affinities to lamproites (Fig. 8).

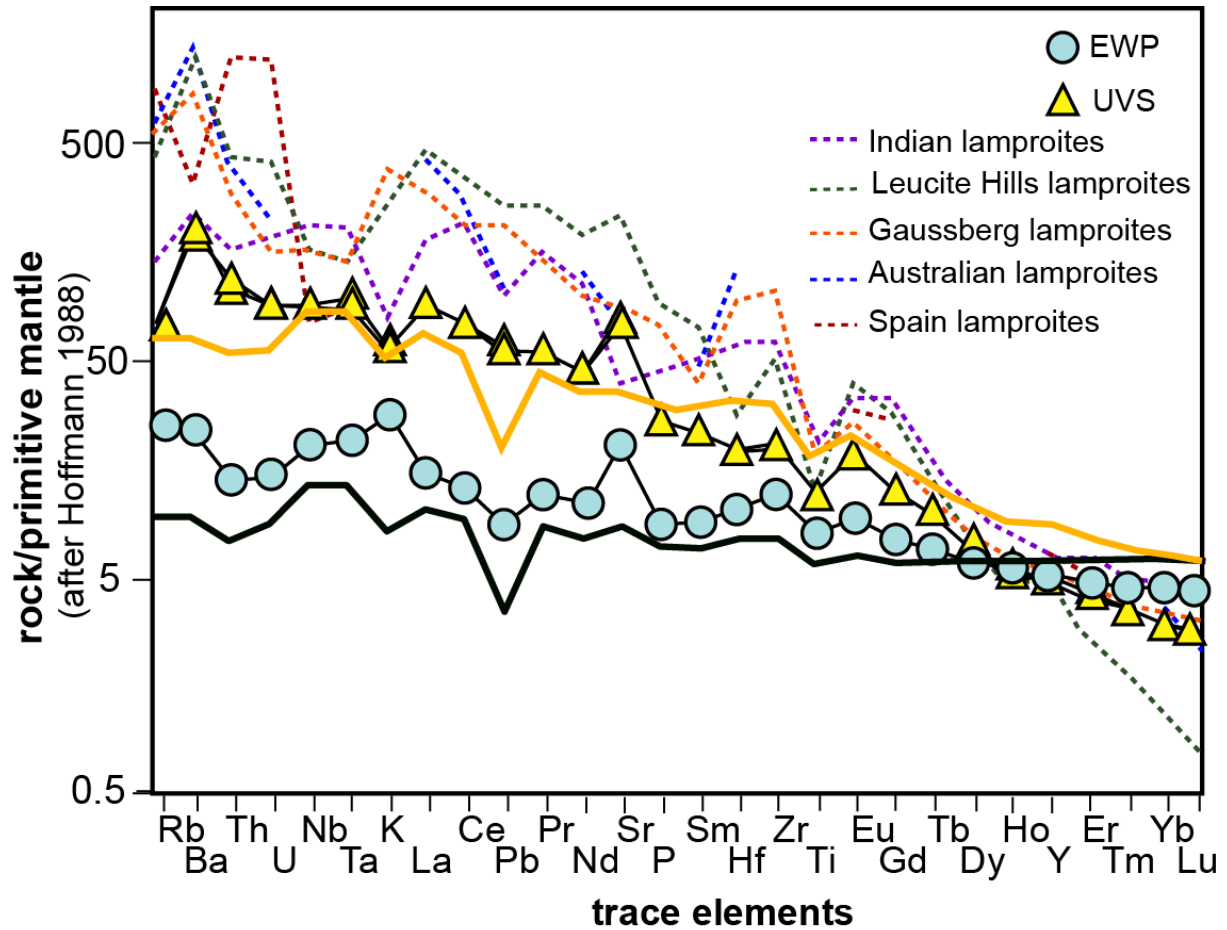


Fig. 8: Most primitive samples of EWP and UVS Christmas Island plotted against Lamproites to implicate source similarities/differences. Symbols as in figure 5a-d.

From uranium to tantalum, the 2 samples of Christmas Island UVS element pattern do not show the Nb-Ta peak normally observed in OIB. This implies that some samples from Christmas Island might be derived from a source slightly depleted in Nb-Ta. Residual rutile in the source may cause such depletions as it has been also suggested for the Leucite Hills lamproites and Gaussberg Lamproites (Mitchell and Bergmann 1991, Murphy et al. 2002, Mirnejad and Bell 2006). Leucite Hills lamproites samples show nearly the same pattern in U-Ta as samples from Christmas Island, but differ in their more pronounced Nb-Ta trough due to the strong enrichment in Th und K in Leucite Hills lamproites. In contrast to Leucite Hills lamproites, Gaussberg Lamproites and Spain lamproites, only samples from the Indian

Lamproites show a similar depletion in Rb and K as observed for the UVS. The negative anomaly in Rb and K is related to the fractionation of phlogopite in the Indian lamproites or the effect of hydrothermal alteration after Chalapathi et al. (2004), but could also reflect residual phlogopite in the Indian lamproite source. It can be assumed that phlogopite was also a residual phase in the source of Christmas Island. From P, Sm, Hf, Zr, Ti and Eu the Christmas Island samples are more depleted than OIBs and lamproites, but their trace element pattern is based on OIB in this section. The MREE to HREE are significantly depleted in Christmas Island alike to samples from Gaussberg Lamproites and Leucite Hills lamproites. The other Lamproite regions are more enriched in HREE related to the Christmas Island samples. Because of the similar pattern in MREE and HREE for all lamproites is suggested the generation of melts in the garnet stability field (Murphy et al. 2002, Mirnejad and Bell 2006), as it is the same for Christmas Island samples. The HREE and MREE were probably retained by residual garnet in the source.

In contrast to the Christmas Island samples, the eastern EWP sample has incompatible element characteristic similar to E-MORB (Fig. 8). In the EWP the trace element pattern of Rb, Ba, Th, U, Nb and Ta are more comparable with those from E-MORB, concluding that the affinity to a depleted source in their trace elements is much stronger than for the UVS. A positive K-peak as seen in Gaussberg Lamproites and Leucite Hills lamproites, is absent in the UVS. The K- enrichment in lamproites from Leucite Hills lamproites is explained by recent metasomatic activity (hydrous fluids or melts) that probably led to addition of K₂O (Mirnejad and Bell 2006). Addition of silicate melts can also cause enrichment in LIL elements (Sun and McDonough 1989). The enrichment in LIL especially in Ba, Rb and K as well as in Sr in EWP hints that this enrichment could be related to a lamproitic source flavor. In the model of Hoernle et al. 2011, SCLM and young MORB were mixed in variable amounts during mantle upwelling at the MOR. This means that the enriched (SCLM) and depleted (MORB, oceanic crust), components were not present in constant proportions. This depends on several factors that may have influenced the composition of EWP and hence all CHRISP volcanism. Hoernle et al. (2011) propose that the longer the stirring and heating and therefore the dismemberment of detached mantle takes, the more SCLM could rise up above the solidus and mix with MORB. Additionally an increase in spreading rates at the W.Burma/Australian MOR from 70 mm at 150 Ma up to 136 mm at 110 Ma could have also led to an increase in uprising SCLM material and mixing with MORB and therefore explain the variations in element enrichments of the CHRISP. In this context the EWP sample may represent mixing of regular MORB with tiny amounts of SCLM at slow spreading rates of the

W. Burma/Australian MOR. Possibly the influence of the depleted component was stronger here than at younger times when CHRISP volcanism was located farther off-axis. VMP and CKP may have formed during times of faster seafloor spreading and the longer heating of detached mantle and increased SCLM upwelling could have led to more enriched melts than the EWP. Another explanation for the enrichment process in these subprovinces is change in the degree of melting. While the EWP was generated at or close to the MOR the VMP and CKP formed further away from the MOR underneath older and thicker lithosphere, leading to a shorter melt column and lower degrees of melting allowing preferential sampling of the SCLM component.

Although the UVS formed in a true intra-plate setting, it tapped an isotopically similarly enriched source as the older CHRISP volcanic structures that formed in the vicinity of a spreading center. The envisioned mechanism for such late stage melting is storage of unmelted SCLM at sublithospheric depths and small scale mantle upwelling beneath the outer rise of the Java trench leading to low degree decompression melting and extraction of near primary SCLM melts as Christmas seamount was rode over the flexural bend and became an island.

5.5 Two component mixing model

This chapter attempts to model the trace element compositions of CHRISP using a two-component mixture of lamproites (SCLM) and MORB as enriched and depleted end member compositions respectively. This exercise shall try to test whether or not the isotopic mixing model of Hoernle et al. 2011 is consistent with the trace element chemistry. The first step explains the choice for source components and the second step contains the modeling.

As known from the tectonic situation in this area, the seamounts were generated near the spreading center of the W-Burma block, Australia and greater India. Before 150 Ma ago India was adjacent to NW-Australia and Antarctica as part of the super continent Gondwana. Lamproites occur on all these continents (e.g., Fraser et al. 1985, Chalapathi et al. 2004 and Chakrabarti et al. 2007, Murphy et al. 2002). During the rifting process, Archaean SCLM from the different continents could have been delaminated into the convecting mantle (Hoernle et al. 2011). Consequentially these areas of SCLM could serve as the potential source of the enriched component in the CHRISP lavas. Due to incomplete trace element data for the Australian lamproites, the Indian lamproites are assumed to be the most representative source composition for the CHRISP. Another lamproitic source with similar characteristics, however, is required to get a closer match to the enrichment processes of the CHRISP

(incompatible elements, Ba, Rb, Sr, K). A mix of Leucite Hills lamproites and Indian lamproites has proved to be the best approximation to CHRISP. As the depleted component, E-MORB, with a more extreme Indian MORB composition was chosen for the modeling.

The spider diagram illustrates the mixing between E-MORB and Leucite Hills lamproites and Indian lamproites. Using percent calculation it is possible to generate different mixing patterns between E-MORB and lamproites (Fig. 9a and 9b).

For the model 80% of Leucite Hills lamproites were mixed with 20% of Indian lamproites to get a hybrid lamproite composition to create mixing proportions. Mixing proportions of 25-30 % hybrid lamproite and 75-70 % Indian E-MORB provide the best fit to the measured composition of the most mafic UVS samples from Christmas Island. Certainly there is not a complete agreement in all trace elements related to the modeled mixing patterns. The largest deviations are observed for Th, Nb, Ta and Sr, the MREE (Ho) and HREE (Y, Er, Tm, Yb and Lu) (see Fig. 10a and 10b). The variations in Th, Nb and Ta seen for the Christmas Island multi element pattern may come from the distinctions in source generation for both areas of Leucite Hills lamproites and Indian lamproites. The Leucite Hills lamproites show greater subduction related characteristics (e.g. figure 7a), with elevated Th/Yb and retention of Nb and Ta in the source (most likely due to residual rutile) of the metasomatic hydrous melts, and the Indian lamproites show less subduction effect. The enriched source for the CHRISP melts may have been SCLM metasomatized by small degree asthenospheric melts from the convecting mantle. The divergence from Sr in the modeled mixing pattern related to Christmas Island is the result on the one hand of Sr fractionation in the Indian lamproites and on the other hand the enrichment process in Sr in Leucite Hills lamproites. From Ho to Lu the influence of Indian MORB is much stronger than those of lamproites. Therefore the modeled mixing line follows the HREE pattern for E-MORB.

The best approaches to model the primitive EWP sample were calculated mixing patterns with 2-3 % lamproite and 97-98% E-MORB (Fig. 10c and 10d). There is not a complete correlation between the modeled pattern and the EWP sample. The mixing pattern for EWP displays strong deviations in the elements Rb, K and Sr. EWP is enriched in all these elements compared to the mixing line. This might happen during alteration of the EWP sample. In summary, the modeled mixing pattern fit well for for most elements of Christmas Island samples but show strong derivation in Th, Nb, Ta and Sr, which might be related to the different source enrichment processes for the SCLM source than generally observed in lamproites, e.g. metasomatism with asthenospheric melts rather than hydrous subduction zone melts. Alternatively, lamproites may form with residual phases such as rutile in their source,

which hold back Nb and Ta. Such phases may no longer have been stable in the CHRISP source due to higher temperatures and greater degrees of melting under a spreading center.

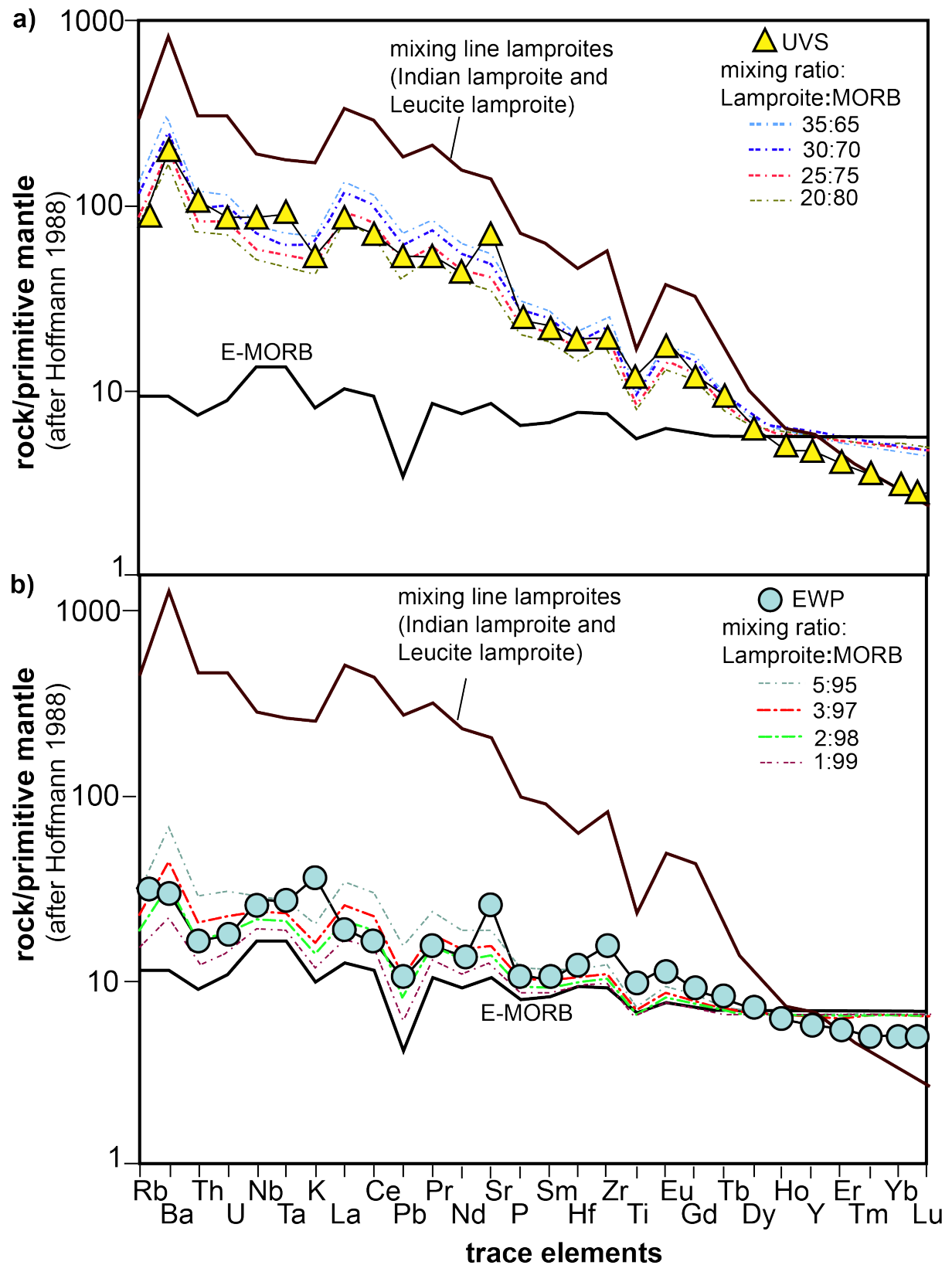
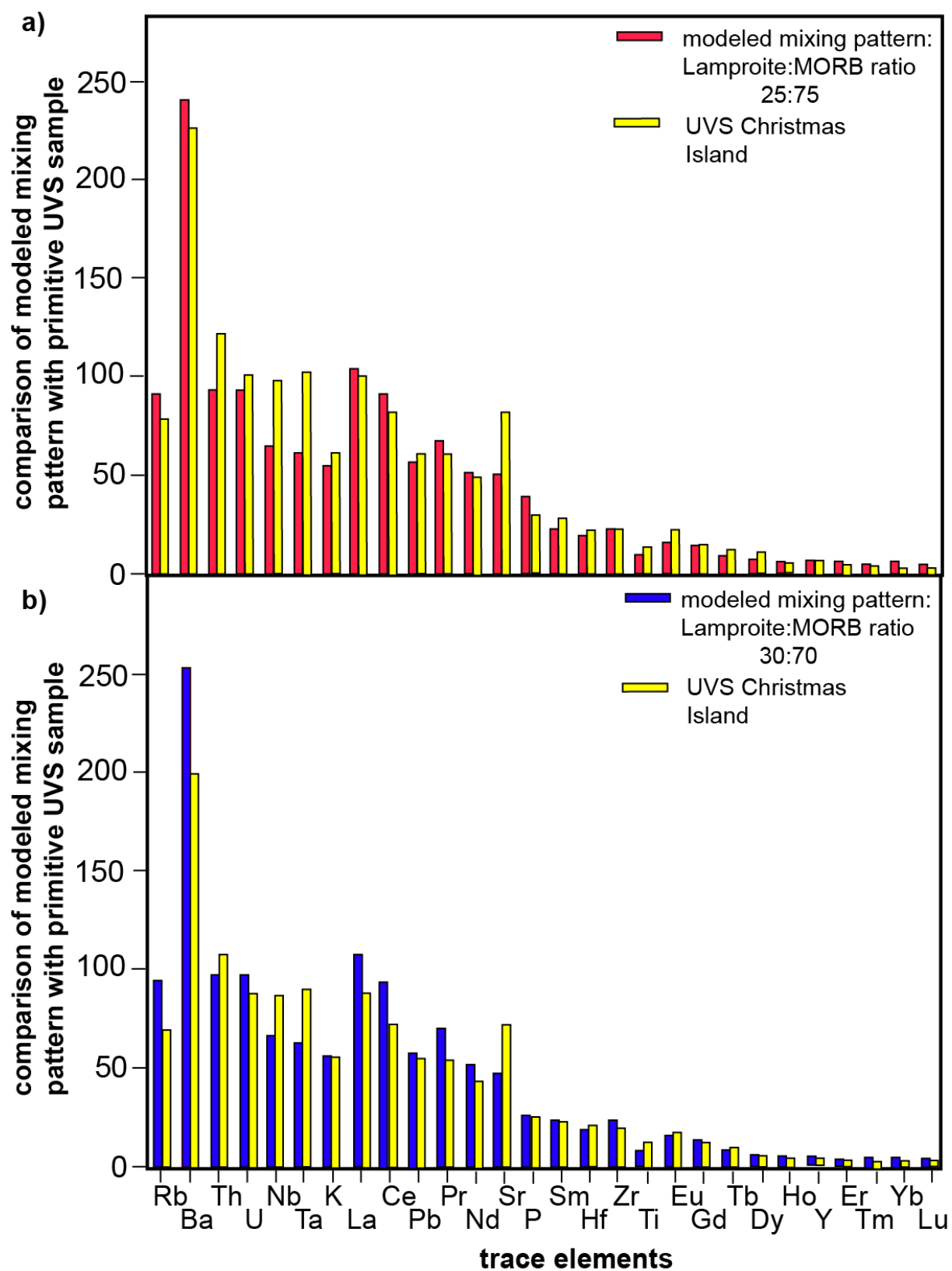


Fig. 9: Modeled mixing lines versus primitive samples of a) UVS Christmas Island and b) EWP. Mixing lines were calculated from Lamproite (mixing between LHL and Indian L.) and E-MORB. a) UVS shows a good

correlation to mixing lines of with 70-75% MORB and 30-25% Lamproite. b) EWP sample may be generated by 2-3% Lamproite and 98-97% MORB.



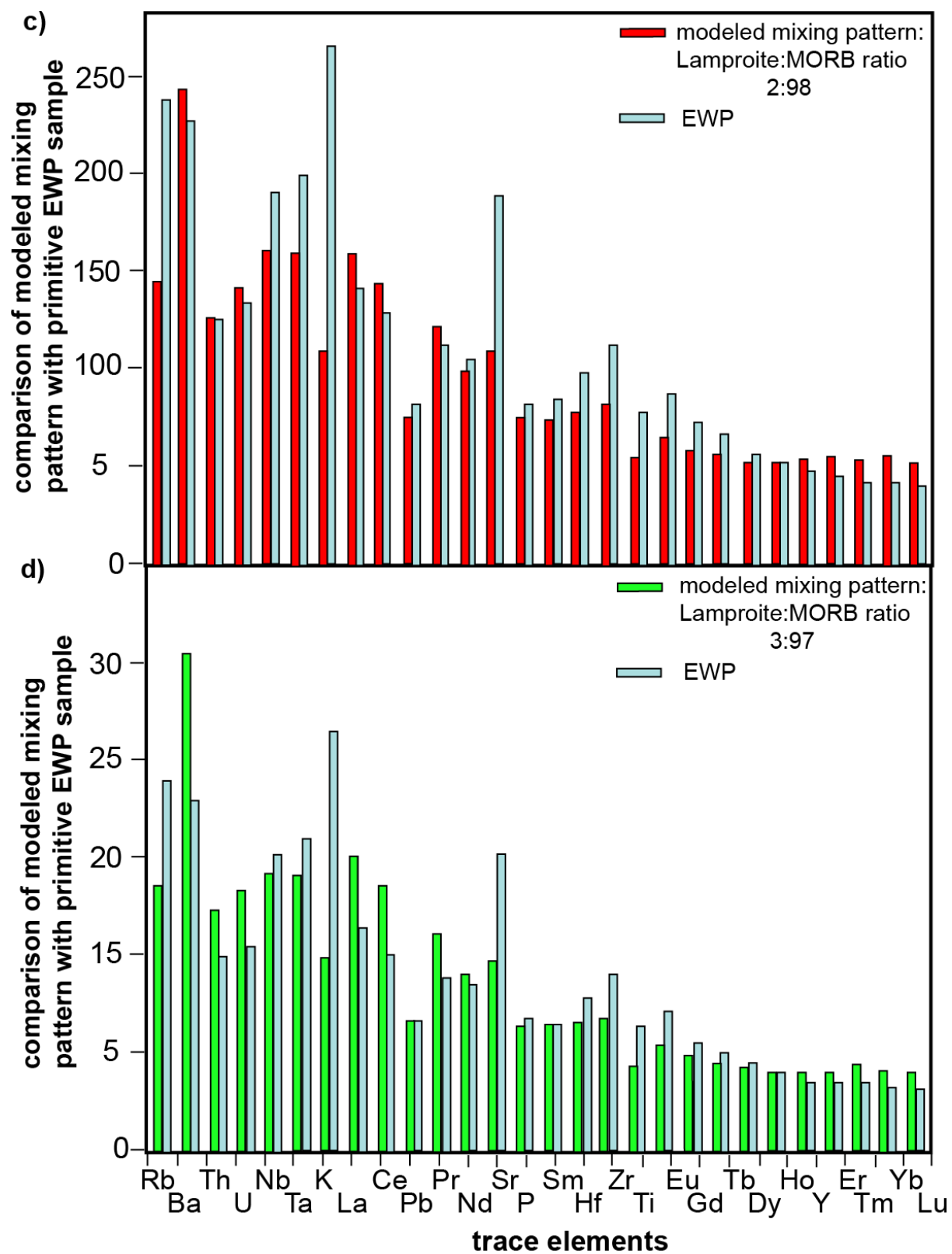


Fig. 10a-d: Derivation in trace elements between modeled mixing line and primitive samples of a) UVS and b) EWP.

6. CONCLUSIONS

This study shows that the major and trace element composition of the CHRISP volcanics is strongly affected by fractional crystallization and alteration processes. Nevertheless, most trace element data sets suggest generation of the CHRISP rocks by mixing of an enriched and a more depleted component in their mantle source, which are potentially lamproites or metasomatized SCLM (lamproitic source) and Indian MORB as postulated by age and isotope study of Hoernle et al. (2011). Modeling using the trace element concentrations of the two most mafic samples from Christmas Island confirm an Indian lamproite/Leucite Hills lamproites mixture and Indian MORB as possible source components. Mixing proportions between 25-30 % of hybrid lamproite, consisting of 19.05 % Indian lamproite and 76.19 % Leucite Hills lamproite, with 4.76 % Indian E-MORB provide the best fit for the measured composition of the two most mafic UVS samples. Mixing proportions for the more evolved EWP sample were 2-3 % hybrid lamproite and 97-98% Indian E-MORB. These calculations display, however, strong deviations in Th, Nb, Ta and Sr, which can be best explained by the complete fusion of accessory phases in the SCLM containing these minerals due to higher degrees of melting beneath a spreading center than at the base of continental lithosphere.

In conclusion, the trace element geochemistry of the most primitive, unaltered CHRISP volcanics can be generated by mixing of lamproitic SCLM melts and E-MORB, but it must be noted, that the majority of the CHRIPS trace element data does not allow a reliable reconstruction of their specific source components.

REFERENCES:

Albarede, F., Tamagnan, V., 1988. Modelling the recent geochemical evolution of the Piton de la Fournaise Volcano, Réunion Island, 1931-1986. *Journal of Petrology* 29 (Part 5) 997-1030.

Chakrabarti, J., Basu, A.R., Paul, D. K., 2007. Nd-Hf-Sr-Pb isotopes and trace element geochemistry of Proterozoic lamproites from southern India: Subducted komatiite in the source. *Chemical Geology* 236, 291-302. doi:10.1016/j.chemgeo.2006.10.006.

Chalapathi, R.N.V., Gibson, S.A., Pyle, D.M. and Dickin, A.P., 2004. Petrogenesis of Proterozoic lamproites and kimberlites from the Cuddapah Basin and Dharwar craton, southern India; *Journal of Petrology* 45, 907–948.

Davies, G.R., Stolz, A.J., Mahotkin, I.L., Nowell, G.M. and Pearson D.G., 2006. Trace element and Sr–Pb–Nd–Hf isotope evidence for ancient, fluid-dominated enrichment of the source of Aldan Shield lamproites. *Journal of Petrology* 47, 1119-1146. doi:10.1093/petrology/egl00.

Foley, S.F., Venturelli, G., Green, D.H., Toscani, L., 1987. The ultrapotassic rocks: characteristics, classification and constraints for petrogenetic models. *Earth-Science Reviews* 24, 81–134.

Fraser, K. J., Hawkesworth, C. J., Erlank, A. J., Mitchell, R. H. & Scott-Smith, B. H., 1985. Sr, Nd and Pb isotope and minor element geochemistry of lamproites and kimberlites. *Earth Planetary Science Letters* 76, 57-70.

Garbe-Schönberg, C.-D., 1993. Simultaneous determination of thirty-seven trace elements in twenty-eight international rock standards by ICP-MS: *Geostandards and Geoanalytical Research* 17, 81-97.

Graham, S., Lambert, D.D., Shee, S.R., Smith, C.B. and Reeves, S. 1999. Re-Os isotopic evidence for Archean lithospheric mantle, beneath the Kimberley block, Western Australia. *Geology* 27, 431-434. doi: 10.1130/0091-7613(1999)027<0431:ROIEFA>2.3.CO;2.

Hawkesworth, C.J., Kempton, P.D., Rogers, N.W., Ellam, R.M., van Calsteren, P.W., 1990. Continental mantle lithosphere, and shallow level enrichment processes in the Earth's mantle. *Earth and Planetary Science Letters* 96, 256-268. [http://dx.doi.org/10.1016/0012-821X\(90\)90006-J](http://dx.doi.org/10.1016/0012-821X(90)90006-J).

Hoernle, K., Hauff, F., Werner, R., van den Bogaard, P., Gibbons, A.D., S. Conrad & Müller R.D., 2011. Origin of Indian Ocean Seamount Province by shallow recycling of continental lithosphere. *Nature Geoscience* 4, 883-887, doi:10.1038/ngeo1331.

Hofmann, A.W., 1988. Chemical differentiation of the Earth: the relationship between mantle, continental and oceanic crust. *Earth and Planetary Science Letters* 90, 297-314, doi: 10.1016/0012-821X(88)90132-X.

Irvine, T.N. and Baragar, W.R.A., 1971. A guide to the chemical classification of the common volcanic rocks. *Canadian Journal of Earth Sciences* 8, 523-548, doi:10.1139/e71-055.

Kipf, A., Hauff, F., Werner, R., Gohl, K., van den Bogaard, P., Hoernle K., Maicher, D., Klügel A., 2013. Seamounts off the West Antarctic margin: A case for non hotspot driven intraplate volcanism. *Gondwana Research*. doi.org/10.1016/j.gr.2013.06.013.

Kononova, V. A., Bogatikov, O.A., Kondrahshov, I. A., 2011. Kimberlites and lamproites: Criteria for similarity and differences. *Petrology* 19, 34-54. doi:10.1134/S0869591111010024.

Korenaga, J., 2005. Firm mantle plumes and the nature of the core-mantle boundary region. *Earth and Planetary Science Letters* 232, 29-37. doi:10.1016/j.epsl.2005.01.016.

Korsch, M. J. and Gulson, B. L., 1986. Nd and Pb isotopic studies of an Archaean layered mafic-ultramafic complex, Western Australia, and implications for mantle heterogeneity. *Geochim. Cosmochim. Acta* 50, 1-10. doi.org/10.1016/0016-7037(86)90042-6.

Lei, J. and Zhao D., 2006. A new insight into Hawaiian plume. *Earth and Planetary Science Letters* 241, 438-453, doi:10.1016/j.epsl.2005.11.038.

le Roux, A.P. Dick, H.J., Watkins, R.T. 1992. Petrogenesis of anomalous K-enriched MORB from the Southwest Indian Ridge: 11°53' E to 14°38' E. *Contribution to Mineralogy and Petrology* 110, 253-268.

Lonsdale, P., 1988. Geography and history of the Louisville hotspot chain in the South Pacific. *Journal of Geophysical Research* 93, 3078-3104, doi: 10.1029/88JB01301.

McKenzie, D. 1989. Some remarks on the movement of small melt fractions in the mantle. *Earth and Planetary Science Letters* 95, 53-72.

Mitchell, R., Bergman, S., 1991. Tectonic Framework of Lamproite Genesis. In: *Petrology of Lamproites*. Springer US, 103-124.

Mirnejad, H. and Bell, K., 2006. Origin and source evolution of the Leucite Hills Lamproites: Evidence from Sr-Nd-Pb-O isotopic composition. *Journal of Petrology* 47, 2463-2489, doi:10.1093/petrology/egl051

Morgan, W.J., 1971. Convection plumes in the lower mantle. *Nature* 230, 42-43,

doi:10.1038/230042a0.

Murphy D.T., Collerson K.D., and Kamber B.S., 2002: Lamproites from Gaussberg, Antarctica: Possible Transition Zone Melts of Archaean Subducted Sediments. *Journal of Petrology* 43, 981-1001, doi:10.1093/petrology/43.6.981.

Nelson, D.R., McCulloch, T.M., Sun, S-S. 1986. The origins of ultrapotassic rocks as inferred from Sr, Nd and Pb isotopes. *Geochimica et Cosmochimica Acta* 50, 231-245.

O'Connor J.M., Steinberger B., Regelous M., Koppers A.A.P., Wijbrans J.R., Haase K.M., Stoffers, P., Jokat, W., Garbe-Schönberg, D., 2013. Constraints on past plate and mantle motion from new ages for the Hawaiian-Emperor Seamount Chain. *Geochemistry, Geophysics, Geosystems* 14, 4564-4584, doi:10.1002/ggge.20267.

Rohde, J. K., van den Bogaard, P., Hoernle, K., Hauff, F. und Werner, R., 2013. *Evidence for an age progression along the Tristan-Gough volcanic track from new $^{40}\text{Ar}/^{39}\text{Ar}$ ages on phenocryst phases* Tectonophysics, 604, 60-71, doi:10.1016/j.tecto.2012.08.026.

Royer, J-Y., Peirce, J. W. and Weissel, J.K., 1991. 38. Tectonic constraints on the hot-spot formation of Ninetyeast Ridge. Proceedings of the Ocean Drilling Program, Scientific Results. 121, 763- 776.

Sun, S. S. and McDonough, W.F., 1989. Chemical and isotopic systematics of oceanic basalts: implications for mantle composition and processes. In: Saunders, A. D. & Norry, M. J. (eds) Magmatism in the Ocean Basins. Geological Society Special Publications 42, 313-345, doi:10.1144/GSL.SP.1989.042.01.19.

Steinberger, B., Sutherland, R., O'Connell, R.J., 2004. Prediction of Emperor-Hawaii seamount locations from a revised model of global plate motion and mantle flow. Nature 430,167-173, doi:10.1038/nature02660.

Tarduno, J.A., Duncan, R.A., Scholl, D.W., Cottrell, R.D., Steinberger, B., Thordason, T., Kerr, B.C., Neal, C.R., Frey, F.A., Torii, M., Carvallo, C., 2003. The Emperor seamounts: Southward motion of the Hawaiian hotspot plume in earth's mantle. Science 301,1064-1069, doi: 10.1126/science.1086442.

Venturelli, G., Capedri, S., Di Battistini, G., Crawford, A., Kogarko, L. N., and Celestini, S. 1984a. The ultrapotassic rocks from southeastern Spain. Lithos 17, 37-54.

Werner, R., Hauff, F. und Hoernle, K., eds .2009. RV SONNE Fahrtbericht / Cruise Report SO199 CHRISP: Christmas Island Seamount Province and the Investigator Ridge: Age and Causes of Intraplate Volcanism and Geodynamic Evolution of the South-Eastern Indian Ocean ; Merak/Indonesia - Singapore, 02.08.2008 - 22.09.2008 *IFM-GEOMAR Report*, 25 . *IFM-GEOMAR, Kiel, Germany*, doi:10.3289/ifm-geomar_rep_25_2009.

Willbold M. and Stracke A. 2006. Trace element composition of mantle end-members:

Implications for recycling of oceanic and upper and lower continental crust Geochemistry
Geophysics Geosystems 7, Q04004, doi:10.1029/2005GC001005.

Wilson, J.T., 1963. Evidence from islands on the spreading of the ocean floor. *Nature* 197,
536-538, doi:10.1038/197536a0.

Woodroffe C.D., 1988. Vertical movement of isolated oceanic islands at plate margins:
evidence from emergent reefs in Tonga (Pacific Ocean), Cayman Islands (Caribbean Sea) and
Christmas Island (Indian Ocean). *Zeitschrift für Geomorphology, Suppl.- Band 69*. 17-37.

Workman, R. K. and Hart, S.R., 2005. Major and trace element composition of the depleted
MORB mantle (DMM). *Earth Planetary Science Letters* 231, 53-72,
<http://dx.doi.org/10.1016/j.epsl.2004.12.005>.

APPENDICES:

Appendix I (CHAPTER I)

ANALYTICAL METHODS

Age Dating

$^{40}\text{Ar}/^{39}\text{Ar}$ analyses were carried out by laser step-heating on plagioclase phenocrysts, microcrystalline matrix and basalt glass, using Taylor Creek Rhyolite Sanidine (TCR-2: 27.87 ± 0.04 Ma; Lanphere and Dalrymple, 2000) as neutron flux monitor, following the methods described in Kipf et al. (2012). Alteration is monitored by calculating alteration indices (A.I.), based on the measured $^{36}\text{Ar}/^{37}\text{Ar}$ ratios (Baksi, 2007). Internal errors are reported at the 2 sigma confidence level. Analytical results are given in Table A1.

Sample preparation for Geochemistry

Samples selected for geochemistry were first crushed to small pieces in a steel jaw crusher, then repeatedly washed in deionized water and carefully hand-picked under a binocular microscope. Sample powders were prepared in a agate mortar and agate swing mill.

Major elements

Major element analyses were carried out on fused glass beads using a Phillips X'Unique PW 1480 X-ray fluorescence spectrometer using a Rh-tube at GEOMAR. To produce homogenous glass beads, 0.6mg of dry sample powder, lithium tetraborate and ammonium nitrate were mixed in platinum cups and then fused in four heat-steps. H_2O and CO_2 were analyzed upon ignition of powders at 1200°C using a Rosemount CWA 5003 infrared photometer. The accuracy of major-element concentrations for reference material JB-2, JB-3, and JA-2, measured along with the samples, is generally better than 6.5% of the suggested working values (Govindaraju 1994, Jochum et al. 2005). Measured and reference values of these standards are given in Table A2.

Trace elements

Trace elements (Rb, Sr, Ba, Y, Nb, Zr, Ta, Hf, U, Th, Pb and all REE) were determined after microwave digestion on an ELEMENT 2 at the University of Bremen after the methods of Geldmacher et al. (2008). Measured and "GeoReM" preferred values for BHVO-2, BCR-2, and BIR-1 are given in Table A3. The accuracy of the reference material BCR-2 and BHVO-2, BCR-2, and BIR-1, obtained along with the samples, is generally within $\leq 8\%$ of the "GeoReM" preferred values (Jochum et al. 2005). Exceptions are noted for Ta in all three

standards and for Zr (11.3%) and Ba (12.4%) in the depleted BIR-1 tholeiite standard. Replicate analyses of individual sample digestions are within 2.0% for most elements (except Pb, Er, Tm; Table 2).

Sr-Nd-Pb-Hf isotopes

Sr-Nd-Pb-Hf isotope analyses were carried out on 0.5-2 mm sized whole rock or fresh glass chips. 100-250 mg of sample were leached in warm ultra pure 2N HCl (70 °C, 1h) and subsequently rinsed three times in ELGA water in order to minimize the effects of sample handling. The leached chips were dissolved for 2 days in a 5:1 mixture of ultra pure HF and HNO₃ at 150 °C and ion exchange procedures followed established standard procedures (Hoernle et al 2008). Isotope analyses were carried out in static multi-collection mode on a Finnigan MAT 262 RPQ²⁺ (Pb) and on a Thermo Finnigan TRITON-TI (Sr, Nd) thermal ionization mass spectrometer (TIMS). Sr and Nd isotopic ratios were normalized within run to $^{86}\text{Sr}/^{88}\text{Sr} = 0.1194$ and $^{146}\text{Nd}/^{144}\text{Nd} = 0.7219$ respectively and all errors are reported as 2 sigma of the mean. Sr and Nd standards were measured every 4th to 5th sample. For each sample turret a normalization value was obtained by subtracting the average measured standard values from the preferred value of the standard. The normalization value was then applied to the sample and standard data. This procedure ensures maximum comparability of data generated from 2006-2010. Following this procedure, NBS987 gave $^{87}\text{Sr}/^{86}\text{Sr} = 0.710250 \pm 0.000007$ (n=14) and La Jolla $^{143}\text{Nd}/^{144}\text{Nd} = 0.511850 \pm 0.000008$ (n=38) on the TRITON. A subset of Sr samples (marked with two asterisk in Table 4) were measured on the MAT262 where NBS987 gave $^{87}\text{Sr}/^{86}\text{Sr} = 0.710250 \pm 0.000014$ (n=18).

Pb isotope ratios (with the exception of sample PS69-PI-1) were determined using the Pb Double-Spike (Pb-DS) technique described in Hoernle et al. (2011). The double spike corrected NBS981 values measured along with the samples are $^{206}\text{Pb}/^{204}\text{Pb} = 16.9416 \pm 0.0021$, $^{207}\text{Pb}/^{204}\text{Pb} = 15.4996 \pm 0.0020$, $^{208}\text{Pb}/^{204}\text{Pb} = 36.7231 \pm 0.0052$, $^{207}\text{Pb}/^{206}\text{Pb} = 0.91488 \pm 0.00005$ and $^{208}\text{Pb}/^{206}\text{Pb} = 2.16763 \pm 0.00011$ (n=45). Total Pb chemistry blanks were 20-40pg and thus considered negligible.

Hf chemical separation followed the procedure of Blichert-Toft et al. (1997) and were measured at GEOMAR on an AXIOM MC-ICP-MS (see Geldmacher et al. 2006 for operating details and machine performance). The JMC-475 Hf standard was run repeatedly and normalized to $^{176}\text{Hf}/^{177}\text{Hf} = 0.282162 \pm 0.000008$ (n=13). Our in-house standard Spex (cross-calibrated to JMC-475) was measured every three samples to monitor machine performance and gave normalized $^{176}\text{Hf}/^{177}\text{Hf} = 0.282173 \pm 0.000006$ (n=43).

References:

Baksi, A. K., 2007. A quantitative tool for detecting alteration in undisturbed rocks and minerals—I: Water, chemical weathering, and atmospheric argon. *Special Paper of the Geological Society of America* 430, 1197, 285–303, doi:10.1130/2007.2430(16).

Blichert-Toft, J., Chauvel, C., Albarede, F., 1997. Separation of Hf and Lu for high-precision isotope analyses of rock samples by magnetic sector-multiple collector ICP-MS. *Contributions to Mineralogy and Petrology* 127, 248-260, doi:10.1007/s004100050278.

Geldmacher, J., Hoernle, K., Klügel, A., Bogaard, P.v.d., Wombacher, F., Berning, B., 2006. Origin and geochemical evolution of the Madeira-Tore Rise (eastern North Atlantic). *Journal of Geophysical Research* 111, doi:10.1029/2005JB003931.

Geldmacher J., Hoernle K.A., Bogaard P.v.d., Hauff F., Klügel A. (2008): Age and geochemistry of the Central American forearc basement (DSDP Leg 67 and 84): Insights into Mesozoic arc volcanism and seamount accretion on the fringe of the Caribbean LIP. *Journal of Petrology* 49, 1781-1815. doi:10.1093/petrology/egn046.

Govindaraju K., 1994. Compilation of working values and sample descriptions for 383 geostandards. *Geostandard Newsletters* 18, 1-158, doi:10.1046/j.1365-2494.1998.53202081.x-i1.

Hoernle K., Abt D.L., Fischer K.M., Nichols H., Hauff F., Abers G.A., van den Bogaard P., Heydolph K., Alvarado G., Protti M., Strauch W., 2008. Arc-parallel flow in the mantle wedge beneath Costa Rica and Nicaragua. *Nature* 451(7182), 1094-1097, doi:10.1038/nature06550.

Hoernle, K., Hauff, F., Kokfelt, T. F., Haase, K., Garbe-Schönberg, D., Werner, R. (2011) On- and off-axis chemical heterogeneities along the South Atlantic Mid-Ocean-Ridge (5-11°S): Shallow or deep recycling of ocean crust and/or intraplate volcanism? *Earth and Planetary Science Letters* 306, 86-97, doi:10.1016/j.epsl.2011.03.032.

Jochum K.P., Nohl U., Herwig K., Lammel E., Stoll B., Hofmann A.W., 2005. GeoReM: A New Geochemical Database for Reference Materials and Isotopic Standards. *Geostandards and Geoanalytical Research* 29 (3), 333-338, doi:10.1111/j.1751-908X.2005.tb00904.x.

Kipf, A., Mortimer, N., Werner, R., Gohl, K., van den Bogaard, P., Hauff, F., Hoernle, K., 2012. Granitoids and dykes of the Pine Island Bay Region, West Antarctica. *Antarctic Science* 24 (5), 473-484, doi:10.1017/S0954102012000259.

Lanphere, M.A., Dalrymple, G.B., 2000. First-Principles Calibration of ^{38}Ar Tracers: Implications for Ages of $^{40}\text{Ar}/^{39}\text{Ar}$ Fluence Monitors. US Geological Survey Professional Paper 1621, 10 pp.

Table A1: $^{40}\text{Ar}/^{39}\text{Ar}$ laser step-heating analysis data

317-1-1gls glass step-heating analysis

Mass = 1.555 mg

J = 3.69E-03 +/- 3.90E-06 (2 Sigma) 0.106 Percent

Step	Laser power (W)	40Ar/39Ar	37Ar/39Ar	36Ar/39Ar	Mol 39ArK	Ca/K	% 40ArA	Cum 39ArK	Age (Ma)	2 Sigma	A.I. (36/37)
1	1.25E-01	2.89E+03	7.62E-01	8.84E+00	3.09E-16	1.50E+00	9.03E+01	4.58E-03	1.28E+03	4.90E+01	4.28E+00
2	2.00E-01	3.03E+02	1.19E+00	9.63E-01	4.00E-15	2.33E+00	9.38E+01	6.38E-02	1.21E+02	1.50E+01	3.00E-01
3	3.00E-01	7.50E+01	1.34E+00	2.15E-01	1.25E-14	2.63E+00	8.47E+01	2.49E-01	7.50E+01	4.72E+00	5.91E-02
4	4.00E-01	3.78E+01	1.57E+00	9.44E-02	9.61E-15	3.08E+00	7.32E+01	3.91E-01	6.65E+01	2.08E+00	2.20E-02
5	5.00E-01	2.96E+01	1.71E+00	6.77E-02	8.22E-15	3.36E+00	6.69E+01	5.13E-01	6.41E+01	1.95E+00	1.45E-02
6	6.00E-01	3.22E+01	1.80E+00	7.65E-02	7.31E-15	3.54E+00	6.95E+01	6.21E-01	6.43E+01	1.91E+00	1.55E-02
7	7.00E-01	3.26E+01	1.85E+00	7.74E-02	5.45E-15	3.63E+00	6.95E+01	7.02E-01	6.52E+01	2.36E+00	1.53E-02
8	8.00E-01	2.88E+01	1.98E+00	6.44E-02	4.98E-15	3.89E+00	6.53E+01	7.75E-01	6.55E+01	2.68E+00	1.19E-02
9	9.00E-01	2.97E+01	2.09E+00	6.81E-02	3.63E-15	4.11E+00	6.68E+01	8.29E-01	6.47E+01	2.27E+00	1.19E-02
10	1.00E+00	2.86E+01	2.30E+00	6.55E-02	2.16E-15	4.52E+00	6.66E+01	8.61E-01	6.27E+01	4.01E+00	1.04E-02
11	1.10E+00	2.69E+01	2.62E+00	5.98E-02	1.28E-15	5.14E+00	6.45E+01	8.80E-01	6.26E+01	3.39E+00	8.29E-03
12	1.20E+00	2.70E+01	2.83E+00	6.44E-02	7.71E-16	5.56E+00	6.90E+01	8.91E-01	5.52E+01	8.06E+00	8.26E-03
13	1.35E+00	2.76E+01	3.23E+00	6.50E-02	1.19E-15	6.35E+00	6.81E+01	9.09E-01	5.79E+01	5.22E+00	7.29E-03
14	1.50E+00	3.68E+01	3.97E+00	9.31E-02	8.78E-16	7.80E+00	7.34E+01	9.22E-01	6.43E+01	8.36E+00	8.52E-03
15	2.00E+00	5.42E+01	5.29E+00	1.49E-01	8.96E-16	1.04E+01	8.03E+01	9.35E-01	7.02E+01	7.48E+00	1.03E-02
16	3.00E+00	6.31E+01	5.53E+00	1.78E-01	1.27E-15	1.09E+01	8.24E+01	9.54E-01	7.30E+01	4.68E+00	1.18E-02
17	5.00E+00	3.91E+01	6.86E+00	1.01E-01	2.51E-15	1.35E+01	7.36E+01	9.91E-01	6.79E+01	3.51E+00	5.27E-03
18	1.00E+01	2.24E+01	8.18E+00	4.37E-02	5.75E-16	1.62E+01	5.28E+01	1.00E+00	6.96E+01	7.71E+00	1.83E-03

Plateau age = 64.73±0.84 Ma (2s, including J-error of .106%), MSWD = 0.95, probability = 0.46, includes 63.1% of the 39Ar, steps 4 through 11

Table A1: continued

317-1-2gls glass step-heating analysis

Mass = 1.564 mg

J = 3.69E-03 +/- 3.90E-06 (2 Sigma) 0.106 Percent

Step	Laser power (W)	40Ar/39Ar	37Ar/39Ar	36Ar/39Ar	Mol 39ArK	Ca/K	% 40ArA	Cum 39ArK	Age (Ma)	2 Sigma	A.I. (36/37)
1	1.25E-01	5.10E+02	8.71E-01	1.64E+00	1.50E-15	1.71E+00	9.49E+01	1.85E-02	1.66E+02	2.22E+01	6.94E-01
2	2.00E-01	8.32E+01	1.23E+00	2.45E-01	5.57E-15	2.41E+00	8.68E+01	8.71E-02	7.17E+01	5.14E+00	7.36E-02
3	3.00E-01	2.58E+01	1.34E+00	5.47E-02	1.86E-14	2.62E+00	6.20E+01	3.16E-01	6.41E+01	1.31E+00	1.50E-02
4	4.00E-01	1.56E+01	1.53E+00	2.11E-02	1.46E-14	3.00E+00	3.88E+01	4.96E-01	6.25E+01	7.04E-01	4.95E-03
5	5.00E-01	1.24E+01	1.77E+00	1.11E-02	8.44E-15	3.47E+00	2.46E+01	6.00E-01	6.13E+01	1.08E+00	2.18E-03
6	6.00E-01	1.29E+01	1.81E+00	1.21E-02	6.72E-15	3.55E+00	2.60E+01	6.83E-01	6.25E+01	1.13E+00	2.33E-03
7	7.00E-01	1.32E+01	1.80E+00	1.32E-02	5.84E-15	3.54E+00	2.78E+01	7.55E-01	6.24E+01	1.04E+00	2.56E-03
8	8.00E-01	1.32E+01	1.86E+00	1.31E-02	4.12E-15	3.65E+00	2.73E+01	8.05E-01	6.30E+01	1.97E+00	2.45E-03
9	9.00E-01	1.37E+01	1.95E+00	1.50E-02	2.80E-15	3.83E+00	3.04E+01	8.40E-01	6.26E+01	2.65E+00	2.69E-03
10	1.00E+00	1.33E+01	2.18E+00	1.34E-02	2.27E-15	4.28E+00	2.76E+01	8.68E-01	6.32E+01	2.62E+00	2.13E-03
11	1.10E+00	1.23E+01	2.40E+00	1.30E-02	1.39E-15	4.71E+00	2.86E+01	8.85E-01	5.79E+01	5.90E+00	1.86E-03
12	1.20E+00	1.21E+01	2.56E+00	1.30E-02	1.38E-15	5.04E+00	2.92E+01	9.02E-01	5.62E+01	5.75E+00	1.73E-03
13	1.35E+00	1.41E+01	2.74E+00	2.04E-02	1.28E-15	5.38E+00	4.01E+01	9.18E-01	5.57E+01	6.74E+00	2.61E-03
14	1.50E+00	1.35E+01	3.39E+00	2.04E-02	9.02E-16	6.66E+00	4.13E+01	9.29E-01	5.23E+01	9.53E+00	2.09E-03
15	2.00E+00	1.33E+01	4.48E+00	1.92E-02	1.41E-15	8.83E+00	3.83E+01	9.46E-01	5.39E+01	5.92E+00	1.44E-03
16	3.00E+00	1.77E+01	5.19E+00	3.26E-02	1.32E-15	1.02E+01	5.05E+01	9.62E-01	5.78E+01	4.08E+00	2.18E-03
17	5.00E+00	1.94E+01	6.65E+00	3.60E-02	1.98E-15	1.31E+01	5.04E+01	9.87E-01	6.33E+01	2.13E+00	1.86E-03
18	1.00E+01	1.53E+01	7.69E+00	2.19E-02	1.05E-15	1.52E+01	3.59E+01	1.00E+00	6.46E+01	6.05E+00	9.12E-04

Plateau age = 62.30±0.44 Ma (2s, including J-error of .106%), MSWD = 0.99, probability = 0.44, includes 56.8% of the 39Ar, steps 4 through 11

Table A1: continued

317-1-2gl2 glass step-heating analysis

Mass = 1.557 mg

J = 3.69E-03 +/- 3.90E-06 (2 Sigma) 0.106 Percent

Step	Laser power (W)	40Ar/39Ar	37Ar/39Ar	36Ar/39Ar	Mol 39ArK	Ca/K	% 40ArA	Cum 39ArK	Age (Ma)	2 Sigma	A.I. (36/37)
1	1.25E-01	3.46E+02	1.81E+00	1.09E+00	1.81E-15	3.55E+00	9.29E+01	2.29E-02	1.58E+02	1.88E+01	2.22E-01
2	2.00E-01	2.72E+01	1.38E+00	5.72E-02	5.65E-15	2.70E+00	6.15E+01	9.45E-02	6.84E+01	3.37E+00	1.52E-02
3	3.00E-01	2.04E+01	1.45E+00	3.69E-02	1.39E-14	2.85E+00	5.26E+01	2.71E-01	6.33E+01	1.86E+00	9.25E-03
4	4.00E-01	1.29E+01	1.56E+00	1.22E-02	1.45E-14	3.05E+00	2.65E+01	4.54E-01	6.20E+01	9.75E-01	2.76E-03
5	5.00E-01	1.17E+01	1.72E+00	9.05E-03	1.01E-14	3.37E+00	2.10E+01	5.83E-01	6.05E+01	8.09E-01	1.80E-03
6	6.00E-01	1.16E+01	1.88E+00	8.62E-03	7.21E-15	3.68E+00	1.99E+01	6.74E-01	6.07E+01	1.09E+00	1.56E-03
7	7.00E-01	1.11E+01	1.92E+00	6.57E-03	4.86E-15	3.77E+00	1.52E+01	7.35E-01	6.19E+01	1.53E+00	1.12E-03
8	8.00E-01	1.11E+01	1.95E+00	6.65E-03	3.90E-15	3.82E+00	1.54E+01	7.85E-01	6.17E+01	2.12E+00	1.12E-03
9	9.00E-01	1.11E+01	1.93E+00	5.61E-03	3.21E-15	3.79E+00	1.27E+01	8.25E-01	6.33E+01	2.11E+00	9.32E-04
10	1.00E+00	1.09E+01	2.05E+00	6.07E-03	2.93E-15	4.03E+00	1.41E+01	8.63E-01	6.12E+01	2.52E+00	9.50E-04
11	1.10E+00	1.14E+01	2.28E+00	8.81E-03	1.70E-15	4.48E+00	2.02E+01	8.84E-01	5.97E+01	3.75E+00	1.28E-03
12	1.20E+00	1.21E+01	2.34E+00	1.19E-02	1.62E-15	4.60E+00	2.67E+01	9.05E-01	5.81E+01	3.29E+00	1.74E-03
13	1.35E+00	1.31E+01	2.87E+00	1.48E-02	1.40E-15	5.64E+00	3.06E+01	9.22E-01	5.97E+01	3.36E+00	1.76E-03
14	1.50E+00	1.48E+01	3.38E+00	2.15E-02	8.33E-16	6.65E+00	3.98E+01	9.33E-01	5.87E+01	6.49E+00	2.20E-03
15	2.00E+00	1.29E+01	4.01E+00	1.42E-02	1.47E-15	7.89E+00	2.84E+01	9.52E-01	6.08E+01	2.83E+00	1.17E-03
16	3.00E+00	1.51E+01	5.09E+00	2.06E-02	1.49E-15	1.00E+01	3.60E+01	9.70E-01	6.33E+01	4.67E+00	1.35E-03
17	5.00E+00	1.46E+01	7.23E+00	2.07E-02	1.80E-15	1.43E+01	3.54E+01	9.93E-01	6.23E+01	3.58E+00	9.18E-04
18	1.00E+01	1.30E+01	8.15E+00	1.61E-02	5.10E-16	1.61E+01	2.84E+01	1.00E+00	6.15E+01	1.33E+01	5.87E-04
19	1.50E+01	2.09E+01	6.46E+00	-3.92E-03	2.12E-17	1.27E+01	-9.57E+00	1.00E+00	1.47E+02	2.82E+02	-3.64E-04
20	2.00E+01	8.13E+01	8.25E+00	1.09E-01	7.12E-18	1.63E+01	3.81E+01	1.00E+00	3.10E+02	9.38E+02	4.72E-03

Plateau age = 61.15±0.45 Ma (2s, including J-error of .106%), MSWD = 1.19, probability = 0.27, includes 72.9% of the 39Ar, steps 4 through 20

Table A1: continued

321-1-2fss plagioclase step-heating analysis

Mass = 1.495 mg

J = 3.70E-03 +/- 3.59E-06 (2 Sigma) 0.097 Percent

Step	Laser power (W)	40Ar/39Ar	37Ar/39Ar	36Ar/39Ar	Mol 39ArK	Ca/K	% 40ArA	Cum 39ArK	Age (Ma)	2 Sigma	A.I. (36/37)
1	1.25E-01	7.53E+02	1.48E+01	2.46E+00	7.97E-17	2.94E+01	9.62E+01	7.27E-03	1.84E+02	1.01E+02	6.13E-02
2	2.00E-01	3.83E+02	9.17E+00	1.18E+00	4.84E-16	1.81E+01	9.09E+01	5.14E-02	2.22E+02	8.30E+01	4.75E-02
3	3.00E-01	4.23E+02	3.93E+01	1.33E+00	1.53E-16	8.00E+01	9.15E+01	6.54E-02	2.34E+02	8.35E+01	1.24E-02
4	4.00E-01	2.54E+02	5.94E+01	7.94E-01	1.77E-16	1.23E+02	8.92E+01	8.16E-02	1.85E+02	1.38E+02	4.81E-03
5	5.00E-01	4.42E+02	6.61E+01	1.37E+00	3.72E-16	1.38E+02	8.95E+01	1.16E-01	3.04E+02	9.48E+01	7.51E-03
6	6.00E-01	2.14E+02	1.65E+02	7.80E-01	1.47E-16	3.84E+02	9.76E+01	1.29E-01	4.01E+01	7.21E+01	1.61E-03
7	7.00E-01	2.68E+02	1.66E+02	9.43E-01	1.42E-16	3.85E+02	9.60E+01	1.42E-01	8.29E+01	7.13E+01	1.97E-03
8	8.00E-01	1.91E+02	1.78E+02	6.66E-01	9.59E-17	4.19E+02	9.10E+01	1.51E-01	1.33E+02	6.71E+01	1.25E-03
9	1.00E+00	1.31E+02	3.29E+01	4.05E-01	2.45E-16	6.65E+01	8.81E+01	1.73E-01	1.04E+02	1.98E+01	4.41E-03
10	1.20E+00	2.01E+01	3.35E+01	5.33E-02	3.41E-16	6.79E+01	5.66E+01	2.04E-01	5.91E+01	1.51E+01	4.47E-04
11	1.35E+00	4.78E+01	3.41E+01	1.34E-01	3.16E-16	6.91E+01	7.33E+01	2.33E-01	8.61E+01	1.68E+01	1.31E-03
12	1.50E+00	2.61E+01	2.28E+01	6.41E-02	3.04E-16	4.56E+01	6.11E+01	2.61E-01	6.80E+01	1.97E+01	9.00E-04
13	2.00E+00	1.16E+01	2.77E+01	2.20E-02	9.16E-16	5.57E+01	2.49E+01	3.44E-01	5.89E+01	5.48E+00	1.54E-04
14	3.00E+00	1.00E+01	2.79E+01	1.74E-02	2.38E-15	5.62E+01	1.50E+01	5.62E-01	5.75E+01	3.33E+00	8.99E-05
15	4.00E+00	9.57E+00	3.99E+01	2.19E-02	1.53E-15	8.14E+01	1.32E+01	7.01E-01	5.67E+01	4.43E+00	6.20E-05
16	6.00E+00	1.13E+01	1.95E+01	1.82E-02	1.52E-15	3.90E+01	2.51E+01	8.40E-01	5.67E+01	3.69E+00	2.05E-04
17	8.00E+00	9.13E+00	1.39E+01	1.03E-02	8.61E-16	2.76E+01	1.37E+01	9.18E-01	5.25E+01	6.66E+00	1.35E-04
18	1.00E+01	8.76E+00	1.88E+01	1.09E-02	6.05E-16	3.76E+01	8.80E+00	9.74E-01	5.35E+01	1.16E+01	7.38E-05
19	1.50E+01	8.56E+00	1.61E+01	1.16E-02	2.90E-16	3.20E+01	1.56E+01	1.00E+00	4.83E+01	1.74E+01	1.26E-04

Plateau age = 56.7±1.9 Ma (2s, including J-error of .097%), MSWD = 0.61, probability = 0.72, includes 73.9% of the 39Ar, steps 13 through 19

Table A1: continued

321-1-2mx2 matrix step-heating analysis

Mass = 1.703 mg

J = 3.70E-03 +/- 3.59E-06 (2 Sigma) 0.097 Percent

Step	Laser power (W)	40Ar/39Ar	37Ar/39Ar	36Ar/39Ar	Mol 39ArK	Ca/K	% 40ArA	Cum 39ArK	Age (Ma)	2 Sigma	A.I. (36/37)
1	1.25E-01	4.52E+01	3.89E-01	1.29E-01	5.57E-15	7.63E-01	8.44E+01	4.38E-02	4.66E+01	3.63E+00	1.23E-01
2	2.00E-01	3.74E+01	4.97E-01	9.70E-02	6.53E-15	9.75E-01	7.66E+01	9.52E-02	5.76E+01	3.89E+00	7.20E-02
3	3.00E-01	5.79E+01	5.09E-01	1.65E-01	9.94E-15	9.99E-01	8.43E+01	1.73E-01	5.99E+01	3.18E+00	1.20E-01
4	4.00E-01	4.67E+01	7.66E-01	1.28E-01	9.59E-15	1.50E+00	8.07E+01	2.49E-01	5.93E+01	2.16E+00	6.16E-02
5	5.00E-01	5.09E+01	6.63E-01	1.42E-01	1.24E-14	1.30E+00	8.24E+01	3.47E-01	5.88E+01	2.69E+00	7.93E-02
6	6.00E-01	5.20E+01	5.80E-01	1.46E-01	1.49E-14	1.14E+00	8.25E+01	4.64E-01	5.97E+01	1.91E+00	9.27E-02
7	7.00E-01	5.20E+01	6.43E-01	1.46E-01	1.25E-14	1.26E+00	8.26E+01	5.62E-01	5.94E+01	2.14E+00	8.37E-02
8	8.00E-01	4.88E+01	6.86E-01	1.35E-01	1.26E-14	1.35E+00	8.16E+01	6.61E-01	5.89E+01	1.71E+00	7.26E-02
9	9.00E-01	4.57E+01	8.20E-01	1.26E-01	9.60E-15	1.61E+00	8.10E+01	7.37E-01	5.72E+01	2.48E+00	5.66E-02
10	1.00E+00	4.22E+01	1.00E+00	1.13E-01	7.51E-15	1.97E+00	7.88E+01	7.96E-01	5.89E+01	1.68E+00	4.15E-02
11	1.10E+00	3.72E+01	1.33E+00	9.52E-02	4.73E-15	2.60E+00	7.52E+01	8.33E-01	6.07E+01	1.64E+00	2.64E-02
12	1.20E+00	3.36E+01	1.84E+00	8.59E-02	3.31E-15	3.62E+00	7.48E+01	8.59E-01	5.59E+01	4.54E+00	1.71E-02
13	1.35E+00	3.15E+01	2.12E+00	7.89E-02	2.85E-15	4.17E+00	7.32E+01	8.82E-01	5.57E+01	2.78E+00	1.36E-02
14	1.50E+00	2.88E+01	2.26E+00	6.86E-02	2.03E-15	4.45E+00	6.94E+01	8.98E-01	5.81E+01	4.06E+00	1.11E-02
15	2.00E+00	3.01E+01	2.32E+00	7.38E-02	2.99E-15	4.55E+00	7.15E+01	9.21E-01	5.64E+01	4.89E+00	1.16E-02
16	3.00E+00	2.96E+01	2.40E+00	7.14E-02	3.89E-15	4.72E+00	7.03E+01	9.52E-01	5.77E+01	2.06E+00	1.09E-02
17	5.00E+00	3.09E+01	2.68E+00	7.49E-02	4.07E-15	5.27E+00	7.05E+01	9.84E-01	6.01E+01	2.11E+00	1.02E-02
18	1.00E+01	3.35E+01	2.98E+00	8.45E-02	1.64E-15	5.87E+00	7.34E+01	9.97E-01	5.86E+01	4.65E+00	1.03E-02
19	1.50E+01	3.59E+01	3.68E+00	8.90E-02	2.42E-16	7.24E+00	7.20E+01	9.99E-01	6.61E+01	2.00E+01	8.81E-03
20	2.00E+01	3.62E+01	3.99E+00	9.35E-02	1.75E-16	7.85E+00	7.48E+01	1.00E+00	6.01E+01	2.44E+01	8.53E-03

Plateau age = 58.93±0.58 Ma, (2s, including J-error of .097%), MSWD = 1.10, probability = 0.34, includes 95.6% of the 39Ar, steps 2 through 20

Table A1: continued

321-1-5fss plagioclase step-heating analysis

Mass = 1.483 mg

J = 3.70E-03 +/- 3.59E-06 (2 Sigma) 0.097 Percent

Step	Laser power (W)	40Ar/39Ar	37Ar/39Ar	36Ar/39Ar	Mol 39ArK	Ca/K	% 40ArA	Cum 39ArK	Age (Ma)	2 Sigma	A.I. (36/37)
1	1.25E-01	3.78E+03	2.10E+01	1.28E+01	4.91E-17	4.19E+01	1.00E+02	2.38E-03	-6.98E+00	3.61E+02	2.26E-01
2	2.00E-01	2.69E+03	1.47E+01	9.04E+00	6.68E-17	2.92E+01	9.93E+01	5.61E-03	1.23E+02	2.83E+02	2.27E-01
3	3.00E-01	3.89E+02	5.46E+00	1.26E+00	3.15E-16	1.08E+01	9.58E+01	2.09E-02	1.06E+02	3.53E+01	8.55E-02
4	4.00E-01	7.57E+01	4.97E+00	2.08E-01	7.05E-16	9.79E+00	8.02E+01	5.50E-02	9.78E+01	2.23E+01	1.53E-02
5	5.00E-01	3.58E+01	7.53E+00	9.06E-02	8.87E-16	1.49E+01	7.21E+01	9.80E-02	6.61E+01	8.84E+00	4.31E-03
6	6.00E-01	1.81E+01	8.96E+00	3.50E-02	9.98E-16	1.77E+01	5.07E+01	1.46E-01	5.92E+01	7.86E+00	1.31E-03
7	7.00E-01	1.50E+01	9.88E+00	2.12E-02	9.27E-16	1.95E+01	3.33E+01	1.91E-01	6.62E+01	6.77E+00	6.54E-04
8	8.00E-01	1.64E+01	1.04E+01	2.71E-02	8.27E-16	2.06E+01	4.05E+01	2.31E-01	6.47E+01	7.94E+00	8.22E-04
9	1.00E+00	2.29E+01	9.91E+00	4.49E-02	1.09E-15	1.96E+01	5.23E+01	2.84E-01	7.22E+01	1.17E+01	1.54E-03
10	1.20E+00	1.82E+01	9.85E+00	3.62E-02	7.62E-16	1.95E+01	5.19E+01	3.21E-01	5.79E+01	1.17E+01	1.22E-03
11	1.35E+00	1.04E+01	1.07E+01	8.43E-03	5.75E-16	2.12E+01	1.06E+01	3.49E-01	6.14E+01	1.14E+01	1.51E-04
12	1.50E+00	1.06E+01	1.03E+01	1.18E-02	5.49E-16	2.03E+01	2.02E+01	3.76E-01	5.62E+01	1.12E+01	2.84E-04
13	2.00E+00	1.10E+01	1.01E+01	1.37E-02	8.43E-16	2.01E+01	2.48E+01	4.16E-01	5.47E+01	7.55E+00	3.59E-04
14	3.00E+00	9.74E+00	1.17E+01	7.49E-03	1.08E-15	2.33E+01	7.01E+00	4.69E-01	6.01E+01	5.76E+00	9.52E-05
15	4.00E+00	8.95E+00	1.18E+01	6.01E-03	3.66E-15	2.33E+01	2.73E+00	6.46E-01	5.78E+01	1.50E+00	4.86E-05
16	6.00E+00	8.66E+00	1.27E+01	6.24E-03	4.90E-15	2.53E+01	2.14E+00	8.84E-01	5.63E+01	1.13E+00	4.08E-05
17	8.00E+00	8.58E+00	1.13E+01	3.98E-03	8.17E-16	2.24E+01	-3.47E+00	9.23E-01	5.89E+01	6.82E+00	-1.04E-05
18	1.00E+01	8.65E+00	1.10E+01	4.88E-03	1.11E-15	2.17E+01	1.77E-01	9.77E-01	5.73E+01	4.60E+00	2.43E-05
19	1.20E+01	8.72E+00	1.15E+01	-7.33E-03	1.64E-16	2.27E+01	-4.20E+01	9.85E-01	8.16E+01	2.67E+01	-3.77E-04
20	1.50E+01	8.46E+00	1.41E+01	2.07E-03	3.10E-16	2.80E+01	-1.45E+01	1.00E+00	6.43E+01	1.82E+01	-8.63E-05

Plateau age = 57.03±0.87 Ma (2s, including J-error of .097%), MSWD = 1.3, probability = 0.23, includes 58.4% of the 39Ar, steps 14 through 20

Table A1: continued

321-1-5mx2 matrix step-heating analysis

Mass = 1.452 mg

J = 3.70E-03 +/- 3.59E-06 (2 Sigma) 0.097 Percent

Step	Laser power (W)	40Ar/39Ar	37Ar/39Ar	36Ar/39Ar	Mol 39ArK	Ca/K	% 40ArA	Cum 39ArK	Age (Ma)	2 Sigma	A.I. (36/37)
1	1.25E-01	1.06E+02	4.36E-01	3.33E-01	5.00E-15	8.56E-01	9.31E+01	5.55E-02	4.79E+01	6.08E+00	2.82E-01
2	2.00E-01	3.69E+01	6.04E-01	9.66E-02	3.36E-15	1.18E+00	7.72E+01	9.28E-02	5.53E+01	6.27E+00	5.90E-02
3	3.00E-01	2.05E+01	6.54E-01	3.89E-02	3.75E-15	1.28E+00	5.56E+01	1.34E-01	5.99E+01	3.57E+00	2.19E-02
4	4.00E-01	1.39E+01	6.16E-01	1.81E-02	5.70E-15	1.21E+00	3.80E+01	1.98E-01	5.67E+01	1.86E+00	1.08E-02
5	5.00E-01	1.23E+01	6.21E-01	1.28E-02	7.50E-15	1.22E+00	3.01E+01	2.81E-01	5.63E+01	1.38E+00	7.47E-03
6	6.00E-01	1.12E+01	5.75E-01	9.56E-03	7.47E-15	1.13E+00	2.45E+01	3.64E-01	5.57E+01	1.28E+00	6.01E-03
7	7.00E-01	1.05E+01	7.88E-01	7.25E-03	6.63E-15	1.55E+00	1.94E+01	4.38E-01	5.57E+01	1.33E+00	3.26E-03
8	8.00E-01	1.06E+01	1.49E+00	7.69E-03	6.74E-15	2.92E+00	1.96E+01	5.12E-01	5.61E+01	1.25E+00	1.77E-03
9	9.00E-01	1.08E+01	1.87E+00	8.78E-03	5.06E-15	3.68E+00	2.17E+01	5.69E-01	5.58E+01	1.61E+00	1.59E-03
10	1.00E+00	1.08E+01	2.27E+00	9.96E-03	3.36E-15	4.45E+00	2.45E+01	6.06E-01	5.39E+01	2.40E+00	1.49E-03
11	1.10E+00	1.15E+01	2.59E+00	1.11E-02	2.81E-15	5.09E+00	2.57E+01	6.37E-01	5.61E+01	1.96E+00	1.45E-03
12	1.20E+00	1.12E+01	2.61E+00	1.01E-02	2.97E-15	5.13E+00	2.36E+01	6.70E-01	5.64E+01	2.51E+00	1.29E-03
13	1.35E+00	1.12E+01	2.56E+00	1.10E-02	2.96E-15	5.03E+00	2.62E+01	7.03E-01	5.44E+01	2.02E+00	1.46E-03
14	1.50E+00	1.12E+01	2.39E+00	9.37E-03	2.03E-15	4.70E+00	2.19E+01	7.26E-01	5.78E+01	2.78E+00	1.31E-03
15	2.00E+00	1.11E+01	2.39E+00	1.06E-02	4.03E-15	4.70E+00	2.53E+01	7.70E-01	5.49E+01	1.58E+00	1.50E-03
16	3.00E+00	1.16E+01	2.36E+00	1.17E-02	6.59E-15	4.64E+00	2.72E+01	8.43E-01	5.55E+01	1.20E+00	1.69E-03
17	5.00E+00	1.16E+01	2.48E+00	1.17E-02	8.96E-15	4.87E+00	2.69E+01	9.43E-01	5.59E+01	1.26E+00	1.60E-03
18	1.00E+01	1.17E+01	2.94E+00	1.22E-02	4.56E-15	5.78E+00	2.75E+01	9.94E-01	5.61E+01	1.27E+00	1.40E-03
19	1.50E+01	1.20E+01	2.43E+00	1.04E-02	4.94E-16	4.77E+00	2.30E+01	9.99E-01	6.08E+01	1.23E+01	1.44E-03
20	2.00E+01	1.03E+01	1.24E+00	-2.18E-03	8.47E-17	2.43E+00	-7.82E+00	1.00E+00	7.27E+01	4.29E+01	-7.91E-04

Plateau age = 55.71±0.45 Ma (2s, including J-error of .097%), MSWD = 0.78, probability = 0.68, includes 63.5% of the 39Ar, steps 7 through 19

Table A1: continued

325-1-2Bfss plagioclase step-heating analysis

Mass = 1.482 mg

J = 3.70E-03 +/- 3.59E-06 (2 Sigma) 0.097 Percent

Step	Laser power (W)	40Ar/39Ar	37Ar/39Ar	36Ar/39Ar	Mol 39ArK	Ca/K	% 40ArA	Cum 39ArK	Age (Ma)	2 Sigma	A.I. (36/37)
1	1.25E-01	1.59E+03	5.54E+00	5.38E+00	2.40E-17	1.09E+01	1.00E+02	8.27E-04	-2.25E+01	4.02E+02	3.59E-01
2	2.00E-01	4.76E+03	1.14E+01	1.60E+01	9.50E-17	2.25E+01	9.95E+01	4.11E-03	1.51E+02	2.09E+02	5.22E-01
3	3.00E-01	1.22E+03	7.82E+00	4.06E+00	9.59E-17	1.54E+01	9.80E+01	7.41E-03	1.56E+02	1.09E+02	1.92E-01
4	4.00E-01	2.22E+02	7.57E+00	7.01E-01	1.26E-16	1.50E+01	9.27E+01	1.18E-02	1.06E+02	5.41E+01	3.41E-02
5	5.00E-01	5.58E+01	1.03E+01	1.64E-01	2.23E-16	2.05E+01	8.44E+01	1.95E-02	5.77E+01	2.85E+01	5.73E-03
6	6.00E-01	9.47E+01	1.44E+01	2.94E-01	3.26E-16	2.85E+01	8.97E+01	3.07E-02	6.50E+01	2.39E+01	7.42E-03
7	7.00E-01	1.95E+01	1.66E+01	4.57E-02	4.48E-16	3.31E+01	5.81E+01	4.62E-02	5.47E+01	1.43E+01	8.77E-04
8	8.00E-01	2.09E+01	1.62E+01	4.74E-02	5.30E-16	3.23E+01	5.69E+01	6.45E-02	6.02E+01	1.55E+01	9.41E-04
9	1.00E+00	1.37E+01	1.22E+01	2.25E-02	8.43E-16	2.42E+01	3.69E+01	9.35E-02	5.75E+01	6.85E+00	5.41E-04
10	1.20E+00	1.70E+01	8.51E+00	3.44E-02	9.64E-16	1.68E+01	5.33E+01	1.27E-01	5.27E+01	6.68E+00	1.36E-03
11	1.35E+00	1.17E+01	7.54E+00	1.76E-02	9.66E-16	1.49E+01	3.62E+01	1.60E-01	4.93E+01	6.13E+00	7.24E-04
12	1.50E+00	1.18E+01	7.50E+00	1.62E-02	9.25E-16	1.48E+01	3.25E+01	1.92E-01	5.26E+01	6.19E+00	6.60E-04
13	2.00E+00	1.87E+01	6.29E+00	3.81E-02	2.39E-15	1.24E+01	5.57E+01	2.75E-01	5.48E+01	3.06E+00	2.10E-03
14	3.00E+00	1.16E+01	8.88E+00	1.52E-02	3.32E-15	1.76E+01	2.89E+01	3.89E-01	5.45E+01	1.71E+00	4.94E-04
15	4.00E+00	9.23E+00	5.91E+00	5.17E-03	5.07E-15	1.16E+01	8.21E+00	5.64E-01	5.60E+01	1.04E+00	1.83E-04
16	6.00E+00	9.10E+00	6.44E+00	4.80E-03	6.78E-15	1.27E+01	6.37E+00	7.98E-01	5.63E+01	1.04E+00	1.35E-04
17	1.00E+01	9.19E+00	9.41E+00	7.70E-03	5.79E-16	1.86E+01	1.14E+01	8.18E-01	5.40E+01	1.13E+01	1.62E-04
18	1.20E+01	8.76E+00	6.17E+00	3.91E-03	1.69E-15	1.22E+01	4.02E+00	8.76E-01	5.55E+01	2.51E+00	9.40E-05
19	1.50E+01	9.22E+00	3.70E+00	3.21E-03	3.58E-15	7.28E+00	5.04E+00	1.00E+00	5.77E+01	1.34E+00	1.80E-04

Plateau age = 56.45±0.63 Ma (2s, including J-error of .097%), MSWD = 1.2, probability = 0.30, includes 61.1% of the 39Ar, steps 15 through 19

Table A1: continued

324-1-3mxs matrix step-heating analysis

Mass = 1.855 mg

J = 3.70E-03 +/- 3.59E-06 (2 Sigma) 0.097 Percent

Step	Laser power (W)	40Ar/39Ar	37Ar/39Ar	36Ar/39Ar	Mol 39ArK	Ca/K	% 40ArA	Cum 39ArK	Age (Ma)	2 Sigma	A.I. (36/37)
1	1.25E-01	1.26E+03	1.15E+00	4.17E+00	5.64E-16	2.25E+00	9.76E+01	7.96E-03	1.93E+02	4.07E+01	1.34E+00
2	2.00E-01	1.67E+02	1.08E+00	5.40E-01	1.20E-15	2.12E+00	9.54E+01	2.49E-02	5.02E+01	1.36E+01	1.84E-01
3	3.00E-01	3.46E+01	1.11E+00	1.13E-01	2.59E-15	2.17E+00	9.58E+01	6.15E-02	9.67E+00	5.67E+00	3.75E-02
4	4.00E-01	1.52E+01	1.15E+00	5.00E-02	4.00E-15	2.26E+00	9.62E+01	1.18E-01	3.91E+00	3.12E+00	1.60E-02
5	5.00E-01	1.07E+01	1.18E+00	3.54E-02	5.24E-15	2.31E+00	9.61E+01	1.92E-01	2.80E+00	1.39E+00	1.10E-02
6	6.00E-01	8.24E+00	1.35E+00	2.70E-02	5.89E-15	2.64E+00	9.48E+01	2.75E-01	2.86E+00	9.52E-01	7.28E-03
7	7.00E-01	8.66E+00	1.65E+00	2.89E-02	6.10E-15	3.23E+00	9.62E+01	3.61E-01	2.19E+00	1.08E+00	6.36E-03
8	8.00E-01	8.92E+00	2.25E+00	2.97E-02	4.37E-15	4.41E+00	9.51E+01	4.22E-01	2.93E+00	2.37E+00	4.75E-03
9	9.00E-01	1.03E+01	2.74E+00	3.49E-02	2.94E-15	5.38E+00	9.70E+01	4.64E-01	2.06E+00	3.11E+00	4.58E-03
10	1.00E+00	1.54E+01	3.03E+00	5.07E-02	3.34E-15	5.95E+00	9.51E+01	5.11E-01	5.08E+00	2.51E+00	6.06E-03
11	1.10E+00	2.52E+01	3.08E+00	8.42E-02	4.29E-15	6.06E+00	9.70E+01	5.72E-01	5.00E+00	3.27E+00	9.97E-03
12	1.20E+00	2.52E+01	3.62E+00	8.51E-02	4.39E-15	7.12E+00	9.78E+01	6.34E-01	3.74E+00	2.75E+00	8.56E-03
13	1.35E+00	2.34E+01	4.22E+00	7.99E-02	5.50E-15	8.31E+00	9.86E+01	7.11E-01	2.22E+00	2.45E+00	6.87E-03
14	1.50E+00	2.17E+01	5.03E+00	7.40E-02	3.67E-15	9.91E+00	9.78E+01	7.63E-01	3.17E+00	2.53E+00	5.30E-03
15	2.00E+00	2.36E+01	6.25E+00	7.92E-02	5.58E-15	1.23E+01	9.56E+01	8.42E-01	6.89E+00	3.59E+00	4.55E-03
16	3.00E+00	2.14E+01	7.59E+00	7.25E-02	4.64E-15	1.50E+01	9.56E+01	9.07E-01	6.33E+00	3.88E+00	3.39E-03
17	5.00E+00	1.79E+01	8.80E+00	6.14E-02	5.20E-15	1.74E+01	9.51E+01	9.81E-01	5.90E+00	1.96E+00	2.44E-03
18	1.00E+01	1.80E+01	1.21E+01	6.22E-02	1.29E-15	2.40E+01	9.32E+01	9.99E-01	8.30E+00	1.01E+01	1.76E-03
19	1.50E+01	3.26E+01	1.57E+01	8.42E-02	8.18E-17	3.13E+01	7.01E+01	1.00E+00	6.49E+01	6.47E+01	1.84E-03
20	2.00E+01	7.10E+01	2.16E+01	-1.74E-02	9.54E-18	4.33E+01	-1.12E+01	1.00E+00	4.71E+02	5.00E+02	-4.38E-04

Plateau age = 3.02±0.52 Ma (2s, including J-error of .097%), MSWD = 1.3, probability = 0.21, includes 84.6% of the 39Ar, steps 4 through 16

Table A1: continued

327-1-2mx2 matrix step-heating analysis

Mass = 1.445 mg

J = 3.70E-03 +/- 3.59E-06 (2 Sigma) 0.097 Percent

Step	Laser power (W)	40Ar/39Ar	37Ar/39Ar	36Ar/39Ar	Mol 39ArK	Ca/K	% 40ArA	Cum 39ArK	Age (Ma)	2 Sigma	A.I. (36/37)
1	1.25E-01	6.91E+01	2.36E+00	2.02E-01	4.50E-15	4.63E+00	8.60E+01	9.55E-02	6.35E+01	6.61E+00	3.16E-02
2	2.00E-01	6.38E+01	3.02E+00	1.90E-01	3.21E-15	5.93E+00	8.72E+01	1.64E-01	5.39E+01	9.31E+00	2.31E-02
3	3.00E-01	4.62E+01	3.34E+00	1.37E-01	3.54E-15	6.56E+00	8.64E+01	2.39E-01	4.15E+01	5.34E+00	1.50E-02
4	4.00E-01	2.71E+01	4.10E+00	6.73E-02	3.39E-15	8.07E+00	7.14E+01	3.11E-01	5.12E+01	2.85E+00	5.94E-03
5	5.00E-01	2.19E+01	4.55E+00	4.62E-02	2.99E-15	8.96E+00	5.96E+01	3.74E-01	5.86E+01	3.20E+00	3.62E-03
6	6.00E-01	1.62E+01	3.45E+00	2.53E-02	3.48E-15	6.79E+00	4.35E+01	4.48E-01	6.01E+01	2.04E+00	2.57E-03
7	7.00E-01	1.44E+01	2.92E+00	1.94E-02	4.19E-15	5.75E+00	3.70E+01	5.37E-01	5.98E+01	1.39E+00	2.31E-03
8	8.00E-01	1.57E+01	3.21E+00	2.40E-02	3.38E-15	6.31E+00	4.27E+01	6.09E-01	5.91E+01	1.42E+00	2.63E-03
9	9.00E-01	2.02E+01	3.39E+00	4.02E-02	2.70E-15	6.66E+00	5.67E+01	6.66E-01	5.77E+01	2.65E+00	4.25E-03
10	1.00E+00	2.21E+01	3.40E+00	4.72E-02	2.22E-15	6.68E+00	6.11E+01	7.13E-01	5.66E+01	2.49E+00	5.00E-03
11	1.10E+00	2.47E+01	3.80E+00	5.74E-02	1.64E-15	7.48E+00	6.68E+01	7.48E-01	5.40E+01	5.30E+00	5.45E-03
12	1.20E+00	2.81E+01	3.77E+00	6.99E-02	1.23E-15	7.41E+00	7.18E+01	7.74E-01	5.23E+01	6.58E+00	6.72E-03
13	1.35E+00	3.09E+01	3.89E+00	7.67E-02	1.26E-15	7.64E+00	7.18E+01	8.01E-01	5.74E+01	6.09E+00	7.17E-03
14	1.50E+00	3.13E+01	3.69E+00	8.11E-02	1.03E-15	7.26E+00	7.51E+01	8.23E-01	5.13E+01	8.03E+00	7.99E-03
15	2.00E+00	3.40E+01	3.78E+00	8.73E-02	2.11E-15	7.44E+00	7.45E+01	8.67E-01	5.71E+01	4.58E+00	8.40E-03
16	3.00E+00	3.21E+01	5.26E+00	8.53E-02	2.43E-15	1.04E+01	7.65E+01	9.19E-01	5.00E+01	4.11E+00	5.86E-03
17	5.00E+00	3.42E+01	6.09E+00	9.09E-02	2.92E-15	1.20E+01	7.63E+01	9.81E-01	5.36E+01	2.50E+00	5.38E-03
18	1.00E+01	2.98E+01	5.49E+00	7.68E-02	8.81E-16	1.08E+01	7.38E+01	1.00E+00	5.17E+01	8.06E+00	5.03E-03
19	1.50E+01	7.20E+01	2.01E+01	1.75E-01	1.49E-17	4.01E+01	6.82E+01	1.00E+00	1.49E+02	2.50E+02	3.09E-03

Plateau age = 58.74±0.75 Ma (2s, including J-error of .097%), MSWD = 1.9, probability = 0.040, includes 55.7% of the 39Ar, steps 5 through 15

Table A1: continued

244-1-1gls glass step-heating analysis

Mass = 1.404 mg

J = 3.70E-03 +/- 3.59E-06 (2 Sigma) 0.097 Percent

Step	Laser power (W)	40Ar/39Ar	37Ar/39Ar	36Ar/39Ar	Mol 39ArK	Ca/K	% 40ArA	Cum 39ArK	Age (Ma)	2 Sigma	A.I. (36/37)
1	1.25E-01	2.50E+02	1.40E+00	8.40E-01	1.35E-16	2.74E+00	9.94E+01	2.20E-03	1.01E+01	5.84E+01	2.23E-01
2	2.00E-01	6.98E+01	2.07E+00	2.39E-01	2.35E-16	4.06E+00	1.01E+02	6.04E-03	-3.89E+00	2.34E+01	4.26E-02
3	3.00E-01	1.51E+01	2.52E+00	2.07E-02	2.11E-15	4.95E+00	3.85E+01	4.05E-02	6.10E+01	2.43E+00	2.90E-03
4	4.00E-01	1.85E+00	2.51E+00	6.20E-03	8.79E-15	4.92E+00	8.16E+01	1.84E-01	2.27E+00	8.35E-01	7.75E-04
5	5.00E-01	2.08E+00	2.62E+00	7.27E-03	9.83E-15	5.14E+00	8.72E+01	3.45E-01	1.77E+00	6.89E-01	8.87E-04
6	6.00E-01	1.79E+00	2.63E+00	6.61E-03	8.74E-15	5.17E+00	9.04E+01	4.88E-01	1.14E+00	8.19E-01	7.88E-04
7	7.00E-01	2.07E+00	2.71E+00	6.93E-03	5.80E-15	5.32E+00	8.20E+01	5.82E-01	2.49E+00	1.30E+00	8.07E-04
8	8.00E-01	1.65E+00	2.80E+00	5.94E-03	3.46E-15	5.50E+00	8.47E+01	6.39E-01	1.68E+00	1.42E+00	6.44E-04
9	9.00E-01	1.72E+00	2.82E+00	6.32E-03	2.18E-15	5.54E+00	8.74E+01	6.75E-01	1.45E+00	2.59E+00	6.89E-04
10	1.00E+00	1.11E+00	2.72E+00	3.59E-03	4.46E-15	5.34E+00	6.36E+01	7.47E-01	2.70E+00	1.10E+00	3.47E-04
11	1.10E+00	9.90E-01	2.94E+00	3.65E-03	4.63E-15	5.78E+00	7.06E+01	8.23E-01	1.93E+00	7.49E-01	3.19E-04
12	1.20E+00	1.23E+00	3.00E+00	4.27E-03	2.49E-15	5.90E+00	7.10E+01	8.64E-01	2.38E+00	1.89E+00	3.87E-04
13	1.35E+00	9.27E-01	3.00E+00	1.77E-03	8.92E-16	5.90E+00	1.45E+01	8.78E-01	5.27E+00	5.42E+00	7.81E-05
14	1.50E+00	1.16E+00	3.00E+00	2.41E-03	1.35E-15	5.89E+00	2.79E+01	9.00E-01	5.55E+00	2.92E+00	1.57E-04
15	2.00E+00	1.25E+00	3.18E+00	3.14E-03	1.20E-15	6.26E+00	4.13E+01	9.20E-01	4.88E+00	6.16E+00	2.24E-04
16	3.00E+00	1.43E+00	3.73E+00	4.82E-03	3.51E-15	7.33E+00	6.58E+01	9.77E-01	3.27E+00	1.78E+00	3.38E-04
17	5.00E+00	6.94E-01	6.26E+00	4.99E-03	1.23E-15	1.23E+01	9.58E+01	9.97E-01	1.93E-01	4.53E+00	1.54E-04
18	1.00E+01	1.59E+00	1.45E+01	3.45E-02	1.46E-16	2.88E+01	5.26E+02	1.00E+00	-4.62E+01	4.46E+01	7.42E-04
19	1.50E+01	-6.81E-02	1.88E+01	1.67E-01	1.20E-17	3.75E+01	-6.34E+04	1.00E+00	-3.51E+02	5.98E+02	3.14E-03

Plateau age = 1.93±0.33 Ma (2s, including J-error of .097%), MSWD = 1.03, probability = 0.41, includes 83.8% of the 39Ar, steps 4 through 13

Table A1: continued

244-1-3gl2 glass step-heating analysis

Mass = 1.499 mg

J = 3.70E-03 +/- 3.59E-06 (2 Sigma) 0.097 Percent

Step	Laser power (W)	40Ar/39Ar	37Ar/39Ar	36Ar/39Ar	Mol 39ArK	Ca/K	% 40ArA	Cum 39ArK	Age (Ma)	2 Sigma	A.I. (36/37)
1	1.25E-01	2.06E+02	1.99E+00	6.87E-01	4.71E-17	3.90E+00	9.85E+01	7.78E-04	2.05E+01	1.14E+02	1.28E-01
2	2.00E-01	1.25E+02	-9.45E-01	3.80E-01	6.01E-17	-1.85E+00	8.99E+01	1.77E-03	8.28E+01	8.87E+01	-1.49E-01
3	3.00E-01	3.48E+00	2.42E+00	1.09E-02	4.35E-16	4.76E+00	8.32E+01	8.96E-03	3.90E+00	1.05E+01	1.52E-03
4	4.00E-01	4.24E+01	2.90E+00	4.94E-03	1.67E-15	5.70E+00	2.55E+00	3.65E-02	2.57E+02	2.96E+00	4.90E-04
5	5.00E-01	5.12E-01	2.74E+00	1.95E-03	4.69E-15	5.38E+00	4.35E+01	1.14E-01	1.91E+00	8.73E-01	1.23E-04
6	6.00E-01	3.78E-01	2.74E+00	1.69E-03	5.85E-15	5.39E+00	3.81E+01	2.11E-01	1.54E+00	6.63E-01	8.73E-05
7	7.00E-01	3.18E-01	2.82E+00	1.32E-03	8.60E-15	5.54E+00	7.54E+00	3.52E-01	1.93E+00	4.60E-01	3.30E-05
8	8.00E-01	3.22E-01	2.85E+00	1.57E-03	6.40E-15	5.60E+00	2.88E+01	4.58E-01	1.51E+00	8.56E-01	6.25E-05
9	9.00E-01	4.13E-01	2.85E+00	1.86E-03	6.03E-15	5.60E+00	4.39E+01	5.58E-01	1.53E+00	7.38E-01	1.01E-04
10	1.00E+00	3.18E-01	2.94E+00	1.45E-03	4.84E-15	5.78E+00	1.47E+01	6.38E-01	1.78E+00	6.59E-01	4.22E-05
11	1.10E+00	2.69E-01	2.95E+00	1.53E-03	3.41E-15	5.79E+00	2.59E+01	6.94E-01	1.31E+00	1.62E+00	5.16E-05
12	1.20E+00	2.57E-01	2.96E+00	1.98E-03	2.94E-15	5.81E+00	7.90E+01	7.43E-01	3.52E-01	1.92E+00	1.07E-04
13	1.35E+00	2.45E-01	2.97E+00	1.90E-03	2.13E-15	5.83E+00	7.31E+01	7.78E-01	4.31E-01	2.30E+00	9.62E-05
14	1.50E+00	3.56E-01	3.10E+00	1.65E-03	1.54E-15	6.10E+00	2.35E+01	8.03E-01	1.79E+00	3.89E+00	5.57E-05
15	2.00E+00	3.37E-01	2.94E+00	1.53E-03	4.38E-15	5.78E+00	2.11E+01	8.75E-01	1.75E+00	1.81E+00	5.22E-05
16	3.00E+00	3.44E-01	3.06E+00	2.01E-03	4.13E-15	6.01E+00	5.79E+01	9.44E-01	9.53E-01	1.33E+00	1.03E-04
17	5.00E+00	2.87E-01	3.58E+00	2.03E-03	3.32E-15	7.04E+00	4.75E+01	9.98E-01	9.90E-01	1.90E+00	6.93E-05
18	1.00E+01	1.09E+00	1.04E+01	1.50E-02	9.54E-17	2.06E+01	2.83E+02	1.00E+00	-1.34E+01	4.42E+01	3.92E-04

Plateau age = 1.65±0.25 Ma (2s, including J-error of .097%), MSWD = 0.58, probability = 0.87, includes 96.4% of the 39Ar, steps 5 through 18

Table A2: RFA standard measurements and reference values.

Oxide (wt%)	JB-2^g	JB2 (N=2)	SD	Diff. (abs.)	Diff. (%)	JB-3*	JB-3 (N=2)	SD	Diff. (abs.)	Diff. (%)	JA-2^h	JA-2 (N=2)	SD	Diff. (abs.)	Diff. (%)
SiO ₂	53.20	52.80	0.28	0.40	0.8	51.04	50.70	0.24	0.34	0.7	56.42	56.13	0.21	0.29	0.5
TiO ₂	1.19	1.17	0.02	0.02	2.1	1.45	1.42	0.02	0.03	2.4	0.66	0.68	0.01	-0.02	2.3
Al ₂ O ₃	14.67	14.74	0.05	-0.06	0.4	16.89	17.18	0.21	-0.29	1.7	15.41	15.35	0.04	0.06	0.4
Fe ₂ O ₃	14.34	14.42	0.06	-0.08	0.6	11.88	12.01	0.09	-0.12	1.1	6.21	6.38	0.12	-0.17	2.7
MnO	0.20	0.21	0.01	-0.01	5.0	0.16	0.17	0.01	-0.01	6.3	0.11	0.11	0.00	0.00	1.9
MgO	4.66	4.73	0.05	-0.07	1.5	5.20	5.22	0.01	-0.01	0.3	7.60	7.99	0.28	-0.39	5.1
CaO	9.89	9.86	0.02	0.03	0.3	9.86	9.78	0.06	0.09	0.9	6.29	6.26	0.02	0.04	0.6
Na ₂ O	2.03	2.10	0.05	-0.06	3.2	2.82	2.83	0.00	-0.01	0.2	3.11	3.07	0.03	0.04	1.4
K ₂ O	0.42	0.41	0.01	0.01	2.4	0.78	0.78	0.00	0.01	0.6	1.81	1.76	0.04	0.06	3.0
P ₂ O ₅	0.10	0.10	0.00	0.01	5.0	0.29	0.30	0.00	-0.01	1.7	0.15	0.16	0.01	-0.01	6.2
total	100.70	100.52				100.37	100.36				97.76	97.86			

^g reference values from Govindaraju 1994

^h GeoReM preferred values (Jochum et al. 2005), i.e. primarily certified data as well as data from high precision and definitive methods.

Table A3: ICP-MS standard measurements and reference values.

Element	BCR-2 ppm pref. ⁱ	± ppm	BCR-2 ppm (n=6)	SD ppm	RSD %	Diff. abs.	Diff. %	BHVO-2 ppm pref.	± ppm	BHVO-2 ppm (n=6)	SD ppm	RSD %	Diff. abs.	Diff. %	BIR-1 ppm pref.	± ppm	BIR-1 ppm (n=6)	SD ppm	RSD %	Diff. abs.	Diff. %
Rb	46.9	0.1	50.4	1.39	2.76	-3.5	7.6	9.11	0.04	9.81	0.31	3.12	-0.7	7.7	0.2	0.01	0.209	0.04	19.55	0.0	4.4
Ba	677	2	708	11.44	1.62	-30.9	4.6	131	1	136	2.89	2.13	-4.5	3.4	7.14		8.03	0.27	3.42	-0.9	12.4
Th	5.7	0.5	6.10	0.14	2.38	-0.4	6.9	1.22	0.06	1.24	0.06	4.83	0.0	1.8	0.032	0.004	0.032	0.00	5.92	0.0	0.5
U	1.69	0.19	1.68	0.06	3.68	0.0	0.8	0.403	0.001	0.412	0.02	4.72	0.0	2.2	0.01	0.001	0.011	0.00	2.98	0.0	9.6
Nb	12.6	0.4	12.4	0.21	1.73	0.2	1.5	18.1	1	18.2	0.37	2.05	-0.1	0.4	0.55	0.05	0.560	0.02	3.55	0.0	1.9
Ta	0.74	0.02	0.842	0.01	1.08	-0.1	13.8	1.14	0.06	1.23	0.04	3.47	-0.1	8.0	0.0357	0.0004	0.095	0.02	15.94	-0.1	166
La	24.9	0.2	26.1	0.38	1.43	-1.2	5.0	15.2	0.1	15.9	0.18	1.11	-0.7	4.4	0.615	0.021	0.661	0.02	2.73	0.0	7.4
Ce	52.9	0.2	54.9	0.57	1.04	-2.0	3.8	37.5	0.2	38.3	0.51	1.33	-0.8	2.2	1.92	0.08	2.04	0.05	2.59	-0.1	6.3
Pb	11	1	9.98	0.16	1.65	1.0	9.2	1.6	0.3	1.56	0.04	2.32	0.0	2.7	3.1	0.3	2.91	0.10	3.31	0.2	6.2
Pr	6.7	0.1	6.97	0.09	1.23	-0.3	4.0	5.35	0.17	5.44	0.13	2.35	-0.1	1.8	0.37	0.02	0.391	0.01	2.81	0.0	5.6
Nd	28.7	0.1	29.5	0.52	1.76	-0.8	2.9	24.5	0.1	25.2	0.87	3.47	-0.7	2.7	2.38	0.01	2.503	0.12	4.70	-0.1	5.2
Sr	340		365	9.61	2.63	-24.8	7.3	396	1	423	6.41	1.51	-27.0	6.8	109	2	118	0.91	0.77	-8.7	8.0
Sm	6.58	0.02	6.93	0.15	2.20	-0.4	5.4	6.07	0.01	6.33	0.08	1.31	-0.3	4.2	1.12	0.02	1.17	0.04	3.30	-0.1	4.5
Hf	4.9	0.1	5.02	0.13	2.63	-0.1	2.5	4.36	0.14	4.40	0.12	2.67	0.0	1.0	0.582	0.004	0.606	0.03	5.27	0.0	4.1
Zr	184	1	198	3.49	1.77	-13.6	7.4	172	11	179	2.97	1.66	-7.1	4.1	14	0.1	15.6	0.33	2.13	-1.6	11.3
Eu	1.96	0.01	2.01	0.03	1.52	0.0	2.5	2.07	0.02	2.08	0.04	1.87	0.0	0.4	0.53		0.550	0.02	3.66	0.0	3.8
Gd	6.75	0.03	6.93	0.13	1.86	-0.2	2.6	6.24	0.03	6.24	0.20	3.20	0.0	0.1	1.87	0.04	2.00	0.06	3.22	-0.1	6.7
Tb	1.07	0.03	1.05	0.03	3.09	0.0	1.5	0.92	0.03	0.901	0.03	3.11	0.0	2.1	0.36	0.03	0.373	0.02	5.45	0.0	3.6
Dy	6.41	0.05	6.42	0.23	3.64	0.0	0.2	5.31	0.02	5.17	0.25	4.78	0.1	2.7	2.51		2.63	0.12	4.74	-0.1	4.8
Ho	1.28	0.03	1.28	0.05	4.11	0.0	0.2	0.98	0.04	0.949	0.04	4.52	0.0	3.2	0.56	0.05	0.584	0.04	6.50	0.0	4.3
Y	37	2	35.8	1.02	2.85	1.2	3.2	26	2	25.7	0.55	2.13	0.3	1.3	15.6	0.9	15.7	0.23	1.45	-0.1	0.6
Er	3.66	0.01	3.60	0.18	4.99	0.1	1.5	2.54	0.01	2.42	0.12	4.78	0.1	4.7	1.66		1.74	0.10	5.81	-0.1	5.0
Tm	0.54	0.04	0.507	0.03	5.34	0.0	6.1	0.33	0.01	0.317	0.02	7.54	0.0	3.9	0.25	0.03	0.251	0.02	6.14	0.0	0.3
Yb	3.38	0.02	3.54	0.10	2.71	-0.2	4.6	2	0.01	2.01	0.05	2.68	0.0	0.5	1.65		1.75	0.05	3.06	-0.1	5.9
Lu	0.503	0.009	0.512	0.01	1.93	0.0	1.8	0.274	0.005	0.282	0.01	3.82	0.0	3.0	0.25	0.02	0.266	0.00	1.35	0.0	6.5

ⁱ GeoReM preferred values (Jochum et al. 2005), i.e. primarily certified data as well as data from high precision and definitive methods.

Table A4: A full table with sample locations, radiometric ages and geochemical data

Sample No	Location	Lat S	Long W	Depth (mbsl)	Age (Ma)	±2s.e. (Ma)	Rb ppm	Sr ppm	⁸⁷ Sr/ ⁸⁶ Sr	±2s.e.	⁸⁷ Rb/ ⁸⁶ Sr	⁸⁷ Sr/ ⁸⁶ Sr _i	Sm ppm	Nd ppm	¹⁴³ Nd/ ¹⁴⁴ Nd	±2s.e.
Marie Byrd Smnts																
PS69/317-1-1	Haxby	69,172	123,424	1983	64,7	0,8	28,2	760	0,703093	3	0,107	0,70299	12,1	55,6	0,512885	3
PS69/317-1-1*	Haxby	69,172	123,424	1983												
PS69/317-1-2	Haxby	69,172	123,424	1983	61,2	0,5	6,66	1219	0,704186	3	0,016	0,70417	13,3	57,6	0,512881	3
PS69/321-1-2	Miller	69,359	121,532	1670	56,7	1,9	53,4	825	0,703384	3	0,187	0,70323	12,6	63,2	0,512798	3
PS69/321-1-4	Miller	69,359	121,532	1670	56,9		37,3	969	0,703277	2	0,111	0,70319	9,86	46,0	0,512806	2
PS69/321-1-5	Miller	69,359	121,532	1670	57,0	0,9	50,4	925	0,703335	2	0,157	0,70321	9,49	44,3	0,512816	3
PS69/321-1-12a	Miller	69,359	121,532	1670	56,9		23,9	891	0,703230	3	0,078	0,70317	12,5	61,6	0,512811	3
PS69/324-1-3	Miller	69,501	121,006	2622	3,0	0,5	24,1	626	0,703094	3	0,111	0,70309	6,69	30,1	0,512906	3
PS69/324-1-4	Miller	69,501	121,006	2622	3,0		35,8	967	0,704027	3	0,107	0,70402	9,97	46,5	0,512881	3
PS69/324-1-4*	Miller	69,501	121,006	2622	3,0		35,8	967	0,704043	3	0,107	0,70404	9,97	46,5	0,512870	3
PS69/324-1-6	Miller	69,501	121,006	2622	3,0		28,0	568	0,703108	3	0,143	0,70310	8,08	35,5	0,512899	3
PS69/324-1-6*	Miller	69,501	121,006	2622	3,0											
PS69/325-1-2a	Miller	69,454	120,932	1560	56,5		90,1	674	0,703502	3	0,387	0,70319	12,9	62,4	0,512809	3
PS69/325-1-2b	Miller	69,454	120,932	1560	56,5	0,6	57,3	717	0,703417	2	0,231	0,70323	13,3	62,3	0,512817	3
PS69/327-1-1	Smnt C	69,184	117,644	2957	58,7		27,2	811	0,702888	3	0,097	0,70281	8,09	39,0	0,512913	6
PS69/327-1-2	Smnt C	69,184	117,644	2957	58,7	0,8	21,5	843	0,702805	3	0,074	0,70274	7,89	35,6	0,512918	9
PS69/327-1-2*	Smnt C	69,184	117,644	2957	58,7		21,5	843	0,702831	3	0,074	0,70277	7,89	35,6	0,512927	4
De Gerlach Smnts.																
PS-2693-1_(1)**	Belgica	65,305	90,587	800	20,1	1,0	1,80	582	0,703015	5	0,009	0,70301	9,70	37,0	0,512967	2
PS-2693-1_(2)**	Belgica	65,305	90,587	800	23,2	1,2	2,50	591	0,703023	5	0,012	0,70302	10,0	39,0	0,512966	3
PS-2693-1_(3)**	Belgica	65,305	90,587	800	22,6	1,1	1,60	599	0,703029	5	0,008	0,70303	9,90	38,0	0,512966	3
PS-2693-1_(4)**	Belgica	65,305	90,587	800	22,0		12,0	741	0,703029	4	0,047	0,70301	11,0	43,0	0,512957	3
PS-2693-1_(5)**	Belgica	65,305	90,587	800	22,0				0,702998	5					0,512983	4
PS-2693-1_(6)**	Belgica	65,305	90,587	800	22,0				0,702994	5					0,512975	3
Peter I Island																
PS69/244-1-1	NE-Flank	68,741	90,348	1853	1,9	0,3	20,3	624	0,703748	3	0,094	0,70375	7,57	32,7	0,512759	2
PS69/244-1-3	NE-Flank	68,741	90,348	1853	1,7	0,3	19,8	622	0,703752	3	0,092	0,70375	7,54	30,8	0,512750	3
PS69/244-1-5	NE-Flank	68,741	90,348	1853												
PS69/PI-1***	Michajlovodden	68,864	90,426	40m absl	0,23		23,9	797	0,703759	5	0,087	0,70376	9,80	43,0	0,512805	2
PS69/PI-3	Michajlovodden	68,864	90,426	40m absl	0,23		26,5	804	0,703837	2	0,095	0,70384	10,2	43,6	0,512782	2
PS69/PI-4	Michajlovodden	68,864	90,426	40m absl	0,23		26,3	871	0,703871	2	0,087	0,70387	11,0	48,5	0,512775	3

Table A4 continued

Sample No	Location	Lat S	Long W	Depth (mbsl)	Age (Ma)	¹⁴⁷ Sm/ ¹⁴⁴ Nd	¹⁴³ Nd/ ¹⁴⁴ Nd _i	eNd	eNd _i	U ppm	Th ppm	Pb ppm	²⁰⁶ Pb/ ²⁰⁴ Pb ±2s.e.	²⁰⁷ Pb/ ²⁰⁴ Pb ±2s.e.	
Marie Byrd Smnts															
PS69/317-1-1	Haxby	69,172	123,424	1983	64,7	0,132	0,51283	4,82	5,36	2,75	1,52	4,79	20,7725	15	15,7739
PS69/317-1-1*	Haxby	69,172	123,424	1983											
PS69/317-1-2	Haxby	69,172	123,424	1983	61,2	0,139	0,51283	4,75	5,19	2,41	0,427	4,60	20,4116	20	15,7561
PS69/321-1-2	Miller	69,359	121,532	1670	56,7	0,120	0,51275	3,12	3,68	3,81	1,75	6,89	20,2467	16	15,7229
PS69/321-1-4	Miller	69,359	121,532	1670	56,9	0,129	0,51276	3,27	3,76	2,44	0,816	4,57	20,1075	6	15,7153
PS69/321-1-5	Miller	69,359	121,532	1670	57,0	0,129	0,51277	3,48	3,97	2,65	0,695	4,43	20,1005	8	15,7160
PS69/321-1-12a	Miller	69,359	121,532	1670	56,9	0,122	0,51277	3,38	3,92	3,37	0,296	7,31	19,9595	8	15,7082
PS69/324-1-3	Miller	69,501	121,006	2622	3,0	0,134	0,51290	5,23	5,25	2,47	0,743	2,99	19,6713	11	15,6140
PS69/324-1-4	Miller	69,501	121,006	2622	3,0	0,129	0,51288	4,73	4,76	0,82	4,72	2,30	18,7063	6	15,6189
PS69/324-1-4*	Miller	69,501	121,006	2622	3,0	0,129	0,51287	4,53	4,55	0,82	4,72	2,30	18,7110	6	15,6184
PS69/324-1-6	Miller	69,501	121,006	2622	3,0	0,137	0,51290	5,09	5,11	1,89	0,982	3,91	19,8645	9	15,6339
PS69/324-1-6*	Miller	69,501	121,006	2622	3,0					1,89	0,982	3,91	19,8661	13	15,6331
PS69/325-1-2a	Miller	69,454	120,932	1560	56,5	0,124	0,51276	3,34	3,87	3,38	1,34	6,93	20,1218	8	15,7193
PS69/325-1-2b	Miller	69,454	120,932	1560	56,5	0,128	0,51277	3,49	3,98	3,21	1,33	7,02	20,0871	8	15,7180
PS69/327-1-1	Smnt C	69,184	117,644	2957	58,7	0,125	0,51286	5,36	5,90	3,07	1,78	5,21	19,8152	10	15,6835
PS69/327-1-2	Smnt C	69,184	117,644	2957	58,7	0,133	0,51287	5,46	5,94	2,24	1,43	5,06	19,8530	8	15,6903
PS69/327-1-2*	Smnt C	69,184	117,644	2957	58,7	0,133	0,51288	5,64	6,11	2,24	1,43	5,06			
De Gerlach Smnts.															
PS-2693-1_(1)**	Belgica	65,305	90,587	800	20,1	0,158	0,51295	6,43	6,53	1,60	0,910	2,30	19,8515	21	15,6878
PS-2693-1_(2)**	Belgica	65,305	90,587	800	23,2	0,154	0,51294	6,40	6,52	1,60	1,10	2,50	19,8376	25	15,6795
PS-2693-1_(3)**	Belgica	65,305	90,587	800	22,6	0,157	0,51294	6,40	6,51	1,60	1,00	2,40	19,8278	32	15,6804
PS-2693-1_(4)**	Belgica	65,305	90,587	800	22,0	0,154	0,51294	6,23	6,35	4,10	0,370	2,70	19,9238	37	15,6834
PS-2693-1_(5)**	Belgica	65,305	90,587	800	22,0								19,7441	25	15,6641
PS-2693-1_(6)**	Belgica	65,305	90,587	800	22,0								19,7447	16	15,6601
Peter I Island															
PS69/244-1-1	NE-Flank	68,741	90,348	1853	1,9	0,139	0,51276	2,36	2,38	2,30	0,887	2,85	19,2360	15	15,7437
PS69/244-1-3	NE-Flank	68,741	90,348	1853	1,7	0,147	0,51275	2,19	2,20	2,26	0,725	2,68	19,2517	6	15,7520
PS69/244-1-5	NE-Flank	68,741	90,348	1853											
PS69/PI-1***	Michajlovodden	68,864	90,426	40m absl	0,23	0,137	0,51280	3,25	3,25	2,26	0,920	3,53	19,3013	12	15,7216
PS69/PI-3	Michajlovodden	68,864	90,426	40m absl	0,23	0,140	0,51278	2,81	2,81	2,46	0,984	3,74	19,3015	7	15,7409
PS69/PI-4	Michajlovodden	68,864	90,426	40m absl	0,23	0,136	0,51277	2,67	2,68	2,31	1,02	3,78	19,3244	7	15,7456

Table A4 continued

Sample No	Location	Lat S	Long W	Depth (mbsl)	Age (Ma)	$^{208}\text{Pb}/^{204}\text{Pb}$	$\pm 2\text{s.e.}$	$^{238}\text{U}/^{204}\text{Pb}$	$^{232}\text{Th}/^{204}\text{Pb}$	$^{206}\text{Pb}/^{204}\text{Pb}_i$	$^{207}\text{Pb}/^{204}\text{Pb}_i$	$^{208}\text{Pb}/^{204}\text{Pb}_i$	Lu ppm	Hf ppm	$^{176}\text{Hf}/^{177}\text{Hf}$	$\pm 2\text{s.e.}$
Marie Byrd Smnts																
PS69/317-1-1	Haxby	69,172	123,424	1983	64,7	40,1472	56	37,1	121	20,40	15,76	39,76	0,450	8,06	0,282871	5
PS69/317-1-1*	Haxby	69,172	123,424	1983												
PS69/317-1-2	Haxby	69,172	123,424	1983	61,2	39,9679	75	11,8	131	20,30	15,75	39,57	0,554	8,35	0,282875	4
PS69/321-1-2	Miller	69,359	121,532	1670	56,7	40,0393	57	30,6	124	19,98	15,71	39,69	0,496	8,83	0,282879	3
PS69/321-1-4	Miller	69,359	121,532	1670	56,9	39,9521	18	22,2	129	19,91	15,71	39,59	0,359	6,36	0,282880	4
PS69/321-1-5	Miller	69,359	121,532	1670	57,0	39,9815	28	17,4	115	19,95	15,71	39,66	0,332	5,94		
PS69/321-1-12a	Miller	69,359	121,532	1670	56,9	39,9274	28	5,82	148	19,91	15,71	39,51	0,366	9,36	0,282875	4
PS69/324-1-3	Miller	69,501	121,006	2622	3,0	39,5216	44	19,7	81,9	19,66	15,61	39,51	0,278	4,30	0,282787	7
PS69/324-1-4	Miller	69,501	121,006	2622	3,0	38,4900	20	22,7	135	18,70	15,62	38,47	0,350	6,35	0,282877	4
PS69/324-1-4*	Miller	69,501	121,006	2622	3,0	38,4973	19	22,7	135	18,70	15,62	38,48				
PS69/324-1-6	Miller	69,501	121,006	2622	3,0	39,7163	27	34,2	141	19,85	15,63	39,70	0,364	5,55	0,283003	4
PS69/324-1-6*	Miller	69,501	121,006	2622	3,0	39,7173	48	34,2	141	19,85	15,63	39,70	0,364	5,55		
PS69/325-1-2a	Miller	69,454	120,932	1560	56,5	39,9100	16	26,3	141	19,89	15,71	39,52	0,515	7,99	0,282862	4
PS69/325-1-2b	Miller	69,454	120,932	1560	56,5	39,8863	17	27,5	150	19,85	15,71	39,47	0,506	8,02		
PS69/327-1-1	Smnt C	69,184	117,644	2957	58,7	39,2970	31	38,0	115	19,47	15,67	38,96	0,674	4,99	0,282927	4
PS69/327-1-2	Smnt C	69,184	117,644	2957	58,7	39,3447	24	42,0	153	19,47	15,67	38,90	0,377	5,37		
PS69/327-1-2*	Smnt C	69,184	117,644	2957	58,7			42,0	153	19,46	15,66	38,87	0,377	5,37		
De Gerlach Smnts.																
PS-2693-1_(1)**	Belgica	65,305	90,587	800	20,1	39,5057	49	37,4	97,6	19,73	15,68	39,41				
PS-2693-1_(2)**	Belgica	65,305	90,587	800	23,2	39,4705	56	45,1	106	19,68	15,67	39,35				
PS-2693-1_(3)**	Belgica	65,305	90,587	800	22,6	39,4777	63	41,0	102	19,69	15,67	39,37				
PS-2693-1_(4)**	Belgica	65,305	90,587	800	22,0	39,4845	81	5,93	44,7	19,90	15,68	39,44				
PS-2693-1_(5)**	Belgica	65,305	90,587	800	22,0	39,3550	69									
PS-2693-1_(6)**	Belgica	65,305	90,587	800	22,0	39,3438	32									
Peter I Island																
PS69/244-1-1	NE-Flank	68,741	90,348	1853	1,9	39,3779	56	25,2	83,5	19,23	15,74	39,37	0,192	5,22	0,282798	3
PS69/244-1-3	NE-Flank	68,741	90,348	1853	1,7	39,4162	19	20,9	79,6	19,25	15,75	39,41	0,193	5,19		
PS69/244-1-5	NE-Flank	68,741	90,348	1853												
PS69/PI-1***	Michajlovodden	68,864	90,426	40m absl	0,23	39,3230	26	26,5	105	19,30	15,72	39,32	0,206	7,03		
PS69/PI-3	Michajlovodden	68,864	90,426	40m absl	0,23	39,3865	15	26,1	102	19,30	15,74	39,39	0,209	7,42		
PS69/PI-4	Michajlovodden	68,864	90,426	40m absl	0,23	39,4265	14	28,9	111	19,32	15,75	39,43	0,203	7,59		

Table A4 continued

Sample No	Location	Lat S	Long W	Depth (mbsl)	Age (Ma)	$^{176}\text{Lu}/^{177}\text{Hf}$	$^{176}\text{Hf}/^{177}\text{Hf}_i$	eHf	eHf _i	SiO ₂ wt%	TiO ₂ wt%	Al ₂ O ₃ wt%	Fe ₂ O ₃ wt%	MnO wt%	MgO wt%	CaO wt%	Na ₂ O wt%
Marie Byrd Smnts																	
PS69/317-1-1	Haxby	69,172	123,424	1983	64,7	0,008	0,28286	3,49	4,61	46,13	3,39	16,33	14,81	0,21	3,46	7,72	3,82
PS69/317-1-1*	Haxby	69,172	123,424	1983													
PS69/317-1-2	Haxby	69,172	123,424	1983	61,2	0,010	0,28286	3,65	4,64	42,03	3,57	18,20	15,91	0,21	3,41	9,02	3,51
PS69/321-1-2	Miller	69,359	121,532	1670	56,7	0,008	0,28287	3,77	4,75	50,22	1,89	17,15	11,49	0,22	2,58	6,39	4,57
PS69/321-1-4	Miller	69,359	121,532	1670	56,9	0,008	0,28287	3,82	4,80	46,23	3,59	17,59	14,19	0,19	2,85	8,84	3,54
PS69/321-1-5	Miller	69,359	121,532	1670	57,0					45,95	3,44	16,62	13,95	0,22	3,96	8,44	3,53
PS69/321-1-12a	Miller	69,359	121,532	1670	56,9	0,006	0,28287	3,65	4,72	50,19	2,09	18,46	11,09	0,17	2,07	6,76	4,53
PS69/324-1-3	Miller	69,501	121,006	2622	3,0	0,009	0,28279	0,53	0,57	45,80	2,60	15,02	13,05	0,19	8,13	10,65	3,29
PS69/324-1-4	Miller	69,501	121,006	2622	3,0	0,008	0,28288	3,72	3,77	52,85	0,85	17,18	8,63	0,18	5,52	8,68	3,99
PS69/324-1-4*	Miller	69,501	121,006	2622	3,0												
PS69/324-1-6	Miller	69,501	121,006	2622	3,0	0,009	0,28300	8,15	8,20	46,74	3,26	14,86	14,73	0,20	4,87	10,31	3,65
PS69/324-1-6*	Miller	69,501	121,006	2622	3,0												
PS69/325-1-2a	Miller	69,454	120,932	1560	56,5	0,009	0,28285	3,18	4,10	47,72	2,52	16,78	11,58	0,14	2,54	7,93	3,88
PS69/325-1-2b	Miller	69,454	120,932	1560	56,5					47,72	2,49	17,24	12,02	0,14	1,34	7,40	4,19
PS69/327-1-1	Smnt C	69,184	117,644	2957	58,7	0,019	0,28291	5,48	6,04	41,98	2,26	18,15	8,92	0,08	0,97	12,84	3,55
PS69/327-1-2	Smnt C	69,184	117,644	2957	58,7					46,00	2,70	20,31	11,30	0,15	1,24	8,73	3,44
PS69/327-1-2*	Smnt C	69,184	117,644	2957	58,7												
De Gerlach Smnts.																	
PS-2693-1_(1)**	Belgica	65,305	90,587	800	20,1												
PS-2693-1_(2)**	Belgica	65,305	90,587	800	23,2												
PS-2693-1_(3)**	Belgica	65,305	90,587	800	22,6												
PS-2693-1_(4)**	Belgica	65,305	90,587	800	22,0												
PS-2693-1_(5)**	Belgica	65,305	90,587	800	22,0												
PS-2693-1_(6)**	Belgica	65,305	90,587	800	22,0												
Peter I Island																	
PS69/244-1-1	NE-Flank	68,741	90,348	1853	1,9	0,005	0,28280	0,91	0,95	49,48	2,79	13,68	12,58	0,14	8,18	9,00	3,17
PS69/244-1-3	NE-Flank	68,741	90,348	1853	1,7					49,09	2,74	13,26	12,55	0,15	9,20	8,68	3,03
PS69/244-1-5	NE-Flank	68,741	90,348	1853						49,26	2,75	13,61	12,85	0,14	8,55	8,91	3,00
PS69/PI-1***	Michajlovodden	68,864	90,426	40m absl	0,23					47,79	3,53	12,79	13,48	0,15	9,64	9,03	3,07
PS69/PI-3	Michajlovodden	68,864	90,426	40m absl	0,23					47,26	3,48	12,52	13,36	0,15	9,86	8,83	3,03
PS69/PI-4	Michajlovodden	68,864	90,426	40m absl	0,23					48,15	3,46	12,73	13,03	0,14	9,42	8,67	3,17

Table A4 continued

Sample No	Location	Lat S	Long W	Depth (mbsl)	Age (Ma)	K ₂ O wt%	P ₂ O ₅ wt%	H ₂ O wt%	CO ₂ wt%	TOTAL wt%	Rb ppm	Ba ppm	Th ppm	U ppm	Nb ppm	Ta ppm	La ppm	Ce ppm	Pb ppm	Pr ppm
Marie Byrd Smnts																				
PS69/317-1-1	Haxby	69,172	123,424	1983	64,7	1,54	0,91	1,91	0,06	100,29	28,1	330	4,79	1,52	70,3	4,21	49,6	106	2,75	13,1
PS69/317-1-1*	Haxby	69,172	123,424	1983							28,1	330	4,72	1,52	70,6	4,18	48,9	106	2,35	13,1
PS69/317-1-2	Haxby	69,172	123,424	1983	61,2	0,74	1,44 [§]	2,38	0,17	100,59	6,7	264	4,60	0,427	68,1	4,27	64,4	114	2,41	14,4
PS69/321-1-2	Miller	69,359	121,532	1670	56,7	2,61	0,73	2,23	0,30	100,38	53,4	725	6,89	1,75	123	6,60	76,8	154	3,81	17,0
PS69/321-1-4	Miller	69,359	121,532	1670	56,9	2,09	0,92	1,80	0,08	101,91	37,3	462	4,57	0,816	78,5	4,59	52,4	106	2,44	12,2
PS69/321-1-5	Miller	69,359	121,532	1670	57,0	2,05	0,79	1,86	0,07	100,88	50,4	493	4,43	0,695	77,2	4,45	51,4	103	2,65	11,6
PS69/321-1-12a	Miller	69,359	121,532	1670	56,9	2,15	0,87	2,10	0,07	100,55	23,9	784	7,31	0,296	119	6,97	65,9	146	3,37	16,1
PS69/324-1-3	Miller	69,501	121,006	2622	3,0	1,04	0,48	0,74	0,13	101,12	24,1	311	2,99	0,743	46,0	2,78	32,1	66,2	2,47	7,74
PS69/324-1-4	Miller	69,501	121,006	2622	3,0	1,45	0,21	0,98	0,07	100,59	35,8	455	4,72	0,819	78,5	4,60	53,1	107	2,30	12,3
PS69/324-1-4*	Miller	69,501	121,006	2622	3,0															
PS69/324-1-6	Miller	69,501	121,006	2622	3,0	1,24	0,54	0,82	0,08	101,30	28,0	320	3,91	0,982	56,6	3,39	38,3	78,4	1,89	8,98
PS69/324-1-6*	Miller	69,501	121,006	2622	3,0															
PS69/325-1-2a	Miller	69,454	120,932	1560	56,5	2,74	1,69 [§]	2,12	0,59	100,23	90,1	469	6,93	1,34	95,6	5,38	73,5	141	3,38	16,3
PS69/325-1-2b	Miller	69,454	120,932	1560	56,5	3,24	2,12 [§]	2,13	0,18	100,21	57,3	480	7,02	1,33	96,8	5,44	73,8	144	3,21	16,3
PS69/327-1-1	Smnt C	69,184	117,644	2957	58,7	1,74	5,02 [§]	2,92	0,56	98,99	27,2	404	5,21	1,78	55,6	3,48	66,2	80,4	3,07	10,4
PS69/327-1-2	Smnt C	69,184	117,644	2957	58,7	1,38	1,62 [§]	3,03	0,24	100,14	21,5	427	5,06	1,43	58,7	3,58	44,6	84,5	2,24	9,36
PS69/327-1-2*	Smnt C	69,184	117,644	2957	58,7															
De Gerlach Smnts.																				
PS-2693-1_(1)**	Belgica	65,305	90,587	800	20,1															
PS-2693-1_(2)**	Belgica	65,305	90,587	800	23,2															
PS-2693-1_(3)**	Belgica	65,305	90,587	800	22,6															
PS-2693-1_(4)**	Belgica	65,305	90,587	800	22,0															
PS-2693-1_(5)**	Belgica	65,305	90,587	800	22,0															
PS-2693-1_(6)**	Belgica	65,305	90,587	800	22,0															
Peter I Island																				
PS69/244-1-1	NE-Flank	68,741	90,348	1853	1,9	1,16	0,50	0,86	0,05	101,59	20,3	240	2,85	0,887	30,2	1,88	27,2	58,5	2,30	7,49
PS69/244-1-3	NE-Flank	68,741	90,348	1853	1,7	1,08	0,51	0,87	0,05	101,21	19,8	228	2,68	0,725	29,4	1,83	26,7	57,1	2,26	7,20
PS69/244-1-5	NE-Flank	68,741	90,348	1853		1,15	0,48	0,94	0,06	101,70	19,2	226	2,57	0,704	28,9	1,76	26,1	55,6	2,22	6,95
PS69/PI-1***	Michajlovodden	68,864	90,426	40m absl	0,23	1,37	0,64	0,28	0,04	101,81	23,9	308	3,53	0,920	48,5	2,82	38,0	80,9	2,26	10,2
PS69/PI-3	Michajlovodden	68,864	90,426	40m absl	0,23	1,42	0,69	0,45	0,04	101,09	26,5	315	3,74	0,984	48,7	2,89	40,3	85,2	2,46	10,4
PS69/PI-4	Michajlovodden	68,864	90,426	40m absl	0,23	1,47	0,78	0,38	0,04	101,44	26,3	332	3,78	1,02	50,6	2,90	43,1	92,4	2,31	11,4

Table A4 continued

Sample No	Location	Lat S	Long W	Depth (mbsl)	Age (Ma)	Nd ppm	Sr ppm	Sm ppm	Hf ppm	Zr ppm	Eu ppm	Gd ppm	Tb ppm	Dy ppm	Ho ppm	Y ppm	Er ppm	Tm ppm	Yb ppm	Lu ppm
Marie Byrd Smnts																				
PS69/317-1-1	Haxby	69,172	123,424	1983	64,7	55,6	760	12,1	8,06	404	3,79	10,8	1,45	7,98	1,43	42,3	3,59	0,457	3,13	0,450
PS69/317-1-1*	Haxby	69,172	123,424	1983		55,2	756	12,1	8,02	402	3,75	10,7	1,47	7,89	1,46	42,0	3,72	0,479	3,14	0,447
PS69/317-1-2	Haxby	69,172	123,424	1983	61,2	57,6	1219	13,3	8,35	413	4,14	11,4	1,56	8,36	1,54	51,6	3,84	0,475	3,84	0,554
PS69/321-1-2	Miller	69,359	121,532	1670	56,7	63,2	825	12,6	8,83	475	3,92	10,2	1,40	7,50	1,33	43,6	3,47	0,455	3,54	0,496
PS69/321-1-4	Miller	69,359	121,532	1670	56,9	46,0	969	9,86	6,36	323	3,09	8,00	1,05	5,40	0,970	32,5	2,49	0,310	2,57	0,359
PS69/321-1-5	Miller	69,359	121,532	1670	57,0	44,3	925	9,49	5,94	317	2,91	7,45	0,979	5,04	0,920	31,5	2,31	0,291	2,45	0,332
PS69/321-1-12a	Miller	69,359	121,532	1670	56,9	61,6	891	12,5	9,36	446	4,12	9,66	1,29	6,58	1,14	35,5	2,79	0,345	2,76	0,366
PS69/324-1-3	Miller	69,501	121,006	2622	3,0	30,1	626	6,69	4,30	205	2,19	5,89	0,814	4,38	0,787	25,2	2,07	0,261	2,08	0,278
PS69/324-1-4	Miller	69,501	121,006	2622	3,0	46,5	967	10,0	6,35	321	3,04	8,10	1,02	5,49	0,971	31,6	2,50	0,325	2,49	0,350
PS69/324-1-4*	Miller	69,501	121,006	2622	3,0															
PS69/324-1-6	Miller	69,501	121,006	2622	3,0	35,5	568	8,08	5,55	261	2,49	7,17	1,02	5,74	1,02	31,8	2,66	0,350	2,65	0,364
PS69/324-1-6*	Miller	69,501	121,006	2622	3,0															
PS69/325-1-2a	Miller	69,454	120,932	1560	56,5	62,4	674	12,9	7,99	412	3,59	10,9	1,48	7,39	1,35	48,7	3,50	0,458	3,63	0,515
PS69/325-1-2b	Miller	69,454	120,932	1560	56,5	62,3	717	13,3	8,02	417	3,56	10,9	1,41	7,51	1,36	46,1	3,52	0,449	3,54	0,506
PS69/327-1-1	Smnt C	69,184	117,644	2957	58,7	39,0	811	8,09	4,99	250	2,45	7,78	1,07	6,32	1,33	66,5	3,71	0,509	4,21	0,674
PS69/327-1-2	Smnt C	69,184	117,644	2957	58,7	35,6	843	7,89	5,37	258	2,49	6,87	0,957	5,30	0,979	32,0	2,70	0,349	2,72	0,377
PS69/327-1-2*	Smnt C	69,184	117,644	2957	58,7															
De Gerlach Smnts.																				
PS-2693-1_(1)**	Belgica	65,305	90,587	800	20,1															
PS-2693-1_(2)**	Belgica	65,305	90,587	800	23,2															
PS-2693-1_(3)**	Belgica	65,305	90,587	800	22,6															
PS-2693-1_(4)**	Belgica	65,305	90,587	800	22,0															
PS-2693-1_(5)**	Belgica	65,305	90,587	800	22,0															
PS-2693-1_(6)**	Belgica	65,305	90,587	800	22,0															
Peter I Island																				
PS69/244-1-1	NE-Flank	68,741	90,348	1853	1,9	32,7	624	7,57	5,22	233	2,43	6,78	0,874	4,69	0,792	22,5	1,83	0,226	1,53	0,192
PS69/244-1-3	NE-Flank	68,741	90,348	1853	1,7	30,8	622	7,54	5,19	230	2,48	6,55	0,882	4,54	0,737	21,6	1,72	0,207	1,50	0,193
PS69/244-1-5	NE-Flank	68,741	90,348	1853		29,2	632	7,48	5,03	227	2,39	6,38	0,854	4,40	0,706	21,6	1,73	0,204	1,49	0,186
PS69/PI-1***	Michajlovodden	68,864	90,426	40m absl	0,23	43,1	797	9,80	7,03	315	3,14	8,50	1,14	5,70	0,924	24,9	2,14	0,255	1,58	0,206
PS69/PI-3	Michajlovodden	68,864	90,426	40m absl	0,23	43,6	804	10,2	7,42	326	3,21	8,63	1,13	5,52	0,894	24,9	2,05	0,246	1,54	0,209
PS69/PI-4	Michajlovodden	68,864	90,426	40m absl	0,23	48,5	871	11,0	7,59	344	3,52	9,61	1,19	5,85	0,963	25,7	2,14	0,256	1,56	0,203

* Replicate analysis

**⁸⁷Sr/⁸⁶Sr determined on MAT262 TIMS

*** without Pb-DS

±2s.e. refers to the last significant digits

Age and trace element concentration data for the De Gerlach Smnts. from Hagedorn et al. (2007)

Ages for subaerial samples from Peter I Island inferred from Prestvik et al. (1991)

Ages in Italics are Smnt averages or inferred from dated samples of the same dredge

§ Results with unusual high values not shown in Fig. 6

Appendix II CHAPTER II

Table S1: 40Ar/39Ar laser step-heating analysis data

277-1 biotite (analysis 277-1bts)

Mass =	1.505 mg									
J =	3,70E-03	±	3,56E-06	(2 Sigma)						
Step	Laser power (W)	40Ar/39Ar	37Ar/39Ar	36Ar/39Ar	Mol 39ArK	Ca/K	% 40ArA	Cum 39ArK	Age [Ma]	2 Sigma
1	5,00E-02	3,56E+03	-1,44E-01	1,12E+01	1,87E-16	-2,83E-01	9,29E+01	4,38E-04	1,19E+03	6,62E+01
2	1,00E-01	1,22E+03	-6,02E-02	3,82E+00	1,88E-16	-1,18E-01	9,30E+01	8,78E-04	4,96E+02	7,17E+01
3	1,50E-01	4,68E+02	4,72E-02	1,54E+00	2,17E-15	9,25E-02	9,76E+01	5,97E-03	7,44E+01	1,72E+01
4	2,00E-01	1,12E+02	2,29E-02	3,36E-01	5,06E-15	4,49E-02	8,86E+01	1,78E-02	8,35E+01	5,95E+00
5	2,50E-01	5,26E+01	9,30E-03	1,29E-01	1,09E-14	1,82E-02	7,27E+01	4,34E-02	9,34E+01	2,72E+00
6	3,00E-01	3,98E+01	8,23E-03	8,57E-02	1,46E-14	1,61E-02	6,36E+01	7,77E-02	9,44E+01	1,44E+00
7	4,00E-01	3,46E+01	8,29E-03	6,71E-02	3,22E-14	1,63E-02	5,73E+01	1,53E-01	9,62E+01	1,33E+00
8	5,00E-01	2,35E+01	5,79E-03	2,91E-02	5,14E-14	1,13E-02	3,66E+01	2,74E-01	9,71E+01	5,57E-01
9	6,00E-01	2,02E+01	6,82E-03	1,76E-02	6,22E-14	1,34E-02	2,58E+01	4,20E-01	9,75E+01	5,75E-01
10	7,00E-01	1,82E+01	7,38E-03	1,07E-02	6,33E-14	1,45E-02	1,73E+01	5,68E-01	9,81E+01	5,35E-01
11	8,00E-01	1,72E+01	8,63E-03	7,03E-03	5,37E-14	1,69E-02	1,21E+01	6,94E-01	9,83E+01	4,65E-01
12	9,00E-01	1,71E+01	1,12E-02	6,76E-03	3,47E-14	2,19E-02	1,17E+01	7,75E-01	9,84E+01	7,67E-01
13	1,00E+00	1,72E+01	1,46E-02	6,95E-03	2,66E-14	2,86E-02	1,19E+01	8,38E-01	9,85E+01	8,47E-01
14	1,10E+00	1,74E+01	1,86E-02	7,56E-03	1,54E-14	3,64E-02	1,28E+01	8,74E-01	9,88E+01	1,18E+00
15	1,20E+00	1,70E+01	1,90E-02	6,14E-03	1,22E-14	3,72E-02	1,07E+01	9,03E-01	9,86E+01	1,39E+00
16	1,50E+00	1,70E+01	2,37E-02	6,38E-03	1,48E-14	4,65E-02	1,11E+01	9,37E-01	9,84E+01	8,81E-01
17	3,00E+00	1,71E+01	1,12E-02	6,40E-03	1,97E-14	2,20E-02	1,11E+01	9,84E-01	9,89E+01	9,29E-01
18	5,00E+00	1,72E+01	1,81E-02	6,69E-03	4,40E-15	3,54E-02	1,15E+01	9,94E-01	9,86E+01	2,43E+00
19	1,00E+01	1,67E+01	2,38E-02	5,02E-03	2,34E-15	4,67E-02	8,87E+00	9,99E-01	9,88E+01	3,59E+00
20	1,50E+01	2,48E+01	-6,49E-02	1,99E-02	2,76E-16	-1,27E-01	2,37E+01	1,00E+00	1,22E+02	3,86E+01

Total Gas Age = 9,80E+01 ± 2,10E-01 Ma (2Sigma)
 Plateau age = 98.38 ± 0.27 Ma (2s, including J-error of .096%)
 MSWD = 0.50, probability = 0.89
 58% of the 39Ar, steps 10 through 20

Table S1 continued

277-1 biotite (analysis 277-1bt2)

Mass = 1.025 mg
J = 3,70E-03 ± 3,56E-06 (2 Sigma)

Step	Laser power (W)	40Ar/39Ar	37Ar/39Ar	36Ar/39Ar	Mol 39ArK	Ca/K	% 40ArA	Cum 39ArK	Age [Ma]	2 Sigma
1	5,00E-02	5,44E+03	4,65E+00	1,71E+01	6,12E-17	9,16E+00	9,27E+01	2,27E-04	1,64E+03	1,53E+02
2	1,00E-01	2,12E+03	7,19E-01	7,17E+00	5,40E-16	1,41E+00	1,00E+02	2,23E-03	1,93E+00	3,68E+01
3	1,50E-01	8,79E+02	4,29E-01	2,95E+00	4,90E-16	8,42E-01	9,91E+01	4,04E-03	5,03E+01	4,59E+01
4	2,00E-01	5,35E+02	3,78E-01	1,78E+00	8,65E-16	7,41E-01	9,81E+01	7,24E-03	6,83E+01	1,95E+01
5	2,50E-01	1,62E+02	1,20E-01	5,04E-01	2,52E-15	2,36E-01	9,20E+01	1,66E-02	8,46E+01	8,80E+00
6	3,00E-01	8,40E+01	7,68E-02	2,37E-01	4,98E-15	1,50E-01	8,33E+01	3,50E-02	9,16E+01	6,35E+00
7	4,00E-01	6,99E+01	2,23E-02	1,87E-01	1,08E-14	4,37E-02	7,89E+01	7,48E-02	9,62E+01	1,89E+00
8	5,00E-01	4,14E+01	1,72E-02	8,90E-02	1,57E-14	3,37E-02	6,36E+01	1,33E-01	9,79E+01	2,39E+00
9	6,00E-01	3,47E+01	2,19E-02	6,76E-02	2,20E-14	4,30E-02	5,75E+01	2,14E-01	9,60E+01	1,52E+00
10	7,00E-01	2,78E+01	2,16E-02	4,37E-02	2,71E-14	4,24E-02	4,63E+01	3,15E-01	9,71E+01	1,31E+00
11	8,00E-01	2,48E+01	1,04E-02	3,34E-02	2,80E-14	2,03E-02	3,98E+01	4,18E-01	9,73E+01	9,89E-01
12	9,00E-01	2,16E+01	3,41E-03	2,20E-02	2,94E-14	6,69E-03	3,01E+01	5,27E-01	9,80E+01	8,42E-01
13	1,00E+00	1,87E+01	2,38E-02	1,21E-02	3,29E-14	4,66E-02	1,91E+01	6,49E-01	9,83E+01	9,05E-01
14	1,10E+00	1,79E+01	3,79E-02	9,46E-03	2,65E-14	7,42E-02	1,56E+01	7,47E-01	9,82E+01	8,81E-01
15	1,20E+00	1,76E+01	4,22E-02	8,21E-03	1,99E-14	8,26E-02	1,38E+01	8,21E-01	9,84E+01	9,58E-01
16	1,50E+00	1,74E+01	5,39E-02	7,68E-03	2,58E-14	1,06E-01	1,30E+01	9,16E-01	9,84E+01	7,92E-01
17	3,00E+00	1,75E+01	1,03E-01	7,87E-03	1,74E-14	2,03E-01	1,32E+01	9,81E-01	9,85E+01	1,15E+00
18	5,00E+00	1,76E+01	-5,58E-05	8,62E-03	4,81E-15	-1,09E-04	1,45E+01	9,98E-01	9,79E+01	2,18E+00
19	1,00E+01	1,60E+01	-7,78E-01	-7,54E-05	4,14E-16	-1,52E+00	4,93E-01	1,00E+00	1,03E+02	2,28E+01

Total Gas Age
= 9,75E+01 ± 3,15E-01 Ma
(2Sigma)

Plateau age = 98.27±0.38 Ma (2s, including J-error of .096%)

MSWD = 0.15, probability = 0.99

58% of the 39Ar, steps 12 through 18

Table S1 continued

277-7 biotite (analysis 277-7bts)

Mass = 1.438 mg
J = 3,70E-03 ± 3,56E-06 (2 Sigma)

Step	Laser power (W)	40Ar/39Ar	37Ar/39Ar	36Ar/39Ar	Mol 39ArK	Ca/K	% 40ArA	Cum 39ArK	Age [Ma]	2 Sigma
1	5,00E-02	1,02E+04	2,97E-04	3,20E+01	1,13E-16	5,82E-04	9,31E+01	4,11E-04	2,30E+03	1,98E+02
2	1,00E-01	2,84E+03	-2,98E-01	8,85E+00	7,58E-17	-5,83E-01	9,20E+01	6,86E-04	1,10E+03	1,90E+02
3	1,50E-01	7,38E+02	2,95E-02	2,45E+00	1,39E-15	5,78E-02	9,81E+01	5,74E-03	9,20E+01	2,97E+01
4	2,00E-01	1,68E+02	2,14E-02	5,20E-01	4,41E-15	4,20E-02	9,14E+01	2,18E-02	9,36E+01	7,38E+00
5	2,50E-01	7,31E+01	1,21E-02	1,98E-01	1,03E-14	2,38E-02	8,01E+01	5,93E-02	9,44E+01	3,15E+00
6	3,00E-01	4,62E+01	8,60E-03	1,07E-01	1,68E-14	1,69E-02	6,82E+01	1,20E-01	9,55E+01	1,59E+00
7	4,00E-01	3,63E+01	5,52E-02	6,98E-02	3,90E-15	1,08E-01	5,68E+01	1,35E-01	1,02E+02	1,99E+00
8	5,00E-01	2,48E+01	7,08E-02	3,12E-02	1,13E-14	1,39E-01	3,71E+01	1,76E-01	1,01E+02	9,87E-01
9	6,00E-01	2,02E+01	4,27E-02	1,74E-02	5,75E-14	8,37E-02	2,55E+01	3,84E-01	9,76E+01	6,96E-01
10	7,00E-01	1,91E+01	2,01E-02	1,36E-02	4,63E-14	3,94E-02	2,10E+01	5,52E-01	9,79E+01	9,80E-01
11	8,00E-01	1,88E+01	1,75E-02	1,24E-02	3,06E-14	3,44E-02	1,95E+01	6,64E-01	9,84E+01	1,04E+00
12	9,00E-01	1,90E+01	1,57E-02	1,33E-02	2,04E-14	3,07E-02	2,08E+01	7,38E-01	9,76E+01	1,55E+00
13	1,00E+00	1,85E+01	1,33E-02	1,15E-02	1,28E-14	2,60E-02	1,83E+01	7,84E-01	9,81E+01	2,16E+00
14	1,10E+00	1,83E+01	1,40E-02	1,13E-02	8,22E-15	2,74E-02	1,82E+01	8,14E-01	9,75E+01	2,87E+00
15	1,20E+00	1,86E+01	9,93E-03	1,21E-02	7,92E-15	1,95E-02	1,92E+01	8,43E-01	9,77E+01	2,87E+00
16	1,50E+00	1,88E+01	4,12E-02	1,25E-02	1,05E-14	8,08E-02	1,97E+01	8,81E-01	9,80E+01	1,44E+00
17	3,00E+00	1,87E+01	6,70E-02	1,22E-02	2,21E-14	1,31E-01	1,92E+01	9,61E-01	9,80E+01	9,00E-01
18	5,00E+00	1,79E+01	1,36E-01	9,82E-03	5,41E-15	2,66E-01	1,61E+01	9,81E-01	9,76E+01	3,24E+00
19	1,00E+01	1,74E+01	2,30E-02	8,04E-03	4,83E-15	4,50E-02	1,36E+01	9,99E-01	9,78E+01	2,69E+00
20	1,50E+01	2,23E+01	-8,41E-03	1,60E-02	4,09E-16	-1,65E-02	2,13E+01	1,00E+00	1,13E+02	3,48E+01

Total Gas Age = 9,89E+01 ± 3,40E-01 Ma (2Sigma)

Plateau age = 97.88±0.39 Ma (2s, including J-error of .096%)

MSWD = 0.24, probability = 0.995

82.4% of the 39Ar, steps 9 through 20

Table S1 continue

LI-1 plagioclase (analysis LI1fss)

Mass = 1.718 mg
J = 3,70E-03 ± 3,56E-06 (2 Sigma)

Step	Laser power (W)	40Ar/39Ar	37Ar/39Ar	36Ar/39Ar	Mol 39ArK	Ca/K	% 40ArA	Cum 39ArK	Age [Ma]	2 Sigma
1	1,25E-01	4,24E+03	3,03E+00	1,42E+01	3,44E-17	5,95E+00	9,92E+01	6,12E-04	2,10E+02	2,81E+02
2	2,00E-01	1,30E+03	2,04E+00	4,32E+00	1,21E-16	4,01E+00	9,78E+01	2,76E-03	1,79E+02	8,67E+01
3	3,00E-01	3,32E+02	2,39E+00	1,06E+00	4,09E-16	4,70E+00	9,47E+01	1,00E-02	1,15E+02	2,97E+01
4	4,00E-01	1,33E+02	2,59E+00	4,03E-01	7,92E-16	5,08E+00	8,93E+01	2,41E-02	9,33E+01	1,18E+01
5	5,00E-01	8,59E+01	2,33E+00	2,39E-01	1,28E-15	4,57E+00	8,19E+01	4,70E-02	1,02E+02	8,36E+00
6	6,00E-01	4,87E+01	2,36E+00	1,15E-01	1,71E-15	4,63E+00	6,94E+01	7,73E-02	9,72E+01	3,44E+00
7	7,00E-01	3,09E+01	2,36E+00	5,48E-02	1,89E-15	4,63E+00	5,14E+01	1,11E-01	9,79E+01	4,58E+00
8	8,00E-01	2,29E+01	2,32E+00	2,67E-02	1,97E-15	4,56E+00	3,32E+01	1,46E-01	9,94E+01	1,88E+00
9	1,00E+00	2,40E+01	2,11E+00	3,25E-02	3,43E-15	4,14E+00	3,88E+01	2,07E-01	9,57E+01	1,72E+00
10	1,20E+00	2,27E+01	2,14E+00	2,76E-02	3,01E-15	4,19E+00	3,48E+01	2,60E-01	9,65E+01	2,36E+00
11	1,35E+00	2,47E+01	2,23E+00	3,44E-02	2,66E-15	4,39E+00	4,00E+01	3,08E-01	9,64E+01	3,18E+00
12	1,50E+00	2,52E+01	2,26E+00	3,58E-02	1,94E-15	4,44E+00	4,07E+01	3,42E-01	9,75E+01	3,79E+00
13	2,00E+00	2,89E+01	2,36E+00	4,86E-02	4,43E-15	4,63E+00	4,86E+01	4,21E-01	9,67E+01	1,71E+00
14	3,00E+00	3,10E+01	3,10E+00	5,59E-02	1,13E-14	6,09E+00	5,20E+01	6,22E-01	9,70E+01	1,57E+00
15	4,00E+00	2,42E+01	2,97E+00	3,29E-02	1,64E-14	5,84E+00	3,85E+01	9,14E-01	9,72E+01	6,25E-01
16	6,00E+00	2,25E+01	3,08E+00	2,73E-02	3,12E-15	6,06E+00	3,40E+01	9,69E-01	9,70E+01	2,17E+00
17	8,00E+00	2,10E+01	3,20E+00	2,19E-02	9,77E-16	6,29E+00	2,88E+01	9,87E-01	9,74E+01	5,58E+00
18	1,00E+01	2,13E+01	3,14E+00	1,71E-02	3,43E-16	6,18E+00	2,18E+01	9,93E-01	1,08E+02	1,61E+01
19	1,20E+01	2,32E+01	3,04E+00	2,05E-02	1,17E-16	5,97E+00	2,45E+01	9,95E-01	1,14E+02	4,10E+01
20	1,50E+01	2,17E+01	3,36E+00	1,78E-02	2,80E-16	6,60E+00	2,22E+01	1,00E+00	1,10E+02	2,34E+01

Total Gas Age = 9,76E+01 ± 4,62E-01 Ma (2Sigma)

Plateau age = 97.11±0.48 Ma (2s, including J-error of .096%)

MSWD = 1.08, probability = 0.37

87.6% of the 39Ar, steps 8 through 17

Table S1 continued

LI-2 plagioclase (analysis LI2fs2)

Mass = 2.049 mg
J = 3,70E-03 ± 3,56E-06 (2 Sigma)

Step	Laser power (W)	40Ar/39Ar	37Ar/39Ar	36Ar/39Ar	Mol 39ArK	Ca/K	% 40ArA	Cum 39ArK	Age [Ma]	2 Sigma
1	1,25E-01	1,51E+03	7,93E-01	5,03E+00	4,26E-17	1,56E+00	9,84E+01	9,06E-04	1,51E+02	2,27E+02
2	2,00E-01	9,44E+02	3,80E+00	3,16E+00	1,51E-16	7,48E+00	9,88E+01	4,11E-03	7,40E+01	9,90E+01
3	3,00E-01	3,66E+02	3,38E+00	1,20E+00	4,63E-16	6,65E+00	9,71E+01	1,40E-02	7,02E+01	1,52E+01
4	4,00E-01	1,57E+02	3,48E+00	4,86E-01	9,48E-16	6,85E+00	9,14E+01	3,41E-02	8,83E+01	1,58E+01
5	5,00E-01	7,01E+01	3,59E+00	1,89E-01	1,72E-15	7,06E+00	7,89E+01	7,06E-02	9,64E+01	5,53E+00
6	6,00E-01	3,87E+01	3,34E+00	8,31E-02	2,23E-15	6,56E+00	6,25E+01	1,18E-01	9,47E+01	3,98E+00
7	7,00E-01	2,57E+01	3,39E+00	3,96E-02	2,39E-15	6,67E+00	4,37E+01	1,69E-01	9,45E+01	2,93E+00
8	8,00E-01	3,33E+01	3,51E+00	6,38E-02	2,33E-15	6,91E+00	5,52E+01	2,18E-01	9,74E+01	3,74E+00
9	1,00E+00	3,32E+01	3,35E+00	6,41E-02	3,45E-15	6,59E+00	5,57E+01	2,92E-01	9,60E+01	2,64E+00
10	1,20E+00	3,89E+01	3,31E+00	8,40E-02	3,52E-15	6,50E+00	6,27E+01	3,67E-01	9,46E+01	2,39E+00
11	1,35E+00	3,80E+01	3,15E+00	7,87E-02	3,28E-15	6,20E+00	6,02E+01	4,36E-01	9,85E+01	1,78E+00
12	1,50E+00	3,22E+01	3,05E+00	5,93E-02	2,76E-15	6,00E+00	5,32E+01	4,95E-01	9,81E+01	2,53E+00
13	2,00E+00	3,70E+01	3,25E+00	7,59E-02	4,31E-15	6,39E+00	5,94E+01	5,87E-01	9,80E+01	3,29E+00
14	3,00E+00	2,92E+01	3,57E+00	5,00E-02	5,51E-15	7,03E+00	4,91E+01	7,04E-01	9,70E+01	2,00E+00
15	4,00E+00	2,52E+01	3,27E+00	3,48E-02	2,45E-15	6,43E+00	3,92E+01	7,56E-01	9,99E+01	2,73E+00
16	6,00E+00	2,55E+01	3,83E+00	3,78E-02	6,34E-15	7,54E+00	4,20E+01	8,91E-01	9,64E+01	1,80E+00
17	8,00E+00	2,96E+01	2,84E+00	5,13E-02	4,18E-16	5,59E+00	4,99E+01	8,99E-01	9,67E+01	1,46E+01
18	1,00E+01	2,37E+01	4,05E+00	3,15E-02	4,28E-15	7,96E+00	3,70E+01	9,90E-01	9,77E+01	2,21E+00
19	1,50E+01	2,08E+01	4,04E+00	1,51E-02	4,47E-16	7,94E+00	1,90E+01	1,00E+00	1,09E+02	9,55E+00

Total Gas Age = 9,66E+01 ± 6,93E-01 Ma (2Sigma)
Plateau age = 97.05±0.71 Ma (2s, including J-error of .096%)
MSWD = 1.5, probability = 0.12
92% of the 39Ar, steps 6 through 18

Table S1 continued

DR193.1 plagioclase

Mass = 1.788 mg
J = 3,83E-03 ± 5,61E-06 (2 Sigma)

Step	Laser power (W)	40Ar/39Ar	37Ar/39Ar	36Ar/39Ar	Mol 39ArK	Ca/K	% 40ArA	Cum 39ArK	Age [Ma]	2 Sigma
1	1,25E-01	2,00E+02	7,19E-01	4,85E-01	1,77E-17	1,41E+00	7,15E+01	3,90E-04	3,56E+02	9,60E+01
2	2,00E-01	5,86E+02	1,01E+00	1,87E+00	3,86E-17	1,98E+00	9,45E+01	1,24E-03	2,09E+02	6,08E+01
3	3,00E-01	4,38E+02	6,30E-01	1,40E+00	1,79E-16	1,24E+00	9,43E+01	5,18E-03	1,65E+02	1,71E+01
4	4,00E-01	1,46E+02	4,97E-01	4,35E-01	3,88E-16	9,75E-01	8,81E+01	1,37E-02	1,16E+02	8,15E+00
5	5,00E-01	8,73E+01	6,00E-01	2,41E-01	6,60E-16	1,18E+00	8,14E+01	2,83E-02	1,09E+02	4,08E+00
6	6,00E-01	8,48E+01	9,05E-01	2,35E-01	7,92E-16	1,77E+00	8,16E+01	4,57E-02	1,05E+02	6,48E+00
7	7,00E-01	6,54E+01	1,02E+00	1,69E-01	9,06E-16	1,99E+00	7,60E+01	6,57E-02	1,05E+02	3,96E+00
8	8,00E-01	3,64E+01	1,18E+00	7,29E-02	8,80E-16	2,31E+00	5,87E+01	8,51E-02	1,01E+02	3,79E+00
9	1,00E+00	3,80E+01	1,22E+00	7,69E-02	1,70E-15	2,39E+00	5,94E+01	1,22E-01	1,04E+02	8,61E-01
10	1,20E+00	2,47E+01	1,31E+00	3,29E-02	1,45E-15	2,58E+00	3,87E+01	1,54E-01	1,02E+02	1,79E+00
11	1,35E+00	1,86E+01	1,29E+00	1,31E-02	1,09E-15	2,53E+00	1,99E+01	1,78E-01	1,00E+02	1,71E+00
12	1,50E+00	1,80E+01	1,15E+00	1,02E-02	9,33E-16	2,26E+00	1,59E+01	1,99E-01	1,02E+02	1,70E+00
13	2,00E+00	2,69E+01	8,24E-01	3,94E-02	2,74E-15	1,62E+00	4,30E+01	2,59E-01	1,03E+02	1,02E+00
14	3,00E+00	2,87E+01	9,57E-01	4,60E-02	3,68E-15	1,88E+00	4,69E+01	3,40E-01	1,03E+02	8,51E-01
15	4,00E+00	2,61E+01	1,10E+00	3,63E-02	1,53E-15	2,16E+00	4,06E+01	3,74E-01	1,04E+02	1,41E+00
16	6,00E+00	2,21E+01	1,06E+00	2,29E-02	8,15E-15	2,09E+00	3,01E+01	5,54E-01	1,04E+02	4,32E-01
17	8,00E+00	1,86E+01	7,99E-01	1,14E-02	8,28E-15	1,57E+00	1,75E+01	7,36E-01	1,03E+02	4,87E-01
18	1,20E+01	1,87E+01	6,87E-01	1,16E-02	6,55E-15	1,35E+00	1,79E+01	8,81E-01	1,03E+02	5,98E-01
19	1,50E+01	1,74E+01	5,30E-01	6,93E-03	5,41E-15	1,04E+00	1,14E+01	1,00E+00	1,04E+02	4,06E-01

Total Gas Age = 1,04E+02 ± 2,05E-01 Ma (2Sigma)

Plateau age = 103.51±0.28 Ma (2s, including J-error of .147%)

MSWD = 1.8, probability = 0.13

66% of the 39Ar, steps 15 through 19

Table S1 continued

LI-3 K-feldspar (analysis LI3fss)

Mass = 1.532 mg
J = 3,70E-03 ± 3,56E-06 (2 Sigma)

Step	Laser power (W)	40Ar/39Ar	37Ar/39Ar	36Ar/39Ar	Mol 39ArK	Ca/K	% 40ArA	Cum 39ArK	Age [Ma]	2 Sigma
1	1,25E-01	1,77E+03	1,08E+00	5,90E+00	5,07E-17	2,13E+00	9,86E+01	1,77E-03	1,58E+02	1,41E+02
2	2,00E-01	5,53E+02	8,68E-01	1,83E+00	6,71E-17	1,70E+00	9,80E+01	4,10E-03	7,15E+01	1,16E+02
3	3,00E-01	2,11E+02	3,34E-01	6,44E-01	3,39E-16	6,55E-01	9,02E+01	1,59E-02	1,33E+02	2,75E+01
4	4,00E-01	5,80E+01	9,28E-02	1,45E-01	8,07E-16	1,82E-01	7,37E+01	4,40E-02	9,90E+01	9,99E+00
5	5,00E-01	4,43E+01	1,08E-01	9,80E-02	1,04E-15	2,11E-01	6,53E+01	8,01E-02	9,99E+01	6,23E+00
6	6,00E-01	2,87E+01	1,19E-01	4,66E-02	1,05E-15	2,33E-01	4,80E+01	1,17E-01	9,68E+01	6,93E+00
7	7,00E-01	2,77E+01	1,31E-01	4,39E-02	1,08E-15	2,57E-01	4,67E+01	1,54E-01	9,61E+01	5,39E+00
8	8,00E-01	2,25E+01	9,60E-02	2,62E-02	1,12E-15	1,88E-01	3,43E+01	1,93E-01	9,61E+01	5,99E+00
9	1,00E+00	2,09E+01	1,24E-01	2,14E-02	2,00E-15	2,43E-01	3,02E+01	2,63E-01	9,49E+01	2,86E+00
10	1,20E+00	1,85E+01	8,62E-02	1,43E-02	1,74E-15	1,69E-01	2,28E+01	3,24E-01	9,29E+01	4,03E+00
11	1,35E+00	1,90E+01	8,55E-02	1,50E-02	1,43E-15	1,68E-01	2,33E+01	3,73E-01	9,47E+01	3,34E+00
12	1,50E+00	2,00E+01	5,62E-02	1,87E-02	1,56E-15	1,10E-01	2,77E+01	4,28E-01	9,41E+01	3,83E+00
13	2,00E+00	1,89E+01	3,36E-02	1,47E-02	4,28E-15	6,59E-02	2,30E+01	5,77E-01	9,48E+01	1,27E+00
14	3,00E+00	1,85E+01	1,86E-02	1,33E-02	4,81E-15	3,64E-02	2,12E+01	7,44E-01	9,49E+01	1,12E+00
15	4,00E+00	1,78E+01	1,70E-02	9,48E-03	3,20E-15	3,33E-02	1,58E+01	8,55E-01	9,72E+01	1,66E+00
16	6,00E+00	2,10E+01	3,69E-02	2,18E-02	2,20E-15	7,23E-02	3,07E+01	9,32E-01	9,48E+01	2,58E+00
17	8,00E+00	2,92E+01	1,06E-01	4,99E-02	7,89E-16	2,08E-01	5,05E+01	9,59E-01	9,39E+01	6,53E+00
18	1,00E+01	3,72E+01	7,96E-02	7,43E-02	7,40E-16	1,56E-01	5,90E+01	9,85E-01	9,90E+01	8,60E+00
19	1,20E+01	4,60E+01	1,95E-01	1,04E-01	2,58E-16	3,83E-01	6,69E+01	9,94E-01	9,91E+01	1,99E+01
20	1,50E+01	1,18E+02	2,67E-01	3,36E-01	1,69E-16	5,24E-01	8,40E+01	1,00E+00	1,22E+02	3,56E+01

Total Gas Age = 9,62E+01 ± 6,41E-01 Ma (2Sigma)

Plateau age = 95.17±0.67 Ma (2s, including J-error of .096%)

MSWD = 1.2, probability = 0.29

73.9% of the 39Ar, steps 9 through 16

Table S1 continued

PIB-1 biotite (analysis PIB1bt3)

Mass = 1.819 mg
J = 3,70E-03 ± 3,56E-06 (2 Sigma)

Step	Laser power (W)	40Ar/39Ar	37Ar/39Ar	36Ar/39Ar	Mol 39ArK	Ca/K	% 40ArA	Cum 39ArK	Age [Ma]	2 Sigma
1	5,00E-02	3,19E+03	-4,02E-01	9,89E+00	1,30E-16	-7,88E-01	9,16E+01	6,72E-04	1,24E+03	9,55E+01
2	1,00E-01	7,57E+02	7,54E-02	2,49E+00	1,39E-15	1,48E-01	9,71E+01	7,82E-03	1,42E+02	3,35E+01
3	1,50E-01	2,70E+02	-5,79E-03	8,57E-01	1,55E-15	-1,13E-02	9,39E+01	1,58E-02	1,07E+02	1,44E+01
4	2,00E-01	1,08E+02	-8,49E-03	2,95E-01	4,34E-15	-1,66E-02	8,07E+01	3,82E-02	1,34E+02	4,51E+00
5	2,50E-01	5,49E+01	1,59E-03	1,10E-01	1,05E-14	3,11E-03	5,90E+01	9,23E-02	1,44E+02	2,52E+00
6	3,00E-01	4,03E+01	5,51E-03	5,87E-02	1,85E-14	1,08E-02	4,31E+01	1,88E-01	1,47E+02	1,82E+00
7	4,00E-01	3,27E+01	-5,59E-02	2,87E-02	4,58E-15	-1,09E-01	2,59E+01	2,11E-01	1,55E+02	2,06E+00
8	5,00E-01	2,80E+01	6,67E-03	1,25E-02	9,04E-15	1,31E-02	1,32E+01	2,58E-01	1,55E+02	1,02E+00
9	6,00E-01	2,64E+01	3,07E-02	7,55E-03	1,13E-14	6,01E-02	8,44E+00	3,16E-01	1,55E+02	9,71E-01
10	7,00E-01	2,57E+01	5,26E-02	5,89E-03	9,55E-15	1,03E-01	6,74E+00	3,65E-01	1,54E+02	1,40E+00
11	8,00E-01	2,47E+01	-4,85E-02	2,85E-03	4,04E-15	-9,51E-02	3,42E+00	3,86E-01	1,53E+02	4,89E+00
12	9,00E-01	2,47E+01	3,55E-02	6,01E-03	3,45E-14	6,97E-02	7,16E+00	5,63E-01	1,47E+02	1,06E+00
13	1,00E+00	2,48E+01	3,36E-02	6,63E-03	2,37E-14	6,60E-02	7,88E+00	6,85E-01	1,47E+02	1,45E+00
14	1,10E+00	2,45E+01	4,63E-02	6,19E-03	1,30E-14	9,08E-02	7,43E+00	7,52E-01	1,46E+02	2,18E+00
15	1,20E+00	2,47E+01	8,18E-02	6,57E-03	1,03E-14	1,60E-01	7,83E+00	8,05E-01	1,46E+02	2,47E+00
16	1,50E+00	2,52E+01	1,46E-01	6,82E-03	1,68E-14	2,87E-01	7,94E+00	8,92E-01	1,48E+02	1,39E+00
17	3,00E+00	2,51E+01	2,44E-01	7,61E-03	1,92E-14	4,79E-01	8,85E+00	9,91E-01	1,46E+02	1,35E+00
18	5,00E+00	2,40E+01	3,39E-01	6,85E-03	1,56E-15	6,64E-01	8,24E+00	9,99E-01	1,42E+02	7,21E+00
19	1,00E+01	2,05E+01	-3,23E+00	-4,25E-02	8,46E-17	-6,30E+00	-5,93E+01	9,99E-01	2,05E+02	1,27E+02
20	1,50E+01	1,29E+01	-2,87E+00	-4,10E-02	1,58E-16	-5,61E+00	-9,08E+01	1,00E+00	1,57E+02	6,88E+01

Total Gas Age = 1,48E+02 ± 4,03E-01 Ma (2Sigma)

Plateau age = 147.02±0.61 Ma (2s, including J-error of .096%)

MSWD = 1.3, probability = 0.23

61.4% of the 39Ar, steps 12 through 20

Table S1 continued

PIB-1 biotite (analysis PIB1bt4)

Mass = 1.484 mg
J = 3,70E-03 ± 3,56E-06 (2 Sigma)

Step	Laser power (W)	40Ar/39Ar	37Ar/39Ar	36Ar/39Ar	Mol 39ArK	Ca/K	% 40ArA	Cum 39ArK	Age [Ma]	2 Sigma
1	5,00E-02	2,95E+03	-9,16E-01	9,25E+00	6,79E-17	-1,79E+00	9,26E+01	2,97E-04	1,06E+03	1,67E+02
2	1,00E-01	5,47E+02	-1,60E-01	1,78E+00	1,19E-15	-3,13E-01	9,60E+01	5,51E-03	1,41E+02	2,57E+01
3	1,50E-01	1,54E+02	-2,56E-02	4,54E-01	1,74E-15	-5,02E-02	8,72E+01	1,31E-02	1,26E+02	9,36E+00
4	2,00E-01	6,83E+01	-4,09E-02	1,56E-01	4,92E-15	-8,02E-02	6,77E+01	3,47E-02	1,42E+02	3,81E+00
5	2,50E-01	4,50E+01	-1,05E-02	7,66E-02	1,10E-14	-2,06E-02	5,03E+01	8,28E-02	1,43E+02	2,16E+00
6	3,00E-01	3,48E+01	4,77E-03	4,01E-02	1,85E-14	9,34E-03	3,40E+01	1,64E-01	1,47E+02	1,40E+00
7	4,00E-01	2,90E+01	7,01E-03	2,01E-02	4,44E-14	1,37E-02	2,05E+01	3,58E-01	1,48E+02	1,07E+00
8	5,00E-01	2,62E+01	2,07E-02	7,21E-03	7,72E-15	4,06E-02	8,13E+00	3,92E-01	1,54E+02	9,17E-01
9	6,00E-01	2,51E+01	2,05E-02	4,22E-03	8,27E-15	4,02E-02	4,97E+00	4,28E-01	1,53E+02	1,02E+00
10	7,00E-01	2,46E+01	4,31E-02	3,83E-03	1,65E-14	8,46E-02	4,56E+00	5,01E-01	1,51E+02	8,24E-01
11	8,00E-01	2,42E+01	2,70E-02	4,10E-03	3,73E-14	5,28E-02	4,98E+00	6,64E-01	1,48E+02	1,04E+00
12	9,00E-01	2,43E+01	4,38E-02	4,35E-03	2,24E-14	8,58E-02	5,27E+00	7,62E-01	1,48E+02	1,47E+00
13	1,00E+00	2,46E+01	5,30E-02	4,94E-03	1,36E-14	1,04E-01	5,91E+00	8,22E-01	1,48E+02	2,03E+00
14	1,10E+00	2,46E+01	6,82E-02	5,48E-03	9,34E-15	1,34E-01	6,56E+00	8,63E-01	1,47E+02	2,51E+00
15	1,20E+00	2,46E+01	8,84E-02	6,10E-03	8,39E-15	1,73E-01	7,29E+00	9,00E-01	1,46E+02	2,54E+00
16	1,50E+00	2,48E+01	1,65E-01	6,52E-03	1,03E-14	3,24E-01	7,68E+00	9,45E-01	1,47E+02	1,79E+00
17	3,00E+00	2,47E+01	2,78E-01	6,67E-03	1,16E-14	5,45E-01	7,83E+00	9,96E-01	1,46E+02	1,84E+00
18	5,00E+00	2,84E+01	1,01E+00	2,57E-02	6,46E-16	1,98E+00	2,63E+01	9,98E-01	1,35E+02	1,54E+01
19	1,00E+01	2,39E+01	-8,13E-01	1,27E-02	3,65E-16	-1,59E+00	1,62E+01	1,00E+00	1,29E+02	2,53E+01

Total Gas Age = 1,48E+02 ± 3,57E-01 Ma (2Sigma)

Plateau age = 147.32±0.64 Ma (2s, including J-error of .096%)

MSWD = 1.18, probability = 0.31

49.9% of the 39Ar, steps 11 through 19

Table S1 continued

PIB-1 biotite (analysis PIB1bt6)

Mass = 0.325 mg
J = 3,70E-03 ± 3,56E-06 (2 Sigma)

Step	Laser power (W)	40Ar/39Ar	37Ar/39Ar	36Ar/39Ar	Mol 39ArK	Ca/K	% 40ArA	Cum 39ArK	Age [Ma]	2 Sigma
1	5,00E-02	1,88E+03	-4,12E-01	6,31E+00	2,71E-16	-8,07E-01	9,93E+01	2,80E-03	8,70E+01	8,88E+01
2	1,00E-01	3,70E+02	5,92E-01	1,18E+00	3,18E-16	1,16E+00	9,46E+01	6,09E-03	1,29E+02	2,38E+01
3	1,50E-01	1,34E+02	-2,21E-01	3,93E-01	5,48E-16	-4,34E-01	8,67E+01	1,18E-02	1,15E+02	1,40E+01
4	2,00E-01	5,97E+01	9,20E-02	1,31E-01	1,70E-15	1,80E-01	6,49E+01	2,93E-02	1,35E+02	5,01E+00
5	2,50E-01	3,81E+01	-1,49E-02	4,97E-02	4,33E-15	-2,92E-02	3,85E+01	7,40E-02	1,50E+02	2,25E+00
6	3,00E-01	3,06E+01	1,83E-02	2,30E-02	6,54E-15	3,59E-02	2,22E+01	1,42E-01	1,53E+02	1,36E+00
7	4,00E-01	2,74E+01	-1,49E-03	1,25E-02	1,33E-14	-2,93E-03	1,35E+01	2,79E-01	1,52E+02	7,63E-01
8	5,00E-01	2,52E+01	1,39E-02	5,22E-03	1,91E-14	2,72E-02	6,10E+00	4,76E-01	1,52E+02	4,88E-01
9	6,00E-01	2,49E+01	2,47E-03	3,92E-03	1,75E-14	4,85E-03	4,64E+00	6,57E-01	1,52E+02	6,07E-01
10	7,00E-01	2,50E+01	9,12E-03	3,04E-03	1,44E-14	1,79E-02	3,59E+00	8,05E-01	1,54E+02	7,05E-01
11	8,00E-01	2,46E+01	3,26E-02	5,15E-03	5,92E-15	6,38E-02	6,16E+00	8,66E-01	1,48E+02	1,41E+00
12	9,00E-01	2,46E+01	6,97E-02	6,14E-03	3,50E-15	1,37E-01	7,35E+00	9,03E-01	1,46E+02	1,44E+00
13	1,00E+00	2,48E+01	1,91E-01	7,56E-03	1,76E-15	3,74E-01	8,91E+00	9,21E-01	1,45E+02	2,64E+00
14	1,10E+00	2,48E+01	1,99E-01	7,59E-03	1,39E-15	3,90E-01	8,93E+00	9,35E-01	1,45E+02	3,12E+00
15	1,20E+00	2,47E+01	1,13E-01	7,20E-03	1,50E-15	2,21E-01	8,57E+00	9,51E-01	1,45E+02	3,29E+00
16	1,50E+00	2,47E+01	1,21E-01	6,62E-03	2,27E-15	2,38E-01	7,85E+00	9,74E-01	1,46E+02	2,88E+00
17	3,00E+00	2,49E+01	1,46E-01	6,49E-03	2,46E-15	2,87E-01	7,62E+00	9,99E-01	1,48E+02	2,55E+00
18	5,00E+00	2,17E+01	3,48E-01	-9,73E-03	5,41E-17	6,82E-01	-1,35E+01	1,00E+00	1,57E+02	9,63E+01

Total Gas Age
= 1,50E+02 ± 2,77E-01 Ma
(2Sigma)

Plateau age = 151.90±0.36 Ma (2s, including J-error of .096%)

MSWD = 1.3, probability = 0.26

62.8% of the 39Ar, steps 5 through 9

Table S1 continued

BI-5 biotite (analysis BI5bts)

Mass = 1.750 mg
J = 3,70E-03 ± 3,56E-06 (2 Sigma)

Step	Laser power (W)	40Ar/39Ar	37Ar/39Ar	36Ar/39Ar	Mol 39ArK	Ca/K	% 40ArA	Cum 39ArK	Age [Ma]	2 Sigma
1	5,00E-02	-5,73E+02	8,36E-01	-1,47E+00	-2,22E-17	1,64E+00	7,57E+01	0,00E+00	-1,30E+03	1,31E+03
2	1,00E-01	3,23E+03	-1,73E-02	1,01E+01	2,80E-16	-3,40E-02	9,25E+01	1,11E-03	1,15E+03	8,49E+01
3	1,50E-01	9,14E+02	5,11E-02	2,83E+00	4,56E-16	1,00E-01	9,14E+01	2,92E-03	4,59E+02	4,01E+01
4	2,00E-01	2,16E+02	6,95E-02	6,79E-01	5,93E-15	1,36E-01	9,30E+01	2,64E-02	9,85E+01	7,14E+00
5	2,50E-01	1,18E+02	3,20E-02	3,24E-01	7,55E-16	6,27E-02	8,08E+01	2,94E-02	1,46E+02	1,22E+01
6	3,00E-01	6,74E+01	3,18E-02	1,65E-01	1,94E-14	6,24E-02	7,25E+01	1,06E-01	1,20E+02	3,35E+00
7	4,00E-01	4,38E+01	3,95E-02	8,04E-02	5,86E-15	7,73E-02	5,43E+01	1,29E-01	1,29E+02	2,77E+00
8	5,00E-01	3,19E+01	4,48E-02	3,94E-02	1,21E-14	8,77E-02	3,65E+01	1,77E-01	1,31E+02	1,60E+00
9	6,00E-01	2,34E+01	5,03E-02	1,64E-02	9,93E-15	9,86E-02	2,07E+01	2,17E-01	1,20E+02	1,60E+00
10	7,00E-01	2,12E+01	6,13E-02	1,18E-02	5,10E-14	1,20E-01	1,64E+01	4,18E-01	1,15E+02	1,19E+00
11	8,00E-01	2,01E+01	1,07E-01	1,01E-02	3,71E-14	2,10E-01	1,47E+01	5,65E-01	1,11E+02	1,22E+00
12	9,00E-01	2,04E+01	1,41E-01	1,19E-02	2,63E-14	2,77E-01	1,72E+01	6,69E-01	1,09E+02	1,52E+00
13	1,00E+00	2,02E+01	2,39E-01	1,23E-02	1,86E-14	4,69E-01	1,78E+01	7,43E-01	1,08E+02	1,92E+00
14	1,10E+00	2,00E+01	2,28E-01	1,07E-02	1,33E-14	4,47E-01	1,57E+01	7,96E-01	1,09E+02	2,48E+00
15	1,20E+00	1,92E+01	1,97E-01	8,45E-03	1,04E-14	3,87E-01	1,29E+01	8,37E-01	1,08E+02	2,83E+00
16	1,50E+00	1,89E+01	2,51E-01	9,11E-03	1,40E-14	4,93E-01	1,41E+01	8,92E-01	1,05E+02	1,28E+00
17	3,00E+00	2,13E+01	4,35E-01	1,32E-02	1,92E-14	8,54E-01	1,80E+01	9,68E-01	1,13E+02	1,09E+00
18	5,00E+00	2,07E+01	5,21E-01	1,08E-02	2,69E-15	1,02E+00	1,51E+01	9,79E-01	1,13E+02	4,46E+00
19	1,00E+01	1,99E+01	6,42E-01	1,15E-02	5,16E-15	1,26E+00	1,66E+01	9,99E-01	1,08E+02	3,61E+00
20	1,50E+01	2,60E+01	2,34E+00	7,94E-03	1,89E-16	4,59E+00	7,85E+00	1,00E+00	1,54E+02	6,69E+01

Total Gas Age = 1,15E+02 ± 4,48E-01 Ma (2Sigma)

Best steps mean age = 109.82±0.78 Ma (2s, including J-error of .096%)

MSWD = 3.0, probability = 0.019

41.8% of the 39Ar, steps 10 through 14

Table S1 continued

BI-5 biotite (analysis BI5bt3)

Mass = 1.550 mg
J = 3,70E-03 ± 3,56E-06 (2 Sigma)

Step	Laser power (W)	40Ar/39Ar	37Ar/39Ar	36Ar/39Ar	Mol 39ArK	Ca/K	% 40ArA	Cum 39ArK	Age [Ma]	2 Sigma
1	5,00E-02	1,13E+04	-5,38E-01	3,53E+01	1,14E-16	-1,05E+00	9,25E+01	5,58E-04	2,56E+03	1,28E+02
2	1,00E-01	3,07E+03	-7,43E-01	9,55E+00	2,15E-16	-1,45E+00	9,20E+01	1,61E-03	1,17E+03	5,42E+01
3	1,50E-01	6,45E+02	2,43E-02	2,14E+00	1,90E-15	4,76E-02	9,80E+01	1,09E-02	8,51E+01	3,23E+01
4	2,00E-01	3,03E+02	2,36E-01	9,71E-01	4,28E-15	4,62E-01	9,47E+01	3,18E-02	1,04E+02	1,11E+01
5	2,50E-01	1,77E+02	2,03E-01	5,24E-01	4,25E-15	3,97E-01	8,77E+01	5,25E-02	1,39E+02	7,62E+00
6	3,00E-01	9,80E+01	1,57E-01	2,70E-01	1,33E-14	3,08E-01	8,16E+01	1,17E-01	1,17E+02	2,85E+00
7	4,00E-01	5,48E+01	3,11E-01	1,13E-01	4,08E-15	6,10E-01	6,10E+01	1,37E-01	1,37E+02	5,84E+00
8	5,00E-01	3,03E+01	2,64E-01	3,74E-02	5,88E-15	5,18E-01	3,64E+01	1,66E-01	1,24E+02	2,73E+00
9	6,00E-01	2,25E+01	4,30E-01	1,62E-02	3,52E-15	8,43E-01	2,11E+01	1,83E-01	1,15E+02	2,59E+00
10	7,00E-01	2,13E+01	1,27E-01	1,24E-02	5,07E-14	2,49E-01	1,71E+01	4,31E-01	1,15E+02	6,37E-01
11	8,00E-01	2,07E+01	7,26E-02	1,10E-02	3,37E-14	1,42E-01	1,56E+01	5,96E-01	1,13E+02	8,06E-01
12	9,00E-01	2,07E+01	1,13E-01	1,18E-02	2,02E-14	2,22E-01	1,68E+01	6,94E-01	1,11E+02	1,14E+00
13	1,00E+00	2,07E+01	1,39E-01	1,30E-02	1,50E-14	2,72E-01	1,84E+01	7,67E-01	1,09E+02	1,39E+00
14	1,10E+00	2,05E+01	1,59E-01	1,30E-02	9,30E-15	3,11E-01	1,87E+01	8,12E-01	1,08E+02	2,28E+00
15	1,20E+00	2,01E+01	2,04E-01	1,21E-02	5,63E-15	3,99E-01	1,77E+01	8,40E-01	1,07E+02	3,31E+00
16	1,50E+00	2,02E+01	4,03E-01	1,26E-02	6,49E-15	7,90E-01	1,82E+01	8,72E-01	1,07E+02	2,28E+00
17	3,00E+00	2,13E+01	3,15E-01	1,46E-02	1,27E-14	6,17E-01	2,01E+01	9,33E-01	1,10E+02	1,36E+00
18	5,00E+00	2,10E+01	2,17E-01	1,39E-02	7,60E-15	4,26E-01	1,94E+01	9,71E-01	1,10E+02	1,70E+00
19	1,00E+01	2,17E+01	1,58E-02	1,51E-02	5,80E-15	3,09E-02	2,06E+01	9,99E-01	1,11E+02	1,89E+00
20	1,50E+01	2,61E+01	-1,96E+00	1,45E-02	2,26E-16	-3,83E+00	1,74E+01	1,00E+00	1,38E+02	4,18E+01

Total Gas Age = 1,16E+02 ± 3,68E-01 Ma (2Sigma)

Best steps mean age = 111.0±1.5 Ma (95% conf.), including J-error of .096%)

MSWD = 7.4, probability = 0.000

56.8% of the 39Ar, steps 11 through 19

Table S1 continued

BI-5 biotite (analysis BI5bt6)

Mass = 0.352 mg
J = 3,70E-03 ± 3,56E-06 (2 Sigma)

Step	Laser power (W)	40Ar/39Ar	37Ar/39Ar	36Ar/39Ar	Mol 39ArK	Ca/K	% 40ArA	Cum 39ArK	Age [Ma]	2 Sigma
1	5,00E-02	7,10E+03	1,47E+00	2,40E+01	1,56E-16	2,89E+00	9,98E+01	1,93E-03	8,83E+01	1,66E+02
2	1,00E-01	1,99E+03	3,52E-01	6,66E+00	2,64E-16	6,90E-01	9,91E+01	5,19E-03	1,21E+02	1,26E+02
3	1,50E-01	3,64E+02	2,24E-01	1,17E+00	5,60E-16	4,39E-01	9,53E+01	1,21E-02	1,10E+02	3,15E+01
4	2,00E-01	2,52E+02	3,07E-01	8,09E-01	9,65E-16	6,03E-01	9,48E+01	2,40E-02	8,50E+01	2,16E+01
5	2,50E-01	1,34E+02	9,82E-02	3,98E-01	2,18E-15	1,93E-01	8,78E+01	5,10E-02	1,06E+02	8,52E+00
6	3,00E-01	5,87E+01	7,44E-02	1,42E-01	3,43E-15	1,46E-01	7,15E+01	9,34E-02	1,08E+02	3,89E+00
7	4,00E-01	3,32E+01	5,02E-02	5,44E-02	9,55E-15	9,84E-02	4,83E+01	2,11E-01	1,11E+02	1,55E+00
8	5,00E-01	2,23E+01	3,26E-02	1,57E-02	1,40E-14	6,39E-02	2,08E+01	3,84E-01	1,15E+02	1,16E+00
9	6,00E-01	2,03E+01	5,52E-02	9,57E-03	1,33E-14	1,08E-01	1,39E+01	5,49E-01	1,13E+02	1,14E+00
10	7,00E-01	1,94E+01	1,11E-01	8,02E-03	1,13E-14	2,18E-01	1,22E+01	6,89E-01	1,10E+02	1,23E+00
11	8,00E-01	1,93E+01	1,27E-01	7,80E-03	8,55E-15	2,48E-01	1,19E+01	7,94E-01	1,10E+02	1,19E+00
12	9,00E-01	1,89E+01	2,69E-01	8,85E-03	5,71E-15	5,27E-01	1,36E+01	8,65E-01	1,06E+02	1,74E+00
13	1,00E+00	1,97E+01	4,44E-01	1,17E-02	2,72E-15	8,71E-01	1,72E+01	8,99E-01	1,06E+02	3,16E+00
14	1,10E+00	2,06E+01	7,85E-01	1,40E-02	1,35E-15	1,54E+00	1,95E+01	9,15E-01	1,08E+02	5,56E+00
15	1,20E+00	2,02E+01	8,52E-01	1,04E-02	8,72E-16	1,67E+00	1,47E+01	9,26E-01	1,11E+02	8,26E+00
16	1,50E+00	2,08E+01	4,31E-01	1,63E-02	6,74E-16	8,45E-01	2,28E+01	9,35E-01	1,04E+02	7,90E+00
17	3,00E+00	2,02E+01	1,72E-01	1,22E-02	2,93E-15	3,36E-01	1,77E+01	9,71E-01	1,08E+02	2,10E+00
18	5,00E+00	2,01E+01	2,08E-01	1,28E-02	1,89E-15	4,08E-01	1,86E+01	9,94E-01	1,06E+02	3,18E+00
19	1,00E+01	1,75E+01	-6,05E-02	3,92E-03	4,64E-16	-1,19E-01	6,65E+00	1,00E+00	1,06E+02	9,46E+00

Total Gas Age = 1,10E+02 ± 4,88E-01 Ma (2Sigma)

Best steps mean age = 108.9±1.4 Ma (95% conf.), including J-error of .096%)

MSWD = 3.2, probability = 0.001

45.1% of the 39Ar, steps 10 through 19

Appendix III (CHAPTER III)

Table 1: RFA standard measurements and reference values.

Oxide (wt%)	JB-2^a	JB2 (N=2)	SD	Diff. (abs.)	Diff. (%)	JB-3^b	JB-3 (N=2)	SD	Diff. (abs.)	Diff. (%)	JA-2^b	JA-2 (N=2)	SD	Diff. (abs.)	Diff. (%)	JR-I^b	JR-I (N=2)	SD	Diff. (abs.)	Diff. (%)
SiO ₂	53.20	53.09	0.08	0.12	0.2	51.04	50.79	0.18	0.26	0.50	56.42	56.26	0.21	0.29	0.5	75.28	75.03	0.18	0.25	0.34
TiO ₂	1.19	1.17	0.01	0.02	1.7	1.45	1.41	0.03	0.05	3.20	0.66	0.67	0.01	-0.02	2.3	0.11	0.11	0.00	0.00	0.00
Al ₂ O ₃	14.67	14.85	0.12	-0.18	1.2	16.89	17.31	0.29	-0.41	2.40	15.41	15.44	0.04	0.06	0.4	12.56	12.77	0.14	-0.21	1.61
Fe ₂ O ₃	14.34	14.34	0.08	-0.12	0.8	11.88	11.96	0.06	-0.12	0.67	6.21	6.38	0.12	-0.17	2.7	0.86	0.86	0.00	0.01	0.58
MnO	0.20	0.21	0.01	-0.01	4.8	0.16	0.18	0.01	-0.08	11.11	0.11	0.11	0.00	0.00	1.9	0.10	0.11	0.01	-0.01	9.09
MgO	4.66	4.78	0.08	-0.12	2.5	5.20	5.25	0.04	-0.02	0.95	7.60	8.05	0.28	-0.39	5.1	0.13	0.14	0.00	-0.01	3.70
CaO	9.89	9.91	0.01	-0.02	0.2	9.86	9.78	0.06	0.09	0.87	6.29	6.27	0.02	0.04	0.6	0.68	0.70	0.01	-0.02	2.86
Na ₂ O	2.03	2.17	0.10	-0.14	6.5	2.82	2.86	0.03	-0.04	1.40	3.11	3.05	0.03	0.04	1.4	3.97	4.15	0.12	-0.17	4.22
K ₂ O	0.42	0.42	0.00	0.00	0.0	0.78	0.78	0.00	0.01	0.65	1.81	1.75	0.04	0.06	3.0	4.51	4.46	0.04	0.05	1.12
P ₂ O ₅	0.10	0.10	0.00	0.00	0.0	0.29	0.30	0.01	-0.01	3.33	0.15	0.16	0.01	-0.01	6.2	0.02	0.03	0.00	-0.01	20.00
total	100.70	101.14				100.37	100.60				97.76	98.12				98.22	98.33			

^a reference values from Govindaraju 1994

^b data from GeoReM

Table 2: ICP-ES standard measurement and reference values (IFG Data)

Element	BCR-2 (ref. value)	BCR-2 (measured value)	BCR-2 (measured value)	BCR-2 (mean)	STD	RSD %	Diff (abs.)	Diff (%)
Rb	46.9	47.49	46.83	46.9	0.47	0.99	-0.26	0.55
Ba	677	683.95	667.96	675.96	11.31	1.67	1.04	0.15
Th	5.7	5.98	5.90	5.94	0.05	0.91	-0.24	4.02
U	1.69	1.70	1.67	1.68	0.02	1.16	0.01	0.36
Nb	12.6	12.19	11.93	12.06	0.29	1.48	0.54	4.49
Ta	0.74	0.76	0.75	0.75	0.01	1.52	-0.01	1.79
La	24.9	25.60	25.60	25.30	0.43	1.70	-0.40	1.59
Ce	52.9	54.17	53.35	53.76	0.58	1.09	-0.86	1.60
Pb	11	10.25	10.18	10.21	0.05	0.54	0.79	7.70
Pr	6.7	6.92	6.77	6.84	0.11	1.56	-0.14	2.08
Nd	28.7	29.55	28.80	29.17	0.53	1.80	-0.47	1.63
Sr	340	342.65	339.51	341.08	2.22	0.65	-1.08	0.32
Sm	6.58	6.70	6.58	6.64	0.09	1.29	-0.06	0.83
Hf	4.9	4.89	4.79	4.84	0.07	1.39	0.06	1.29
Zr	184	188.30	184.48	186.39	2.70	1.45	-2.39	1.28
Eu	1.96	1.99	1.96	1.97	0.02	1.17	-0.01	0.73
Gd	6.75	6.92	6.80	6.86	0.08	1.20	-0.11	1.64
Tb	1.07	1.10	1.07	1.09	0.02	1.55	-0.02	1.49
Dy	6.41	6.47	6.39	6.43	0.05	0.85	-0.02	0.33
Ho	1.28	1.30	1.28	1.29	0.01	0.91	-0.01	0.70
Y	37	35.62	34.74	35.18	0.63	1.79	1.82	5.17
Er	3.66	3.52	3.47	3.49	0.04	1.08	0.17	4.78
Tm	0.54	0.51	0.51	0.51	0.00	0.34	0.03	5.37
Yb	3.38	3.41	3.33	3.37	0.06	1.74	0.01	0.32
Lu	0.503	0.50	0.50	0.50	0.01	1.06	0.00	0.93

Table 2: continued BHVO-2

Element	BHVO-2 (ref. value)	BHVO-2 (measured value)	BHVO-2 (measured value)	BHVO-2 (mean)	STD	RSD %	Diff (abs.)	Diff (%)
Rb	9.11	9.26	9.23	9.24	0.02	0.22	-0.13	1.42
Ba	131	130.45	131.44	130.94	0.70	0.54	0.06	0.04
Th	1.22	1.22	1.21	1.21	0.00	0.21	0.01	0.50
U	0.40	0.42	0.42	0.42	0.00	0.40	-0.02	3.62
Nb	18.1	17.99	17.87	17.93	0.09	0.48	0.17	0.93
Ta	1.14	1.12	1.12	1.12	0.00	0.34	0.02	1.61
La	15.2	15.36	15.34	15.35	0.01	0.10	-0.15	1.00
Ce	37.5	37.89	38.08	37.98	0.13	0.35	-0.48	1.27
Pb	1.6	1.58	2.68	2.13	0.77	36.34	-0.53	24.88
Pr	5.35	5.34	5.31	5.33	0.02	0.41	0.02	0.39
Nd	24.5	25.04	24.80	24.92	0.17	0.66	-0.42	1.68
Sr	396	399.20	390.55	394.87	6.12	1.55	1.13	0.28
Sm	6.07	6.13	6.08	6.10	0.03	0.57	-0.03	0.52
Hf	4.36	4.34	4.36	4.35	0.01	0.20	0.01	0.23
Zr	172	173.11	173.03	173.07	0.06	0.03	-1.07	0.62
Eu	2.07	2.07	2.07	2.07	0.01	0.32	0.00	0.01
Gd	6.24	6.26	6.24	6.25	0.02	0.27	-0.01	0.18
Tb	0.92	0.96	0.96	0.96	0.00	0.37	-0.04	4.11
Dy	5.31	5.34	5.33	5.34	0.00	0.09	-0.03	0.51
Ho	0.98	0.98	0.97	0.98	0.00	0.46	0.00	0.25
Y	26	25.79	25.73	25.76	0.04	0.17	0.24	0.94
Er	2.54	2.44	2.43	2.43	0.01	0.25	0.11	4.35
Tm	0.33	0.33	0.33	0.33	0.00	0.16	0.00	1.24
Yb	2	2.00	2.01	2.01	0.01	0.25	-0.01	0.28
Lu	0.274	0.27	0.28	0.28	0.00	0.92	0.00	0.74

Table 2: continued

Element	BIR-1 (ref. value)	BIR -1 (measured value)	BIR-1 (measured value)	BIR-1 (mean)	STD	RSD %	Diff (abs.)	Diff (%)
Rb	0.20	0.20	0.19	0.19	0.00	2.10	0.01	3.36
Ba	7.14	6.48	6.47	6.48	0.01	0.12	0.66	10.21
Th	0.03	0.03	0.03	0.03	0.00	3.08	0.00	3.29
U	0.01	0.01	0.01	0.01	0.00	2.87	0.00	15.70
Nb	0.55	0.53	0.54	0.53	0.01	2.25	0.02	3.10
Ta	0.03	0.05	0.04	0.05	0.00	3.36	-0.01	20.67
La	0.61	0.60	0.61	0.60	0.01	2.05	0.01	1.67
Ce	1.92	1.89	1.90	1.90	0.00	0.14	0.02	1.26
Pb	3.10	2.89	3.17	3.03	0.20	6.49	6.49	2.33
Pr	0.37	0.36	0.38	0.37	0.01	2.85	0.00	0.34
Nd	2.38	2.42	2.44	2.43	0.01	0.59	-0.05	1.95
Sr	109	107.66	111.63	109.65	2.81	2.56	-0.65	0.59
Sm	1.12	1.10	1.12	1.11	0.01	1.30	0.01	0.80
Hf	0.58	0.57	0.59	0.58	0.01	1.77	0.00	0.23
Zr	14	14.44	15.08	14.76	0.45	3.07	-0.76	5.14
Eu	0.53	0.52	0.53	0.52	0.01	2.09	0.01	1.15
Gd	1.87	1.75	1.80	1.77	0.03	1.69	0.10	5.39
Tb	0.36	0.36	0.36	0.36	0.00	0.96	0.00	0.21
Dy	2.51	2.56	2.60	2.58	0.03	0.98	-0.07	2.74
Ho	0.56	0.56	0.57	0.57	0.01	1.16	-0.01	1.39
Y	15.60	15.47	15.53	15.50	0.04	0.26	0.10	0.64
Er	1.66	1.60	1.62	1.61	0.01	0.79	0.05	3.06
Tm	0.25	0.25	0.25	0.25	0.00	0.28	0.00	1.79
Yb	1.65	1.63	1.64	1.63	0.01	0.54	0.02	1.13
Lu	0.25	0.24	0.24	0.24	0.00	0.01	0.01	2.91

Table 3: Reproducibility ICP-MS (Acme Lab)

Element	BIR-1 (ref. value)	BIR-1 (measured value)	BIR-1 (measured value)	BIR-1 (mean)	STD	RSD %	Diff (abs.)	Diff (%)
Rb	0.2	0.2	0.1	0.15	0.07	47.14	0.05	33.33
Ba	7.14	6	6	6	0.00	0.00	1.14	19.00
Th	0.032	0.2	0.2	0.2	0.00	0.00	-0.17	84
U	0.01	0.1	0.1	0.1	0.00	0.00	-0.09	90
Nb	0.55	0.8	0.6	0.7	0.14	20.20	-0.15	21.43
Ta	0.0357	0.1	0.1	0.1	0.00	0.00	-0.06	64.30
La	0.615	0.6	0.6	0.6	0.00	0.00	0.02	2.50
Ce	1.92	2	1.9	1.95	0.07	3.63	-0.03	1.54
Pb	3.1	2.9		2.9			0.20	6.90
Pr	0.37	0.34	0.33	0.335	0.01	2.11	0.04	10.45
Nd	2.38	2.1	2.2	2.15	0.07	3.29	0.23	10.70
Sr	109	109	110.1	109.55	0.78	0.71	-0.55	0.50
Sm	1.12	1.01	1.03	1.02	0.01	1.39	0.10	9.80
Hf	0.582	0.6	0.6	0.6	0.00	0.00	-0.02	3.00
Zr	14	14.4	14.1	14.25	0.21	1.49	-0.25	1.75
Eu	0.53	0.47	0.51	0.49	0.03	5.77	0.04	8.16
Gd	1.87	1.74	1.74	1.74	0.00	0.00	0.13	7.47
Tb	0.36	0.35	0.35	0.35	0.00	0.00	0.01	2.86
Dy	2.51	2.37	2.19	2.28	0.13	5.58	0.23	10.09
Ho	0.56	0.54	0.55	0.545	0.01	1.30	0.02	2.75
Y	15.6	14.2	14.4	14.3	0.14	0.99	1.30	9.09
Er	1.66	1.46	1.57	1.515	0.08	5.13	0.15	9.57
Tm	0.25	0.25	0.25	0.25	0.00	0.00	0.00	0.00
Yb	1.65	1.5	1.58	1.54	0.06	3.67	0.11	7.14
Lu	0.25	0.23	0.24	0.235	0.01	3.01	0.02	6.38

Table 3: Accuracy ICP-MS (Acme Lab)

Element	BHVO-2 (ref. value)	BHVO-2 (measured value)	STD	Diff. (abs.)	Diff. (%)
Rb	9.11	8.4	0.50	0.71	8.45
Ba	131	126	3.54	5.00	3.97
Th	1.22	1.2	0.01	0.02	1.67
U	0.403	0.5	0.07	-0.10	19.40
Nb	18.1	17.0	0.78	1.10	6.47
Ta	1.14	1.1	0.03	0.04	3.64
La	15.2	14.1	0.78	1.10	7.80
Ce	37.5	37.6	0.07	-0.10	0.27
Pb	1.6	0.8	0.57	0.80	100.00
Pr	5.35	4.96	0.28	0.39	7.86
Nd	24.5	23.6	0.64	0.90	3.81
Sr	396	396.6	0.42	-0.60	0.15
Sm	6.07	5.63	0.31	0.44	7.82
Hf	4.36	4.4	0.03	-0.04	0.91
Zr	172	155.1	11.95	16.90	10.90
Eu	2.07	1.88	0.13	0.19	10.11
Gd	6.24	5.72	0.37	0.52	9.09
Tb	0.92	0.91	0.01	0.01	1.10
Dy	5.31	4.61	0.49	0.70	15.18
Ho	0.98	0.90	0.06	0.08	8.89
Y	26	23.5	1.77	2.50	10.64
Er	2.54	2.33	0.15	0.21	9.01
Tm	0.33	0.32	0.01	0.01	3.13
Yb	2.0	1.82	0.13	0.18	9.89
Lu	0.274	0.26	0.01	0.01	5.38

Table 3: continued

Element	BCR-2 (ref. value)	BCR-2 (measured value)	STD	Diff (abs.)	Diff. (%)
Rb	46.9	44.6	1.63	2.3	5.16
Ba	677	663	9.90	14	2.11
Th	5.7	6.1	0.08	-0.11	6.56
U	1.69	1.8	0.01	-0.02	6.11
Nb	12.6	11.9	0.49	0.7	5.88
Ta	0.74	0.70	0.03	0.04	5.71
La	24.9	24.3	0.42	0.6	2.47
Ce	52.9	54.7	1.27	-1.8	3.29
Pb	11	2.8	5.80	8.2	292.86
Pr	6.7	6.56	0.1	0.14	2.13
Nd	28.7	27.4	0.92	1.3	4.74
Sr	340	337.6	1.70	2.4	0.71
Sm	6.58	6.12	0.33	0.46	7.52
Hf	4.9	4.9	0.00	0	0.00
Zr	184	173.5	7.42	10.5	6.05
Eu	1.96	1.86	0.07	0.1	5.38
Gd	6.75	6.25	0.35	0.5	8.00
Tb	1.07	1.06	0.01	0.01	0.94
Dy	6.41	5.81	0.42	0.6	10.33
Ho	1.28	1.29	0.01	-0.01	0.78
Y	37	32.1	3.46	4.9	15.26
Er	3.66	3.44	0.16	0.22	6.40
Tm	0.54	0.51	0.02	0.03	5.88
Yb	3.38	3.24	0.10	0.14	4.32
Lu	0.503	0.49	0.01	0.01	2.65

Table 3: continued

Element	AGV-2 (ref. value)	AGV-2 (measured value)	STD	Diff (abs.)	Diff. (%)
Rb	68	63.2	3.39	4.8	7.59
Ba	1140	1080	42.43	60	5.56
Th	6.1	6.5	0.01	-0.04	6.15
U	1.88	1.9	0.01	-0.02	1.05
Nb	15	13.5	1.06	1.5	11.11
Ta	0.89	0.9	0.01	-0.01	1.11
La	38	35.5	1.77	2.5	7.04
Ce	68	68.9	0.64	-0.9	1.31
Pb	13	4.3	6.15	8.7	202.33
Pr	8.3	7.59	0.50	0.71	9.35
Nd	30	28.3	1.20	1.7	6.01
Sr	685	670.1	8.56	-12.1	1.81
Sm	5.7	5.10	0.42	0.6	11.76
Hf	5.08	5.3	0.16	-0.22	4.15
Zr	230	216.9	9.26	13.1	6.04
Eu	1.54	1.42	0.08	0.12	8.45
Gd	4.69	3.99	0.49	0.70	17.54
Tb	0.64	0.63	0.01	0.01	1.59
Dy	3.6	3.11	0.35	0.49	15.76
Ho	0.71	0.62	0.06	0.09	14.52
Y	20	17.5	1.77	2.5	14.29
Er	1.79	1.69	0.07	0.1	5.92
Tm	0.26	0.25	0.01	0.01	4.00
Yb	1.6	1.43	0.12	0.17	11.89
Lu	0.25	0.23	0.01	0.02	8.70

Table 4: Instrument stability ICP-MS (Acme-Lab)

Element	STD SO-18	STD SO-18	STD SO-18	STD SO-18	STD SO-18 (mean)	STD	RSD %
Rb	28.00	27.5	29.0	28.5	28.25	0.65	2.88
Ba	503	509	534	521	516.75	13.72	2.66
Th	10.2	10.1	10.7	10.7	10.43	0.32	3.07
U	16.4	16.2	17.3	16.9	16.7	0.50	2.97
Nb	20.7	20.7	21.5	21.4	21.08	0.43	2.06
Ta	6.9	7.0	7.3	7.3	7.13	0.21	2.89
La	12.0	11.8	12.7	12.2	12.18	0.39	3.17
Ce	27.1	27.1	29.7	28.2	28.03	1.23	4.39
Pb							
Pr	3.34	3.27	3.49	3.47	3.37	0.09	2.73
Nd	13.8	13.1	14.2	13.8	13.73	0.46	3.33
Sr	402.4	399.2	451.5	410.6	408.43	9.95	2.44
Sm	2.87	2.79	2.95	2.87	2.87	0.07	2.28
Hf	9.6	9.3	10.1	9.7	9.68	0.33	3.42
Zr	282.8	281.2	299.9	292.4	289.08	8.75	3.03
Eu	0.87	0.85	0.89	0.87	0.87	0.02	1.88
Gd	2.91	2.81	3.04	2.90	2.94	0.09	3.25
Tb	0.50	0.49	0.52	0.51	0.51	0.02	2.56
Dy	2.93	2.89	3.01	2.91	2.92	0.05	1.79
Ho	0.62	0.60	0.63	0.62	0.62	0.01	2.04
Y	31.1	30.7	32.6	31.7	31.53	0.83	2.62
Er	1.82	1.80	1.88	1.83	1.83	0.03	1.86
Tm	0.27	0.27	0.28	0.28	0.28	0.01	2.10
Yb	1.77	1.72	1.80	1.78	1.77	0.03	1.93
Lu	0.27	0.26	0.28	0.27	0.27	0.01	3.02
